



Mario Bandiera

Mestre em Ciência para a Conservação e Restauro

**Technological study and chemical- archaeometric
characterization of Roman opaque red glass from *opus
sectile* decoration in the *Lucius Verus Villa*, 2nd century AD**

Dissertação para obtenção do Grau de Doutor em Conservação e
Restauro do Património, Especialidade em Ciências da Conservação

Orientador: Doutora Márcia Gomes Vilarigues, Professora Auxiliar
com agregação, Faculdade de Ciências e Tecnologia da
Universidade NOVA de Lisboa

Co-orientador: Doutor Marco Verità, Research Collaborator, LAMA
Laboratory, IUAV University, Venice (Italy)

Júri:

Presidente: Doutora Maria João Seixas de Melo, Professora Catedrática,
Faculdade de Ciências e Tecnologia da Universidade NOVA de
Lisboa

Arguentes: Doutora Alberta Silvestri, Professora Associada do Dipartimento di
Geoscienze da Università di Padova Italy

Doutora Yael Gorin-Rosen, Diretora do Glass Branch Archaeological
Research Department-Israel Antiquities Authority

Vogais: Doutora Márcia Gomes Vilarigues, Professora Auxiliar com
agregação, Faculdade de Ciências e Tecnologia da Universidade
NOVA de Lisboa

Doutora Andreia Filipa Cardoso Ruivo, Investigadora Auxiliar da
VICARTE Vidro e Cerâmica para as Artes da Universidade NOVA de
Lisboa

Doutor Virgílio Hipólito Correia, Arqueólogo do Museu Monográfico
e Ruínas de Conimbriga



Outubro/2021



Technological study and chemical-archaeometric characterization of Roman opaque red glass from *opus sectile* decoration in the *Lucius Verus* Villa, 2nd century AD

Mario Bandiera

Mario Bandiera

Mestre em Ciência para a Conservação e Restauro

**Technological study and chemical- archaeometric
characterization of Roman opaque red glass from *opus
sectile* decoration in the *Lucius Verus Villa*, 2nd century AD**

Dissertação para obtenção do Grau de Doutor em Conservação e
Restauro do Património, Especialidade em Ciências da Conservação

Orientador: Doutora Márcia Gomes Vilarigues, Professora Auxiliar com
agregação, Faculdade de Ciências e Tecnologia da Universidade
NOVA de Lisboa

Co-orientador: Doutor Marco Verità, Research Collaborator, LAMA Laboratory,
IUAV University, Venice (Italy)

Júri:

Presidente: Doutora Maria João Seixas de Melo, Professora Catedrática, Faculdade de
Ciências e Tecnologia da Universidade NOVA de Lisboa

Arguentes: Doutora Alberta Silvestri, Professora Associada do Dipartimento di Geoscienze
da Università di Padova Italy

Doutora Yael Gorin-Rosen, Diretora do Glass Branch Archaeological Research
Department-Israel Antiquities Authority

Vogais: Doutora Márcia Gomes Vilarigues, Professora Auxiliar com agregação,
Faculdade de Ciências e Tecnologia da Universidade NOVA de Lisboa

Doutora Andreia Filipa Cardoso Ruivo, Investigadora Auxiliar da VICARTE Vidro
e Cerâmica para as Artes da Universidade NOVA de Lisboa

Doutor Virgílio Hipólito Correia, Arqueólogo do Museu Monográfico e Ruínas de
Conimbriga



10/2021

TECHNOLOGICAL STUDY AND CHEMICAL- ARCHAEOOMETRIC CHARACTERIZATION OF ROMAN OPAQUE RED GLASS FROM *OPUS SECTILE* DECORATION IN THE *LUCIUS VERUS VILLA*, 2ND CENTURY AD.

Copyright © Mario Bandiera, Faculdade de Ciências e Tecnologia, Universidade Nova de Lisboa.

A Faculdade de Ciências e Tecnologia e a Universidade Nova de Lisboa têm o direito, perpétuo e sem limites geográficos, de arquivar e publicar esta dissertação através de exemplares impressos reproduzidos em papel ou de forma digital, ou por qualquer outro meio conhecido ou que venha a ser inventado, e de a divulgar através de repositórios científicos e de admitir a sua cópia e distribuição com objectivos educacionais ou de investigação, não comerciais, desde que seja dado crédito ao autor e editor.

Acknowledgments

This PhD was funded by Fundação para a Ciência e Tecnologia – Ministério da Educação e Ciência (FCT-MEC), through doctoral grant Cores PhD program PD/BD/135053/2017.

Because it would not have been possible to accomplish this work alone, I would like to thank the people who have been helpful to reach the main goals of this project.

I would like to start with my Supervisor (Prof. Marcia Vilarigues) who gave me the possibility to work in VICARTE, trusting in me, helping to provide all the support needed to conduct this research, involving me in several projects that helped to develop my skills.

Thanks to my co-supervisor (Dr. Marco Verità), who supported and cared for me with patience in these four years (as mentor), giving me so many suggestions, information and helps that they made me grow up, develop and enrich my knowledge and passion about glassmaking.

Prof. Lucia Saguì that allowed to have access to the Gorga collection and to the *Soprintendenza Archeologica di Roma*. Thanks to her, it was possible to collect and select the samples studied in this research. Without her help, all this work could not start. Moreover, she provided useful information and material for the archaeological section of this work.

The analytical results are the result of the collaboration with several institution such as C2TN, and for this I am very grateful with Dr. Luis Cerquiera, who performed several PIXE analyses for my project; CENIMAT, thanks to Dr. Joana Pinto for the X-ray diffraction analyses. Dr. Bernard Gratuze that gave the possibility to characterize the entire set of my samples enriching enormously the information that this research contains.

Thank to Dr. Elena Tesser, for her kind support, hence, a special thanks to the entire LAMA laboratory, directed by Prof. Fabrizio Antonelli.

Thanks to Dr. Antonio Daneo, who helped to make the measurements at *La Stazione Sperimentale del Vetro* (Murano, Venice).

A special thank is for the director of the C2RMF of the Louvre Dr. Isabelle Biron, who gave access to their laboratory to perform the FEG-SEM analyses. In particular, Dr. Patrice Lehuédé, who not only performed the FEG-SEM analyses, but he gave me so much useful information for my research, and shared part of his knowledge that helped to understand many aspects of my investigation. Thank you very much.

Thanks to Cristiano Ferro (Effe3, Murano), who gave me the glass for my laboratory reproductions, making this part more fruitful.

I would like to give a special acknowledgement to other researchers that helped to shed light in specific aspects of my work. Thanks to Dr. Eva Angelin, who helped a lot as friend and as researcher. I am very grateful to Dr. Sarah Maltoni, who helped to me providing useful and precious information, sharing her deep knowledge about Roman glass, and being very kind friend. Dr. Andreia Ruivo for sharing with me part of her knowledge about copper-ruby glass, nanotechnology, and expertise to make red glass. Mark Taylor (The Roman Glassmaker) who aided to understand better some part of the laboratory reproduction. Thanks to Prof. I.C. Freestone for his suggestions on the topic of my work, for his kind willingness, and to share useful information and suggestions for this project.

Thanks to Prof. Daniel Caurant, Anne Bouquillon, the entire staff of Villa Borg, Marianne Stern, Sylvia Fünfschilling, Paola Santopadre, the Italian committee of AIHV (Maria Diani, Teresa Medici, Marina Ubaldi, Luciana Mandruzzato), Sven Duprè, Jo Wheeler, Sandro Zecchin, Dr. Inês Coutinho, Dr. Susana Cuentro, Dr. Prashant Dabas Robert Wiley, Dr. V. Otero, Prof. M.J. Melo, Prof. Pina and Prof. Pires do Mato for their precious talks and suggestions.

Thanks to Augusta Lima that helped me in the first stage of my investigation.

Thanks to my friends Ana Maria Martins, Fred, Alexandra, Sofia, Raquel, Sara, Daniel, Angelica, Alessandro, Manlio, Felice Fernanda Carvalho, Dr. Teresa Palomar, Dr. Rafael Javier Diaz Hidalgo, Angela Santos, Carla Machado to supported and put up with me.

Finally. I thank my family, and Ilaria, that although we spent four years far away, they sent me their support and love in each moment of this special journey in the Roman glass.

Resumo

O vidro vermelho opaco tem sido produzido desde o início da tecnologia de produção vidreira. No entanto, esta pode ser considerada uma das cores mais difíceis de produzir. Tem vindo a ser amplamente investigado nas áreas da ciência do vidro e da arqueometria, fornecendo uma vasta literatura. Contudo, alguns aspetos relativos à sua produção durante a Idade Romana estão ainda por clarificar, tais como: onde era produzido, que matérias-primas era usadas, e no geral, como era preparado. Além disso, a ausência de fontes escritas técnicas sobre vidro Romano aumenta a complexidade desta investigação.

O objetivo deste estudo é investigar a tecnologia de produção do vidro vermelho opaco durante o século II d.C. no Império Romano, de forma a:

1. Identificar que tipos de vidro vermelho opaco de cobre eram manufaturados no Império Romano durante o século II d.C.
2. Investigar, através de uma abordagem multi-analítica, quais os fatores que determinam a origem dos diferentes tons de vermelho e laranja (composição química, a natureza do agente colorante, bem como a sua quantidade e tamanho das partículas).
3. Esclarecer quais os aspetos tecnológicos envolvidos na produção de tons de vidro vermelho de cobre durante o século II d.C.

Para alcançar estes objetivos, a investigação abordou o vidro vermelho opaco de três principais pontos de vista, que apesar de serem focados em aspetos distintos, estarão interligados. Em primeiro lugar foi necessária uma revisão da literatura para identificar as principais características do vidro vermelho opaco do ponto de vista da ciência do vidro para perceber qual o agente colorante e a formação e produção da cor. Por outro lado, as análises químicas de estudos arqueométricos anteriores foram recolhidas a fim de contruir uma espécie de história do vidro vermelho opaco deste a Idade do Bronze Final até ao período medieval.

Após esta primeira etapa deu-se início à parte central deste projeto, a investigação arqueométrica do vidro *sectilia* (placas de vidro) que decorava a *villa* do Imperador Romano *Lucius Verus*. Estas amostras de vidro são parte da coleção Gorga que se encontra armazenada/preservada na *Soprintendenza Archeologica di Roma*, e representam uma oportunidade excepcional de estudar a tecnologia de vidro Romano do século II d.C. Estes *sectilia* foram selecionados como caso de estudo por duas razões principais: encontram-se bem datados, atribuídos ao século II d.C.; apresentam diferentes tons vermelhos e laranjas. Isso, tornou possível o estudo da origem dos diversos tons vermelhos (composição química, agente colorante e tecnologia de produção específica). A investigação científica foi realizada recorrendo a uma abordagem multi-analítica, que incluiu FORS, OM, EPMA, FEG-SEM, LA-ICP-MS, μ XRD e espectroscopia μ Raman.

A tecnologia de produção do vidro vermelho opaco (neste caso apenas o tipo vermelho-acastanhado) foi estudado através de reproduções sistemáticas em laboratório. Ferro e cobre foram testados de forma a perceber que matérias-primas podiam ser empregues, em que estado de oxidação o ferro podia ser adicionado e a concentração necessária para produzir vidro vermelho opaco. Foram testadas várias metodologias para identificar qual o método mais provavelmente utilizado pelos vidreiros Romanos.

A presente investigação delineou a história da produção do vidro vermelho de cobre opaco, que pode ser muito útil para compreender o desenvolvimento tecnológico da indústria vidreira. O vidro vermelho *sectilia* estudado neste trabalho, revelou a presença de quatro tons vermelhos e três tons laranjas. Para além de enriquecer a literatura referente a análises químicas de vidro vermelho opaco datado do século II d.C., estes resultados salientam o uso de mais do que uma receita pelos vidreiros Romanos por forma a alargar a escala cromática do vidro vermelho opaco. Cada tonalidade vermelha foi conseguida através do controlo preciso das matérias-primas, composição do vidro e tratamentos de calor.

As dificuldades na produção de vidro vermelho opaco que emergiram com as reproduções em laboratório reforçaram que os bons resultados podem ser alcançados mediante o controlo preciso das condições de fusão redox através da composição de vidro correta e do uso das matérias-primas adequadas. Provavelmente, o vidro vermelho opaco não resultou da sorte, mas sim de várias experiências falhadas que permitiram o domínio das técnicas de coloração.

Palavra chave: Vidro romano, vidro vermelho opaco, arqueometria, *opus sectile*, estudo multi analítico, reprodução de laboratório.

Abstract

Opaque red glass has been manufactured since the beginning of glassmaking technology. However, it can be considered one of the most difficult colours to produce. It has been widely investigated by both glass science and archaeometry fields, providing vast literature. However, several aspects concerning its production during the Roman age are still unclear such as: where it was produced, which raw materials were used, and overall, how it was made. Moreover, the absence of written technical sources for Roman glass makes the investigation more complex.

This research aims to investigate the production technology of opaque red glass during the 2nd century AD in the Roman Empire, in order to:

1. Identify which types of opaque copper red glass were manufactured in the Roman Empire during the 2nd century AD.
2. Investigate, through a multi-analytical approach, which factors determine the origin of the different red and orange hues (chemical composition, the nature of the colouring agent as well as their number and sizes).
3. To shed light on the technological aspects involved in making copper-red glass hues during the 2nd century AD.

To reach these goals the research faced opaque red glass from three main different points of view. Although they are focused on distinct aspects, they will be interconnected. First, a literature review was necessary to identify the main features of copper red glass from a glass science point of view to understand the colouring agent, the formation and production of the colour. On the other hand, chemical analyses from previous archaeometric investigations were collected from the literature to make the history of opaque red glass from the Late Bronze Age until the medieval period.

After this first step, the core of this work is the archaeometric investigation of the glass *sectilia* (sheets of glass) which decorated the villa of the Roman Emperor *Lucius Verus*. The glass *sectilia* are part of the Gorga collection, which is stored in the *Soprintendenza Archeologica di Roma*, and they represent an exceptional opportunity to study Roman glass technology of the 2nd century AD. These *sectilia* were chosen for this case study for two main reasons: they are well dated, attested to the 2nd century AD; they show the presence of several red and orange hues. This made it possible to examine the origin of the different red hues (chemical composition, colouring agent and specific production technology). The scientific investigation was conducted through a multi-analytical approach, which included: FORS, OM, EPMA, FEG-SEM, LA-ICP-MS, μ XRD and μ Raman spectroscopy.

The production technology of opaque red glass (in this case only red brown type) has been studied through systematic laboratory reproductions. Iron and copper were tested to understand which raw materials could be employed, in which oxidation state iron should be added and the concentration needed to produce opaque red glass. Several procedures were attempted to recognise the most probable method used by the Roman glassmakers.

This study outlined the history of the production of opaque copper-red glass, which could be very useful to understand the technological development of the glassmaking industry. The red glass *sectilia* investigated in this work revealed the presence of four red hues and three orange hues. Beyond enriching the literature of chemical analyses of opaque red glass dated to the 2nd century AD, these results have highlighted the use of more than one recipe used by the Roman glassmaker to broaden the chromatic scale of opaque red glass. Each red hue was obtained through the accurate control of the raw materials, glass composition and heat treatments. The difficulties in making opaque red glass that emerged through the laboratory reproductions underlined that the good results could be achieved through accurate control of the melt redox condition through the correct glass composition and use of the appropriate raw materials. Likely, opaque red glass was not the result of fortune but of several failed experiments which allowed to master the colouring technique.

Key words: Roman glass, opaque red glass, archaeometry, *opus sectile*, multi analytical approach, laboratory reproduction

INDEX

List of figures	xxiv
List of tables	xxxiii

Introduction.....	1
References	4

-Section One-

A literature review of the field of archaeometry and glass science

1 Early glassmaking technology.....	7
1.1 Brief introduction to glassmaking in ancient times.....	7
1.2 Roman and Late Antique glassmaking.....	9
1.2.1. Raw materials.....	10
1.2.2. Melting techniques: primary and secondary furnaces.....	11
References	13
2 A literature review of the glass science studies on copper-red glass.....	19
2.1. The main type of copper-red glass.....	19
2.2. Physical principle of colour in copper-red glass.....	21
2.3. The debate about the nature of the colouring agent.....	22
2.4. Solubility and formation of metallic particles in glass, a redox affaire.....	26
2.4.1. Temperature.....	26
2.4.2. Oxidation state of the furnace atmosphere.....	27
2.4.3. Base glass composition.....	28
2.4.4. Interaction with another polyvalent element.....	28
2.5 Control of the crystallisation process: heat treatment and striking.....	32
References	36
3. The history of opaque red glass across the centuries	40
3.1. Identification of the types of opaque copper-red glass produced in ancient times	40
3.2 Types of opaque copper-red glass through the analytical data reported in the literature	44
3.2.1 High copper – no lead (14 th – 9 th centuries BC)	45

3.2.1.1 History and use	45
3.2.1.2 Chemical composition.....	46
3.2.1.3 The colouring agent	48
3.2.1.4 Hypothesis about the production technology	49
3.2.2 Sealing wax (High copper – high lead 8 th century BC to the 2 nd century AD)	50
3.2.2.1. History and use	50
3.2.2.2 Chemical analyses	52
3.2.2.3. The colouring agent	54
3.2.2.4 Hypothesis about the production technology	55
3.2.3 Red brown (low copper low lead 3 rd century BC to 13 th century AD)	55
3.2.3.1 History and use	55
3.2.3.2. Chemical composition	57
3.2.3.3. The colouring agent	59
3.2.3.4 Hypothesis about the production technology	60
3.2.4 Orange glass	60
3.2.4.1 History and use	60
3.2.4.2 Chemical composition	61
3.2.4.3 The colouring agent	62
3.2.4.4 Hypothesis about the production technology	63
3.2.5 Aventurine glass (Cu ^o -aventurine)	63
3.2.5.1 History and use	63
3.2.5.2 Chemical composition	64
3.2.5.3 The colouring agent	64
3.2.5.4 Hypothesis about the production technology.....	65
3.3 Discussion and Conclusions	66
3.3.1 High copper-no lead - some considerations	66
3.3.2. Sealing wax - some considerations	67
3.3.3. Red Brown - some considerations	67
3.3.4. Orange glass - some considerations	68
References	69

-Section Two –

Opaque red glass *sectilia* from the Lucius Verus villa. Archaeometric study

4. Archaeological context: sites and materials	76
4.1. The history of the archaeological site	76
4.1.2. The Roman villa from the 1 st century BC to the 4 th century AD	77

4.1.2.1. Before being an Imperial villa (2 nd century BC – 1 st century AD)	78
4.1.2.2. The Imperial villa of Lucius Verus (2 nd century AD)	78
4.1.2.3. The villa from 3 rd to 4 th century AD	81
4.2. The Gorga collection and the <i>opus sectile</i> decoration from the Lucius Verus villa	82
4.2.1 The Gorga collection	82
4.2.2. The <i>opus sectile</i> technique	84
References	86
5. Sampling	87
5.1. Sampling Methodology	87
5.2. Grouping and description of the samples	88
References	96
6. Analytical Method	97
6.1 Identification of the colour	97
6.1.1. OM (Optical Microscope)	97
6.1.2. FORS (Fiber Optics Reflectance Spectroscopy)	97
6.1.3. Colorimetric measurements	97
6.2 Chemical analyses	98
6.2.1 Electron Probe Micro Analyses (EPMA)	98
6.2.2 Laser Ablation Inducted Couple Plasma Mass spectroscopy (LA-ICP-MS)	98
6.2.3 FEG-SEM (Field Emission Electron Gun Scanning Electron Microscope)	99
6.3 Crystalline phases	99
6.3.1 μ -Raman microscopy	99
6.3.2 X-ray diffraction (XRD)	99
References	100
7. Results	101
7.1. Optical microscope observation	101
7.2. UV-Vis reflectance spectroscopy with optical fibers (FORS)	105
7.3. Colorimetry	108
7.4. Chemical analyses	110
7.4.1 The base glass composition	119
7.4.2 Colouring and reducing agents	126
7.5 Crystalline phase	128
7.5.1 Low copper – low lead (Gr-1, Gr-2, Gr-3 groups)	128
7.5.1.1 FEG-SEM analyses	128

7.5.1.2 μ -Raman spectroscopy	133
7.5.1.3 X-ray diffraction analyses	135
7.5.1.4 Other crystalline phases	136
7.5.2 High copper – high lead (groups Gr-4 and Gr-5)	139
7.5.2.1 FEG-SEM analyses	139
7.5.2.2 μ -Raman spectroscopy	142
7.5.2.3 X-ray diffraction analyses	143
7.5.2.4 Other crystalline phases	144
Reference	147
8. Discussion	150
8.1 Presence of two colouring techniques: Cu° and Cu_2O	150
8.1.1 Raw materials, technology production	152
8.1.1.1 Fluxing agent	152
8.1.1.2 Silica source	156
8.1.2 Colouring, reducing agent and other compounds	157
8.1.2.1 Cu° group	157
8.1.2.2 Cuprite (Cu_2O) group	160
8.1.3. Production technology	162
8.1.3.1 Cu° technology	162
8.1.3.2 Cu_2O technology	164
8.2 Conclusion	164
References	166

-Section Three-
Recipes and laboratory reproductions

9 Laboratory reproductions	173
9.1 Introduction	173
9.2 The Venetian recipes: information about raw materials and melting procedures	174
9.2.1 The Venetian manuscripts	174
9.2.2 The raw materials in the recipe books	174
9.2.3 The Procedures	174
9.2.4 Colour control	177

10. Materials and methods	178
10.1 Materials: crucible, raw materials, base glass, furnace	178
10.1.1 Glass composition, colouring and reducing reagents	178
10.1.2 Crucibles, furnace	178
10.2 Procedure	178
10.2.1 P-F procedure	181
10.2.2 P-S procedure	182
10.3 Heat treatment	182
11. Results	183
11.1 Procedures	183
11.2 The effect of the different iron and copper oxidation states	183
11.3 The effect of different iron and copper content	184
11.4 Optical microscope	188
11.5 FORS spectroscopy	190
11.6 Colorimetric measurement	190
11.7 Raman spectroscopy and X-ray diffraction	192
11.8 Heat treatment	194
References	198
12. Discussion and Conclusions	199
Main Conclusions	201
Appendix	
A. How many recipes were there for manufacturing red brown during the Roman Age (1st-4th c. AD)? Raw glass, colouring techniques, trade and production	
A.1. Introduction	204
A.2. Methodology	206
A.3. Results	207
A.3.1 Base glass	207
A.3.2. Colouring and reducing agents	210
A.4. Discussion	211
A.4.1 Base glass	211
A.4.1.1.1 A simple anomaly?	211
A.4.1.1.2 High phosphorus	213

A.4.1.1.3. Addition of fuel ash	214
A.4.1.1.4 Recycling glass, pollutants from the furnace atmosphere	215
A.4.1.2 Silica source	216
A.4.1.3. Production centres	217
A.4.2. Colouring techniques	218
A.5 Conclusion	219
References	221
B. Adulteration of natron Roman glass with wood ash	225
B.1. The aim	225
B.2. Methodology	225
B.3. Results	226
B.3.1. Adulteration of natron glass with wood ash	226
B.3.2 Comparison of the PA group samples with the adulterated soda plant ash glass	230
B.4. Conclusions	231
Referencences	232
C. Archaeometric analysis of a Roman opaque red jar in the <i>Museu da Farmácia</i>, Lisbon	
C.1 Introduction	234
C.2 Materials and method	234
C.3 Results	236
C.4 Conclusions	238
References	239
D. A comparison between recipes and chemical analyses of Venetian red brown	241
D.1 Materials and method	241
D.2 Results	243
References	246
E. First attempts to reproduce opaque red glass in the laboratory	247

List of figures

2.1	The main types of copper-red glass, and the colour given depending on the particles sizes.	20
2.2	Opaque red glass produced by metallic copper particles	20
2.3	Opaque red glass produced by cuprite crystals.	20
2.4	Plotted the fugacity, potential of reduction and ratio of log red/Ox at constant temperature. Picture taken from Schreiber 1986.	30
2.5	The two curves represent the two rates: Nucleation and crystal growth. Taken by Varshney, 1994.	34
3.1	Chronological timeline of the production of opaque red glass	43
3.2	Binary graph with weight % of lead oxide (PbO) versus copper oxide (CuO). Opaque red and orange glass dating from the 14 th century BC to 13 th century AD.	45
3.3	Inlay head of Egyptian opaque red glass, 14 th century BC. Image taken from Stern 1994.	46
3.4	Opaque red bead from Frattesina (picture from Santopadre et al., 2000).	46
3.5	Binary graphs reporting the weight % of the reduced composition of potash (K ₂ O) content versus magnesia content (MgO).	47
3.6	Ingot from Qantir, picture taken from Rehren, 1997; b) opaque red glass produced in the workshop of Qantir (picture from Rehren, 1997) showing cuprite crystals (white crystals)	48
3.7	a) Cross section of a red bead produced at Frattesina. The white dots are metallic copper particles which produce the opaque red layer on the surface of a blue bead; b) Cu ⁰ particles in cubic shape (black squares) identified by TEM analyses (picture from Angelini, 2004).	48
3.8	Number of chemical analyses performed on sealing wax red glass objects.	51
3.9	a) globular bottle, 1 st century BC/1 st century AD (picture taken from Weinberg 1992); b) skyphos from Pydna 1 st century BC (picture taken from Ignatiadou 2009); c) patellas cup 1 st c. BC/1 st c. AD, Italy-Greece (?) (picture taken from Stern, 1994); d) Late Iron Age sealing wax from Britain: strap end from Stanton, Norfolk (picture taken from Davis, 2007)	51
3.10	Binary graphs with the weight % of a) potash (K ₂ O) versus magnesia (MgO); b) alumina (Al ₂ O ₃) versus sodium oxide (Na ₂ O). Sealing wax red glass from 8 th c. BC to 2 nd c. AD.	54
3.11	Cuprite crystals a) under an optical microscope (picture taken from Verità, 2017); b) SEM-EDS imagen of cuprite crystals from the cake of Tara Hill (picture taken from Freestone et al., 2003).	55
3.12	Number of chemical analyses performed on red brown glass objects.	57

3.13	Red brown sample observed by a) optical microscope (picture taken from Verità et al., 2015); b) euhedral sub-micrometrical particles of metallic copper in red brown sample (Picture taken from Maltoni et al., 2018)	59
3.14	4 th – 3 rd c. BC glass object (Picture from Stern 1994; 5000 years of glass).	60
3.15	Number of chemical analyses performed on orange glass objects.	61
3.16	Bi-plot graph of the wt% concentration of potash (K ₂ O) versus magnesium (MgO) in orange glass (reduced composition).	62
3.17	Orange glass tesserae showing common heterogeneous morphology, with cuprite crystals of different sizes and shapes: dendritic in the red band, smaller and with geometrical shapes in the orange layer (from Verità, 2017).	63
3.18	a) Block of aventurine glass; b) sample of aventurine prepared in a thin section and observed under the optical microscope. Picture taken from Moretti et al., 2013.	65
3.19	Bar graph with the number of analyses for each red type divided by date.	66
3.20	Timeline of the main phases of red brown glass.	68
4.1	City of modern Rome, to identify the position of the <i>Lucius Verus</i> villa	76
4.2	Planimetry of the Lucius Verus villa. Picture taken from Caserta et al. 2012.	78
4.3	Planimetry of the sector B and C. Picture taken from Caserta et al. 2012.	79
4.4	Planimetry of the sector C showing the presence of pavement preparation for the opus sectile decoration. Picture taken from Caserta et al. 2012.	80
4.5	The preparation layer for <i>opus sectile</i> decoration of the Lucius Verus villa uncovered in sector C (room 16) revealed by the archaeological excavations in 1988-1989. Picture taken from Caserta et al. 2012.	81
4.6	Panels of the <i>opus sectile</i> decoration from the Lucius Verus villa, with <i>cancellum</i> motif. They exhibit the round rosette with 8 yellow petals which suggested a common provenance. a) Picture taken from Saguì et al., 2005; b) picture taken from the Victoria and Albert Museum, London; c)-d) picture taken from the <i>Palazzo Altemps</i> Rome.	83
5.1	Boxes containing opaque red glass <i>sectilia</i> (both monochrome and polychrome) from the Lucius Verus villa excavations, and stored in the storehouse of the <i>Soprintendenza Archeologica di Roma</i> . Picture of single boxes was taken in the storehouse of <i>Soprintendenza Archeologica di Roma</i> , in St. Croce in Gerusalemme square (Rome), and then assembled by me in this picture.	87
5.2	Fragmentary samples, and thin samples in geometrical shapes.	88
5.3	a) round <i>sectilia</i> with the visible marks of the tools used to cut the glass in order to create the rounded shape; b) maker of the tool (likely) to stretch the molten glass; c) sample with the	88

	“becco di civetta” edge; d) front of a thicker sample of the Gr-1 group, composed of the juxtaposition of several canes.	
5.4	Polychrome sectilia a)-b) red with white dots; c) cross section; d)-e) fragment of the framework.	89
5.5	Comparison between R13 (Gr-4 group) and R16 (Gr-1 group). The samples of Gr-4 group were excluded from the Gr-1 group after several visual examinations.	89
5.6	Five of the brownish samples (Gr-2 group) front a) and back b) .	89
5.7	Markers of the tool.	89
5.8	Samples of the Gr-3 group	90
5.9	a) rods of Gr-4 samples with the visible corrosion layer; b) geometrical <i>sectilia</i> with fresh fractures; c)- d) rods with fresh fractures.	90
5.10	Orange samples, Gr-5 group.	91
7.1	Optical micrographs: a) sample R4 and its magnification b) ; c) sample R31 with pronounced orange-brown heterogeneity, and its magnification d) .	101
7.2	Optical micrographs from the Gr-2 group: samples R10 a-b) and R17 c-d) .	102
7.3	Optical micrographs from the Gr-3 group: samples R1 (a, b) and R22 (c, d) showing the different red layers and the presence of a large dark transparent area.	103
7.4	Optical micrographs from Gr-4: a)-b) sample R12; c)-d) sample R13.	104
7.5	Optical micrographs from Gr-5 group: samples a) AR1; b) AR2; c)-d) AR4.	105
7.6	a) reflectance spectra of Gr-1 samples and b) the calculated first derivative; reflectance spectra of Gr-2 samples c) and d) their first derivative.	106
7.7	Reflectance spectra of Gr-3 groups with a) red and c) dark transparent layer. The first derivative of the red b) and dark transparent layers d) .	107
7.8	a) FORS spectra of Gr-4 samples, in which cuprous oxide could be present as a colouring agent with b) their respective first derivative.	108
7.9	FORS spectra of orange samples. a) yellowish orange samples; b) reddish orange sample (AR4); c) first derivative of the orange samples	108
7.10	CIE Lab graphic representation composed of the chromatic coordinate a^* (x axis) and b^* (y axis).	109
7.11	CIE Lab graphic representation: L^* a^* b^* chromatic coordinates of the samples projected on the L^* a^* b^* space.	110

7.12	Binary graph: a) magnesia concentration (MgO) against potash (K ₂ O) concentration; b) phosphorus concentration (P ₂ O ₅) versus potash concentration (K ₂ O). (Reduced composition)	119
7.13	Binary graphs: strontium (Sr ppm) concentration versus calcium oxide concentration (CaOwt%). (Reduced composition)	120
7.14	Binary graph: a) Rubidium content (Rb) in ppm versus potash concentration (K ₂ O wt%); b) Rubidium content (Rb) in ppm versus sodium concentration (Na ₂ O wt%). (Reduced composition)	121
7.15	Binary graph: Rubidium content (Rb) in ppm versus barium content (Ba) in ppm. (Reduced composition)	121
7.16	Binary graph: a) Barium content in ppm (Ba) against the weight percentage (wt%) of potash (K ₂ O). b) Barium content in Ba ppm content against P ₂ O ₅ wt%. (Reduced composition)	122
7.17	Binary graphs: a) silica (SiO ₂) content against zirconium (Zr) content (ppm); b) silica (SiO ₂) content against alumina content (Al ₂ O ₃ wt%). (Reduced composition)	122
7.18	a) titanium (TiO ₂) content against alumina concentration (Al ₂ O ₃); b) titanium (TiO ₂) content against zirconium (Zr) content (ppm). (Reduced composition)	123
7.19	Binary graph: chromium content (Cr ppm) versus vanadium content (V ppm). (Reduced composition)	123
7.20	Binary graph iron concentration (Fe ₂ O ₃) against titanium content (TiO ₂).	124
7.21	Binary graphs a) Caesium (Ce ppm) concentration against zircon content (Zr ppm); b) hafnium (Hf ppm) concentration against zircon content (Zr ppm).	125
7.22	Binary graph: a) The concentration of tin oxide (SnO ₂) against copper oxide (Cu). b) concentration of lead oxide (PbO) against tin oxide (SnO ₂). The squares are representative of the analyses performed on the Cu-metal particles identified by FEG-SEM analyses in the Gr-1 group samples.	128
7.23	FEG-SEM micrographs of Gr-1 samples: a) sample R2, copper spherical nanoparticles; b) copper spherical and cubic nanoparticles in sample R4.	129
7.24	FEG-SEM micrographs of Gr-1 samples. Different red layer with different number and size of particles in sample R14: a) light red layer and b) dark red layer; sample R31 c) orange layer and d) red layer.	130
7.25	FEG-SEM micrographs: presence of black layers in sample R5.	131
7.26	FEG-SEM micrographs of Gr-2 group samples: a) hexagonal and triangular crystals of metallic copper in sample R10; b) hexagonal crystals of metallic copper in sample R10.	131
7.27	Gr-3 group sample: a) R22 at optical micrograph and b) FEG-SEM micrographs of R22.	132
7.28	Raman spectra of the samples in the Gr-1a group a) , and in the Gr-1b group b) ; samples R29 and R31 richer in iron c) .	134
7.29	Raman spectra of the samples in the Gr-3 group a) , and in the Gr-2 group b) .	134

7.30	X-ray diffraction on the samples of Gr-1 (R2- R4-R5) and Gr-2 (R10), showing the typical peaks of metallic copper. No cuprite crystals were detected.	135
7.31	a) metallic inclusion in sample R8, observed by OM; b)-c) FEG-SEM micrographs and chemical characterisation of the inclusion by EDS.	136
7.32	FEG-SEM micrographs a) metallic inclusion in sample R16 with particles rich in Ag; b) iron rich inclusion probably magnetite in sample R6; c) calcium and phosphate particles in sample R6 and R26.	137
7.33	FEG-SEM micrographs: a) metallic inclusion rich in copper and sulphur, likely Cu_2S , detected in the R17 sample; b) inclusions rich in Si-Al-Fe-K-Na detected in sample R10.	138
7.34	FEG-SEM micrographs: inclusion rich in copper and sulphur, likely Cu_2S , detected in the R22 sample.	138
7.35	FEG-SEM micrographs cuprite crystal in sample R9 (Gr-4).	139
7.36	FEG-SEM micrographs: a) sample R9 which is more homogeneous than sample R11 b) in which lighter layers formed.	139
7.37	FEG-SEM micrographics of Gr-5 group samples: cuprite crystals observed in sample AR1 a) and AR2 b) ; AR8 c) and AR4 d) .	140
7.38	Optical a) and FEG-SEM micrographs b) of the red layer and orange layer in sample AR4 (Gr-5).	141
7.39	Raman spectrum of cuprite (Cu_2O) detected in Gr-4 a) and Gr-5 b) groups.	142
7.40	X-ray diffraction of the R13 (Gr-4 group), showing the fingerprint of cuprite crystals.	143
7.41	X-ray diffraction for the three orange samples of Gr-5 group. The diffractograms show the typical peaks of cubic cuprite crystals. No metallic copper crystals were detected.	143
7.42	FEG-SEM micrographs: metallic inclusion rich in copper revealed in sample R9.	144
7.43	FEG-SEM micrographs: a) metallic inclusion rich in copper revealed in sample R11; b) same inclusion observed at higher magnification.	144
7.44	FEG-SEM micrographs: a) inclusion rich antimony, tin and calcium; b) same inclusion observed at higher magnification.	145
7.45	Biplot graphs of a) the calcium concentration (CaO) against antimony content (Sb_2O_3); b) tin oxide (SnO_2) versus antimony content (Sb_2O_3) – EDS analyses	146
7.46	Raman spectra of two crystalline phase detected in the sample AR-2 and identified as $\text{Ca}_2\text{Sb}_2\text{O}_7$ (calcium antimonate).	146
8.1	The colour changes with the increase in the size of the colouring agent (Cu° on the right; Cu_2O on the left).	151
8.2	Binary graph showing the concentration of potash (K_2O wt%) against magnesia (MgO wt%) content. The samples from the literature were taken from [27-32].	154

8.3	Binary graph showing the concentration of phosphorus (P_2O_5 wt%) against magnesia (MgO wt%) content. The samples from the literature were taken from [27-32].	154
8.4	Biplot of the concentration of zirconium concentration (Zr ppm) and titanium content (TiO_2 wt%) of the typical Roman natron glass dating from the 1 st c. AD to 4 th c. AD and the Lucius Verus copper-red glass. Roman natron glass taken from [20, 36, 40-43].	156
8.5	Biplot graphs: a) Tin content (SnO_2) against copper concentration (CuO); b) zinc content (ZnO) against copper concentration (CuO); c) lead content (PbO) against copper concentration (CuO); d) lead content (PbO) against tin concentration (SnO_2).	159
8.6	Biplot graphs: a) lead content (PbO) against copper concentration (CuO); b) zinc content (ZnO) against copper concentration (CuO); c) lead content (PbO) against tin concentration (SnO_2); d) zinc content (ZnO) against copper concentration (CuO).	161
8.7	Comparison of two fragments of copper red glass: sealing wax a) and brick red b) .	162
8.8	Picture of the R17 sample illuminated, generating a shining and glassy effect on its surface.	163
10.1	a) Crucible C.101 Fossati; b) furnace K-9 Barracha;	178
10.2	a) Steel mortar used to crush the raw glass; b) crushed raw glass.	179
10.3	a) Crushed glass in the crucible; b) crucible inside the furnace at room temperature	179
10.4	Sequence of the definitive procedure: a) the crucible was taken out from the furnace; b) the crucible was deposited on the container with sand; c) addition of the reagents into the molten glass; d) stirring the melt; e) returning the crucible with the molten glass containing the reagents to the furnace.	180
10.5	a) Warmed iron table with iron bars heated in furnace at about 700°C; b) pouring of the molten glass; c) cutting of the glass to gather the samples which will be transferred into the muffle furnace.	181
10.6	a) - b) Transfer of the sample into the muffle furnace at 550 °C, heated for 1h.	181
10.7	a) The set-up for the heat treatment TT-1; b) The set-up for the heat treatment TT-2.	183
11.1	a) FORS spectra of samples P_FA3, P_F2a, P_F3, P_F4, P_F5; b) Spectra of the first derivative of samples P_FA3, P_F2a, P_F3, P_F4, P_F5.	190
11.2	a) CIE Lab graphic representation: L^* a^* b^* chromatic coordinates of the samples (P_F) projected on the L^* a^* b^* space; b) CIE Lab graphic representation composed of the chromatic coordinate a^* (x axis) and b^* (y axis).	191
11.3	a) CIE Lab graphic representation: L^* a^* b^* chromatic coordinates of the samples (S_F) projected on the L^* a^* b^* space; b) CIE Lab graphic representation composed of the chromatic coordinate a^* (x axis) and b^* (y axis).	192
11.4	a) Raman spectra of the samples P_FA3, P_F2a, P_F3 and P_F4; b) Raman spectra of the samples P_F1 and P_F6.	193

11.5	X-ray diffraction on the samples a) P_F2a and b) P_F3, showing typical peaks of metallic copper particles. No cuprite crystals were revealed.	193
11.6	Optical microscope picture of a) TT-1 P_F2; b) TT-2 P_F2; c) TT-1 P_F4; d) TT-2 P_F4.	194
11.7	Optical microscope micrographs at 50X of magnification of a) P_F2a (no heat treatment); b) TT-1 P_F2; c) TT-2 P_F2.	199
11.8	CIE Lab graphic representation: L* a* b* chromatic coordinates of the samples produced by heat treatments, projected on the L* a* b* space.	196
11.9	Raman spectra of the samples TT-2_P_F4.	197
11.10	X-ray diffraction on the sample TT-1_F4, showing typical peaks of metallic copper particles. No cuprite crystals were revealed.	197
A.1	Bi-plot of weight % a) potash (K ₂ O) versus magnesia (MgO) and b) phosphorus (P ₂ O ₅) and magnesia (MgO) in opaque red glass between the 1 st century AD and the 4 th century AD.	207
A.2	Bi-plot/Binary graph of a) weight % sodium oxide (Na ₂ O) versus potash (K ₂ O); b) weight % sodium oxide (Na ₂ O) versus calcium oxide (CaO), in opaque red glass between the 1 st century AD and the 4 th century AD.	208
A.3	a) Binary graph of Strontium ppm versus weight % of calcium oxide (CaO), b) binary graph of barium (Ba ppm) versus weight % of calcium oxide (CaO), in opaque red glass between the 1 st century AD and the 4 th century AD.	208
A.4	Binary graph of a) weight % of magnesia (MgO) against barium (Ba) ppm, b) weight % of manganese oxide (MnO) versus barium (Ba) ppm, in opaque red glass between the 1 st century AD and the 4 th century AD.	209
A.5	Binary graph of weight % titanium oxide (TiO ₂) versus alumina (Al ₂ O ₃), in opaque red glass between the 1 st century AD and the 4 th century AD.	209
A.6	Binary graph of weight % iron oxide (Fe ₂ O ₃) versus titanium oxide (TiO ₂), in Roman opaque red glass (1 st - 4 th century AD).	210
A.7	Histogram showing the number of PA, NA and INT samples reported in the literature and divided into three different periods: Roman Age (1 st -4 th c. AD); Lat Antique (5 th -8 th c. AD); Medieval (9 th -13 th c. AD).	211
A.8	Binary graph with the concentration of potash (K ₂ O wt%) versus magnesia (MgO) content detected in the Roman PA and NA samples (1 st -4 th c. AD), and medieval opaque red glass (9 th -13 th c. AD).	212
A.9	Binary graph with the concentration of potash (K ₂ O wt%) versus magnesia (MgO wt%) content detected in the Roman PA and the soda-plant ash glass from different regions of the Eastern coast of the Mediterranean Sea and ancient Mesopotamian region. Comparative data: [31-34] .	212
A.10	Binary graph with the concentration of phosphorus versus magnesium content detected in the Roman PA and NA red brown samples, compared with Medieval opaque red glass and French soda-plant ash glass dated to the 16 th c. AD.	214

A.11	A binary graph of strontium content (Sr ppm) versus weight % calcium oxide (CaO wt%), comparing the PA group samples with the Islamic soda plant ash glass. Comparative data: [31-34].	215
A.12	a) Binary graph of weight % potash versus magnesia content; b) Binary graph of weight % phosphorus versus magnesia content. NA samples compared with natural/ colourless Roman natron glass. Comparative data: [23, 37-41].	215
A.13	Binary graph with titanium concentration vs alumina concentration in the PA and NA samples, Comparative data: [23, 37-41].	216
A.14	binary graph with zircon concentration (Zr ppm) versus titania concentration (TiO ₂ wt%). Comparative data: [23, 37-41].	217
A.15	Binary graph with the concentration of copper oxide (CuO wt%) versus the iron content (Fe ₂ O ₃ wt%); b) Binary graph with the concentration of copper oxide (CuO wt%) versus the ratio between iron and copper (Fe ₂ O ₃ /CuO).	218
B.1	Histogram showing the variation in sodium, potassium, calcium, magnesium and phosphorus by addition of different amounts of beech ashes to the N_16 natron glass. The composition of the PA group is also reported.	226
B.2	Histogram showing the variation in sodium, potassium, calcium, magnesium and phosphorus by addition of different amounts of bracken ashes to the N_16 natron glass. The composition of the PA group is also reported.	227
B.3	Histograms showing the variation in sodium, potassium, calcium, magnesium and phosphorus by addition of different amounts of oak ashes to the N_16 natron glass. The composition of the PA group is also reported.	227
B.4	a) Binary graph between sodium content (Na ₂ O) versus lime content (CaO) Roman natron base glass adulterated with 5% of beech ashes compared with the PA and INT samples. b) Binary graph of sodium content (Na ₂ O) versus potassium content (K ₂ O) between adulterated natron glass (with 5% of beech ashes) and the PA and INT samples.	228
B.5	a) Binary graph of potash (K ₂ O wt%) versus magnesia (MgO). N_16 type natron glass adulterated by 5 wt% of bracken, beech and oak ashes. b) Binary graph of potash (K ₂ O wt%) versus phosphorus (P ₂ O ₅ wt%) of the Roman natron glass adulterated by 5 wt% of bracken, beech and oak ashes.	229
B.6	a) Binary graph of weight % strontium (SrO wt%) versus calcium oxide (CaO wt%) of the adulterated Roman natron glass, and compared with the PA and INT. b) Binary graph of weight % barium oxide (BaO) versus potash (K ₂ O), of the adulterated Roman natron glass, and compared with the PA and INT.	229
B.7	a) Binary graph with the concentration of potash (K ₂ O wt%) versus magnesia (MgO) content detected in the Roman PA and the adulterated soda-plant ash. b) Binary graph with the concentration of phosphorus (P ₂ O ₅ wt%) versus magnesia content detected in the Roman PA and the adulterated soda-plant ash glass.	230
B.8	a) Binary graph with the concentration of sodium (Na ₂ O wt%) versus calcium oxide (CaO wt%) content detected in the Roman PA and the adulterated soda plant ash glass. b) Binary graph with the concentration of strontium (SrO wt%) versus calcium (CaO wt%) content detected in the Roman PA and the adulterated soda plant ash.	231

C.1	The red jar (N°. inv. 13829) from the Museu da Farmácia, Lisbon.	234
C.2	a) the white greenish layer, probably a decayed product on the mouth of the jar; b) the neck with two different red hues; c) on the round body the presence of an area with fragments showing different red hues.	235
C.3	Dentric crystals observed by optical microscope on the rounded body.	236
C.4	a) Presence of coating/consolidant layer on the surface of the vessel, observed by reflected light; b) observation by optical microscope by using UV-light.	237
C.5	Some of the points analysed on the vessel. a) Analysing the original part of the neck; b) analysing the original part on the rounded body.	237
C.6	a) one of the Raman analyses point; b) Raman cuprite spectra.	238
C.7	The interior of the neck vessel, with uneven surface, not smooth.	239
D.1	Alumina vs manganese content (wt% of oxides) of the base glass of analysed red samples (black diamonds) compared with Venetian transparent glass (cristallo: open circles; vitrum blanchum: grey circles; common glass: grey triangles).	243
D.2	Calcium vs. potassium contents (wt% of oxides) of the base glass of analysed red samples (black diamonds) compared with Venetian transparent glass (cristallo: open circles; vitrum blanchum: grey circles; common glass: grey triangles).	244
E.1	Sequences of the P1 procedure: a) three batches in the furnace melted at 1300 °C for 3 hours; b) the three crucibles after half hour at 1100 °C and the addition of iron; c) the crucibles were placed in the muffle furnace for the entire night at 550 °C.	247

Table list

2.1	Standard electrode potential values calculated in the melt (E'), and in the aqueous (E°) solution at 25°C. Data taken by Schreiber 1994.	29
3.1	The number of samples with the respective date and location.	45
3.2	References of the analyses	46
3.3	Average chemical composition in wt % of the 17 samples from the Near East regions.	47
3.4	Average chemical composition in wt % of the 6 samples from the site of Frattesina.	47
3.5	Number of analysed samples for each age and region.	52
3.6a	Average chemical composition in wt % of the sealing wax red glass from different regions. N.E: Near East; Hell/Rom: Hellenistic/Roman; Ang-Sax: early Anglo-Saxon.	52
3.6b	Average chemical composition in wt % of sealing wax red glass from different regions. N.E: Near East; Hell/Rom: hellenistic/Roman; Ang-Sax: early Anglo-Saxon.	54
3.7	Data source for the mosaic <i>tesserae</i> (from 1 st BC to 13 th AD), providing city/site, date range and number of analyses.	56
3.8	Data source for the <i>opus sectile</i> (from 3 rd to 6 th AD), providing city/site, date range and number of analyses.	56
3.9	Data source for the canes in mosaic glass (from 3 rd BC to 9 th AD), providing city/site, date range and number of analyses.	56
3.10	Data source for the beads (from 5 th to 8 th AD), providing city/site, date range and number of analyses.	56
3.11	Average chemical composition in wt % of red brown samples from the 3 rd century BC to 13 th century AD.	59
3.12	Average chemical composition in wt % of orange samples from the 3 rd century BC to 12 th century AD.	61
3.13	Average chemical composition in wt % of Merovingian orange samples dated 5 th -8 th c. AD.	62
3.14	Average chemical composition in wt % of aventurin glass dated 19 th – 20 th c. AD.	64
4.1	Number of sectilia pieces divided by colour. Data taken from Saguì et al., 2009.	82
4.2	Number of monochrome and polychrome glass sectilia uncovered in the last excavation in 2005 by Messineo (data reported from [1])	84
5.1	Samples collected from the <i>Soprintenza Archeologica of Rome</i> . Fragments representing the different red hues, they are showed through their retro-verso and cross-section. L: length; W: width; Th: thickness. * Fragments, without regular shape, difficult to measure and understand their side.	92
7.1	Average chromatic and colorimetric coordinates of the five groups.	110

7.2	Data of major and minor elements [wt%] obtained by the three techniques (EPMA, FEG-SEM, LA-ICP-MS). Colour description: BrR: brick red; Br: brown; BdR: banded red; SW: Sealing wax; Or: orange. Type of base glass: PA: plant ash; INT: intermediate; N: natron. ¹ EPMA analyses; ² FEG-SEM analyses; * LA-ICP-MS analyses. Std. dev.: standard deviation. Five measurements were performed (at least) for each sample.	112
7.3	LA-ICP-MS data of the trace elements [ppm] detected in the samples..	114
7.4	Data of major and minor elements [wt%] obtained by the reduced composition. Colour description: BrR: brick red; Br: brown; BdR: banded red; SW: Sealing wax; Or: orange. Type of base glass: PA: plant ash; INT: intermediate; N: natron. ¹ EPMA + analyses; ² FEG-SEM analyses; *samples analysed by LA-ICP-MS. Sr, Ba and Zr detected by LA-ICP-MS.	118
7.5	Concentration of the colouring and reducing agents, major and minor elements [wt%], trace elements in ppm (by LA-ICP-MS). PA: plant ash; INT: intermediate; N: natron. ¹ EPMA + analyses; ² FEG-SEM analyses; *samples analysed by LA-ICP-MS.	126
7.6	Average (crystals + glassy phase) and regular (glassy phase) EDS analyses performed on the Gr-1 and Gr-2 groups. S.D.: Standard Deviation; five measurements were performed (at least) for the area investigated.	133
7.7	Average (crystals + glassy phase) and punctual (glassy phase) EDS analyses performed on the Gr-4 and Gr-5 groups. S.D.: Standard Deviation; five measurements were performed (at least) for the area investigated.	142
7.8	Colouring, metallic and devitrification particles investigated by FEG-SEM, Raman spectroscopy and X-ray diffraction. Cu ^o : metallic copper; Cu ₂ O: cuprite; W: wollastonite (CaOSiO ₂); Dt: Devitrite (Na ₂ O.3CaO.6SiO ₂), Dp: diopside (CaO.MgO.2SiO ₂). Pol.: polyphase (Al-Si-Na-Fe-Ca); C: Chalcocite (Cu ₂ S); CP: calcium phosphate; CA: calcium antimonate (Ca ₂ Sb ₂ O ₇); Mgn: magnetite (Fe ₃ O ₄); Hem: Haematite (Fe ₂ O ₃); Inc.A: inclusions composed of Cu-Ag-Sb; Inc.B: PbS-Cu ₂ S; Inc.C: inclusions rich in Fe ₂ O ₃ , SiO ₂ , Al ₂ O ₃ and TiO ₂ .	147
8.1	Average composition (wt%) of a hypothetical copper-alloy used in the three red hues produced by Cu ^o particles.	158
8.2	Average composition (wt%) of the hypothetical copper-alloy used in the sealing wax (Gr-4) and orange (Gr-5) glass. They were obtained by normalising the chemical composition for copper, tin and zinc.	160
9.1	Venetian recipes compatible with the analytical data. Amounts of lead-tin calx, iron (flakes or steel) and red copper prescribed in the recipes to be added to 100 parts of translucent glass to obtain opaque red glass.	177
10.1	The procedures are summarised indicating the reagents with their amounts used in the manufacturing of opaque red.	182
11.1	Picture of the glass produced by adding 2 g of metallic iron (Fe ^o) or 2 g of stannous oxide (SnO) to the batch at the room temperature.	183

11.2	Picture of the glass produced by the different reducing agents (using P_F procedure). The concentration of cuprous oxide was fixed at 2 g, as well as the concentration of the reductants used in these experiments.	184
11.3	Picture of opaque red glass produced by adding 2 g of metallic iron (Fe ⁰) and 2 g of cuprous oxide (Cu ₂ O) according to the P_F procedure.	185
11.4	Picture of the unsuccessful results by using 2 g of metallic iron (Fe ⁰) and 2 g of cuprous oxide (Cu ₂ O) according to the P_F procedure.	185
11.5	Picture of opaque red glass produced starting with 2 g of metallic iron (Fe ⁰) and 2 g of cuprous oxide (Cu ₂ O) according to the P_F procedure, and continue with progressive addition of Fe ⁰ and Cu ₂ O until the formation of opaque red.	185
11.6	Results of the composition P_F in which Cu ₂ O addition was constant at 2 g, and Fe ⁰ varied from 1 to 6 g.	187
11.7	Results of the second composition (S_F) in which copper content was constant at 1 g, and iron varied from 1 to 5 g.	187
11.8	Results of the composition P_F in which Cu ₂ O addition was constant at 2 g, and Fe ⁰ varied from 1 to 6 g.	189
11.9	Results of the composition P_S in which Cu ₂ O addition was constant at 1 g, and Fe ⁰ varied from 1 to 5 g.	189
11.10	Average colorimetric coordinates of the different compositions used in the tests.	191
11.11	Comparison of the optical microscope observation of the polished section of the samples obtained by the different heat treatments, using two different chemical compositions (P_F2: Cu ₂ O 2 g and Fe ⁰ 2 g; P_F4 Cu ₂ O 2 g and Fe ⁰ 4 g).	195
A.1	Average chemical composition (reduced composition) of opaque red glass (mosaic tesserae, <i>opus sectile</i> , rods/canes) from the 1 st century AD to 4 th century AD.	207
A.2	Average chemical composition (weight %) of opaque red glass (mosaic tesserae, canes/rods, and <i>opus sectile</i>) from the 1 st century AD to 4 th century AD.	210
A.3	Average chemical composition of the base glass (calculated by mean of reduced composition) of opaque red glass (mosaic tesserae, <i>opus sectile</i> , rods/canes) from the 1 st to 4 th century AD and mosaic tesserae from the 5 th to 13 th century AD.	213
C.1	Average oxide composition of the red ampoule	237
C.2	Average oxide concentration of the base glass composition (by reduced composition).	238
D.1	Quantitative chemical composition (wt% of oxides) of the analysed samples. n.a.: not analysed; searched for and not detected: Sb, As, Ba, Zn, Co, Ni. Glass type: VB, vitrum blanchum; CR, cristallo glass.	245
E.1	Results by using the P1 procedure.	247
E.2	Results by using the P2 procedure.	248
E.3	Results by using the P1 procedure.	249

Introduction

According to the historian Michel Pastoureau, red was one of the first colours to be used and applied in early prehistoric artistic representations, and due to it being associated with life and strength, it was considered the “*king of the colours*” in early civilisations. Red retained this association until the Roman Age [1], and it is possible to see this in several aspects of everyday Roman life and culture. Some historians have shown that this colour had different names according to the shade of red referred to, including: *minium*, *indica cinnabar* and *rubrica*. *Minium*, according to Pliny, was considered the “*sacrum pigmentum*”, a sacred pigment used to paint the face of the statues of *Jupiter Optimus Maximus* [2].

The colour red is also frequently found in private and public buildings, in which columns, *opera sectilia*, sculptures, tabletops, vases and tubs were made of precious red marbles such as *Marmor taenarium rubrum* (rosso antico) or *Lapis porphyrites*. These were among the most expensive marbles (according to Diocletian edict), and they were imperial property, which were worked in exclusive quarries [3].

The colour red was abundantly used in clothes and jewellery such as amulets, in which coral or red glass were used. Red in these objects signified strength, authority and vital energy [1]. Although they date from before the complete dominance of Rome in the Mediterranean basin, some red glass objects (*skyphos*, or bowls) were used as ornaments in royal burials, indicating the status of the deceased, or associated with the deities protecting them [4, 5]. Beyond these examples with their complex meanings, red glass was abundantly used in wall and pavement mosaic decorations, and can be found in the excavations in Pompei, or the churches of Ravenna or other Roman and Late Antique sites.

The colour red colour has also attracted the attention of numerous glass science and archaeometric surveys, because the manufacture of red glass (or red glaze) is very sensitive to several factors which could prevent the formation of red in the glass. There is an extensive literature devoted to red glass, which can be divided into two main aspects: the mechanism for forming the colour red in the glass and the nature of the colouring agent. Despite the numerous scientific studies about these two main topics, however, some aspects still remain unclear.

This aim of this research is to investigate the technology for producing opaque red glass during the 2nd century AD in the Roman Empire, in order to:

1. Identify which types of opaque copper red glass were manufactured in the Roman Empire during the 2nd century AD.
2. Investigate, through a multi-analytical approach, which factors determine the origin of the different red and orange hues (chemical composition, the nature of the colouring agent as well as their number and sizes).
3. To shed light on the technological aspects involved in making copper-red glass hues during the 2nd century AD.

To reach these goals, the study was divided into three distinct but interconnected parts: an in-depth and broad literature review, archaeometric research into the red glass *sectilia* from the *Lucius Verus* villa, and systematic laboratory reproductions.

“Why study Roman opaque red glass?” Although the Roman period has provided a massive amount of archaeological evidence which can tell us how they lived, how they constructed their buildings, or what they read, on the glassmaking industry there are some aspects that are still not understood. In the last few decades, archaeometric analyses have provided fundamental and outstanding information which has shed light on Roman glassmaking. However, these were focused mainly on the glassware, glass vessels, jewellery, their provenance and how they were traded and made. In contrast, where coloured glasses were produced, or at which step of the production process they were made is still the subject of debate. Although opaque red glass was produced in abundance during the Roman Age, as the numerous glass *tesserae* uncovered in Pompeii, Rome or in other mosaic spread across the Roman Empire, attest, it is still unclear where it was produced, which raw materials were used, and overall, how it was made. Previous archaeometric analyses have highlighted the high compositional variability of specific compounds (which do not enable us to make any useful generalisations) and in some cases, the chemical compositions have been defined as “anomalies” for the Roman Age. While all these aspects have been covered and investigated in part, a definitive answer has been still not found. Moreover, the absence of written technical sources for Roman glass make the survey more complex.

Therefore, studying opaque red glass *sectilia* from the *Lucius Verus* villa is a rare opportunity to obtain crucial information on the production of opaque red glass during the Roman Age. They may not provide a definitive answer to all the aspects mentioned above, but they do supply data for the literature, which could help us to get closer to the answer.

Section One of the thesis is devoted to the literature review which has three main aims:

1. To provide an overview of the main features of the ancient glassmaking industry, underlining how the Roman glassmaking was organised (production centres, trade, use), and which materials were used to manufacture glass on such a massive scale.
2. To summarise the main research carried out by glass scientists into the origin and the production technology used for copper-red glass. The main theories advanced since the 19th century are reported, as well as crucial technological aspects concerning its manufacturing, such as: the mechanism for forming red glass, the melting conditions, raw materials and heat treatments.
3. To carry out a wide-ranging literature review of the studies on opaque copper-red glass from an archaeometric point of view. This attempts to shed light on the chronological development of the manufacture of copper-red glass. The main features (chemical composition, colouring agent, use and technical aspects) of copper-red glass produced in the Late Bronze Age, Iron Age, Roman Age until the Medieval Age (and briefly in the 16th century for aventurine glass only) are reported.

This broad literature review therefore aims to show the reader the main technical difficulties in making opaque red glass, which have led glassmakers and glass scientists to invest many energies into understanding its manufacture. In contrast, the archaeometric literature review aims to provide a broad view of opaque red glass production in ancient times, highlighting the main types of opaque red produced in the Roman Age, and some critical points from the chemical analyses. This information should be helpful for the reader to better understand the archaeometric analysis included in the Section Two of the thesis.

Section Two is entirely dedicated to the archaeometric analysis of 2nd century AD Roman opaque red glass. The objects studied are glass *sectilia* (sheets of glass) which decorated the villa of the Roman Emperor *Lucius Verus*. They were part of the Gorga collection, which is stored in the *Soprintendenza Archeologica di Roma*, and have been studied by Professor Lucia Sagui who gave me access to the storehouse of the *Soprintendenza* and allowed me to collect the samples. She also contributed to this research, giving fundamental information and suggestions. These *sectilia* were chosen for this case study for two main reasons: they are well dated, attested to the 2nd century AD; they show the presence of several red and orange hues among the red and orange glass *sectilia*. This made it possible to examine the origin of the different red hues (the chemical composition, the colouring agent or specific production technology).

The scientific investigation focused on determining the origin of the different red and orange hues (chemical compositional, the nature of the colouring agent as well as their number and sizes) and was conducted through a multi-analytical approach, including:

- FORS (Fiber Optics Reflectance Spectroscopy), UV-VIS-NIR spectroscopy and colorimetric analysis to study the colour/measure the samples and specify the presence of different shades.
- OM (Optical Microscope) in reflected light for the observation of the main textural morphology features.
- EPMA (Electron Probe Micro Analysis) to carry out a micro analysis on the samples with even better quantitative analyses.
- FEG-SEM (Field Emission Gun Scanning Electrons Microscope with Energy Dispersive Spectrometry) for elemental and morphological analysis of the glass phase and the crystalline phase.
- LA-ICP-MS (Laser Ablation Inductively Coupled Plasma Mass Spectrometry) to investigate trace elements which are useful to identify the nature of raw materials used.
- μ XRD (micro X-Ray Diffraction) and μ Raman microscopy for a detailed study of crystalline phases and to clarify the colouring and opacifying agents.

The data obtained by this scientific research provide further information about the chemical composition of opaque red glass and its technology. Furthermore, these analyses helped enrich the literature on this period, which has few archaeometric studies.

Section Three of the thesis aims to investigate the production of opaque copper-red glass through systematic laboratory reproduction. Based on the information gathered from the literature review, iron and copper were selected to be tested in order to understand:

- a) which oxidation state iron should be used to produce opaque red glass, hence the identification of the probable iron-bearing materials.
- b) when copper and iron should be added to the glass, if directly to a batch at room temperature or to the molten glass. It sought to identify a probable procedure to make opaque red.
- c) the amounts of copper and iron required to make opaque red glass.
- c) how to obtain several different red hues.

Through these experiments it was possible to gain empirical information about the probable procedure used by the glass master and highlight the practical difficulties which could occur. However, the samples produced were analysed through colorimetry and FORS spectroscopy to measure the colour, were then observed by optical microscope to identify the main textural features and studied by X-ray diffraction and μ Raman spectroscopy to identify the colouring agent.

This part took longer than expected and due to the COVID-19 pandemic, it was not possible to test other factors or compounds to produce opaque red glass.

In the appendices is reported material that emerged through the literature review and from the analyses on the red glass *sectilia* from the villa of Lucius Verus. They were not reported in the main text since not considered as the primary goals of this project, but they provided useful (I wish) data and information about Roman opaque red glass, hence their presence is also relevant.

The chemical analyses on some of the red *sectilia* from the villa of Lucius Verus, revealed the presence of anomalous values for the glass dated to the Roman Age. This aspect was a very intriguing topic and it has been the subject of many debates in the last decade. So, these anomalous values were investigated through a comparison with the data reported in the literature. The main theories advanced to explain them are reported in the appendix.

Moreover, in the appendix the research into a Roman opaque red glass jar, found in the *Museu da Farmácia* in Lisbon is reported. Since opaque red glass was rarely used to make glass vessels or jars, it was interesting to analyse this jar in order to identify the type of opaque red glass used to make it.

In appendix are also reported some data that are the result of the study of Venetian manuscripts, which gave significant information for the laboratory reproduction.

References

1. Pastaoureau, M. *Rouge. Histoire d'une couleur*. Seuil, Paris, France, 2016.
2. Bradley, M. Pliny the Elder and the unnatural history of color. In *Colour and Meaning in Ancient Rome*. 1st ed.; Hunter, R.; Osborne, R.; Millett, M.; Sedley, D.N.; Horrocks, G.C.; Oakley, S.P.; Bread, W.M. Eds.; Publisher: Cambridge University Press, UK, 2011, pp. 94-100.

3. Lazzarini, L. Ancient Mediterranean polychrome stones. *Mineralogy* 2019, 20 (10), 367–392.
4. E. Marianne Stern, “Hellenistic Glass from Kush (Modern Sudan),” In *Proceeding 8eAnnales de l’Association Internationale pour l’Histoire du Verre*, v. 8, London/Liverpool, 1979 (Liège, 1981), pp. 35–59.
5. Ignatiadou, D. A Haematinon bowl from Pydna. In *Proceedings of the Annales du 18e Congrès de l’Association Internationale pour l’Histoire du Verre, Thessaloniki, Greece, 20–25 September 2009*; Ignatiadou, D., Antonaras, A., Eds.; ZITI Publishing: Thessaloniki, Greece, 2012; pp. 69–74.

-Section One-

**A literature review of the field of archaeometry and
glass science**

1 Early glassmaking technology

1.1 Brief introduction to glassmaking in ancient times

Glass is already present in nature, formed from volcanic magma, such as obsidian; however, it can be produced artificially through a fusion process, by melting a mixture of silica, sodium and calcium at high temperature. Silica is considered the network former, while sodium is a fluxing agent necessary to lower the melting temperature of the silica (1710°C), and calcium is a stabiliser which increases the chemical durability of the glass. The early glassmakers found these compounds in nature; indeed, the main sources of silica were quartz pebbles or sand, sodium was provided by halophytes plants (such as *Salicornia*) or by evaporitic salt composed of sodium carbonate (natron). Calcium was often already present (calcite or aragonite) in the mineralogical composition of the siliceous-calcareous sand chosen to make the glass; otherwise, it entered the process through soda plant ash (used as a fluxing agent).

The production of glass required specific skills in the melting process and special knowledge of the materials properties to choose the correct raw materials. Nevertheless, the origins of glassmaking technology are still uncertain.

One of the most widely accepted hypotheses is that the first vitreous materials were faience objects, produced around the 4th millennium BC in Egypt and Mesopotamia, probably by mixing quartz powder (or quartz sand) with sodium-rich fluxing and water, left to dry and heated at high temperature [1-3]. These materials were used to fabricate small amulets, rings, scarabs, and beads [2, 3].

From the middle of the 2nd millennium BC (probably between 1600 and the 1500 BC) early glassmakers started to manufacture glass vessels [4]. However, it is still debated if these originated in Mesopotamia or in Egypt. These vessels were made by dipping a clay body into a crucible containing molten glass. From the 1st millennium BC more techniques were developed such as core-forming, rod-forming, casting in open or closed moulds, the use of canes and bars to make polychrome glass objects (glass mosaic technique) and tooling on a potter's wheel [5].

The glass produced between the 14th century BC and the 13th century AD in the Mediterranean basin, can be considered soda-lime-silica glass, made by mixing a silica source, such as sand or quartzite pebbles, and a soda source, in order to lower the melting temperature. Based on the nature of the soda source, scholars usually distinguished different glassmaking traditions and different steps in the evolution of glassmaking.

Glass artefacts recovered in Mycenaean Greece, Anatolia, Crete, Egypt, the Mesopotamian region and southwestern Persia dating from between 1500 and 800 BC are characterised by high levels of sodium (12-18 wt%), potash (K₂O 2-4 wt%) and magnesia (MgO 2-4wt%) and were known as high magnesia glass (HMG) [6]. The concentration of potash and magnesia detected in this glass suggests the use of soda-plant ash as a fluxing agent [3, 7-9]. However, high variability is noted in the composition of the species of plant, which is affected by the soil in which the soda plants grow, how they are burned and prepared, and also which part of the plant was used [8-11].

In the same period (1300 – 900 BC), a glass with potash detected between 2-10 wt%, and low sodium (Na_2O usually 2-9wt%) was produced in continental Europe and the North of Italy (Frattesina). These glasses are usually referred to as low magnesia high potash (LMHK) or mixed alkali [7, 12-14].

From the 8th century BC until the 8th century AD in the Mediterranean basin, a mineral source of soda replaced the vegetable ash (soda ash) and was the main fluxing agent during the Iron Age and Roman/Late Antique period [15]. However, in the same period, in the regions of the Tigris and Euphrates valley and in the Persian lands, soda plant ash continued to be used as a source of soda in the glassmaking industry [16-18].

This mineral source is an evaporitic deposit (trona) extracted from salt lakes, such as in Wadi-El-Natron and therefore called natron, composed of sesquicarbonate $\text{Na}_2\text{OCO}_3 \cdot \text{NaHCO}_3 \cdot 2\text{H}_2\text{O}$ and small percentage of other contaminant elements [4, 15]. The glass produced by natron is characterised by sodium content varying between 13-22 wt%, while potash and magnesia have been frequently detected below 1 wt% (which entered mainly through the silica source – sand), and for this reason is known as low magnesia glass (LMG) [6].

The use of natron continued until the mid-8th century AD. Archaeological evidence and chemical analyses attested the presence of soda plant ash glass manufactured in the Palestinian region about the mid-8th century AD. The use of plant ash, as alkali source for glass making, substituted natron glass about the mid-9th century AD (in the Syro-Palestinian regions). The same occurred in Egypt, in which natron glass was abundantly produced until the 9th century AD and was substituted by soda plant ash about the mid-10th century AD [19, 23]. In this period of transition, natron and soda-plant ash glass coexisted in the Mediterranean basin, and often an intermediate composition has been detected, which can be considered a mixture (by recycling) of natron and soda plant ash glass [24, 25]. In North and Central Europe, from the 8th century AD, wood ash was used to make glass, using mainly beechwood or oak trees to obtain the ashes which were very high in potash and calcium content [26]. This type of glass is generally called potash or wood ash glass.

Several hypotheses have been advanced to explain the decline in natron availability. The early studies supposed that weather fluctuations, trade disruption or political instability could be responsible for this technological changing. More recent investigations advanced the hypothesis that environmental climate change is more probably the main factor which restricted natron formation in the lake, and influences of cultural and societal development. All these factors seem to have encouraged the employment of soda plant ash as alkali source in glass making. Indeed, suitable plant ash to produce glass were locally accessible (in the Near-East) and in enough amount to supply local or regional market [19].

Beyond the raw materials for the base glass, the history of glass was characterised by different firing procedures which involved the preparation or not of the raw materials to melt the glass, and the melting procedure.

It was thought that in the Late Bronze Age, the raw materials were heated at temperatures of about 700-850 °C in order to eliminate the carbonates, and a semi-product (frit) was produced. This was then powdered and heated at a higher temperature (probably 1000-1100 °C) in a crucible obtaining molten glass [27].

In contrast, from the early Roman to the Islamic period, the raw materials were put into a large tank furnace and melted using only one firing stage without the prior preparation of a semi-product (frit) [28]. During the

medieval period, the production of glass required the preparation of a frit, afterward it was re-heated and melted at a higher temperature in a pot. To shape and work the glass, it was taken directly from the crucible [26].

Since the beginning of glassmaking technology, coloured glasses (opaque or transparent) were produced by using compounds containing one of these elements: copper (Cu), iron (Fe), manganese (Mn), cobalt (Co), tin (Sn) or antimony (Sb). Through the manipulation of their oxidation states, or by using specific compounds, it was possible to obtain a wide range of colours [26].

The organisation of glass production was a fundamental factor in achieving efficiency and for supplying the market. In general, from the Late Bronze Age until the Byzantine period it is thought that glassmaking (where glass was melted from the batch) and glass working (where a raw glass was re-melted and worked or coloured) were two separate stages of glass production. In the Bronze Age “elite-attached” glass factories produced coloured glass in ingot moulds [3, 29] and sent them to the specialised “elite-attached” workshops which shaped and created glass manufactures. Moreover, archaeological evidence has been found which supports the probable existence of long-trade exportation of coloured glass ingots and glass artifacts from Mesopotamia and Egypt to the Near East and Greece [26, 27, 30]. During the Roman period and in Late Antiquity, glassmaking took place in a few large furnaces, and then the raw glass was shipped to the small furnaces where the raw glass was remelted, coloured or shaped into glass items. In contrast, during the Medieval period in Europe, glassmaking and glass working took place in the same glass factories which produced the raw glass, working it and trading it in the regional/local market [8, 26].

1.2 Roman and Late Antique glassmaking

After this brief and general introduction to the main historical stages in the history of glass, it is time to be more focused on the Roman-Late Antique period.

When Rome started to impose its hegemony on the Mediterranean basin, it incorporated the glassmaking traditions that were already well established in the different regions of the Eastern Mediterranean Sea. Indeed, this area from the 3rd century BC saw the flowering of glass-working and colouring techniques. Cups, dishes, *skyphoi* and large amphorae with complex patterns made by glass, were abundantly produced by improvements in the use of moulds, demonstrates this technological progress [31]. The production of polychrome glass, obtained by the juxtaposition of several canes of different colours, was widely used in the manufacture of plaque, vessels, cups, bowls with elaborated floral or geometrical motifs [5, 32]. During the early Roman period, all these techniques were enhanced thanks to an intensive exchange of knowledge and the movement of glassworkers from one place to another [33].

Examples of the extraordinary technological level reached by the Roman glassmakers are the cameo glass artifacts [34], the production of window glass for public and private Roman architecture, bringing light within buildings. Glass *tesserae* were used in the *opus vermiculatum*, expanding the chromatic scale available for the mosaicist [35]; sheets of glass were used in *opus sectile* techniques to decorate walls and pavements, enabling the artisan to produce pieces with complex shapes [36-38] more easily. Oil lamps were produced to illuminate

the interiors of private and public buildings at night; moreover, *diatreta* cups (or cage cups), such as the Lycurgus cup [39], were produced for the Roman elite, and testify to amazing artistic and technical skills [31]. The most important factor which characterised the Roman glassmaking tradition, and subsequent periods, was the discovery of the blowing technique between 1st century BC and 1st century AD. It has been attested by archaeological evidence, found in the Jewish quarter of Jerusalem, that this technique was discovered and explored in the Syro-Palestinian coastal region in the middle of the 1st BC. Likely it was discovered earlier, but the true advantage that this technique could bring to work the glass was not completely understood. Indeed, recent studies showed that it was only in the second quarter of the 1st AD that glass inflation was used to produce glass object in large scale [40]. Moreover, since glassworkers moved from the East Mediterranean basin to Italy, or other regions of the Roman Empire, this new and revolutionary technique spread very fast. Indeed, archaeological evidence suggests that about the middle of the first century AD glassblowing techniques reached and developed in Avenches, Lyon, Saintes, Northern Italy, Campania (Southern Italy), Spain and Britain [33].

Before the introduction of the blowing technique, glass bowls, bottles and vessels were mainly produced by the core-forming, mosaic glass or casting techniques, which were a long and a slow procedure. By means of the blowing technique, these items were made by blowing small amounts of molten glass into a mould, which reduced the time and the amount of glass required. It is possible to say that glass objects were manufactured on assembly line, increasing the number of products that a glass workshop could make in one day [33, 40]. The Roman glassmaking industry can be considered an example of mass production, which affected the price of the glass vessels, as well glass tableware, transforming them into objects of common use. The archaeological excavation of Pompei confirmed this fact, showing that the amount of glass manufactures were higher than those made in ceramics [31, 41].

Through the chemical analyses and the finding of shipwrecks, it has emerged that recycling glass and re-melting broken glass manufactures were a well-established practice in Roman glassmaking, at least since the Flavian Age (1st century AD) [33, 42-44]. Before the Roman Age, glassmaking was for small-scale production only, while the dimensions reached in the Roman Age are not comparable [33]. However, this mass production of glass was possible thanks to a well-organised manufacturing system.

1.2.1 Raw materials

Roman and Late Antique glass is characterised by its “standardised” composition of the main components with only very narrow variations. Usually, Roman, and Byzantine glass shows high silica content (60-70 wt%), high sodium levels (Na₂O 14-20 wt%) and moderate concentrations of calcium (CaO 5-10 wt%). This reflects the composition of the raw materials and the relative ratios used to melt this glass, which were a fluxing agent and siliceous-calcareous sand [45].

The fluxing agent was *natron*, a sesquicarbonate which is nowadays known as trona (Na₂OCO₃.NaHCO₃.2H₂O) and exploited from the salt lake of Wadi el Natron, approximately 50 km northwest

of the modern-day city of Cairo [4, 46, 47]. This is also mentioned by Pliny the Elder in his *Naturalis Historiae*, written in 77 AD, in which he mentions “*soda preferably from Egypt*” [46].

The other two components, silica and calcium, were supplied by one single raw material - a siliceous-calcareous sand, in which these components are mixed in the correct proportions, and calcium is present as fragments of shells (aragonite and calcite) or calcareous minerals (such as calcite).

According to the Pliny manuscript, the sands from the mouths of the Belus river (close to modern Haifa, Israel) or of the Volturno river (Campania, South of Italy) were used to make glass [46]. Chemical analyses of the Belus River sand have confirmed that this type of sand was suitable for producing soda-lime-silica glass with a chemical composition very close to that of Roman glass. This hypothesis was further confirmed by isotopic analyses and archaeological findings. The early investigation suggested that the sand from the Volturno river was suitable for making glass. Indeed, experimental reproduction produced glass with a composition close to typical Roman natron glass [48]. However, more recent studies using a deep mineralogical characterization of the sand and isotopic analyses (Nd isotope), highlighted that the sand from the Volturno river contains high concentration of heavy minerals, resulting high in Fe_2O_3 and Al_2O_3 . These values make this sand unsuitable as raw material to make Roman glass [49].

Looking at the minor elements, it is possible to find traces of alumina usually varying between 2-3 wt%, with potash, magnesia concentration lower than 1 wt%, and phosphorus below 0.2 wt%; iron ranges between 0.3 and 1 wt% and titanium between 0.01 and 0.5 wt%. They are representative of a siliceous-calcareous sand with low amounts of alkali-feldspars and heavy minerals. However, it is not excluded that the glass composition has been affected by refractories of the furnace, contaminants from the crucibles wall or altered by the fuel ash or recycling glass [50, 51].

1.2.2 Melting techniques: Primary and secondary furnaces

Through the archaeological findings and chemical and geochemical analyses, a model has been drawn up which attempts to explain the production system of Roman and Byzantine natron glass.

As stated in the literature, during the Roman and Byzantine period the glassmaking industry was organised into a two-stage process: primary production (glassmaking) in which raw glass was produced; secondary production (glass working) devoted to re-melting raw glass and producing glass manufactures [46].

The raw glass was produced in large rectangular tank furnaces, consisting of a rectangular melting chamber (about 2 m x 4 m) in which the raw materials (silica-lime sand source and natron) were introduced, and a smaller firing chamber divided into two parts filled by fuel [28]. It was estimated that up to 30 tons of glass could be melted in these furnaces [28].

Melting of the batch occurred probably in a single firing stage, without the preparation of frit, estimated at temperature of about 1100 °C [27, 28, 46, 52]. The melting of the batch took several days or (probably) weeks. Afterwards, the furnace was cooled down, then dismantled and the glass in a singular rectangular slab of

several tons (9 -13 tons) was broken up into shapeless chunks, which were sent to be traded either to the local glasshouse or shipped to reach the countless workshops spread across the various parts of the Empire [28, 53]. In secondary production (glass working, workshops) the chunks were re-melted, most likely in crucibles or in small tanks placed in smaller, circular furnaces. The molten glass was collected to produce glass artifacts to trade in the market. Moreover, it is generally accepted that coloured glass was produced in the secondary workshops (opaque or transparent), by adding colouring elements to the raw glass.

This model is strongly supported by historical written sources (such as Pliny) and archaeological composed of furnaces remains [28, 54] and shipwrecks [42, 43]. Furnaces remains were discovered in Beirut, and it is dated about the 50 BC. It could be the earliest known evidence for primary glass making in the ancient classical world [55]. Unfortunately, no more furnaces of the early Roman period were found. On the contrary tank furnaces dated between the 4th and 8th century AD were uncovered in: Jalame (Israel, 4th AD), Wadi El Natrun valley (Beni Salama, Egypt, 4th-8th century AD) [56, 57], Bet Eli Ezer (Hadera, Israel, 6th-8th AD) [28].

The almost homogeneous chemical composition of the Roman-Byzantine glass, and the archaeological evidence of furnace remains, suggested that the primary production of raw glass took place in the Levantine coast (Syro-Palestinian coast) and in the Egypt [45]. The raw glass produced in these production centers, where broken and shipped to the secondary furnaces, in which the glass was remelted and worked to make glass items [45].

However, in the last two decades some authors advanced the hypothesis that primary glass production could existed also in the western part of the Roman Empire, especially during its early stage (1st – 4th AD). Through the scientific investigation on ceramic crucible, evaluating the probable temperature of melting, Jackson [58] advanced the hypothesis that primary glass production was working in York. By comparing the strontium and barium concentrations, Wedepohl [59] proposed the existence of primary furnaces that made own raw glass in the Hambach Forest (Western Germany) by local raw materials. However, more recent chemical analyses of the glass uncovered in these two regions, revealed that the composition of the glass is very similar with those detected in other sites, such as Bulgaria, Italy, France, Egypt and Israel dated to the same period. This fact suggests that the glass used in York and in the furnaces of the Hambach Forest were more likely imported from the Levantine coast or from Egypt and not locally produced [60, 61].

Brems [62], analysed several beach sands from the Mediterranean coast, and identified some potential sand suitable for producing glass with the same chemical composition as typical Roman glass. They indicated some locations in Italy (Val Basento, Brindisi, Piombino), the South of France and Spain (Huelva, Murcia, Bay of Hyere) [62]. Gallo [63] analysed several shards from North-east Italy dating from the 1st – 5th century AD. For the early Roman glass, they established that most of the glass shows an Eastern Mediterranean provenance, but compositional differences were detected that do not exclude Western Mediterranean production [63]. Furthermore, coloured glass dating between 1st and 4th century AD showed concentrations of potash and magnesia higher than 1.5 wt%, which are considered anomalous values for the standardised Roman natron (K₂O and MgO usually < 1.5wt%) glass, opening other question on the production of coloured glass [64-66].

Although, these data and hypothesis are very suggestive, no archaeological findings have been recovered to confirm and strongly support the presence of primary production furnaces in the Western Mediterranean.

Conversely, for the Late Antique period, the centralised production system is in good agreement with the archaeological evidence (furnaces and shipwreck) and scientific analyses. According to the literature from the 4th century AD, two main types of natron glass circulated in the Mediterranean basin and supplied the Byzantine and Western glass workshop: Levantine 1, produced along the Syro-Palestinian coasts and used from the 5th to 7th century AD [53, 67]; HIMT produced in Egypt from the 4th to 7th century AD, represented a low-quality sand glass with higher concentrations of iron, manganese, and titanium [53, 67]. A third group can be included called Foy 3.2. which was probably produced on the Levantine coast between the 3rd and 5th centuries AD, by using beach sand from a different location [67]. Levantine 1 and HIMT showed several sub-groups, for example two major sub-groups of Levantine 1 have been identified (Levantine 1 and Levantine 2); while HIMT is more variable and four sub-groups are classified (HLMT, HIT, HIMTa and HIMTb) [68-70].

References

1. Pradell, T., Molera, J. Ceramic technology. How to characterise ceramic glazes. *Archaeol. Anthropol. Sci.* **2020**, 12, 189.
2. Tite, M.S.; Manti, P.; Shortland, A.J. A technological study of ancient faience from Egypt. *J. Archaeol. Sci.* **2007**, 34, 1568-1583.
3. Shortland, A.J.; Tite, M. S. Raw materials of glass from Amarna and implications for the origins of egyptian glass. *Archaeometry*, **2000**,42, 141-151.
4. Shortland, A. J., Eremin, K. The analysis of second millennium glass from Egypt and Mesopotamia, part 1: new WDS analyses. *Archaeometry*. **2006**, 48 (4), 581–603.
5. Stern, E.M.; Schlick-Nolte, B. Manufacturin techniques. *Early glass of the ancient world 1600 B.C. - A.D. 50. Ernesto Wolf collection*. Publisher: Verlag Gerd Hatje, Ostfildern, Germany 1994, pp. 27-88.
6. Sayre, E.V.; Smith, R.W. Compositional categories of ancient glass. *Science* **1961**, 133, 1824–1826.
7. Henderson, J. The raw materials of early glass production. *Oxford Journal of Archaeology*, **1985**, 4(3), 267-291.
8. Turner, W. Studies in Ancient glass, and glassmaking process. Raw materials and melting process. *Journal Soc. Glass Technology* **1956**, 40 (5), 277-300.
9. Tite, M.S.; Shortland, A.; Maniatis, Y.; Kavoussanaki, D.; Harris, S.A. The composition of the soda-rich and mixed alkali plant ashes used in the production of glass. *J. Archaeol. Sci.*, **2006**, 33, 1284-1292.
10. Barkoudah, Y.; Henderson, J. Plant ashes from Syria and the manufacture of ancient glass: ethnographic and scientific aspects. *J. Glass Stu.* **2006**,48. 291-231.
11. Verità, M. L'invenzione del cristallo muranese: una verifica analitica delle fonti storiche, *Riv. Staz. Sper. del Vetro*, **1985**, 1, 17-29.
12. Henderson, J. Electron probe microanalysis of mixed-alkali glasses, *Archaeometry*, **1988**, 30, 77-91.
13. Brill, R.H. Chemical analyses of some glasses from Frattesina, *J. Glass Stu.* **1992**, 34, 11–22.

14. Santopadre, P.; Verità M. Analyses of the production technologies of Italian vitreous materials of the Bronze Age. *J. Glass Stu.* **2000**,42, 25–41.
15. Shortland, A.; Schachner, L.; Freestone, I.; Tite, M. Natron as a flux in the early vitreous materials industry: sources, beginnings and reasons for decline. *J. Archaeol. Sci.* **2006**, 33, 521-530
16. Mirti, P.; Pace, M.; Negro Ponzi, M.M.; Aceto, M. ICP–MS Analysis of glass fragments of Parthian and Sasanian epoch from Seleucia and Veh Ardasir (Central Iraq). *Archaeometry* **2008**,50 (3), 429–450.
17. Mirti, P.; Pace, M.; Malandrino, M.; Negro Ponzi, M.M. Sasanian glass from Veh Ardasir: new evidences by ICP-MS analysis. *J. Archaeol. Sci.* **2009**, 36, 1061–1069.
18. Brill, R.H. *Chemical Analyses of Early Glasses. Volume 2 Tables of Analyses*; The Corning Museum of Glass: Corning, NY, USA, 1999; ISBN 0-872900-143-2.
19. Phelps, M.; Freestone, I.C.; Gorin-Rosen, Y.; Gratuze, B. Natron glass production and supply in the late antique and early medieval Near East: The effect of the Byzantine-Islamic transition. *J. Archaeol. Sci.* **2016**, 75, pp.57-71.
20. Schibille, N.; Gratuze, B.; Ollivier, E.; Blondeauc, É. Chronology of early Islamic glass compositions from Egypt. *J. of Archaeol. Sci.* **2019**, 104, 10–18.
21. Phelps, M. Glass supply and trade in early Islamic Ramla: An investigation of the plant ash glass. In *Things that travelled-Mediterranean Glass in the First Millennium CE*. Rosenow, D., Phelps, M., Meek, A., Freestone I., Eds.; Publisher: UCL Press University College London, UK, 2018, pp. 236-282.
22. Henderson J.; Evans, J.A.; Sloane, H.J.; Leng, M.J.; Doherty, C. The use of oxygen, strontium and lead isotopes to provenance ancient glasses in the Middle East, *J. Archaeol. Sci.* **2005**, 32, 665–673.
23. Gratuze, B.; Barrandon, J.-N. Islamic glass weights and stamps: analysis using nuclear techniques, *Archaeometry* **1990**,32 (2), 155-162.
24. Andreescu-Treadgold, I.; Henderson, J.; Roe, M. Glass from the Mosaic of the west wall of the Torcello's Basilica, Extract from *Arte medieval* 2006, 2, 87-140.
25. Verità, M. Tecniche di fabbricazione dei materiali musivi vitrei. Indagini chimiche e mineralogiche. In *Medieval Mosaics Light, Color, Materials*; Borsook, E., Gioffredi Superbi, F., Pagliarulo, G., Eds.; Silvana Editoriale S.p.A.: Cinisello Balsamo, Italy, 2000; pp. 47–64, ISBN 88-8215-265-0.
26. Rehren, Th.; Freestone, I.C. Ancient glass: from kaleidoscope to crystal ball. *J. Archaeol. Sci.* **2015**, 56, 233-241.
27. Rehren, T.; Pusch, E.B. Late Bronze Age glass production at Qantir-Piramesses, Egypt. *Science* **2005**, 308, 1756–1758.
28. Gorin-Rosen, Y. The ancient glass industry in Israel. Summary of the finds and new discoveries. , In *La Route du Verre: Ateliers primaires et secondaires du second millenaire av. J.- C. Au Moyen-Age*. Acte du colloque organisé en 1989 par l'Association française pour l'Archaeologie du Ver (AFAV); Nenna, M-D., Ed; Maison de l'Orient Méditerranéen, Lyon, 2000, 49–64.
29. Rehren, Th. Ramesside glass-colouring crucibles. *Archaeometry* **1997**, 39 (2), 355-368.
30. Jackson, C.M.; Nicholson, P.T. The provenance of some glass ingots from the Uluburun shipwreck. *J. Archaeol. Sci.* **2010**, 37, 295–301.
31. Sagù, L. Il vetro. In *Arte romana*, M.Papini, Milano 2016, pp. 450-466.
32. Grose, D. Fr. The Early Roman Empire 30 B.C. to 50 A.D. In *Early Ancient Glass, The Toledo Museum of Art, core-formed, rod-formed and cast vessels and objects from the late bronze age the early roman empire, 1600 BC to AD 50*. Publisher: Hudson Hills Press, Toledo, USA, 1989, pp. 241-245.

33. Stern E.M. Roman Glassblowing in a Cultural Context. *Amer. J. Archaeol.* **1999**, 103, 441-482.
34. Bimson, D.; Freestone, I.C. The analytical study of the relationship between the Portland vase and other cameo glass. *J. Glass Stu.* **1983**, 25, 55-64.
35. Boschetti, Cr. Vitreous Materials in Early Mosaics in Italy: Faience, Egyptian Blue, and Glass. *J. Glass Stu.* **2011**, 53, 59-91.
36. Saguì, L.; Santopadre, P.; Verità, M. Technology. Colours, Forms, and Shapes in the 2nd Century Glass Opus Sectile Materials from the Villa of Lucius Verus in Rome. In Proceedings of the *Annales du 18e Congrès de l'Association Internationale pour l'Histoire du Verre, Thessaloniki, Greece, 20–25 September 2009*; Ignatiadou, D., Antonaras, A., Eds.; ZITI Publishing: Thessaloniki, Greece, 2012; pp. 133–138.
37. Gliozzo, E., Santagostino Barbone, A., Dacapito, F., Turchiano, M., Memmi, I., and Volpe, G. The sectilia panels of Faragola (Ascoli Satriano, Italy): a multi-analytical study of the red, orange and yellow glass slabs, *Archaeometry*, **2008**, 50(3), 451–73.
38. Gliozzo, E., Santagostino Barbone, A., Turchiano, M., Memmi, I., and Volpe, G., The coloured tesserae decorating the vaults of the Faragola balneum (Ascoli Satriano, Foggia, southern Italy). *Archaeometry* **2012**, 54(2), 311–31.
39. Barber, D.J.; Freestone, I.C. An investigation of the origin of the colour of the Lycurgus cup by analytical transmission electron microscopy. *Archaeometry* 1990, 32 (1), 33-45.
40. Larson, K.A. Cheap, fast, good: the Roman glassblowing revolution reconsidered. *J. Rom. Archaeol.* **2019**, 32, 7-22.
41. Verità, M. Natura e tecnologia dei vetri pompeiani attraverso le analisi chimiche dei reperti. *Vitrum, il vetro fra arte e scienza nel mondo romano*. M. Berretta, G. Pasquale, Eds.; Publisher: Giunti, Italy, 2004, pp. 163-169.
42. Silvestri, A. The coloured glass of Iulia Felix, *J. Archaeol. Scie.* **2008**, 35(6), 1489–501.
43. Silvestri, A., Molin, G., and Salviulo, G. The colourless glass of Iulia Felix, *J. Archaeol. Scie.* **2008**, 35(2), 331–41.
44. Schibille, N., Sterrett-Krause, A., Freestone, I.C. Glass groups, glass supply and recycling in late Roman Carthage. *Archaeol. Anthropol. Scie.* **2017**, 9, 1223–1241.
45. Freestone, I. C., Gorin-Rosen, Y., and Hughes, M. J., 2000, Primary Glass from Israel and the Production of Glass in Late Antiquity and the Early Islamic Period, In *La Route du Verre. Ateliers Primaires et Secondaires du Second Millènaire av. JC au Moyen Age* (ed. M. D. Nenna), 65–83, Maison de l'orient Méditerranéen, Lyon.
46. Freestone, I. C., Pliny on Roman glassmaking, In *Archaeology, History and Science. Integrating Approaches to Ancient Materials* (eds. M. Martinon-Torres, and T. Rehren), UCL Institute of Archaeology Publications, Oxford **2008**, 77–100.
47. Freestone, I. C., Greenwood, R., and Gorin-Rosen, Y. Byzantine and early Islamic glassmaking in the eastern Mediterranean: production and distribution of primary glass. In *Hyalos-Vitrum-Glass. History, technology and conservation of glass in the Hellenic world*, Kordas, G., Eds.; Publisher: Glasnet Publications, Athens, Greek, 2002, pp. 167–74,
48. Silvestri, A.; Molin, G.; Salviulo, G. Sand for roman glass production: An experimental and philological study on source of supply. *Archaeometry* **2006**, 48 (3), 415– 432.
49. Brems, D.; Ganio, M.; Latruwe, K.; Balcaen, L.; Carremans, M.; Gimeno, D.; Silvestri, A.; Vanhaecke, F.; Muechez, P.; Degryse, P. Isotopes on the beach, part 2: neodymium isotopic analysis for the provenancing of Roman glass-making. *Archaeometry* **2013**, 55(3), 449-464.
50. Paynter, S. Experiments in the Reconstruction of Roman Wood-Fired Glassworking Furnaces: Waste Products and Their Formation Processes. *J. Glass Stu.* **2008**, 50, 271-290.

51. Schibille, N., Degryse P., Corremans, M., Specht, Ch.G. Chemical characterisation of glass mosaic tesserae from sixth-century Sagalassos (south-west Turkey): chronology and production techniques. *J. Archaeol. Scie.* **2012**, 39, 1480-1492.
52. Rehren, Th. Rationales in Old World Base Glass Compositions. *J. Archaeol. Scie.* **2000**, 27, 1225–1234.
53. Freestone, I.C. The Provenance of Ancient Glass through Compositional Analysis. In *Materials Issues in Art and Archaeology VII*, edited Vandiver, P.B., Mass, J.L., Murray A. (Mater. Res. Soc. Symp. Proc. 852, Warrendale, PA, 2005), OO8.1.1 -OO8.1.13
54. Nenna, M-D.; Vichy, M.; Picon, M. L'atelier de verrier de Lyon, du 1er siècle après j.-c, et l'origine des verres romains, *Revue d'Archéométrie*, **1991**, 21, 81-87.
55. Kowatli, I.; Curvers, H.H.; Stuart, B.; Sablerolles, Y.; Henderson, J.; Reynolds, P. A pottery and glass production site in Beirut (BEY 015). *Bulletin d'Archéologie et d'Architecture Libanaise* **2006**, 10, 103-129.
56. Nenna, M.D.; Picon, M.; Thirion-Merle V.; Vichy M. Ateliers primaires du Wadi Natrun: nouvelles découvertes. In the Proceeding of *Annales du 16e Congrès de l'Association Internationale pour l'Histoire du Verre, London, Unite Kingdom, 7-13 September 2003*; pp. 59-63
57. Nenna, M.D.. Primary glass workshops in Graeco-Roman Egypt: preliminary report on the excavations of the site of Beni Salama, Wadi Natrun (2003, 2005-9). *Glass of the Roman World*. Oxford: Oxbow Books, 2015, 1-22.
58. Jackson, C.M.; Joyner, L.C.; Booth, A.; Day, P.M.; Wager, E.C.W.; Kilikoglou, V. Roman glass-making at coppergate, york? Analytical evidence for the nature of production. *Archaeometry* **2003**, 45 (3), 435–456.
59. Wedepohl, K. H.; Baumann, A. The use of marine molluscan shells for Roman glass and local raw glass production in the Eifel area (western Germany), *Die Naturwissenschaften*, **2000**, 87(3), 129–32.
60. Jackson, C.M.; Paynter, S. A great big melting pot: exploring patterns of glass supply, consumption and recycling in Roman Coppergate, York. *Archaeometry* **2016**, 58(1), 68-95.
61. Rehren, T.; and Brüggler, M., The Late Antique glass furnaces in the Hambach Forest were working glass-not making it. *J. Archaeol. Scie.: Reports* **2020**, 29, 102072.
62. Brems, D.; Degryse P., Hasendoncks, F.; Gimeno, D.; Silvestri, A.; Vassilieva, Luypaers, E.S., Honings, J. Western Mediterranean sand deposits as a raw material for Roman glass production. *J. Archaeol. Scie.* **2012**, 39, 2897-2907.
63. Ganio, M.; Boyen, S.; Fenn, T.; Scott, R.; Vanhoutte, S.; Gimeno, D.; and Degryse, P. Roman glass across the Empire: an elemental and isotopic characterization, *J. Anal. At. Spectrom.* **2012**, 27(5), 743-753.
64. Nenna, M-D.; Gratuze, B. Etude diachronique des compositions de verres employés dans le vases mosaïque: résultats préliminaires, In Proceedings of the *Annales du 17e Congrès de l'Association Internationale pour l'Histoire du Verre, Antwerp, Belgium, 4–8 September 2006*; Janssens, K., Degryse, P., Cosyns, P., Caen, J., Van't dack, L., Eds.; University Press Antwerp: Antwerp, Belgium, 2009; pp. 199-205.
65. Rosenow, D.; and Rehren, T. Herding cats - Roman to Late Antique glass groups from Bubastis, northern Egypt. *J. Archaeol. Scie.* **2014**, 49(1), 170–84.
66. Jackson, C.M.; Cottam, S. A green thought in a green shade'; Compositional and typological observations concerning the production of emerald green glass vessels in the 1st century A.D. *J. Archaeol Scie* **2015**, 61, 139-148.
67. Foy, D., Vichy, M., and Thirion-Merle, V., Caractérisation des verres de la fin de l'Antiquité en Méditerranée occidentale: l'émergence de nouveaux courants commerciaux , In *Actes du colloque de l'Association Française pour l'Archéologie du Verre*, Aix-en-Pro, Monique Mergoïl, Montagnac, 2003; D. Foy, M. D. Nenna Eds.; pp. 41–85.

68. Ceglia, A., Cosyns, P., Nys, K., Terryn H., Thienpont H., Meulebroeck, W. Late antique glass distribution and consumption in Cyprus: a chemical Study. *J. Archaeol. Scie.* **2015**, 61, 213-222.
69. Rehren, Th., Cholakova, A. The Early Byzantine HIMT Glass From Dichin, Northern Bulgaria. In *Interdisciplinary Research*, **2010**, 81-96.
70. Foster, H.E., Jackson, C.M. The composition of late Romano-British colourless vessel glass: glass production and consumption. *J. Archaeol. Scie.* **2010**, 37(12), 3068-3080.

*A theory is only useful and valid if it explains the empirical data.
(Bamford, 1977)*

*The successful manufacture of copper-red glass depends on such a variety of factors that they are the most difficult of all coloured glass to produce
(Weyl, 1959)*

2 A literature review of the glass science studies on copper-red glass

2.1 The main type of copper-red glass

Copper-red glass has been produced since glassmaking technology began, around the second half of the 2nd millennium BC. It has been one of the most difficult colours to produce due to the high sensitivity of its colouring agent to variations in temperature and redox conditions.

The colouring agent may be cuprite crystals (Cu_2O) or metallic copper (Cu°), mostly depending on the chemical composition of the glass [1-3]. Based on the optical properties of the glass, two main types of copper-red glass exist: transparent red glass, called ruby glass (or copper-ruby glass) and opaque copper-red glass (fig. 2.1).

The nature of copper particles in copper-ruby transparent glass has been debated over the last few centuries both in the archaeological and glass-science fields. However, the particles of Cu_2O or Cu° are of nanometric size, ranging between 5 and 40 nm and are placed in a colloidal system and embedded in a colourless glass [1, 4]. The very small size of the particles and their low quantities dispersed within the glass allows the light to pass through the glass, resulting in transparent red [2, 5]. The manufacture of this glass required small amounts of copper (0.1 wt% or slightly higher) and the presence of another element which helped the formation of the colouring particles, usually tin oxide or metallic tin (SnO 0.5 -1 wt%) [1, 6, 7]. However, the formation of colour is the result of a complex melting and re-heating procedure which makes it possible to strike the colour at specific range of temperatures.

As regards opaque copper-red glass, it can be divided into two colouring techniques: Cu° -opaque red glass Cu_2O -opaque red glass. Sub-micrometre particles of metallic copper in spherical or cubic form are obtained in Cu° -opaque red glass with a moderate concentration of copper (CuO 1-4 wt%) and the presence of considerable amounts of other elements useful for the formation of Cu° particles, such as iron, tin and lead [1, 8, 9]. A special type of Cu° -opaque red glass is Cu° -aventurine glass, which started to be produced at the beginning of the 16th century AD in Murano (Venice) [10]. It is a result of very complex heat-treatment procedure with control of redox conditions, and it contains very large Cu° crystals (in some cases visible to the naked eye), in triangular or hexagonal shapes that give a sparkling effect to the glass (fig. 2.2).

In the Cu_2O -opaque red glass coloured by cuprite, also called Cu_2O -aventurine in the early studies [8, 11], or sealing wax [12, 13], the crystals are in dendritic shapes and range from a few tens of a micrometre to 150 micrometres, embedded in a transparent colourless glass matrix. The Cu_2O -opaque composition is rich in copper (CuO 6-12 wt%) and lead (15-30 wt%) oxide [8, 9, 11, 14]. The shape and the dimensions of the crystals

are the result of a prolonged and slow cooling process, and by modifying the heat treatment (by using different times and temperatures) it is possible to obtain smaller cuprite crystals (60 nm to 10 μm) usually in cubic or hexagonal forms which produce a yellow or orange opaque glass [11] (fig.2.3).

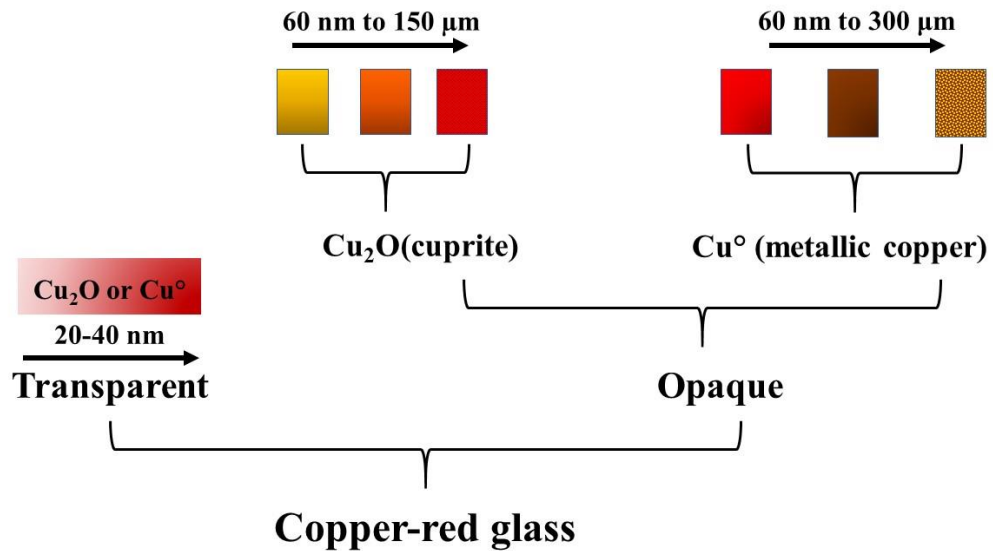


Figure 2.1 The main types of copper-red glass, and the colour given depending on the particles sizes.

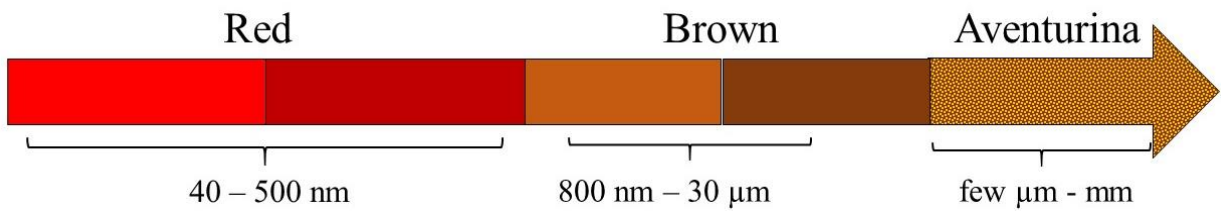


Figure 2.2 Opaque red glass produced by metallic copper particles.

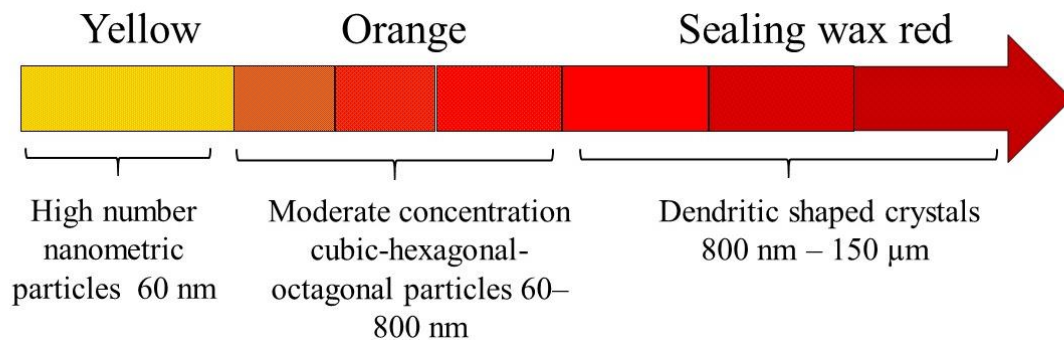


Figure 2.3 Opaque red glass produced by cuprite crystals.

2.2 Physical principle of colour in copper-red glass

The colour in glass is due to the interaction between the visible light (330 nm-770 nm) and the glass, which could produce: a reflection on the air-glass interface, absorption in the glass or a scattering of the light [2]. When the incident light hits absorbing species present in the glass, these will selectively absorb a specific wavelength from the visible light, which is able to excite the electron of the absorbing species causing electronic transition in these atoms. After absorption, the glass will show a colour which will be the sum of the remaining wavelength of the visible light [2].

The structural components of the glass network do not absorb any component of the visible light spectrum, and the resulting glass is transparent and colourless. To colour the glass it is necessary to add the colouring species.

Although a wide range of coloured glasses can be produced by ionic coloration, this has its limits, and it is not able to produce red glass, which forms only by dispersion of metal nanoparticles in a colloidal system [2]. This implies several difficulties which involve the dissolution and solubility of metals in the glass, the equilibrium of redox conditions (reducing condition), the scattering of the light by the metal nanoparticles [1].

The colour produced by metal nanoparticles is due to both absorbing and scattering of the light according to Mie theory [3]. Using the equation reported by Weyl [1], the scattering of the light by particles smaller than the wavelength of the visible light is explained by Rayleigh law's:

$$I_{\beta, r} = (D' - D)^2 / D^2 * (1 \cos^2 \beta) (M \pi V^2) / \lambda^4 r^2 \quad [1]$$

D' is the optical density of the particles, D is the optical density of the medium in which the particles are dispersed, M is the number of particles, λ is the wavelength of the incident light, V the volume of the scattering particles and r the distance from the particles in which the intensity $I_{\beta, r}$ is measured. This formula highlights that the intensity of the scattered light is inversely proportional to the fourth power of the wavelength, and it is proportional to the square of the particles' volume [1].

However, this relationship does not explain the colour produced by metallic nanoparticles which range from 5 to 40 nm in size, so 10 times smaller than the wavelength of the visible light [2]. Indeed, through Mie's theoretical studies on the optical properties of colloidal metals, and the measurements performed by his co-worker Steubing (which solved the Maxwell equations), it was noted that the scattered light play a marginal role in the coloration process [1]. The colour is mainly caused by the "consumptive light absorption" from the metal nanoparticles [1]. The extinction coefficient in the case of metals is the sum of the absorbed and scattered extinction coefficient [2]:

$$Q_{ext} = Q_{scat} + Q_{abs} \quad [2]$$

Q_{ext} is the extinction coefficient, Q_{abs} the intensity light absorbed and Q_{scat} the intensity of the scattered light. The optical transmission will depend on the optical density of the glass and on the radius of nanoparticles.

Indeed, Q_{scat} is a function of the four powers of the nanoparticles' radius, and Q_{abs} is proportional to the radius. Hence it is assumed that in the range between 1-10 nm, Q_{abs} is the predominant contribution. With larger particles, Q_{scat} contribution starts to be more relevant, but the glass is still transparent [2]. However, with particles measuring more than 40 nm the scattering effect is predominant, and with the gradually enlargement of the particles, the glass progressively loses its transparency and turns opaque [2, 15].

It is important at this point to see the interaction between light and metallic nanoparticles.

The interaction between the electromagnetic field of the visible light and the metallic nanoparticles (such as copper, silver, gold) causes the coherent oscillation of the conduction electrons, called surface plasmonic resonance [4, 16, 17]. *“Hence, light absorption occurs when the frequency of the incident light coincides with the time required for one of the electrons to traverse its orbit. In this case the system resonates, and the electron can gain sufficient energy to jump to a larger orbit. If free electrons are placed in an electric field, they will generate a convection current because they are free to move about and are not held back by attractive forces of positive nuclei. This interaction between electromagnetic waves and free electrons links conductively to the optical properties of metals”* [1]. Furthermore, it was established that the oscillation frequency depends on four factors: the density of electrons, the effective electron mass, and the shape and size of the charge distribution [16,17].

The optical properties of the metallic particles have been calculated assuming that they have a spherical shape; moreover, the metallic nanoparticles are much smaller than the wavelength of the light, and their optical absorption coefficient was expressed by [4]:

$$\alpha = (18\pi N_s V n^3 \epsilon_2 / \lambda) / (\epsilon_1 + 2n^2)^2 + \epsilon_2^2 \quad [3]$$

In this equation n is the refractive index of the medium where the particles are embedded, N is the number of spheres per unit volume of volume V , and ϵ_1 and ϵ_2 are the real and imaginary parts of the complex dielectric constant ϵ^* of the particles:

$$\epsilon^* = \epsilon_1 - i\epsilon_2 \quad [4]$$

This absorption coefficient gives an absorption band of Lorentzian shape. The position of this band is assigned to the metallic copper in the range between 560 and 590 nm [4, 6, 7, 15, 18, 19]. However, the true nature of the colouring agent has been debated for several decades, with some arguing that the origin of the colour is due to the metallic copper and others to the cuprous oxide.

2.3 The debate about the nature of the colouring agent

Since the 19th century the nature of the colouring agent in copper red glass has been debated by several authoritative scholars.

In 1856, Pettenkofer proposed the hypothesis that cuprite crystals were the colouring agent for ancient copper red glass (copper ruby, opaque red and Cu° -aventurine) [1, 20]. In contrast, in 1874, Ebell was the first to affirm that copper in the metallic state (Cu°) caused the colour in these glasses [1, 20]. Later, this theory was supported by Weyl [1], Stookey [6], Tress and [8] Brown [21].

To better identify the colouring agent, Brown [21] created personal references to measure the reflectance spectra of a copper metallic foil and of cuprous oxide. He compared these reference spectra with the reflectance spectra obtained from the red glaze produced by their studies. The reflectance spectra of red glazes fitted well with those of metallic copper foil. The presence of only metallic copper was confirmed also by the x-ray diffraction analyses, in which no cuprite peaks were detected [21].

In the same years, several researcher groups mainly composed of Ram and Prasad, Banerjee and Paul, and Wakamatsu and Ishida concluded from their experiment that cuprite crystals are the true colouring agent.

Ram and Prasad [22] worked on the understanding of the development of the red colour in the glass, and through analyses of the macro properties of the glass (such as chemical durability or viscosity) and especially by the comparison between the absorption spectra of ruby glass and those of colloidal cuprite in aqueous solution, they asserted that cuprite crystals are formed in the glass after the required special firing condition (melting temperature, heat-treatments and control of the redox conditions) [22, 23]. According to their studies, copper would be mainly a cuprous ion (Cu^+) during the cooling phase to room temperature, which starts to coordinate with the network structure of the glass. At the re-heating temperature, the Cu^+ , chilled in the structure of the glass, should act as an aggregation centre on which cuprite particles will form [22].

Banerjee and Paul, on the other hand, studied the influence of the partial pressure of the oxygen ($p\text{O}_2$) and temperature in the formation of metallic copper or cuprite in boron-sodium glass [23]. In their results, metallic copper was detected in brown or liverish glass, not in the experiment in which best ruby glass was obtained, suggesting that the colour was imparted by cuprite crystals nanoparticles [23].

After the studies by these two groups of scholars, Bamford provided supporting data for the metallic copper thesis. A good match between the extinction spectrum of copper-ruby glass, or copper-red stained glass with the model elaborated by the Mie theory has been found, reinforcing the hypothesis that copper-ruby glass was coloured by metallic copper nanoparticles [2].

Diwadi and Nath melted soda-lime-silica glass at 1400°C , and after casting it in an iron plate, it was annealed, ground and polished, and the samples were irradiated by ultra-violet irradiation [24]. When poured and cooled at room temperature, the glass was colourless (before the irradiation), indicating the presence only of cuprous ion (Cu^+). During the irradiation, the cuprous ion (Cu^+) captured the electron and formed metallic copper (Cu°). However, at room temperature the complete formation of the red colour was hampered by the high viscosity and *neither electrical forces or ionic structure can be rearranged* [24]. They can occur only through re-heating, with the lowering of the viscosity which allows the colouring process to be completed. Hence the reducing conditions help to maintain copper in cuprous form, which will be chilled in the structure of the glass during the cooling phase. During the re-heating Cu^+ could react with the reducing agent (in this case SnO) and Cu° atoms will diffuse in the glass as an embryo and nuclei and crystallise [24].

Wakamatsu and his fellow researchers affirmed that cuprite was the main colouring agent [25, 26]. They criticised the previous research which used only diffraction or absorption analyses, indeed, the detection of Cu° peaks by XRD does not mean that cuprite is not present, maybe it is not in crystalline structure but in an amorphous state. So, Wakamatsu used ESCA and ESR analyses to differentiate Cu° , Cu_2O and CuO . Their results revealed high concentration of Cu^+ and very faint Cu° content in the glass when red colour was produced. In contrast, when greyish blue glass was obtained, metallic copper photo peaks were observed. According to these results only the presence of cuprite crystals could justify the red colour [25, 26].

Nagao studied red copper-stain glass by means of optical transmittance, x-ray diffraction, EPMA and x-ray fluorescence [15]. To colour the glass, a coating layer composed of a mixture of organic compounds and inorganic powder (in which copper was present as cupric sulphate) was applied to the surface of a piece of soda-lime-silica glass. The samples were annealed at 600°C for 6 to 30 min and colour formed essentially by ion-exchange process. Through optical transmittance the optical properties of colouring particles were calculated and turned out to be in good agreement with the values of metallic copper nanoparticles. Moreover, using the subroutine BHMIE software they studied the curves of the extinction cross-section, scattering cross-section and absorbing cross-section of metallic copper. They revealed that the colour is due to the scattering and absorbing of the light; however, by the progressive enlargement of Cu° particles, the scattering effect becomes dominant, and the glass gradually loses its transparency (as mentioned in the previous paragraph). Furthermore, they revealed the position of the surface plasmonic resonance at longer wavelength from 560 nm to 590 nm identified as Cu° nanoparticles, which was confirmed by x-ray diffraction [15].

Doremus [4] using a soda-lime-silicate glass melted at 1450°C (from 3 to 4h) and poured it onto a brass plate with different cooling rates (530°C for 15 to 20 min) to attempt to identify the colouring agent. The optical absorption coefficient calculated spectra of Otter and Roberts were compared with the spectra obtained by the laboratory reproduction. The absorption position peaks between 560 and 570 nm detected in the laboratory test samples were in good agreement with the theoretical values of metallic copper nanoparticles calculated by Otter and Roberts. Furthermore, the laboratory samples were analysed by x-ray diffraction and by TEM (Transmission Electronic Microscope) detecting Cu° particles about 4.5 nm in size, and no cuprite crystals [4]. Nakai reproduced copper-ruby glass by using a lead-silicate based glass according to a specific Japanese recipe [27]. By using XEFAS analyses, they revealed that copper is present mainly as Cu^+ , as previously proposed by Ram, Banerjee and Wakamatsu, but Cu^+ in this case is coordinated with 3 or 4 oxygen atoms of the silicate anions, in other words with the structure of the glass, and not in form of Cu_2O with the cuprite structure. The calculation of the extinction coefficient is in good agreement with the metallic copper nanoparticle properties, which were not detected by EXAFS analyses because they were probably below the detection limit of the analytical technique [27].

Using the same analytical technique, Padovani [28] studied red lustre from the Italian Renaissance period and confirmed what Nakai revealed from the first analyses by EXAFS. The concentration of metallic copper in red lustre varies between 8 wt% to 20wt%, while the dominant species of copper is Cu^+ (about 80 wt%). However, Cu° was identified as the main colouring agent [28].

Copper-ruby glasses, reproduced in the laboratory, were recently intensively researched by Bring [29], who used several techniques to identify the colouring agent such as: SEM-EDS, TEM, EXAFS, XRD, ESCA, Raman spectroscopy, UV-VIS spectroscopy and colorimetric measurements. Metallic copper nanoparticles were detected throughout all of the analytical techniques, and he proposed that Cu^0 nanoparticles are the colouring agents in copper-ruby glass [29].

Although the particle sizes are larger than those of copper-ruby glass, the identification of the true colouring agent in opaque copper-red glass is complex. As with ruby-glass, the contraposition of two parts started with Pettenkofer (1856) who argued that ancient opaque red glass (called *Hematinon*) was coloured by cuprous oxide and Ebell (1874) who proposed Cu^0 as the main colouring agent of opaque red glass [1, 20].

Although Weyl agreed with Ebell's hypothesis, he did not rule out the possibility that cuprous oxide crystals and metallic copper particles can colour opaque red glass; however, each of them is the result of different chemical compositions and heat treatment procedures. He highlighted that heat-treatment in high copper and high lead glass leads to the formation and crystallisation of cuprite crystals; on the other hand, in a glass with less copper than the previous one, metallic copper precipitated during a fast-cooling phase [1].

Weyl's theory was successively confirmed in studies by Ahmed and Ashour, who investigated the effect of heat treatment in opaque copper-red glass. By using high concentrations of copper and lead (PbO 19.06 wt%; Cu_2O 14.64 wt%) in the glass and adopting a slow cooling phase (with different cooling rates) large dendritic cuprite crystals were revealed [11, 14]. With glass rich in lead and copper (PbO 19.06 wt%; Cu_2O 14.64 wt%), by increasing the iron concentration (Fe_2O_3 from 4% to 8wt%) the formation of metallic copper is favoured rather than cuprite. Crucial factors have been a specific range of temperatures (around 1000 °C) and a fast cooling phase rate, which formed Cu^0 particles not detectable under the microscope, while larger Cu^0 particles developed by prolonged heat-treatment [14].

The scientific investigation of archaeological glass from the 14th century BC to 15th century AD also helped to identify the colouring agent; however, in some cases some contradictions emerged.

Brun [9], using TEM analyses, proposed that the presence of cuprite or metallic copper depends mainly on the chemical composition of the glass. So, in high copper high lead glass ($\text{CuO} > 5$ wt%; $\text{PbO} > 15$ wt%), cuprite was detected while, in copper-red glass with moderate concentrations of copper and lead oxide, metallic copper will form [9].

These results were recently confirmed by XANES and EXAFS analyses performed on Roman orange, red and brown glass. The results confirmed that metallic copper coloured opaque red and brown glass [30, 31]; while cuprite crystals caused the colour in orange glass and Cu_2O -opaque red glass with high concentration of copper and lead [31].

Barber [32], by using TEM analyses revealed a more complex situation. Although this "rigid" distinction of the colouring agent based on the chemical composition can be helpful, it is possible to find (at least in ancient opaque red) some exceptions. Indeed, cuprite crystals were found in glass with low copper (CuO 2.8 wt%) and

lead (PbO 6.4 wt%) content, while Gedzevičiūtė [33] detected cuprite crystals in Ptolemaic opaque red by using Raman spectroscopy. The debate is still open.

2.4 Solubility and formation of metallic particles in glass, a redox affaire

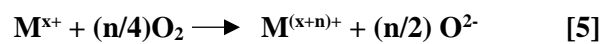
It is well known that metals are not soluble in glass, hence it is necessary to introduce copper in oxide forms such as CuO (Cu²⁺) or Cu₂O (Cu⁺) and induce the reduction of Cu²⁺ to Cu⁺ or to Cu⁰ inside the glass [34]. It is important to remember that as copper is a multivalent element, each oxidation state gives different colours. The cupric ion (Cu²⁺) gives a blue or green-blue (aquamarine) colour to the glass; the cuprous ion (Cu⁺) gives colourless glass; copper in its metallic state (Cu⁰) imparts a red and brown colour [1, 2, 34]. For this reason, reducing conditions are fundamental to obtaining red glass.

The oxidation state of polyvalent elements such as copper strongly depends on oxygen physically dissolved in the melt, (hence the oxidation state of the melt) known as the fugacity of oxygen (fO₂) or the partial pressure of the oxygen (pO₂) [35-37].

The main parameters which can modify pO₂, in the melt and necessary to take into account in this process, are: the melting temperatures, the redox state of the furnace atmosphere, the chemical composition of the base glass, and the presence or the addition of other polyvalent elements [2, 35, 36, 39, 40]. They are strictly connected, and each of them contribute to the formation of the red colour. Beyond these parameters, heat treatment can be considered a further fundamental factor in the formation of colour in ruby glass, sealing wax red and orange glass, and Cu⁰-aventurine glass.

2.4.1 Temperature

If only copper is present as a polyvalent element in the melt, it reacts with oxygen according to the following equation:



In this equation $M^{(x+n)+}$ is the oxidised ion and M^{x+} is the reduced species (n is the number of transferred electrons). The equilibrium between oxidised and reduced species is expressed by the equilibrium constant K_M according to the following equation:

$$K_M = \frac{aM^{(x+n)+} a(O^{2-})^{n/2}}{aM^{x+} (fO_2)^{n/4}} \quad [7]$$

The terms $aM^{(x+n)+}$ or aM^{x+} represent the activity of the oxidised and reduced species, and n the number of the electrons, while $a(O^{2-})$ is a constant [36]. The equilibrium constant K_M is inversely proportional to the temperature according to the equation:

$$-RT \ln K_M = \Delta G = \Delta H - T \Delta S \quad [8]$$

When the temperature increases, the values of K_M decrease favouring the reduced species. During the cooling phase the equilibrium constant K_M should increase and shift the redox equilibrium towards the oxidised species, because the temperature is lowering. This would occur by the diffusion of oxygen into the melt. However, for high viscous melts, such as soda-lime-silica glass, the diffusion of oxygen during the cooling phase is a very slow process, which can be considered an irrelevant factor for glass containing more than 0.1 wt% of polyvalent elements [36, 37, 39]. Due to the very small percentage of dissolved oxygen and the reduced oxygen activity in the melt, during the cooling phase the shift toward the oxidised species will not occur [37, 39]. This indicates that the equilibrium of the redox pair reached at the melting temperature should be the same as that in the quenched glass [37]

It is generally accepted that at the melting temperature copper is dissolved and present in the three oxidation states (Cu^{2+} - Cu^+ - Cu^0) [1, 2, 8, 22]. This phase is named the *critical melting stage*, because it is possible to affect the equilibrium among the three copper oxidation states. Through specific firing conditions, the equilibrium between Cu^+ - Cu^0 (reducing condition) or Cu^{2+} - Cu^+ (oxidising conditions) can be favoured [8, 21-23]. Indeed, several experiments showed that the higher the temperature, the lower the oxidation state [1, 2, 8, 35, 36].

Some writers have pointed out that at the melting temperature, the reducing condition necessary to cause the formation of Cu^0 should be created, allowing a further growth of the particles during the cooling phase or by a suitable re-heating [8, 21]. Other writers who disagree with this statement, explain that similar conditions have to be avoided otherwise brown or liverish red glass will be produced and not the ruby colour [22, 23].

2.4.2 Oxidation state of the furnace atmosphere

The managing of the firing condition involves the temperature and also the oxidation state of the furnace atmosphere.

The works of [21], [22], [23] [25, 26] have demonstrated how the reducing condition applied at the melting temperature causes the formation of copper-red glazes. Although they favour different types of true colouring agent, they agree that very strong reducing conditions have to be avoided because of the formation of black glaze rather than red, such as the oxidising condition which oxidises copper turning the glaze blue-aquamarine [21-26]. These redox conditions play a crucial role mainly at the melting temperature (*critical melting stage*) in which it is possible to affect the direction of the equilibrium between Cu^{2+} - Cu^+ or Cu^+ - Cu^0 [21-26].

Banerjee and Paul melted a boron-soda glass at 900-1050°C using 0.5 wt% of copper, and the $p\text{O}_2$ was obtained by mixing O_2 , N_2 , CO_2 . They established that the correct values of $p\text{O}_2$ to obtain the best ruby glass is at 10^{-14} atm. With values of $p\text{O}_2$ 10^{-13} atm the glass was green/blue, while with $p\text{O}_2$ at 10^{-15} or 10^{-17} atm the colour turned brown. They assumed that over-reduced glass causes too much metallic copper precipitation, and the glass will be brown or liverish red. However, by means of mild reducing condition, the amount of the metallic copper precipitated is irrelevant, so cuprous ions are the dominant species and the colour red is obtained [23]. A similar conclusion has been advanced by Wakamatsu by means of ESCA analyses [25-26]. The different copper oxidation states were studied at the specific firing conditions: R-R, R-O, N-O (R: reducing; O:

oxidising; N: neutral). By R-R conditions, the colour obtained is greyish blue, in which the photo peaks of Cu⁰ were detected clearly by ESCA analyses. In contrast, with the R-O firing condition red glaze was obtained, and Cu⁺ is the dominant species as shown by the photo peaks in ESCA analyses, in which Cu⁰ is very faint [25, 26].

These results highlighted that the strong reducing condition creates a high number of metallic atoms at melting temperature, which start to aggregate during the cooling phase, and continue to enlarge at the re-heating temperatures. Due to the large size of the copper particles, the glass will lose its transparency and red colour [21].

Colomban and Schreiber produced ruby glass by using alkali borosilicate with 0.25 wt% of CuO and melting them at 1150 °C for 24h. By manipulating the pO₂ they obtained an oxidised glass at air condition (pO₂: 10^{-0.7} atm), in which copper was present, 40% of copper as Cu²⁺ and 60% as Cu⁺; at the intermediate condition (pO₂: 10^{-9.6} atm), 100% of the copper was present as Cu⁺; at the reducing condition (pO₂: 10^{-14.5} atm), the copper was 70% Cu⁰ and 30% Cu⁺ [41, 42].

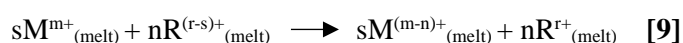
2.4.3 Base glass composition

It is generally accepted that a high concentration of network modifiers (such as soda, potash, barium oxide and lead oxide) facilitates the release of oxygen from the glass, due to the breaking of the oxygen bond and the depolymerisation of the network, causing an increase in the basicity of the melt. In this base glass, the higher valences of the polyvalent elements would be facilitated [8, 35]. In contrast, laboratory experiments have highlighted that copper does not follow this trend, and that the concentration of Cu⁺ is favoured with high content of network modifier in the base glass composition [40]. Hence, in the case of copper-containing glass a rich alkali glass would facilitate the presence of the reduced Cu⁺, which would be easier to reduce to the metallic copper. This is supported by the experiments of Stookey and Weyl who suggested that high alkali glass is better for the production of copper-ruby glass [1, 6]. Moreover, Weyl and Volf suggested that the presence of P₂O₅ (usually present in the soda-plant ash or wood-ash in the ancient glass, or added through bone ash), would improve the formation of the red colour, acting as a nucleant for the Cu⁰ particles [1, 34].

2.4.4 Interaction with another polyvalent element

Although Weyl [1] considered the aforementioned factors (temperature – base glass composition – redox condition control) enough to obtain copper-ruby glass or opaque red glass, many writers have suggested adding another polyvalent element to the batch (or to the melt) which would act as a reducing agent, facilitating the formation and precipitation of Cu⁰ particles [6, 8].

When two or more polyvalent elements are present in the melt, an interaction between them will take place according to the following equation:



The multivalent elements interacting in the redox reaction are M and R and M^{m+} is reduced to the $M^{(m-n)+}$ ion while $R^{(r-s)+}$ is oxidised to the R^+ species with transfer of n and s electrons [35].

In order to calculate the k equilibrium constant, it is possible to use the equation devised by [37]:

$$K_{MR}(T) = (K_M(T))^s / (K_R(T))^n \quad [10]$$

Because the K_M equilibrium constants of each redox couple are temperature dependent [37], K_M and K_R can be written as:

$$-RT \ln K_M(T) = \Delta G_M^0 = \Delta H_M^0 - T \Delta S_M^0 \quad [11]$$

$$-RT \ln K_R(T) = \Delta G_R^0 = \Delta H_R^0 - T \Delta S_R^0$$

So, the equilibrium constant can be written as:

$$\text{Exp}[(n\Delta H_R^0 - s\Delta H_M^0)/(R^*T)] \text{exp}[(s\Delta S_M^0 - n\Delta S_R^0/R) \quad [12]$$

At the melting temperature, the two redox pairs do not interact with each other [35]. Conversely, the two redox pairs start to interact with each other during the cooling phase, since there is no interaction with the oxygen diffusion in this phase [35, 39].

The interaction between the two redox pairs is affected by their reduction potential. The reduction potential is calculated by the standard electrode potential. Based on the reduction potential values, some elements are easier to reduce than others (table 2.1). In other words, the higher (positive) the reduction potential, the lower its reducing strength [44]. Schreiber proposed a graph made by plotting the $\log([M^{(n-m)}] / [M^{n+}])$ versus $-\log(fO_2)$ for each redox couple, a straight line with slope $n/4$ and intercept E' should be yielded, which should help to predict the oxidation state of the specific redox pair fig. 2.4 [39, 43].

Table 2.1. Standard electrode potential values calculated in the melt (E'), and in the aqueous (E^0) solution at 25°C. Data taken by Schreiber 1994.

Redox couple	E'	E^0
$\text{Sn}^{4+} - \text{Sn}^{2+}$	-5,5	+0,14
$\text{Cu}^{2+} - \text{Cu}^+$	-0,8	+0,16
$\text{Cu}^+ - \text{Cu}^0$	-3,3	+0,52
$\text{Sb}^{5+} - \text{Sb}^{3+}$	-0,3	+0,68
$\text{Fe}^{3+} - \text{Fe}^{2+}$	-1,7	+0,77

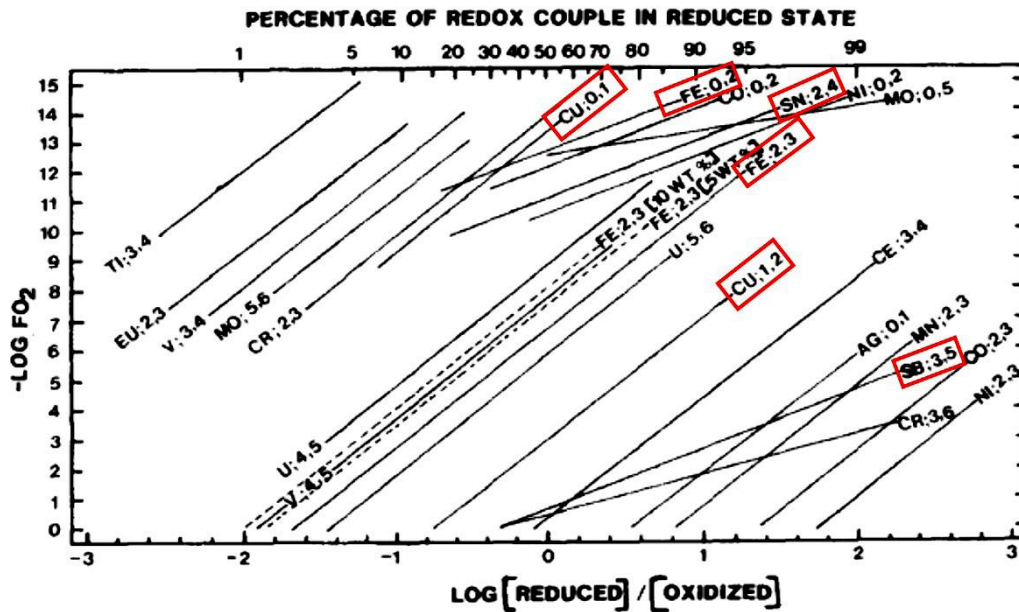
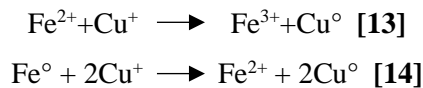


Figure 2.4 Plotted the fugacity, potential of reduction and ratio of log red/Ox at constant temperature. Picture taken from Schreiber 1986.

In the case of (ancient) copper-red glass, two main reducing agents are taken in consideration, iron and tin, because frequently encountered in the ancient opaque red. Iron is considered one of the most common reducing agent, and interacts with copper according the following redox reaction:



The equilibrium constant (K_M) of each redox couple, during the cooling phase, lowering by different rate from another redox couple [8, 39]. In this stage, the ratio value of the redox couple $\text{Fe}^{3+}/\text{Fe}^{2+}$ decreases faster than the couple $\text{Cu}^+/\text{Cu}^{\circ}$, consequently the equilibrium between $\text{Cu}^+/\text{Cu}^{\circ}$ moves towards the most reduced specie. As the temperature continue to decrease, the ratio value of the redox couple $\text{Cu}^+/\text{Cu}^{\circ}$ will continue to decrease which will saturate the melt of Cu° . When the concentration of Cu° will overcome the saturation limit in glass, Cu° particles start to precipitate. This interaction between the two redox pairs $\text{Fe}^{3+}/\text{Fe}^{2+}$ and $\text{Cu}^+/\text{Cu}^{\circ}$ will stop with the increase of the viscosity which will cause a more rigid structure of the melt, hampering further growing and formation of the particles [8, 14, 39, 45].

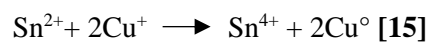
Moreover, the cooling rate could affect the interaction between the redox pairs; indeed, a fast cooling phase, could reduce the required time for the electron transfer between the redox pair (due to also for the increasing of the viscosity) hampering the complete process of redox reactions [39].

A soda-lime-lead silica glass is melted, and then kept at 1000°C , these reactions should lead to the production of Cu° -opaque red [14, 45].

Also, the formation of the Cu⁰-aventurine is mainly based on the interaction between iron and copper redox pairs. According to Tress, the discrepancies of reduction potential between Fe³⁺/Fe²⁺ and Cu⁺/Cu⁰ is not so high and in a slow and prolonged cooling phase Fe²⁺ does not reduced Cu⁺ to Cu⁰ very fast, giving enough time to the Cu⁰ atoms to precipitate and slowly aggregate to form large crystals [45].

Shcheglova [46] considered the interface tension between Cu⁰-particles and glass the driving force for the formation of Cu⁰-aventurine. In this process the amount of FeO in the glass contributes to diminish the interface tension between Cu⁰ and glass, facilitating the growth of the Cu⁰-crystals [46].

Stannous oxide (SnO) is another important polyvalent element often employed in the production of copper-ruby glass such as opaque red glass. However, the role of Sn²⁺ is not completely understood. Tress supported that tin acts mainly as reducing agent during the cooling phase according to the equation [45]:



He suggested that probably Sn²⁺ could be a buffer for the melt oxidation state by neutralizing the oxygen present in the glass. Moreover, free anions of Sn²⁺ could react with the Cu⁺ coordinated with the network structure to form new Cu⁰ particles and favour the strike of the ruby colour [8, 45].

Diwadi [24], considered Sn²⁺ mainly as a reducing agent, and the redox reaction, leading to the precipitation of Cu⁰ particles, occurs mainly during the re-heating phase. During the re-heating, the glass is not affected to the partial pressure of oxygen, so the cuprous ions (Cu⁺), coordinated with the network structure of the glass, reacts with the Sn²⁺ anions facilitating the precipitation of Cu⁰ and the consequently striking of ruby colour.

Weyl supported the hypothesis that Sn²⁺ worked not only as reductant but as *metallophilic* [1]. This term indicates that tin increases the solubility of metals (such as gold, silver, copper) and their diffusion in the glass. Tin would arrange the density of electrons in the outer shell creating a bridge between glass and metal. Brown and Volf agreed with Weyl and advanced the hypothesis that tin works like a barrier against the further crystal growth retarding the further growth of the colouring particles (Cu⁰), and avoiding their overstriking [21, 34]. According to Ram, Sn²⁺ should retard the reduction of Cu⁺ to Cu⁰ during the melting temperature. At this stage, the reduction of the redox couple Sn²⁺ to Sn⁰ is favoured rather than the couple Cu²⁺ to Cu⁺, this should retard the formation of Cu⁰ particles [22, 23]. In other words, Sn²⁺ would prolong the time of the critical melting stage, allowing the aggregation of Cu⁺ ions. Hence, the reduction of Sn²⁺ > Sn⁰ is favoured rather than Cu⁺ > Cu⁰. Ishida by means of ESCA analyses proposed that at a first stage tin reduces Cu⁺ to Cu⁰, and the Cu⁰ already formed are the centres on which the cuprous oxide will aggregate to grow as cuprite [47]. Finally, Capatina suggested that tin protects copper against the oxidation during the cooling and re-heating phase [7]. Lead oxide (Pb²⁺) should bring the same advantage of tin to increase the solubility of metals particles, however, according to Weyl high amount of lead (more than 10wt%,) are required [1, 34]. Moreover, lead oxide should be capable to maintain metals as pyrosol, avoiding the aggregation of metals under reducing conditions [6, 34]. Moreover, according to the studies of Tress, high concentration of lead help to maintain more stable copper in the cuprous state (Cu⁺), facilitating its crystallization during the prolonged heat treatment [8]. Beyond this

specific observation for copper-red glass, lead oxide improves the refractive index making more shining the colour of the glass [34].

2.5 Control of the crystallization process: heat treatment and striking

After the formation of metallic copper or cuprous ion due to the redox reaction observed above, it is necessary a careful control and managing of the precipitation of the colouring particles as well as their number and sizes to obtain coloured glass [1]. These factors depend on the control of the crystallization process which required [48, 49]:

1. the formation of stable and detectable nuclei (nucleation);
2. Crystal growth rate.

The existence of nuclei is essential, which are a periodic aggregation of atoms but with dimensions not detectable, because the crystal growth occurs. The formation of a nucleus is firstly favoured by the constantly vibration and moving of the atoms at high temperature. The atomic vibrations allow to the atoms to join at the nucleus, contributing to its growth, however, because the nucleus continues to grow it is necessary to overcome two energetic barriers [48]:

- a) the kinetic barrier, which is the energy necessary to the atoms to pass through the interface liquid-nucleus, it means to leave the surrounding environment and attach to nucleus “structure”.
- b) thermodynamic barrier which correspond to the change of free energy in the system after the formation of a nucleus. Indeed, when the atoms continue to link with the nucleus to form a cluster, this causes two main effects: the lowering of the free energy in the system, due to the presence of an ordinate structure (crystalline phase); and the increasing of the surface energy between the interface liquid-crystal.

Trough the equations which calculate the rate of nucleation¹ a bell curve is obtained, showing that the maximum of nucleation rate (a peak) occurs at temperature lower than melting temperature (usually indicate as T_m), while at melting temperature there is not nucleation [48, 49].

¹ The nucleation occurs when two energetic barriers have been overcome, which are: **kinetic barrier** ΔE_D , which represents the activation energy necessary for the atoms to cross the liquid-nucleus interface; and the second is **thermodynamic barrier (W)**, that is the net free energy change in the system after a nucleus has formed. The nucleation rate is given by:

$$I = n\nu \exp(-Nw^*/RT) \exp(-\Delta E_D/RT)$$

(**I**) nucleation rate

I = **n** ν the product between the number of atoms (**n**) and the atomic vibration frequency (**ν**):

N: Avogadro's number

R: the gas constant

T: absolute Temperature

If the nucleus is able to overcome these two barriers and reach a specific size (usually called *critical size*), it gained more stability, and the crystal growth can start.

The crystal growth strictly depends on the diffusion of the atoms to cross the interface liquid-crystal, and on the viscosity [1, 48]. As well in the nucleation, the atoms need an activation energy (called free energy of crystallization) to “jump” from one phase (liquid) to another (crystal), which is supplied by the temperature.

During the growth of the crystal, small and large crystals compete. At the beginning of the crystal growth the formation of numerous small crystals is kinetically favoured. If the thermal treatment is prolonged in time, larger crystals prevailing because thermodynamically stable. Indeed, the small crystals have large ratio surface/volume, and their external atoms are unstable and easy to dissolve in the molten glass. On the contrary the larger crystals have lower ratio surface/volume and the atoms attached to their surface encounter a solid and energetically stable. Hence, with a prolonged thermal treatment, larger crystals are favoured while small crystals dissolved in the molten glass. Around the larger crystals, an area without crystals is formed [48].

As well the nucleation, it is possible to calculate the rate of crystal growth² and a curve is obtained, which indicates that at the melting temperature no crystallisation occurs, due to the high free energy which form and dissolve them. On the contrary at temperature below the melting temperature it is possible to have crystallisation, and it shows a maximum at temperature slightly lower than T_m ; while at very low temperature viscosity will increase and the diffusion rate progressively fall, and the crystallisation will stop.

If the two curves (nucleation and crystallization) are plotted together against the temperature, it is possible to observe (fig. 2.5) that their maximum occurs at different temperatures. The maximum of nucleation rate arises at lower temperature than crystal growth. This is a fundamental information for the glassmakers (and of course for the glass scientist) because can help to control the number and size of the crystals.

² The crystallization occurs after that nucleus with critical size are formed. In this process is very important to consider how fast atoms diffuse from liquid to crystal phase. in this process is represented by $\Delta E'$, that it is the activation energy. During the nucleation there is a “jump” frequency (the number of atoms able to jump and reach the crystal phase) expressed by:

$$V_{lx} = v \exp(-\Delta E'/RT)$$

And from crystal to liquid:

$$V_{lx} = v \exp[-(\Delta E' - \Delta G_x)/RT]$$

Another factor to considering is (a), that is so, the velocity of crystallization is given by:

$$u = a v \exp(-\Delta E'/RT) [1 - \exp(\Delta G_x/RT)]$$

u: crystalline rate

a: the distance between two interfaces

v: the jump frequency (the number of atom able to jump from the liquid to crystalline phase)

ΔG_x : the free energy of crystallization

$\Delta E'$: The energy required for an atom to jump from liquid to crystalline phase

At $T > T_m$ the crystals dissolve and $\Delta G_x = 0$, so crystallization occurs when T starts to decrease and ΔG_x become negative, in this way crystallization (u) increase. When the temperatures are very low, the activation energy ($-\Delta E'$), or kinetic term [$\exp(-\Delta E'/RT)$] goes very fast to zero and the crystals growth decreases asymptotically (Varshneya).

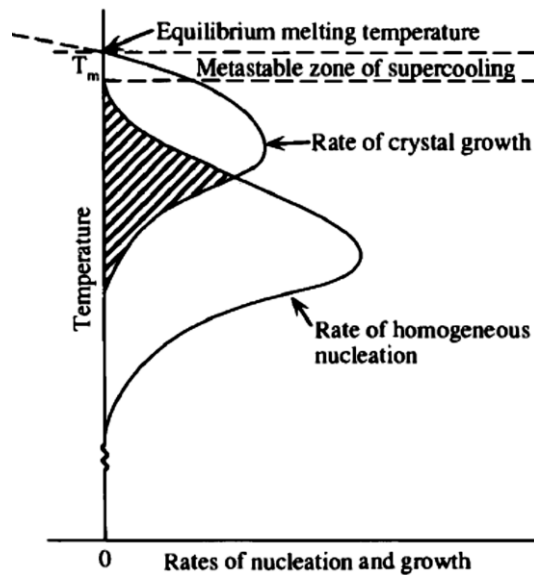


Figure 2.5. The two curves represent the two rates: Nucleation and crystal growth. Taken by Varshney, 1994.

The knowledge of these mechanisms is crucial in the manufacture of ruby-glass. It is generally accepted that the colour forms only after re-heating at a specific temperature using a specific range of time. For this reason, copper-ruby glass is classified as “striking glass”, because the colour starts to strike during the re-heating [5]. Several experiments have indicated that for the manufacture of ruby-glass, the molten glass needs a fast-cooling phase. In this way, the range of crystal growth is cut off and the glass appears colourless. As mentioned above, some writers argued that in this phase only Cu^+ is present in the glass [22, 23, 25, 47], while another group of researchers hypothesised that atoms of metallic copper are already precipitated thanks to the reducing condition at the melting temperature but are too small to colour the glass [1, 6, 8, 21, 45].

After the cooling of the melt at room temperature, the glass is subjected to suitable re-heating. Based on the chemical composition of the base glass, the temperatures can vary. However, in the literature the range of temperature used ranges between 500° and 650°C . These temperatures are often very close to the maximum nucleation rate, favouring the formation of numerous nuclei and preventing a further growth of crystals. If higher temperatures are used, the ruby colour may move towards brownish tint, or the Cu^0 (or Cu_2O) particles may oxidise to Cu^{2+} and the red colour will be lost [7].

The length of the re-heating should be long enough to produce the correct ratio, number and size of particles, to avoid losing the transparency of the glass and the intensity of the red colour. This is crucial to obtaining the correct red hues [7]. Otherwise, if further time is allowed (depending on the temperature), this may favour the growth of a high number of particles and the glass will turn brown, or the gradual oxidation of Cu^0 to Cu^{2+} could occur and the glass will turn greyish, or the transparency could be completely lost [7].

Heat treatments are necessary to obtain sealing wax red glass. Ahmed and Ashour provided fundamental information concerning the firing and cooling procedure to follow in order to manufacture sealing wax red glass [11, 14]. They used high concentrations of copper (CuO 14.64 w%) and lead (PbO 19.06 wt%). Moreover, after identifying the maximum temperature of the nucleation (500°C) and of the crystal growth (850°C) (in this type of glass), they manipulated the rate of cooling or heating. The high concentration of lead

should be helpful to increase the solubility and diffusion of the particles, and reduce the viscosity at lower temperatures, allowing the arrangement of atoms in a crystalline structure. The high concentration of copper is used to encourage the “supersaturation” of cuprous oxide in the glass, which exceeds its solubility limit (12wt%) [11].

When the melt was kept at 500°C, small cubic octahedral crystals of cuprous oxide (5 µm) formed which impart a yellowish colour to the glass. At temperatures of between 500-700°C, the crystals continue to grow and the glass becomes orange. Using temperatures higher than 700°C, dendritic crystals of 150 µm are obtained which give a bright red colour to the glass [11].

The formation of these crystals is based on supersaturation and the coarsening mechanism³. If the cuprous oxide surpasses its solubility limit in the melt, it will dissolve at melting temperature, but during the cooling phase it will separate from the melt. The growth of the crystals follows the coarsening mechanism, in which the nuclei that have reached and overcome a critical radius will continue to grow, while those smaller will dissolve in the molten glass [50]. The dissolved cuprous oxide of the smaller crystals will transfer to the larger ones which continue growing. This is considered the driving force of the coarsening mechanism. Through this mechanism and due to the prolonged heat treatment at high temperature (850 ° - 1000°C), the crystals assume their dendritic shape [11].

However, several failures occurred in manufacturing this glass, and heterogenous glass usually of three layers with different colours were obtained in their experiments. On top is a black layer, below this is a green layer corresponding to the oxidised glass in which no cuprous crystals were detected. Below these two layers, cuprous oxide crystals were detected which showed progressive enlargement from the top to the bottom of the crucible (from orange to red).

Also highlighted by Tress [45], the results mentioned above show that controlling the reducing condition is still the core of red glass production. Indeed, the different oxidation states of the melt can encourage (or not) the correct development of the crystallisation [45].

Cable and Smedley advanced the use of antimony or crushing the glass several times in order to increase the homogeneity of the glass [51].

The Cu⁰-opaque red apparently does not need a specific heat treatment or prolonged cooling phase. A well-engineered chemical composition guarantees the correct reducing condition in the molten glass, to cause the precipitation of Cu⁰ particles during a fast-cooling phase, and the glass should turn red. Otherwise, throughout the prolonged cooling phase, larger particles of Cu⁰ are formed and the glass turns from brownish red to a dark brown colour. In contrast, when the molten glass is cooled to room temperature very slowly, and by a gradual decrease in the temperature (at a very low rate), it is possible obtain aventurine glass [1].

³ Coarsening, also called Ostwald ripening or competitive growth, occurs where large particles grow at the expense of small particles. To better understand this process, a dispersion of solid particles in a matrix has to be considered. In this case, an interfacial area is created between the solid particles and the matrix, which increases the overall energy of the entire system (solid particles and matrix). The system will attempt to minimize the energy, and it will reach this goal by reducing the interface energy, which decreases with time. Usually, a single large particle has less interface area than a large number of smaller particles occupying the same volume. Thus to minimize the energy, the system will favour the formation, with prolonged time, of fewer large particles rather than a high number of small particles, since the excess energy associated with the interface is reduced [50].

Indeed, keeping the molten glass for several hours at a temperature of about 1000° C and then gradually lowering it, the low viscosity of the glass allows the diffusion of the Cu° atoms which can aggregate and form triangular or hexagonal flakes of crystals [14, 45]. In some experiments, the suggestion was to leave the melt at 900°C and 800°C for several hours before switching off the furnace for a spontaneous cooling of the molten glass in the crucible [14, 45]. During this phase, a green glass should form, due to the high concentration of iron oxide in the glass, and Cu° particles would aggregate, favouring the growth of the larger crystals rather than the smallest ones [14, 45]. As for sealing wax red glass, in this case the chemical composition and the control of the redox condition also play a crucial role for the best results of the heat-treatment. The presence of iron (Fe²⁺) would cause the formation of Cu° particles and their growth in size [14, 47]. In this case, iron is not only a reducing agent, but as mentioned above it would decrease the interface tension glass-Cu° particles, favouring crystalline growth [47]. However, too much iron content creates too many reducing conditions, and the lack of enough oxygen to dissolve metallic iron and Cu° particles could cause the formation of large metallic inclusions in the glass [14].

References

1. Weyl, W.A. Copper in copper-ruby glasses (Hematinone and copper aventurine). In *Coloured Glasses*; Society of Glass Technology: Sheffield. UK. 1951, pp. 420-432; ISBN 9780900682063.
2. Bamford, C.R. Colouration by colloidal particles. In *Colour Generation and Control in Glass*; Elsevier Scientific Publishing Company: Amsterdam, The Netherlands, 1977; Volume3, pp. 90-98, ISBN 1520-6378.
3. Navarro J.M.F. Vidrios coloreados por cromoforos en estado colloidal o microcristalina. *El vidrio: constitución, fabricación, propiedades*, 3rd ed.; Consejo Superior de Investigaciones Científicas, Instituto de Cerámica y Vidrio, Madrid, 2003, pp. 460-463, 473-475.
4. Doremus, R.; Kao, S.C.; Garcia, R. Optical absorption of small copper particles and the optical properties of copper. *J. Applied optics* **1992**, 30 (27), 5773-5778.
5. Vogel, W. Glass colored by metal colloids (Ruby glass). *Glass Chemistry*, Springer-Verlag Berlin Heidelberg 1994, pp. 246-249.
6. Stookey, S.D. Coloration of glass by gold, silver and copper. *J. Am. Ceram. Soc.* **1949**, 32 (8), 246-249.
7. Capatina, C. The study of copper ruby glass. *Ceram. Silikàty* **2005**, 49, 283–286.
8. Tress, H.J. Ruby glass and related glasses from standpoint of the chemical potential of oxygen in glass. Part 1. Physics and Chemistry of Glasses. *Glass Technol.* **1962**, 3, 28–36.
9. Brun, N.; Mazerolles, L.; Pernot, M. Microstructure of opaque red glass containing copper. *J. Mater. Sci. Lett.* **1991**, 10, 1418–1420.
10. Zecchin L. Avventurina, lattimo e altri vetri. In *Vetro e vetrai di Murano*. Arsenale Eds.; Venezia, 1987, pp. 327-336.
Paolo Zecchin, La pasta venturina, vetro speciale muranese, *J. Glass Stu.* **2005**, 47, 93-106
11. Ahmed, A.A.; Ashour, G.M. Effect of heat treatment on the crystallisation of cuprous oxide in glass. *Glass Technol.* **1981**, 22, 24–33.
12. Turner W.E.S. Glass Fragments from Nimrud of the Eighth to the Sixth Century B.C. *Iraq*, **1955**, 17 (1), 57-68.
13. Hughes, M.J. A technology study of opaque red glass of the Iron Age in Britain. *Proc. Prehist. Soc.* **1972**, 38, 98–107.

14. Ahmed, A.A.; Ashour, G.M.; El-Shamy, T.M. The effect of melting conditions on the crystallization of cuprous oxide and copper in glass. In *Proceedings of the 11th international Congress of Glass. Prague. Czechoslovakia. 4–8 July 1977*; pp. 177–187.
15. Nagao, H.; Misonou, M.; Kawahara, H. Mechanism of Coloration in Copper-Stained Float Glass. *J. Non-Cryst. Solids* **1990**, *120*, 199–206.
16. Kelly, K.L.; E.Coronado, Zhao, L.L., Schatz, G.C. The Optical Properties of Metal Nanoparticles: The Influence of Size, Shape, and Dielectric Environment, *J. Phys. Chem. B* **2003**, *107*, 668–677.
17. Quinten, M. The color of finely dispersed nanoparticles, *Appl. Phys. B* **2001**, *73*, 317–326
18. Baltă P., Căpărină C., Baltă E.: *Proceedings of the XIIth International Conference Chemistry and Chemical Engineering*, p. 210-215, Bucharest 2001.
19. Johnston. W.D., Chelko, A. Oxidation-Reduction Equilibria in Molten $\text{Na}_2\text{O}_2\text{SiO}_2$, Glass in Contact with metallic Copper and Silver, *J. Am. Ceram. Soc.*, **1966**, *49* (10), 562-564.
20. Beyersdorfer, P. Studien ueber das Aventuringlas. *Glastechnische Berichte*, **1943**, *21*, 1-7.
21. Brown, S.F; Norton, F.H. Constitution of copper-red glaze. *J. Am. Ceram. Soc.* **1959**, *42* (11), 499-503.
22. Ram A.; Prasad S.N.; Srivastava K.P.; Prasad S.S. On the role of tin in copper ruby glass. *Transaction of the Indian Ceramic Society* **1970**, *29* (2), 35-40.
23. Banerjee S.; Paul, A. Thermodynamics of the system Cu-O and Ruby formation in borate glass. *J. Am. Ceram. Soc.* **1973**, *57* (7), 287-290.
24. Dwivedi, R.N.; Nath, P. Mechanism of red colour formation in photosensitive and normal copper-ruby glasses. *Transaction of the Indian Ceramic Society* **1980**, *39* (1), 23-28.
25. Wakamatsu, M.; Takeuchi, N.; Ishida S. Effect of heating and cooling atmospheres on colors of glazes and glass containing copper. *J. of Non-Crystalline Solids*. **1986**, *80*, 412-421.
26. Wakamatsu, M.; Takeuchi, N.; Nagai, H.; Ishida S. Chemical states of copper and tin in copper glazes fired under various atmospheres. *J. Am. Ceram. Soc.* **1989**, *72*, 16-19.
27. Nakai, I.; Numako, C.; Hosono, H.; Yamasaki, K. Origin of the red colour of Satsuma copper-ruby glass as determined by EXAFS and optical absorption Spectroscopy. *J. Am. Ceram. Soc.* **1999**, *82*, 689–784.
28. Padovani, S.; Sada, C.; Mazzoldi, P.; Brunetti, B.; Borgia, I.; Sgamellotti, A.; Giulivi, A.; D'Acapito, F.; Battaglin, G. Copper in glazes of Renaissance luster pottery: Nanoparticles, ions, and local environment. *Appl. Phys.* **2003**, *93*, 10058–10063.
29. Torun Bring, *Red Glass Coloration. A Colorimetric and Structural Study*, PhD Thesis.
30. Arletti, R. Roman coloured and opaque glass: a chemical and spectroscopic study. *Appl. Phys. (A)*, **2006**, *83*, 239–245.
31. Silvestri, A.; Tonietto, S.; D'Acapito, F.; Molin G. The role of copper on colour of palaeo-Christian glass mosaic tesserae: An XAS study. *J. Cult. Herit.* **2012**, *13*, 137–144.
32. Barber, D.J.; Freestone, I.C.; Moulding, K.M. Ancient copper red glasses: Investigation and analysis by microbeam techniques. In *From Mine to Microscope. Advances in the Study of Ancient Technology*; Shortland, A.J., Freestone, I.C., Rehren, T., Eds.; Oxbow Books: Oxford, UK, 2009; pp. 115–127, ISBN 978-1-84217-259-9.
33. Gedzeviciute, V.; Welter, N.; Schüssler, U.; Weiss, C. Chemical composition and colouring agents of Roman mosaic and millefiori glass, studied by electron microprobe analysis and Raman microspectroscopy. *Archaeol. Anthropol. Sci.* **2009**, *1*, 15–29.
34. Volf. M.B. Copper. In *Chemical Approach to Glass*; Elsevier Science Publishing Company Inc.: Amsterdam. The Netherlands. 1984; Volume 7, pp. 477-484 ISBN 0-444-99635-4.
35. Schreiber, H.D. Redox processes in glass-forming melts. *J. Non-Cryst. Solids* **1986**, *84*, 129-141.

36. Chopinet, M-H., Lizarazu, D., Rocanière C. L'importance des phénomènes d'oxydo-réduction dans le verre, *Academie des Sciences. Comptes Rendus. Chimie*, **2002**, 5 (12), 939-949.
37. Kido, L., Muller, M., Russel, Ch. Redox reactions during temperature change in soda-lime–silicate melts doped with copper and iron or copper and manganese, *J. Non-Cryst. Solids* **2006**, 352, 4062–4068.
39. Paul, A. Effect of thermal stabilization on redox equilibria and colour of glass. *J. Non-Cryst. Solids* **1985**, 71, 269-278.
40. H.D. Schreiber, Mary E. Stokes, Amy M. Swink, Using additives for color control in copper-containing glasses. In *Advances in Fusion and Processing of glass III*, James R. Varner, Thomas P. Seward III, Helmut A. Schaeffer Eds; Vol. 141, 2006, pp.315-322.
41. Colomban, P.; Schreiber, H.D. Raman signature modification induced by copper nanoparticles in silicate glass. *J. Raman Spectrosc.* **2005**, 36, 884-890.
42. H.D. Schreiber, Stone, M., Amy A., Swink, M. Novel red–blue dichroic glass containing copper nanocrystals. *J. Non-Cryst. Solids* **2006**, 352, 534–538.
43. Schreiber, H.D., Wilk Jr, N.R., Schreiber, C.W. A comprehensive electromotive force series of redox couples in soda-lime-silicate glass. *J. Non-Cryst. Solids* **1999**, 253, 68-75.
44. Schreiber, H.D., Kochanowski, B.K., Schreiber, C.W., Morgan, A.B., Coolbaugh, M.T., Dunlap, T.G. Compositional dependence of redox equilibria in sodium silicate glasses. *J. Non-Cryst. Solids* **1994**, 177, 340-346
45. Tress, H.J. Ruby glass and related glasses from standpoint of the chemical potential of oxygen in glass. Part 2. Gold and copper glasses. *Glass Technol.* **1962**, 3, 95–106.
46. Shcheglova M.D.; Babenko, T.V.; Polonzhai, S.G.; Svistun, V.M. Mechanism of aventurine formation in copper-containing alkali-lead silicate glass. *J. Glass and Ceramic* **1996**, 53 (1-2), 14-17.
47. Ishida, S.; Takeuchi, N.; Hayashi, M.; Wakamatsu, M. Role of Sn²⁺ in development of red colour during reheating of copper glass. *J. Non-Cryst. Solids* **1987**, 95, 793–800.
48. Varshneya Arun K. The kinetic of glass formation. In *Fundamental of Inorganic glasses*, Published Elsevier, 1994, pp. 43-58.
49. Shelby James E. Kinetic theories of glass formation. *Introduction to glass science and technology*. 2nd ed.; Publisher: Royal Society of Chemistry; 2005, pp. 11-20.
50. Ratke, L.; Voohees, P.W. Coarsening: Basics and Laws. In *Growth and Coarsening. Ostwald Ripening, in Material Processing*, 1st ed.; Springer: New York, NY, USA, 2002; pp. 117-123 ISBN 978-3-642-07644-2.
51. Cable. M.; Smedley. J.W. The Replication of an opaque red glass from Nimrud. In *Early Vitreous Materials; British Museum Occasional Paper 56*; Bimson. M., Freestone. I.C. Eds.; British Museum: London. UK. 1987; pp. 151–164. ISBN 978-0861590568.

When studying the history of glassmaking, one must resist the temptation to oversimplify by adopting too many magic moments and believing that they revolutionized technology simultaneously wherever glass was being made... Different people did things in different ways, and whether or not they changed their ways depended upon cultural factors as well as upon practically. (pag. 22- Brill 1988)

3. The history of opaque red glass across the centuries

3.1 Identification of the types of opaque copper-red glass produced in ancient times

Klaproth (1798) was the first to study opaque red glass through scientific investigation and attempt to identify the colouring agent. He studied one opaque red tessera from Pompei, and some decades later Mercanton (1824) studied a red tessera from Canopus (Egypt). They concluded that ancient opaque red glass was produced essentially by a high concentration of copper (CuO 6.5-13.1 wt%) and lead (PbO 13.0 – 35.7 wt%) [1]. Their first studies were limited by their analytical equipment (which was not able to identify the entire chemical composition of the glass) and by a partial archaeological contextualisation.

In 1857 Pettenfork published “*Ueber einen antiken roten glasfluss (hamatinon) und über das aventurin-glas*”, in which he tried to highlight the main features of ancient opaque red glass until aventurine glass. He selected the samples more rigorously, collecting and analysing opaque red glass from well dated archaeological sites such as Pompei, and described the red hues of the glass as “between cinnabar and red lead”. Moreover, using a microscope with a magnification of 200 he studied the structure of the glass, identifying red crystals embedded in a “clear” glass matrix, which are cuprous oxide. The opaque red glass analysed by him was rich in copper (CuO 11.3 wt%) and lead (PbO 15.5 wt%) too [1].

In 1893 Ball published “*On a block of red glass enamels said to have been found at Tara Hill*”, that represented the first evidence of ancient opaque red glass outside the Mediterranean area. A sort of cake was buried in a slope of the northern portion of ditch of Caelchu at Tara Hill (Ireland). Although this discovery suggested local production, Ball with the chemical analyses of Reynold revealed a Mediterranean provenance for this block of red glass. Indeed, the base glass turned out to be a soda-lead glass and did not show evident compositional differences from other Roman glass. The analyses revealed 32.8 wt% of lead and 9.8 wt% of copper; moreover, the presence of “opaque red particles” in a “transparent yellow glass”, described by Ball, is similar to the pervious opaque red glass studied by Pettenfork [1].

At the beginning of the 20th century, Kotyga analysed a flat rectangular piece of red glass from Tell el-Amarna (14th century BC), belonging to the Berlin Museum, and revealed 12 wt% of copper but no lead was detected (probably below the detection limit). Samples dated to the 2nd century BC from the Island of Elephantine, analysed by Kotyga, showed concentrations of copper ranging between 2.1 wt% and 4.4wt%, and lead content between 1.28 and 6.28 wt% [2].

In the second half of the 20th century, the improvement in analytical techniques, the discoveries of important archaeological evidence and a more systematic approach in the studies of ancient glass helped explain the production technology of glass from the Late Bronze Age until the Byzantine period.

In 1952, through the excavation of the Burnt Palace of Nimrud, Mallowan found in room n° 23 an ingot of opaque red glass with “*bronze alloy, magnetic iron oxide mixed with lead alloy and ferric oxide, a cake of iron oxide, siliceous materials and charcoal*”, which was dated as between 8th – 6th century BC [3]. This round cake (16.5 cm dia, and 3.8 cm thick), was analysed by Turner, who detected 13.1 wt% of copper and 22.8 wt% of lead oxide, and established that cuprous oxide is the main colouring agent (Cu₂O). This type of opaque red was called sealing wax, due to its intense red colour. This discovery was of fundamental importance because it should have attested the intentional use of lead oxide in the glassmaking industry to at least around the 8th century BC [4].

Nevertheless, Turner argued that lead oxide was introduced into Egypt during the 18th dynasty (1500 BC), since chemical analyses on opaque red glass, thought to be from Tell el-Amarna samples (14th century BC), revealed high lead oxide content [4]. This was criticised by Arkell who explained that the sample analysed by Turner was misdated. Turner acknowledged the misdating of the sample but continued to support the idea that lead oxide was introduced in the 14th century BC in Egypt [3, 4].

Hughes analysed 33 artefacts of opaque red glass stored in the British Museum and Colchester Museum dating from between the 1st century BC and 2nd century AD and found in Britain [5]. The chemical analyses revealed concentration of copper from 5.5 up to 8.5 wt%, and lead from 18 up to 35 wt%. Moreover, it observed “*red feathery crystals*” thought to be the colouring agent. These data were compared with the chemical composition of the sealing wax red glass previously analysed and dated to the late Iron Age, revealing strong similarities. This led Hughes to establish that the glass used between the 1st century BC and 2nd century AD in Britain was sealing wax red glass. Like Ball (1893), Hughes disagreed with the hypothesis of the local production of sealing wax red glass, suggesting that it was manufactured in the eastern Mediterranean area [5]. Indeed, based on the lead isotopic values reported by Brill, it was possible to indicate Italy (Naples) or Egypt (Alexandria) as probable manufacturing centres of sealing wax red glass [6].

Moreover, Hughes analyses Roman opaque red tesserae, dated to the 1st and 2nd centuries AD, detecting concentrations of copper usually lower than 3 wt%, and variable amounts of lead from 0.07 up to 13.5 wt%, which are similar to the copper and lead content detected by Kotyga in opaque red dated to the 2nd century BC from the Isle of Elephantine and Salona (Dalmatia) [2]. In these opaque red glasses, no “*feathery crystals*” of cuprous oxide were observed, and Hughes proposed the presence of Cu^o particles as the colouring agent. They can be identified as red brown glass, which is considered less brilliant or duller than sealing wax red glass.

Through these data, there was evidence of the co-existence of two types of opaque red glass in the Mediterranean area between the 2nd century BC and 2nd century AD, distinguished by different chemical compositions and two different colouring agents. Hughes advanced the hypothesis that red brown took the place of sealing wax during the Roman Age, since lower amounts of metals (lead and copper) and fuel were required, making high quantity production of opaque red glass [5] economically more advantageous.

According to Bimson [3] in the mid-2nd millennium, an opaque red glass containing 6-8 wt% of CuO and negligible amounts of lead was produced in Egypt, and it was coloured by cuprous oxide, exhibiting a liverish or dark red. This was confirmed by his analyses performed on samples from Alalakh (15th century BC) and Tell el-Amarna (14th century BC) and stored in the British Museum. He posited the introduction of lead into glassmaking between the 8th-6th century BC in the Near East rather than in Egypt, which was supported by the chemical analyses on a sample from Toprakkale (8th-6th century BC). This dismantled the affirmation of Turner, who argued that lead oxide had been used in glassmaking since the 14th century BC. Indeed, Bimson observed that in the Tel el Amarna sample (analysed by Turner) negligible amounts of lead were detected [3]. During the first millennium BC, this dull opaque red continued to be manufactured, but with lower amounts of copper (lower than 4wt%) than the earlier types and with small amounts of lead, which was used in glass mosaic or *millefiori* glass. The colouring agent of this new opaque red was not specified. Contemporaneously, a new opaque red glass, known as high copper high lead, was produced with a sealing wax red hues and used for mould inlays and other small objects, or enamels, and as a substitute for jasper stone, or to make small bowls and dishes [3].

A well detailed scientific investigation and an exhaustive comparison of opaque red glass from different ages were provided by the works of Freestone [7] and Brill [8], showing the main differences in the chemical composition and colouring agent. Freestone was mainly focused on the glass from the 15th century BC until the 4th century BC, while Brill covered a wider time span from the 14th century BC until the 12th century AD. Both concluded that lead oxide started to be used around the 9th-6th century BC in Mesopotamia and not in Egypt. Moreover, the copper (CuO) and lead (PbO) content were used by Freestone to distinguish three main opaque red types, giving an important contribution to understanding the technical aspect of opaque red glass manufacture: a) high copper (3-12 wt%) – no lead; b) high copper (CuO >5 wt%) – high lead (PbO > 15 wt%) (sealing wax); c) low copper (CuO < 5 wt%) – low lead (PbO < 15 wt%) (red brown). These categories cover different periods: high copper– no lead was produced during the Late Bronze Age (14th – 10th century BC); high copper – high lead started to be manufactured around the 8th century BC until the 1st century AD; finally, low copper – low lead was the main opaque red produced during the Roman and Byzantine Age. However, Freestone is aware that these borders, both date and chemical composition, are too rigid and must be considered artificial, since the transition period occurred from one type of opaque red to another, and several “anomalies” in the chemical composition have been detected [7].

Brill thought that copper was introduced through a compound which could dissolve easily and rapidly in the molten glass [8]. Similar material could be copper alloy, bronze, brass scale which contained lead, tin and zinc in different concentrations. Hence, the analyses would reflect the composition of the bronze, brass or copper alloy produced in that region at that time [8, 9]. This hypothesis could explain the presence of arsenic in copper-red glass, which could be linked with the use of arsenical bronze as a copper source [8, 9].

Freestone highlighted the presence of different colouring agents among the three types of opaque red glass. Well-developed dendritic crystals of cuprite (Cu₂O) were detected in the samples of high copper-no lead and in the sealing wax red glass, while metallic copper was probably the colouring agent in the red brown samples

[7]. Brill argued that the ancient opaque red glass “*invariably contain cuprite and sometimes metallic copper*”, and due to the very small sizes they are difficult to *distinguish under microscopic magnification* [8].

Clearer identification of the nature of the colouring agent in the three types of opaque red has been proved by more recent scientific investigations both in the glass science and archaeometric fields. Brun analysed Celtic opaque red glass [10] classified as sealing wax and Roman opaque red glass (red brown) [11]. By means of TEM analyses they detected two different colouring agents: cuprite crystals in sealing wax (confirming the results of Freestone), and sub-micrometric metallic copper particles in the red brown type [11]. These results were progressively confirmed by further scientific investigations which indicated the main colouring agent for the three types of opaque red. High copper-no lead is generally coloured by dendritic cuprite crystals [7, 12]; however, Cu⁰ particles were revealed through TEM analyses in one sample from Amarna (14th c. BC) [13]. Dendritic crystals of cuprite are the colouring agent in sealing wax and orange glass [7, 8, 10, 11, 14-17]. In contrast, red brown is mainly coloured by sub-micrometre metallic copper particles [11, 13, 16, 17].

In fig. 3.1 the chronological timeline from the 14th century BC until the 4th century AD attempts to summarise and highlight the main steps in the development of opaque red glass production. Due to the comparable chemical composition of Roman red brown (Cu⁰-opaque red) glass with Medieval opaque red glass, the timeline stopped at the 4th century AD. Further details in paragraph 3.3.

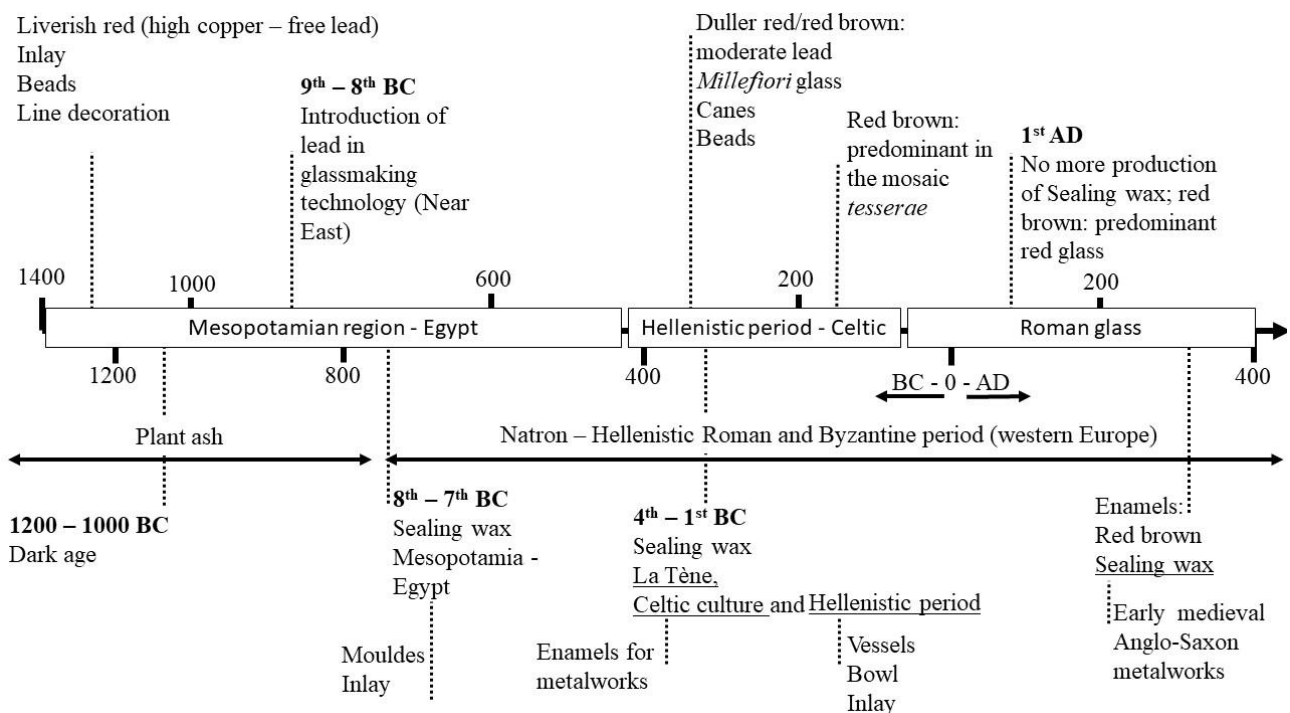


Figure 3.1. Chronological timeline of the production of opaque red glass.

3.2 Types of opaque copper-red glass through the analytical data reported in the literature

Analytical data were collected from the archaeometric investigations found in the literature, which provide useful information to describe the ancient opaque red glass produced from the 15th century BC until the 13th century AD. Orange glass and aventurine glass have been added to this list, because they are considered a special type of opaque copper-red glass.

Through the collection of archaeometric studies, some critical points have emerged which could be helpful to explain before beginning with the description of the single types of opaque copper-red.

The total number of chemical analyses collected in this research is 746, performed by EPMA, LA-ICP-MS, SEM-EDS, XRF, ICP-MS. A considerable number of these analyses could be considered “routine analyses”, in which the red glass represented one of the coloured glasses (tesserae, beads or fragments) studied in that scientific investigation. In these cases, it was not possible to explore technical aspects concerning the production technology of opaque red or characterise in detail the colouring agents. However, they are of extreme importance in obtaining a view on the changes occurring in the chemical composition of opaque red glass and make it possible to identify transition periods. Nevertheless, in the literature are studies which analyse opaque red glass from an archaeological and scientific point of view, providing fundamental details on the colouring agents and the manufacture of opaque red. In the meantime, they shed light on the probable raw materials and the probable recipes [7, 15, 17-33].

Notwithstanding the large number of chemical analyses, some of them are uncompleted, especially in the analyses carried out before the first half of the 20th century, many elements were missed in the composition of the glass. Probably due to the detection limit of the analytical methods used, the following minor and trace elements are frequently missed: TiO₂, P₂O₅, BaO, SrO, ZrO₂, ZnO. In the analyses reported by [18], MgO was not detected. In the sealing wax red glass analysed by [10] SnO₂ and Sb₂O₃ content were not revealed.

The analysis of colour, which makes it possible to identify different red hues that could be related to a specific chemical composition or production technique, was measured by colorimetry or FORS only in a few studies, and only in recent decades have scholars included this aspect more frequently in their studies [17, 19, 20, 32-35]

In [fig. 3.2](#), the three types of copper-red glass are reported, obtained by using the analytical data collected from the literature and by using the value ranges of copper and lead, proposed by [7]. Orange glasses have been included in this graph.

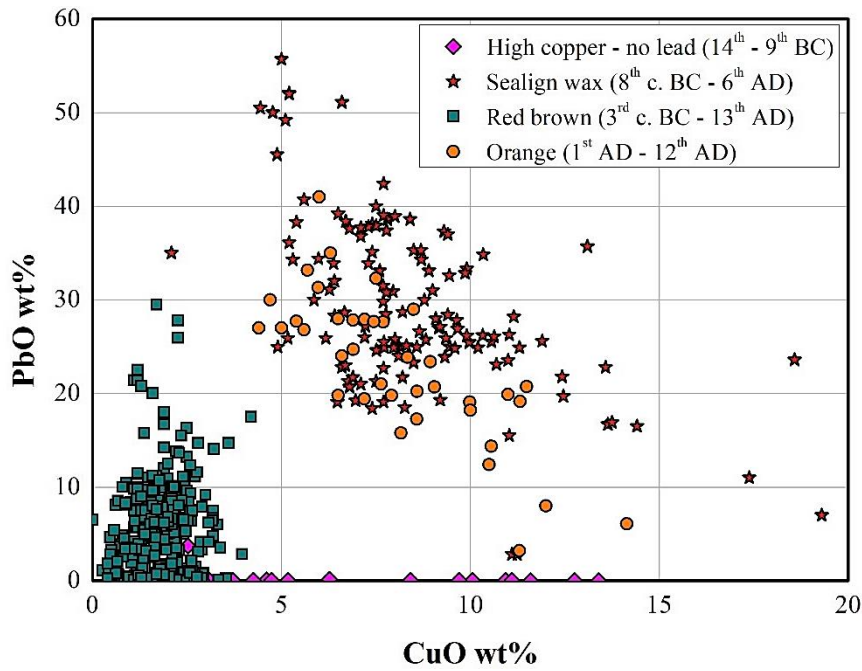


Figure 3.2. Binary graph with weight % of lead oxide (PbO) versus copper oxide (CuO). Opaque red and orange glass dating from the 14th century BC to 13th century AD.

These four copper-red glasses (and aventurine too) will be discussed in detail and separately, later in the text, to explain the main features of their chemical composition, their use and colouring agent.

3.2.1 High copper – no lead (14th – 9th centuries BC)

3.2.1.1 History and use

This category can be considered the earliest type of opaque red glass. It was produced in ancient Egypt and in the Mesopotamian region between 1500 and 1200 BC (table 3.1-3.2). A set of 22 samples, 15 from Egypt (Lisht, Tell el-Amarna, Alalakh, Malkata) dating between 1500 and 1200 BC, represents the early opaque red glass. Moreover, two samples (Sardis, and Egypt) dating from the 7th and 6th century BC, were identified as high copper no lead by Brill [8] and included in this category.

In this category, 6 samples from Frattesina (Italy) dating between the 11th and 9th centuries BC are included, although the concentration of copper does not exceed 5 wt%.

Table 3.1. The number of samples with the respective date and location.

Site	century	n.	Reference
Alalakh (Egypt)	15 th BC	2	7
Amarna (Egypt)	14 th BC	6	7, 8, 36
Lisht (Egypt)	13 th BC	3	8
Qantir (Egypt)	13 th BC	2	12
Frattesina (Italy)	11 th -9 th BC	6	37, 38, 39
Lisht (Egypt)	7 th -5 th BC	1	8
Sardis (Lydian Reign)	6 th -5 th BC	1	8

Table 3.2. References of the analyses

References	
7	Freestone 1987
8	Brill et al., 1988
12	Rehren, 1997
36	Shortland et al. 2006
37	Brill, 1992
38	Santopadre et al. 2000
39	Angelini et al., 2004

Opaque red glass from the Near East and Egypt (fig. 3.3) was used to manufacture inlays and beads, or to substitute cornelian or jasper stone in the creation of jewellery, but not for core-formed vessels [3]. It was probably produced in limited numbers as luxury items for people of high status.



Figure 3.3. Inlay head of Egyptian opaque red glass, 14th century BC. Image taken from Stern 1994.

The archaeological evidence from Frattesina suggests that opaque red glass was mainly used to make beads (fig. 3.4).



Figure 3.4. Opaque red bead from Frattesina (picture from Santopadre et al., 2000).

3.2.1.2 Chemical composition

The samples from Alalakh (15th century BC), Amarna (14th century BC), and from Qantir (table 3.3), are characterised by magnesia content oscillating between 2.2 wt% - 5.5 wt% and potash varying between 1.6 wt% - 2.8 wt%, while sodium content ranges between 15.5 – 21.9 wt%. These values are probably due to the use of soda plant ash as a fluxing agent [40].

The concentration of copper is higher than 4 wt% (CuO 4 wt% – 13.7 wt%) and only a few exceptions have copper content varying between 2.5 wt% and 3.5 wt% [12, 36]. The content of antimony is not constant, and usually varies between 1.1 wt% and 3.8 wt%; however, in some samples it is lower than 1 wt% or not detected. In most of the glass, the iron concentration is usually lower than 1 wt%, while in two samples from Alalakh it is 3.5 wt% [7] and in one sample from Malkata it is 1.9 wt% [36].

Table 3.3. Average chemical composition in wt % of the 17 samples from the near east regions.

		SiO ₂	Al ₂ O ₃	Na ₂ O	K ₂ O	CaO	MgO	P ₂ O ₅	TiO ₂	Fe ₂ O ₃	MnO	Sb ₂ O ₃	SnO ₂	CuO	PbO
Egypt	Av.	59.8	0.8	16.1	2.0	7.1	3.7	0.27	0.10	0.89	0.10	1.5	0.29	7.0	0.37
	St.D.	5.7	0.6	4.3	0.5	1.5	1.0	0.22	0.06	0.90	0.18	1.0	0.31	4.1	1.06

In the samples from Frattesina, the concentration of potash is higher than the previous group, and ranging between 9.1 wt% and 12.7 wt%, while magnesia varies between 0.57 – 1.7 wt% and sodium between 4 and 7.4 wt%. They could be classified as LMHK glass, indicating a mixed alkali as fluxing agent, as supported by [37, 41]. The copper content is lower than the previous group and varies between 1.5 and 4.5 wt%, while antimony oxide is about 0.02 wt% and iron is lower than 1 wt% (table 3.4).

Table 3.4. Average chemical composition in wt % of the 6 samples from the site of Frattesina.

Site	Oxide	SiO ₂	Al ₂ O ₃	Na ₂ O	K ₂ O	CaO	MgO	P ₂ O ₅	TiO ₂	Fe ₂ O ₃	MnO	Sb ₂ O ₃	SnO ₂	CuO	PbO
Frattesina	Av.	73.5	2.5	5.7	10.6	2.0	0.8	0.1	0.1	0.92	0.0	0.01	0.4	3.1	0.001
	St.D.	3.2	1.9	1.2	1.4	0.3	0.4	0.0	0.1	0.8	0.0	0.01	0.1	0.9	0.01

From these data emerged the coexistence of two different production technologies for the opaque red glass during the Late Bronze Age characterised by different fluxers and colouring techniques. In (fig. 3.5) the concentration of K₂O and MgO indicate the use of soda-plant ash the glass produced in the Near East area, and a mixed alkali for the samples from Frattesina.

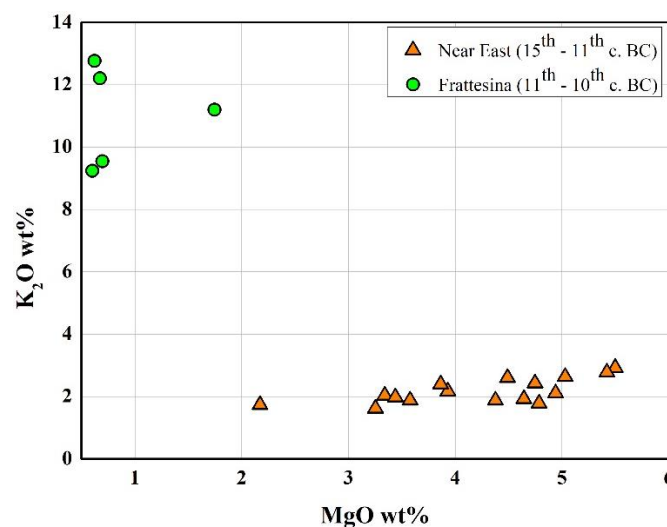


Figure 3.5. Binary graphs reporting the weight % of the reduced composition of potash (K₂O) content versus magnesia content (MgO).

Furhtemore, the concentration of antimony detected in the Egyptian samples (Amarna and Alalakh) suggests an intentional addition of some antimony-bearing, however it is still unclear if antimony was added as a

reducing agent, opacifier or was present in the colourless base glass. In contrast, antimony seems not to be used to make opaque red in the samples from Frattesina.

3.2.1.3 The colouring agent

The colouring agent of the opaque red from Alalakh (15th century BC), Amarna (14th century BC), and Qantir is represented by dendritic cuprite (Cu_2O) crystals about 10 μm as attested by the SEM-EDS analyses performed by Freestone [7] and by Rehren (fig. 3.6a-b) [12]. However, in one of the samples previously investigated by Freestone from Tel el-Amarna (sample 67883), metallic copper particles ranging between 200-500 nm, polygonal and spherical in shape were detected [13]. Freestone subsequently affirmed that metallic copper was only found in that sample, while in the other samples only cuprite crystals were found.

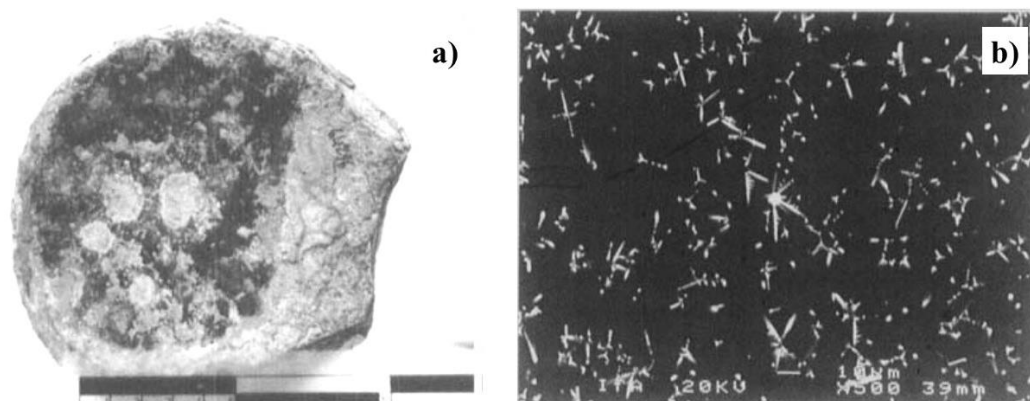


Figure 3.6. a) Ingot from Qantir, picture taken from Rehren, 1997; b) opaque red glass produced in the workshop of Qantir (picture from Rehren, 1997) showing cuprite crystals (white crystals)

A cross section of the beads from Frattesina revealed that the red colour occurred only in a thin external layer, while the entire body was copper-blue glass [37-39]. Through a deep investigation focused on the identification of the colouring agent in the Frattesina red beads, SEM, TEM and XRD analyses were performed by Angelini [39], revealing the presence of only metallic copper particles ranging between 200-400 nm, being octahedral and cubic in shape (fig. 3.7a-b).

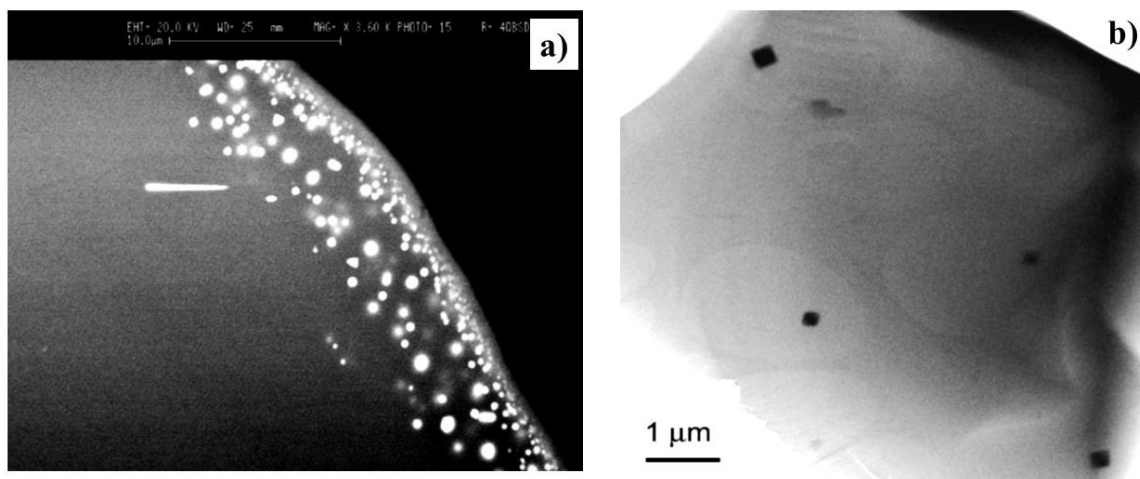


Figure 3.7. a) Cross section of a red bead produced at Frattesina. The white dots are metallic copper particles which produce the opaque red layer on the surface of a blue bead; b) Cu^0 particles in cubic shape (black squares) identified by TEM analyses (picture from Angelini, 2004).

3.2.1.4 Hypothesis about the production technology

It is still unclear how the glassmakers obtained the formation of the colouring agents in these early opaque red glasses. However, the archaeological site at Qantir (1200 BC), on the Nile delta in Egypt, provided interesting clues. Several ingots of opaque red glass and 250 ceramic crucibles (typically with inner diameter of 12-18 cm and height of 15 cm) were uncovered in Qantir [12, 42, 43]. Due to the presence of raw glass, opaque red glass ingots and crucibles in the same site, Rehren deduced that the area could be a specialised workshop devoted only to the manufacture of opaque red glass ingots [12]. According to Rehren, in this workshop the raw glass was firstly melted in two steps (to obtain a more homogenised glass) at 900°C and then 1050°C. Afterwards the colouring agent was added to the molten glass *“to produce glass cakes or ingots weighing 1.5 – 3.0 Kg each”* [43].

Some writers have advanced the hypothesis that the formation of the colouring particles was the result of a careful control of the redox state during the heat treatment, achieved with a charcoal blanket laid on the surface of the molten glass during the cooling phase and a smoky furnace (reduce atmosphere) [7]. Nevertheless, Rehren did not detect any trace of charcoal on the wall of the crucibles and supported the hypothesis that a very prolonged cooling phase had to be applied to the molten glass. He proposed that probably the heat treatment *“was performed in a reverberatory furnace chamber boosted by several localised areas of intensive heat process”*. Rehren suggested that before obtaining the opaque red glass ingots, the glass was crushed several times in order to obtain a more homogenised glass [12]. It is not well understood if the coloured glass was poured or not, but it was probably left to cool spontaneously inside the crucible in the furnace, and then the crucible may have been broken to extract the red ingots.

The site at Qantir and the presence of several ingots and crucibles, together with the shipwreck discovered in the Mediterranean Sea dating from between 1100 and 1000 BC, suggested a probable centralised organisation of glassmaking in the Late Bronze Age [12, 44]. According to this hypothesis, a few “elite-attached” specialised centres produced specific coloured glass in the form of cakes or ingots which were sent to “elite-attached” workshops devoted to re-melting and working the coloured glass. Some of these ingots were required by other workshops located far from Egypt, and so they were shipped to reach various markets located along the Eastern Mediterranean coast [44].

According to Brill [37], the red layer in the Frattesina beads is the result of a complex procedure in which turquoise glass was reheated in a strong reducing furnace, obtained using a closed container and/or a smoky fire. In a kiln chamber, the beads were embedded in calcined lime, furnace ashes, charcoal or a mixture of them. In this way, strong reducing conditions were achieved at the surface of the beads, facilitating the precipitation of metallic copper, and the glass turned opaque red. Several powdery substances were detected on the surface which could be the residues of the material in which the beads were embedded [37].

Santopadre hypothesised that a thin, hot layer of cuprite or metallic copper, previously powdered, was laid on the surface of the beads and by reheating, it stuck to the surface of the beads, preventing the complex and difficult procedure from maintaining the correct redox state in the furnace [38].

Angelini [39] proposed that the process occurred throughout the reheating of the blue glass in a reducing environment as argued by the previous writers [37, 38]. She supported the idea that the red layer on the surface formed throughout an exsolution and migration of the particles from the bulk of the glass to its surface. This phenomenon is caused by the oxidation gradient, achieved in the furnace, which acted as the main reducing agent and facilitated the nucleation of Cu^0 small particles. Moreover, this technique is very similar to the method used to manufacture lustre ceramic [39].

3.2.2 Sealing wax (High copper – high lead 8th century BC to the 2nd century AD)

3.2.2.1. History and use

Sealing wax red glass can be considered a product of the Renaissance which invested in glassmaking technology in the Eastern Mediterranean from the 9th century BC until to the Roman Age [3]. Its production is attested since the 9th-8th century BC, as indicated by chemical analyses of samples from Toprakkale (Iraq), Hasanlu (Iran) and Nimrud (Iraq) [7, 8]. This date is important in glassmaking history because it establishes (approximately) the intentional addition of lead in the production of glass objects, indicating that glassmakers understood the technical advantage given by the addition of this element in the manufacture of glass.

It is thought that sealing wax continued to be produced over the centuries up to the Roman period (1st-2nd century AD). However, it is not clear when exactly sealing wax glass production stopped. Boschetti [45] proposed that after the 1st century AD sealing wax red glass was no longer produced. Nevertheless, opaque red enamels dating from between 1st and 4th century AD were identified as sealing wax [14, 46]. Furthermore, later enamels dated to the early medieval period (6th – 11th century AD) attested the continuation of sealing wax red glass production in Britain [15]. Few glass mosaic tesserae of sealing wax were found in mosaic decorations of the early Medieval or Medieval period, but this could be due to the re-use of old tesserae or fragments from other sites.

Several writers agree that sealing wax red glass production was located somewhere in the Near East and Egypt in specific workshops and traded in the form of ingots to different manufacturing centres located in several area of the Mediterranean basin, central Europe and Britain, where it was worked [3, 5, 8]. This was confirmed by the isotopic analyses performed by Brill, in which the sealing wax discovered in Britain and in Nimrud revealed the same (or very close) values of lead isotopes, supporting the same provenance [6, 8]. More recently, isotopic analyses were performed on Roman sealing wax (from Pompei, Segesta, Milan and Siena), taking into account also the ratio of neodymium and strontium, and confirmed as of Eastern Mediterranean origin, most probably somewhere in Egypt [47].

A wide variety of glass objects (fig. 3.8) were manufactured using sealing wax red glass: large dishes, cups/bowls (*patella cups*), vessels and mould inlays to be used in jewellery to substitute jasper stone (fig. 3.9) [3]. A flourishing production of opaque red glass vessels occurred in Egypt [48] and in Macedonia [49,50], Especially during the Hellenistic period. Stern discovered 13 rounded bowls of opaque red glass in the archaeological site of Sudan, which they are thought to be made from sealing wax [3, 45, 48], while a *skyphos* and a globular bottle were analysed by Ignatiadou and Weinberg [49, 50]. It is probable that they intentionally

imitated the ceramic and metallic vessels; however, how they were made is still unclear. Examples of these objects or fragments of them are to be found in several museum collections around the world [45]. Other examples of vessels made from sealing wax were analysed in this research and reported in [Appendix C](#). Fragments of sealing wax red glass objects were used in mosaic wall/pavement decoration [44], or as glass mosaic tesserae [29]. Sealing wax red glass was widely used, for example as an enamel to decorate metalwork (bronze objects) such as swords, helmets and terrets in the Celtic and La Tène civilisations [5, 10, 51].

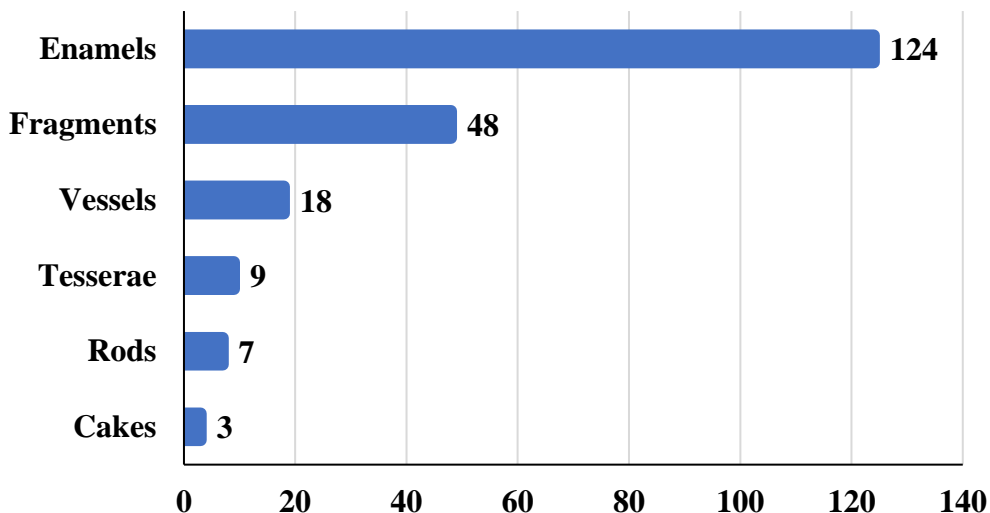


Figure 3.8. Number of chemical analyses performed on sealing wax red glass objects.

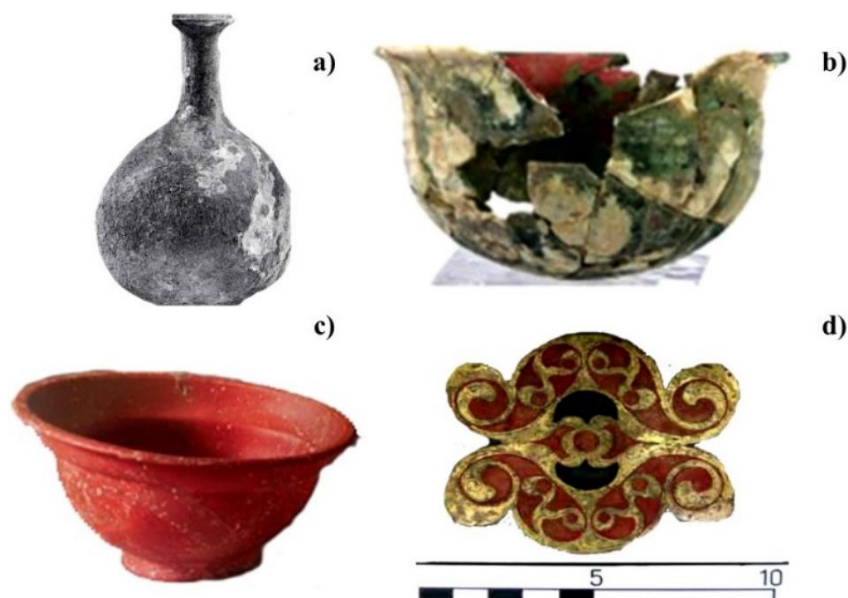


Figure 3.9. **a)** globular bottle, 1st century BC/1st century AD (picture taken from Weinberg 1992); **b)** skyphos from Pydna 1st century BC (picture taken from Ignatiadou 2009); **c)** patellas cup 1st c. BC/1st c. AD, Italy-Greece (?) (picture taken from Stern, 1994); **d)** Late Iron Age sealing wax from Britain: strap end from Stanton, Norfolk (picture taken from Davis, 2007).

3.2.2.2 Chemical analyses

The number of chemical analyses of sealing wax is 211. However, 128 analyses (tab. 3.5) have the entire chemical composition (the average bulk composition is reported in tab. 3.6a).

Table 3.5. Number of analysed samples for each age and region.

City/Site	Period	century	n.	Reference
Tropak Kale (Turkey)	Assyrian	8 th – 6 th BC	1	7
Nimrud (Iraq)		7 th – 4 th BC	9	8, 52
Nimrud (Iraq)		4 th BC	1	7
Hasanlu (Iran)		7 th BC (850 BC)	2	8
Persepoli (Iran)	Persian	5 th BC	2	8
Hungary, France, Belgium, Switzerland, North Italy (Central Europe)	La Tène	4 th – 1 st BC	40	10
Pydna, Macedonia	Hellenistic Emp.	4 th – 1 st BC	1	49
Scotland	Celtic	2 nd BC	12	51
Britain		1 st BC – 2 nd AD	33	5
Pompeii	Roman Italy	1 st BC/1 st AD	8	21, 29
Sussex	Roman Britain	1 st AD	4	32
Cumbria				
London				
Castelford				
	Anglo-Saxon	6 th - 11 th	11	15

Table 3.6a. Average chemical composition in wt % of the sealing wax red glass from different regions. N.E: Near East; Hell/Rom: Hellenistic/Roman; Ang-Sax: early Anglo-Saxon.

		SiO ₂	Al ₂ O ₃	Na ₂ O	K ₂ O	CaO	MgO	P ₂ O ₅	TiO ₂	Fe ₂ O ₃	MnO	Sb ₂ O ₃	SnO ₂	CuO	PbO
Near East	Av.	46.8	0.84	10.0	1.42	3.70	2.2	0.08	0.16	0.65	0.48	3.3	0.18	12.8	17.7
	St.D.	5.02	0.30	2.05	0.69	0.93	0.92	0.07	0.18	0.55	1.2	1.5	0.17	3.1	7.0
La Tène	Av	42.4	1.5	4.8	0.44	4.54	0.44	n.d.	n.d.	1.8	0.14	n.d.	n.d.	7.4	34.5
	St. D	5.9	0.25	0.71	0.14	1.41	0.08	n.d.	n.d.	1.0	0.26	n.d.	n.d.	1.3	8.8
Celtic	Av	42.2	1.6	10.5	0.59	4.80	0.44	0.32	0.10	0.70	0.35	0.92	0.50	9.3	27.7
	St. D	1.09	0.20	1.04	0.19	0.54	0.10	0.10	0.04	0.51	0.11	0.32	0.20	1.1	3.2
Hell/Roman	Av	39.6	1.7	9.4	0.62	3.90	0.64	0.16	0.11	0.92	0.28	0.71	0.64	7.8	33.7
	St. D	6.35	0.47	2.54	0.36	1.36	0.31	0.12	0.08	0.39	0.19	0.54	0.69	2.5	9.1
Angl-Sax.	Av	20.4	2.5	0.34	0.68	0.65	0.33	0.22	0.22	0.59	0.20	0.60	2.24	15.1	57.7
	St. D	7.09	0.82	0.16	0.27	0.43	0.15	0.09	0.06	0.34	0.00	0.00	4.12	9.6	12.5

Taking into account the concentration of lead and copper, it is possible to divide the samples into three main groups.

a) The Near East samples showed concentrations of lead usually lower than 25 wt% (PbO 11-24.8 wt%) and copper higher than 10 wt% (CuO 10.7-17.4 wt%) except one sample from Nimrud (CuO 7 wt%). Antimony ranged between 1.8 and 5.5 wt%.

b) The second group is composed of samples dating from the 4th century BC up to the 2nd – 4th centuries AD and includes: the La Tène, Celtic and Hellenistic-Roman period. They are characterised by a higher lead content (PbO 25-50 wt%) than the previous group, as well as a lower copper concentration (CuO 6.4-11.0 wt%). La Tène samples showed iron content (Fe₂O₃ 1.8-5 wt%) higher than the Celtic and Hell/Roman samples (Fe₂O₃ 0.44 – 1.9 wt%). Despite the samples from the Near East, antimony is often lower than 1 wt%, and only

in a few cases varied between 1.1 and 1.8 wt%. Tin oxide is frequently lower than 1 wt%, and only in four enamels from the Roman-Britain does it surpass 1 wt% (SnO_2 1.1 – 3.2 wt%) [32].

c) The early-Medieval Anglo-Saxon sealing wax showed the highest concentration of lead (PbO 32 -75 wt%), while the amounts of copper ranging between 9 and 42 wt% (except two samples with CuO 2.8 and 3.6 wt%). Antimony was not reported, but tin content is usually about 0.70 wt% and in some cases varies between 1.6 wt% and 16.4 wt% [15].

As regards the raw materials, some writers proposed copper-alloy such as bronze or brass roasted in air used as a copper source [8] and litharge (PbO) as a lead source [23, 32]. Other writers, advanced the hypothesis that waste metal scraps, produced by the silver refining process, composed of copper- and tin-bearing lead-silicate slags, could be used in the production of the Early Anglo-Saxon sealing wax [15, 32]. However, the high concentration of lead detected in all the samples suggests that lead was added through some lead-bearing different from the copper compound [32].

The antimony concentration detected in the samples from the Near East suggests the deliberate addition of an antimony compound. Cable and Smedley observed that the presence of high antimony content affects the formation of the cuprite nuclei [23]. However, it is still unclear if it was added as a reducing agent or as an opacifier/decolouriser to the raw glass [32]. In contrast, in the other two groups antimony content varies widely, not enabling an accurate interpretation.

Through the reduced composition [52] the three main groups continued to exhibit compositional differences. In fig. 3.10a-b, most of the samples belonging to the Near East group exhibit magnesia content higher than 2 wt%, except for a few samples, while the potash concentration is higher than 1.5 wt%. According to the literature, these values could be related to the use of soda plant ash to melt the glass. The alumina content are very low, detected between 0.72 and 1.9 wt%.

The group composed of the samples from the La Tène, Celtic cultures and the samples from the Hellenistic-Roman period, showed concentrations of MgO and K_2O lower than 1.5 wt%, due to the use of natron as a fluxing agent [40, 50, 53]. Among these groups, the samples produced in the La Tène culture have lower sodium (Na_2O 6.5-11 wt%) than the other samples (Na_2O 14-22 wt%)⁴. The amounts of alumina are higher than the Near East sealing wax, varying between 2.0 and 4.4 wt%.

In the early-medieval Anglo-Saxon period, a very complex and different base glass was probably used. All the samples are characterised by low sodium content (ranging between 0.78 and 3.5 wt%), with potash concentration higher than 2wt% (except two samples), magnesia varying between 0.52 and 2.7 wt%, and phosphorus varying between 0.52 – 2.3 wt%. Considering the high concentration of PbO (mentioned above) the sealing wax in the Early Anglo-Saxon was probably produced by a lead-silicate glass employing different raw materials which increased the amount of potash, phosphorus and alumina [15, 32].

⁴ The data from La Tène samples analysed by Brun et al., 1992, should be treated with more caution because they used uncalibrated SEM-EDS, in which case the lead is slightly over-estimated, while the light elements were under-estimated. Personal comment of Professor Ian C. Freestone. So the concentration of sodium should be under-estimated.

Table 3.6b. Average chemical composition in wt % of sealing wax red glass from different regions. N.E: Near East; Hell/Rom: hellenistic/Roman; Ang-Sax: early Anglo-Saxon.

	Base glass	Oxide	SiO ₂	Al ₂ O ₃	Na ₂ O	K ₂ O	CaO	MgO	P ₂ O ₅	Cl	TiO ₂	Fe ₂ O ₃	MnO
Near East	Plant ash	Av.	70.4	1.3	14.9	2.2	5.7	3.6	0.06	0.75	0.10	0.96	0.02
		St.D.	4.2	0.38	2.1	1.1	1.4	1.4	0.10	0.08	0.24	0.65	1.5
La Tène	Natron	Av.	74.8	2.7	8.4	0.78	8.0	0.81	n.d.	0.90	n.d.	3.3	0.21
		St. D.	2.8	0.53	0.84	0.28	2.3	0.23	n.d.	0.11	n.d.	1.8	0.39
Celtic	Natron	Av.	67.8	2.6	16.8	0.93	7.7	0.70	0.47	0.99	0.16	1.2	0.56
		St. D.	1.5	0.27	1.2	0.28	0.68	0.14	0.19	0.15	0.06	0.92	0.17
Hell/Roman	Natron	Av.	68.0	2.8	16.4	1.1	6.9	1.1	0.20	1.0	0.10	1.7	0.36
		St. D.	3.2	0.68	2.4	0.57	1.6	0.59	0.26	0.34	0.12	0.82	0.31
Angl-Sax.	Lead-silicate	Av.	76.7	10.1	1.4	2.6	2.6	1.4	0.87	0.93	0.87	2.5	0.08
		St. D.	6.9	4.0	0.67	0.74	1.7	0.74	0.44	0.27	0.22	1.7	0.19

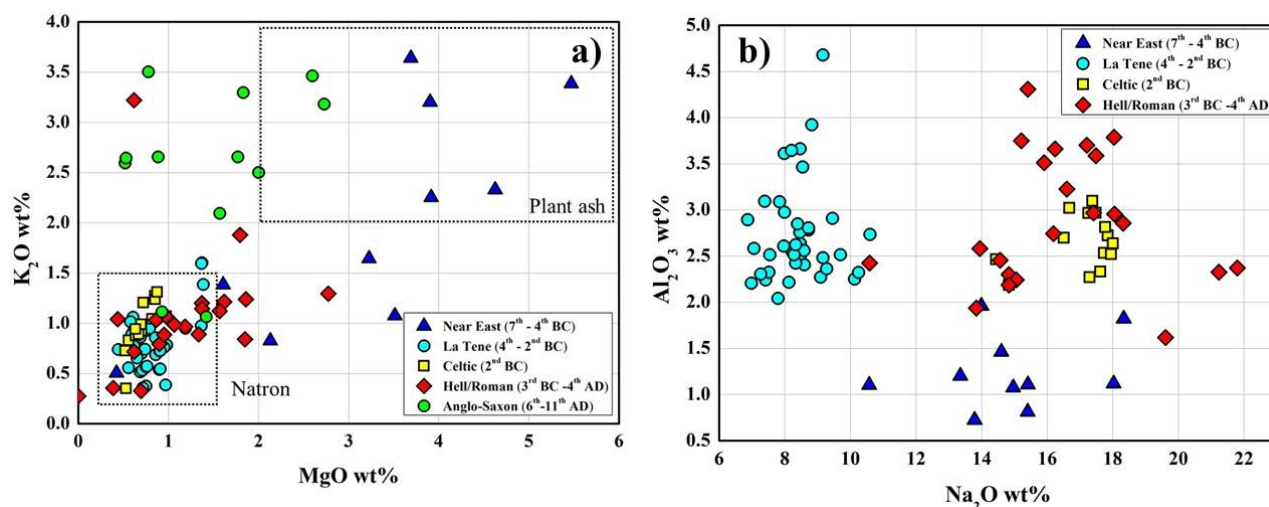


Figure 3.10. Binary graphs with the weight % of **a)** potash (K₂O) versus magnesia (MgO); **b)** alumina (Al₂O₃) versus sodium oxide (Na₂O). Sealing wax red glass from 8th c. BC to 2nd c. AD.

3.2.2.3 The colouring agent

The colour of the sealing wax red glass is due to the scattering of the light by the large cuprite crystals in dendritic shape with 90° and/or 60° branching (fig. 3.11a-b) [13, 23]. These crystals appear red or yellow and are embedded in a colourless glass matrix [23]. Their sizes range between 10-300 μm [7, 10-13], but in some cases cuprite crystals smaller than 500 nm and without branching were detected in Roman enamels [14]. These distinctions could be due to different heat treatments. Indeed, a prolonged heat treatment could promote equiaxed and well-developed dendritic crystals, otherwise coarser dendritic crystals will result [10].

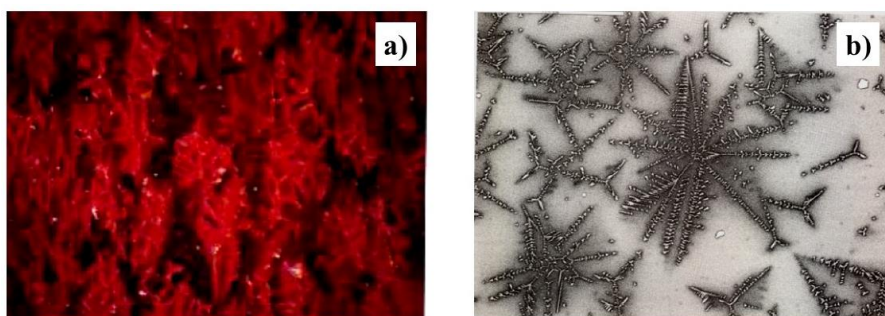


Figure 3.11. Cuprite crystals **a)** under an optical microscope (picture taken from Verità, 2017); **b)** SEM-EDS image of cuprite crystals from the cake of Tara Hill (picture taken from Freestone et al., 2003).

3.2.2.4 Hypothesis about the production technology

Although several laboratory reproductions have been tested to produce sealing wax [23, 24, 54], its manufacture is still unclear. The results obtained by the laboratory reproduction suggested that the melt should be cooled slowly and for prolonged period of time, maintaining reducing conditions [23, 54]. However, all the laboratory tests exhibited layers with different colours from green to red (from the top to the bottom of the crucible) due to the different redox conditions of the melt during the cooling phase [23, 24, 54]. Some writers have suggested adding charcoal in the top of the crucible, or to grind the frit several times to reduce this segregation phenomenon [23], but a definitive solution has not been found.

3.2.3 Red brown (low copper low lead 3rd century BC to 13th century AD)

3.2.3.1 History and use

Bimson showed that during the transition between the high copper-no lead opaque red to sealing wax production, an opaque red with lower copper ($\text{CuO} < 3 \text{ wt\%}$) and a small amount of lead (without specifying the quantities) and coloured by not well-defined copper particles was produced, which was used mainly in *millefiori* and mosaic glass [3]. On the other hand, analyses of samples dated between the 3rd and the 1st centuries BC [2, 5, 55, 56], showed copper and lead concentrations close to the values of the red brown glass indicated by Freestone ($\text{CuO} < 5 \text{ wt\%}$, $\text{PbO} < 15 \text{ wt\%}$) [7]. These data suggest that the production of red brown glass probably started before the Roman Empire had established its control in the Mediterranean area, as hypothesized by Hughes. However, since the 1st century AD, red brown can be considered the main opaque red glass made during the Roman Age up to the present day.

Red brown has been found across a wide area including the Mediterranean basin (Palestine, Egypt, France, Italy, Greece, Spain, Turkey), and continental Europe up to the Roman British regions.

Red brown has been used (Table 3.7 – 3.10; fig. 3.12) as canes/rods (32) in the mosaic glass technique [55, 56], glass mosaic *tesserae* (272), *opus sectile* (19), bracelets (3), game counters (1), beads (87) and enamels (3); while vessels made by red brown have been rarely uncovered, and they have been dated to around the 15th-16th century AD [17-20, 27-29, 33-35, 57-79].

Table 3.7 Data source for the mosaic *tesserae* (from 1st BC to 13th AD), providing city/site, date range and number of analyses.

Site		century	n.
Italy	North-East (Venice-Torcello-Aquileia-Padova-Trento-Vicenza-Pordenone)	1 st BC – 13 th AD	61
	Rome	2 nd AD – 13 th AD	40
	Ravenna	5 th -6 th AD	21
	Naples – Pompei- Herculaneum	1 st AD – 5 th AD	18
	Sicily	3 rd AD – 13 th AD	9
	Milan	1 st – 5 th AD	4
	Siena – Ancona	3 rd AD – 5 th AD	3
Turkey	Amorium	9 th AD	7
	Haghia Sophia	6 th AD	4
	Kilise Tepse	5 th AD- 6 th AD	4
	Sagalassos	6 th AD	4
	Hagios Polyuktos	6 th AD	2
	Sarachane- Sardis - Acheiropoietos -Not specified	5 th AD- 10 th AD	4
Greece	Hosios Lukas	9 th AD – 11 th AD	9
	Daphni	9 th AD – 11 th AD	
	St. Demetrios Thessaloniki	7 th -11 th AD	2
	Athene	11 th AD	1
Near East	Israel	5 th AD- 7 th AD	22
	Syria	2 nd AD	1
	Jordan	6 th AD – 8 th AD	3
Spain	Noheda	4 th AD	33
Britain	West Clacton	2 nd AD	11
France		2 nd AD- 4 th AD	3

Table 3.8. Data source for the *opus sectile* (from 3rd to 6th AD), providing city/site, date range and number of analyses.

City/Site		century	n.
Kenchreai	GRE	4 th AD	9
Faragola	ITA	4 th -6 th AD	5
Ostia Antica	ITA	3 rd AD	3
Fayum	EGY	4 th AD	2

Table 3.9. Data source for the canes in mosaic glass (from 3rd BC to 9th AD), providing city/site, date range and number of analyses.

City/Site		century	n.
Tebtinu	EGY	3 rd BC	3
Delos	GRE	2 nd BC	1
Heis	GRE	1 st BC	6
Avenches	FR	1 st -3 rd AD	5
Augustea	CH	1 st -3 rd AD	9
	ITA	1 st BC/AD	4
Cosa	ITA	1 st AD	1
Amorium	TURK	9 th AD	3
	GRE	1 st BC/AD	4

Table 3.10. Data source for the beads (from 5th to 8th AD), providing city/site, date range and number of analyses.

City/Site		century	n.
Meroving	FRA/BEL	5 th -8 th AD	32
Anglo-Saxon	UK	5 th -7 th AD	27
Longobards	ITA	6 th -7 th AD	19

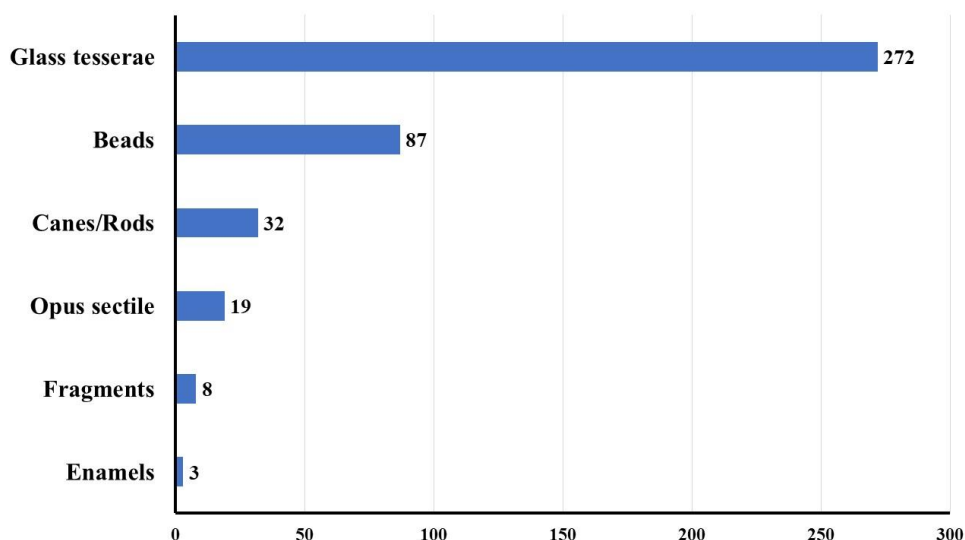


Figure 3.12. Number of chemical analyses performed on red brown glass objects.

3.2.3.2 Chemical composition

The number of chemical analyses is 421. Copper is usually lower than 5 wt%, but high variation was observed. Indeed, the copper content can vary from 0.47 wt% to 4 wt%, with a few samples in which the copper concentration ranges between 7 to 10 wt% (table 3.11). These differences do not seem to depend on regional tradition or on different use (such as beads, glass mosaic tesserae, canes etc) of red brown.

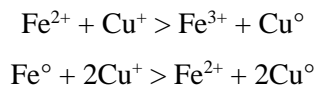
However, focusing on the glass mosaic tesserae (which includes most of the analyses and a wide time span), it is possible to observe that the concentration of copper gradually decreases over the centuries, and moves from an average content of 2 wt% in the Roman Age (1st-4th centuries AD) to an average concentration of 1.5 wt% in the Late Antique (5th – 8th centuries AD).

The concentration of lead is usually below the 15 wt%, but the chemical analyses showed that the amount of lead varies widely. In some red brown used in *millefiori* glass and dated between 3rd century BC and 3rd century AD, the amount of lead varies between 5 and 15 wt% [55, 56], and in the Early Anglo-Saxon beads (5th – 7th century AD), they showed an average lead concentration of 12.4 wt% [25]. In mosaic *tesserae*, as well as in other beads or *sectilia*, the lead content varies between 1 wt% to 2 wt% up to 4 wt% and 9 wt%, reaching in some cases 20 wt%.

It is usually accepted that the concentration of lead lower than 5 wt% does not bring any technical advantage to the glass, so when lead is present in concentrations lower than 2 wt% or 5 wt%, it could have entered as a contaminant from the copper-bearing, or by the addition of complex metallurgical slags [15, 32]. These metallurgical slags, produced by the silver refining process, could include copper, lead, tin, and zinc but their concentration should be very variable. The probable use of this raw material could explain the high variability of the lead and copper content in red brown [15, 32]. Fiori contested this hypothesis, underlining the lack of any correlation between copper and lead in the opaque red mosaic tesserae from Ravenna [28].

Despite the high copper-no lead or sealing wax, red brown glass is characterised by higher concentrations of iron frequently detected between 2 wt% and 4 wt%, reaching in some beads or mosaic *tesserae* 7 wt%. These

values suggest that some iron-bearing material was intentionally added to the glass and acted as the main reducing agent. Ferrous oxide (FeO) or metallic iron (Fe⁰) work as internal reductants, facilitating the precipitation of metallic copper according to the following equation:



Metallic inclusions, which could help to identify the iron compound used as a reducing agent, have rarely been detected in red brown dating from the Roman Age (1st – 4th centuries AD). In contrast, in red brown glass dated to the 5th-8th centuries AD (Byzantine period, Early Anglo-Saxon and Merovingian periods), several metallic inclusions were revealed. They are usually fayalite phase, or metallic inclusions composed of several iron oxides (FeO, Fe₃O₄) or metallic iron [25, 30, 31]. This could indicate the use of a mixture of several iron-oxide powders or metallic iron, or metallic scraps rich in iron oxides [25, 30, 31].

In Roman black glass dated to around the 2nd century AD in modern-day Bulgaria, inclusions of metallic iron were found, indicating an intentional addition to increase the reducing conditions into the melt, and highlighting that the practice of using metallic iron was already present in the Roman glassmaking tradition [80, 81]. Hence, the use of metallic iron in Roman opaque red glass is not to be excluded.

Tin is another potential reducing agent, but its concentration varies widely in red brown glass. When it is detected in concentrations lower than 1wt% it can be considered a contaminant from the bronze or brass scrap used as copper-bearing [32].

Tin has been detected sporadically in red brown dating from the 1st century BC – 1st century AD, ranging between 1.2 wt% - 4 wt%, which indicated an intentional addition [9, 26, 29, 52, 55, 56, 68, 72]. In contrast, in mosaic *tesserae* from Padova, Ravenna, Israel and Amorium, and dating from 5th-7th centuries AD, tin has been frequently detected in concentrations between 1 and 3.5 wt% [17, 18, 28, 60, 79]. Moreover, in several red brown glass artefacts dating from 5th-7th centuries AD (both Byzantine, Merovingian regions) several tin-rich inclusions such as lead-tin, tin-calcium, metallic tin and cassiterite were found [17, 30, 31, 63]. In these samples, the ratio Sn:Cu is higher than that exhibited by the bronze or brass Byzantine objects, and several writers agree that these values indicate a deliberate addition of some tin compounds. Schibille suggested a tin-rich waste metallurgical product [63], Silvestri proposed the addition of cassiterite directly to the batch [17], while Fiori suggested the recycling of some tin-bearing copper alloy, or lead-tin alloy such as pewter [28].

Antimony is usually lower than 1wt% which suggested that it was not intentionally added to this composition. Zinc oxide has been detected in concentrations varying between 0.01 and 0.5 wt%. However, in some mosaic *tesserae* it ranged between 1 up to 5 wt%. Shugar thought that a specific Zn-rich raw material was used [18]. In most of the cases, Zn content is related to the copper-bearing material, and it is accepted that Zn entered as an impurity or contaminant, as well as tin. Indeed, in ancient times, zinc was a rare and expensive material, so it is very difficult to imagine that it was deliberately added to produce opaque red glass [32].

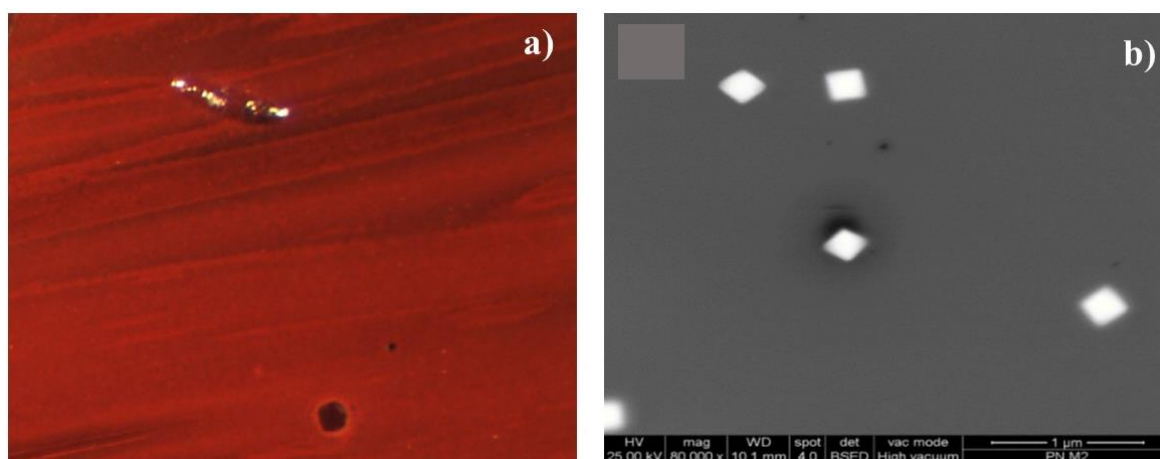
Table 3.11. Average chemical composition in wt % of red brown samples from the 3rd century BC to 13th century AD.

Period	n. analyses		Fe ₂ O ₃	MnO	Sb ₂ O ₃	SnO ₂	CuO	PbO
3 rd -1 st -BC	36	Av.	2.0	0.6	0.6	0.7	2.0	7.8
		St.D.	0.6	0.3	0.6	0.8	0.8	6.0
1 st -4 th AD	112	Av	2.3	0.5	0.4	0.4	1.9	4.4
		St. D	0.9	0.3	0.4	0.6	1.3	4.7
5 th -8 th AD	201	Av	2.8	0.7	0.2	1.0	1.5	4.4
		St. D	1.0	0.4	0.2	0.8	0.6	3.5
9 th -13 th AD	92	Av	3.0	0.9	0.2	0.6	2.1	3.3
		St. D	1.2	0.5	0.2	0.8	1.5	5.9

3.2.3.3 The colouring agent

Despite the cuprite crystals detected in the sealing wax (which are tens of microns), the colouring agent in red brown is metallic copper, and due to its smaller amounts, ranging between 80-500 nm, is possible to investigate only by using specific analytical techniques. Scientific investigations conducted by TEM and SEM analyses have provided the best information. XRD analyses are very helpful; however, only weak peaks indicate the presence of metallic copper. This was confirmed also by the studies on the oxidation state of copper by using XANES and EXAFS analyses. Metallic copper is usually in cubic form, however cubic or spherical shapes are observed by SEM analyses. In darker red or brown glass, the particles of metallic copper exhibit hexagonal or triangle shapes [11, 13, 19-21, 33, 64].

Although Cu⁰ is considered the colouring agent in red brown, cuprite crystals were detected by Barber in one *tesserae* from the Villa Tivoli by using TEM analyses [13]. He proposed an alternative mechanism, already explained by Paul and Ishida, in which the nucleation of copper occurred first; afterwards it passes into the stability field of cuprite, causing the co-precipitation of copper and cuprite [13]. Further examples were detected by Gedzeviciute through Raman spectroscopy, which revealed cuprite crystals (Cu₂O) in opaque red with CuO content below the 3 wt% but with PbO ranging between 6.88 and 25.9 wt% [72].

**Figure 3.13.** Red brown sample observed by a) optical microscope (picture taken from Verità et al., 2015); b) euhedral sub-micrometrical particles of metallic copper in red brown sample (Picture taken from Maltoni et al., 2018).

3.2.3.4 Hypothesis about the production technology

Although, numerous red brown samples have been analysed from the Roman and Byzantine empire, the lack of historical written source makes the comprehension about the red brown production still not completely understood. However, the manufacture of this colour hid several difficulties obtaining several failures [19] which make it a very demanding colour.

3.2.4 Orange glass

3.2.4.1 History and use

Orange glass is most likely to have appeared between the 4th and the 3rd century BC in the palette of early glassmakers, and it was used in some core formed vessels (fig. 3.14), or *millefiori*, as attested by the analyses of Nenna and Gratuze [55]; however, it is difficult to establish the exact date.



Figure 3.14. 4th – 3rd c. BC glass object (Picture from Stern 1994; 5000 years of glass).

Orange glass was used (fig. 3.15) as rods or canes to decorate core-formed vessels, cast polychrome bars from Ptolemaic Egypt, or in mosaic/*millefiori* glass. Afterward, orange glass was used as glass mosaic *tesserae*, as *sectilia* or as cane to make beads [17-19, 30, 31, 34, 58, 61].

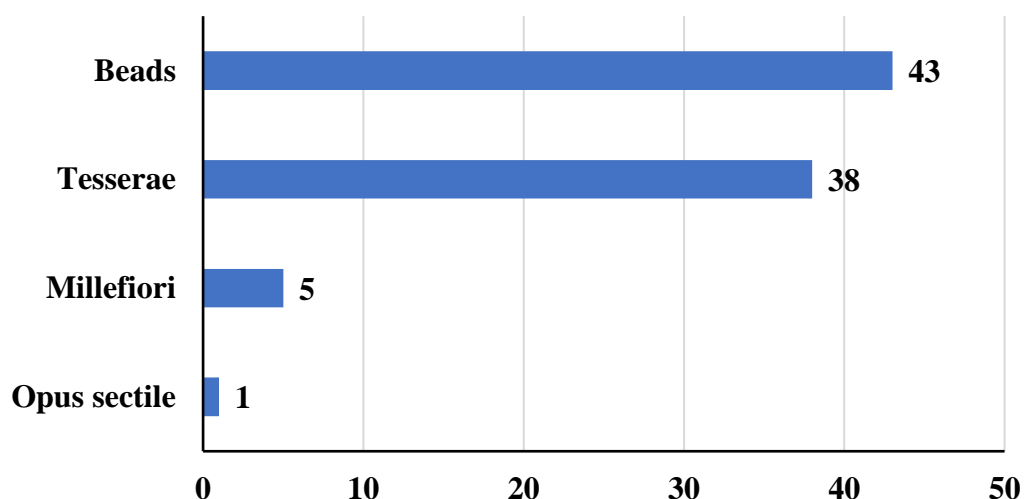


Figure 3.15. Number of chemical analyses performed on orange glass objects.

3.2.4.2 Chemical composition

The chemical analyses of orange glass collected in this research are 87 (table 3.12), and date between the 3rd century BC to 12th century AD. The type of samples varies between mosaic *tesserae*, rods/canes applied in polychrome mosaic glass, *opus sectile* and beads.

The chemical composition of orange glass exhibits a high variation of lead (PbO 8wt% and 34 wt%) and copper (CuO 4.4 and 14.1 wt%) content. The concentration of iron varies between 1.2 wt% and 3.2 wt%, tin content is lower than 1wt% in the samples dating from 3rd and 1st centuries BC, while it was frequently detected between 0.5 wt% and 2.5 wt% in the Roman and Early Byzantine samples. The antimony content is usually lower than 1wt%, and in nine samples it varies from 1.1 wt% up to 2 wt%.

Table 3.12. Average chemical composition in wt % of orange samples from the 3rd century BC to 12th century AD.

Period	n. analyses		Fe ₂ O ₃	Sb ₂ O ₃	SnO ₂	CuO	PbO
3 rd -1 st -BC	5	Av.	2.1	1.1	0.47	8.8	22.2
		St.D.	0.83	0.97	0.32	0.61	4.60
1 st -4 th AD	16	Av	2.2	0.6	1.2	7.6	24.7
		St. D	1.1	0.4	0.6	2.2	8.3
5 th -8 th AD	17	Av	2.9	0.4	1.1	8.1	21.9
		St. D	0.9	0.5	0.4	2.8	7.3
9 th -12 th AD	6	Av	2.2	0.66	1.1	8.1	21.3
		St. D	1.60	0.43	0.96	1.57	6.05

A different chemical composition is exhibited by the Merovingian orange beads dating from between the 5th century and the 8th century AD (table 3.13) which can be divided into two sub-groups.

(a) Beads with lower lead concentration (PbO 5.2-17 wt%) and higher copper content (CuO 8.0 and 14.3 wt%) than the Roman or Byzantine opaque orange; antimony varies between 0.92 and 1.5 wt%. Comparable concentrations of iron have been detected (Fe₂O₃ 1.0 – 3.8 wt%), as well as tin (SnO₂ 0.62 -2.1wt%).

(b) Beads exhibiting concentrations of lead lower than 1 wt%, while copper content ranging from 15.7 wt% up to 22.4 wt%. Tin and antimony are below the 1 wt%, while iron content varies between 0.75 and 4.5 wt%.

Table 3.13. Average chemical composition in wt % of Merovingian orange samples dated 5th-8th c. AD.

Period	Or. type	n. analyses		Fe ₂ O ₃	Sb ₂ O ₃	SnO ₂	CuO	PbO
5 th -8 th AD	a	16	Av.	2.1	1.0	1.1	9.4	10.1
			St.D.	0.8	0.4	0.4	2.1	4.2
5 th -8 th AD	b	27	Av	1.1	0.09	0.14	17.4	0.35
			St. D	0.94	0.39	0.23	2.21	0.32

Through the reduced composition [52], most of the base glass composition of Roman and Byzantine orange glass (fig. 3.16) shows concentrations of potash and magnesia ranging between 1.5 and 2.5 wt%, with a few samples exhibiting values higher than 2.5 wt%. In contrast, the amount of K₂O and MgO in most of the Merovingian orange glass is lower than 1.5 wt%, except for a few samples.

The values of K₂O and MgO detected in the Roman and Byzantine period could be considered anomalous in Roman glassmaking, in which natron was used as a fluxing agent and the base glass showed amounts of K₂O and MgO lower than 1.5wt%.

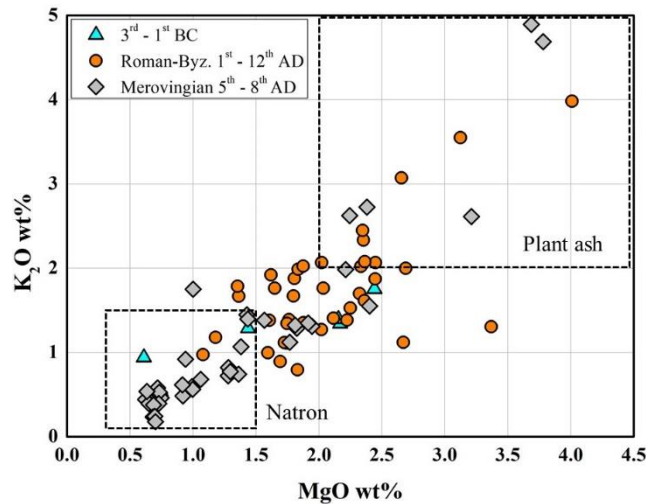


Figure 3.16. Bi-plot graph of the wt% concentration of potash (K₂O) versus magnesium (MgO) in orange glass (reduced composition).

3.2.4.3 The colouring agent

The colouring particles in the orange glass are cuprite crystals of sub-micrometric size ranging between 200 – 800 nm, with cubic or octagonal shapes [17, 19, 61, 62]. In general orange glass appeared heterogenous with the presence of several red bands, in which the cuprite crystals enlarged to reach dendritic shapes and micrometric sizes (fig.3.17) [19, 61]. Generally, no significant compositional differences have been detected between the two layers, but in a few cases the chemical composition of the orange and red layer turned out to be different; it may be supposed that two different glasses were joined to intentionally produce this effect [18].

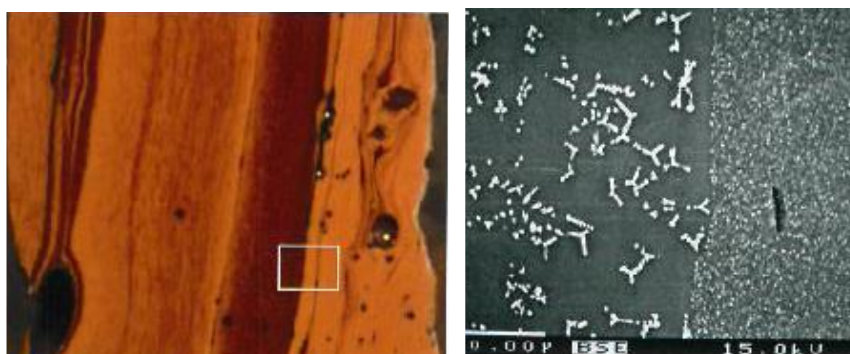


Figure 3.17. Orange glass tesserae showing common heterogeneous morphology, with cuprite crystals of different sizes and shapes: dendritic in the red band, smaller and with geometrical shapes in the orange layer (from Verità, 2017).

3.2.4.4 Hypothesis about the production technology

There is no specific information about the production of orange glass during the Roman and Byzantine period. It is likely that prolonged heat treatments at temperatures between 500-700°C are required to produce a high number of small cuprite crystals, as laboratory reproductions have indicated [54]. However, other production techniques are not ruled out.

3.2.5 Aventurine glass (Cu^o-aventurine)

3.2.5.1 History and use

According to the translation of the cuneiform tablet of Assurbanipal (7th – 6th century BC) by Thompson (1920), the production of aventurine glass was recorded in the ancient region between the Tigris and Euphrates rivers, and then continued to be manufactured in the region of Badakhshan, in modern Afghanistan [82]. According to Fischer (1882), it was Marco Polo, who spent several weeks in this region, who brought these new glass recipes to the Venetian glassmakers [82]. However, archaeological evidence which could confirm these hypotheses have still not been discovered. Hence, the deep investigation of the Venetian archives and the recipes together with chemical analyses of aventurine samples, occurred between 20th and 21st centuries AD by Zecchin and Moretti contributed to shed light on the aventurine history [9, 83-85].

Aventurine glass is mentioned for the first time in the inventory of the goldsmith D. Rimondo Rimondi dated 1626 [83-85]. According to Zecchin, the aventurine glass should start to be manufactured in Venice after the manuscript of Antonio Neri (1612), in which aventurine glass was not still mentioned [84].

The origin of the name aventurine has two hypotheses: the first proposes that the glass took its name from the mineral *aventurine*, a yellowish-brown quartz with sparkling flakes of mica, extracted from the Ural Mountains and Altai region. This hypothesis was advanced by the translation of Thompson, who found in the Assurbanipal table the word *sandumarhasi*, which means aventurine [82]. The

second hypothesis argues that the name is due to the difficulty found in producing this glass (aventurine in Italian sounds like a word indicating adventure), and Darduin said that this glass can be obtained successfully more by chance than by the skill of the glassmakers [84]. The second hypothesis finds confirmation in recipes found in Venetian manuscripts, in which the difficulty of systematically obtaining the same results is explained. Instead, in some manuscripts it is called “*stellaria*” [83].

Aventurine glass was used as a precious stone, so it was cut, ground and polished and used for jewellery, or as a decoration for luxury objects; it was rarely made by the blowing technique, likely due to the sensitivity of the colouring particles to the working temperature [83].

In the literature aventurine has never been found dating from before the second half of the 16th century, and the only chemical analyses used in this research belong to the Venetian aventurine glass dating from the 19th and 20th century AD published by [9, 83] and reported in table 3.14.

3.2.5.2 Chemical composition

The chemical analyses were mainly collected from [83].

The chemical composition of aventurine contains variable amounts of iron (Fe_2O_3 2.2-3.7 wt%), tin (SnO_2 1.9-2.8 wt%) and lead (PbO 0.70 – 2.3 wt%), while the quantities of copper range between 3 and 4.1 wt%.

Table 3.14. Average chemical composition in wt % of aventurin glass dated 19th – 20th c. AD.

	Fe_2O_3	SnO_2	CuO	PbO
Av.	3.6	2.0	4.1	1.1
St. D.	1.2	0.82	0.59	0.68

From the recipes of the Venetian manuscripts it has been possible to identify the raw materials used to manufacture aventurine glass. Flakes of iron or steel were used as an iron-bearing compound, while powdered cuprous oxide (Cu_2O) was used as copper-bearing. In several recipes, lead-tin calx is mentioned as a further compound to add to the batch [83].

3.2.5.3 The colouring agent

As with copper-ruby glass and opaque red, for aventurine the nature of the colouring particles was also debated for several centuries. Pettenfork (1857) and Hautefaille (1861) analysed the nature of the colouring particles of aventurine glass in the second half of the 19th century and argued that they were cuprous oxide (Cu_2O). Ebell and Swartz rejected the results advanced by these writers and established that metallic copper particles are the colouring agents. In more recent scientific investigation, X-ray diffraction and TEM analyses have confirmed that metallic copper represents the

colouring agent in aventurine glass [86, 87]. Metallic copper takes the form of an equilateral triangle with blunt corners and measures between 0.01 and 0.13 mm [82], or as a hexagonal or octahedral shape measuring a few millimetres (fig. 3.18) [83]. Metallic copper can reach these sizes (and shapes) thanks to a very slow cooling procedure and a well-engineered chemical composition which can guarantee the correct reducing conditions [9, 83].

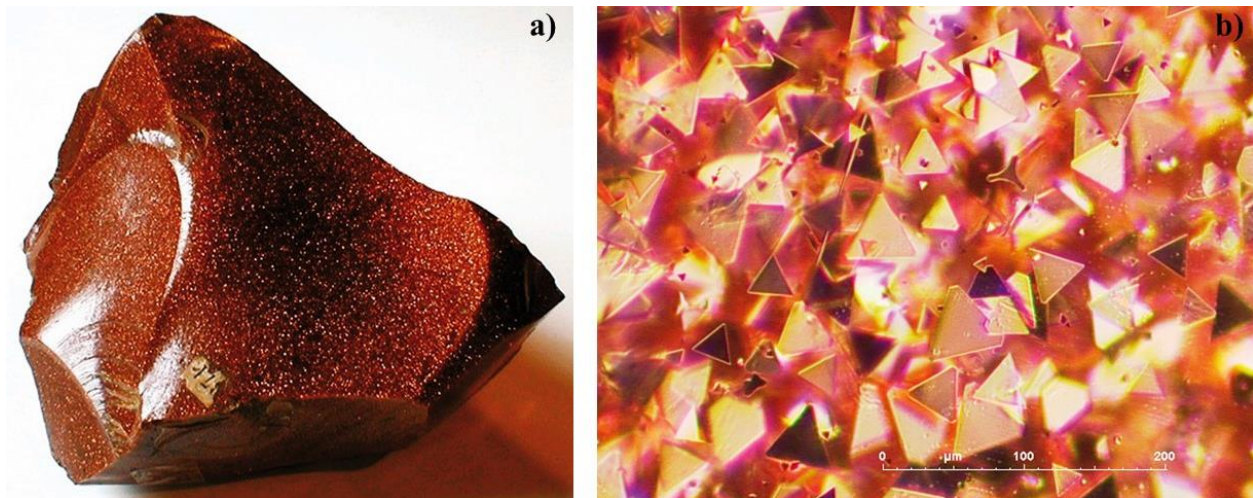


Figure 3.18 a) Block of aventurine glass; b) sample of aventurine prepared in a thin section and observed under the optical microscope. Picture taken from Moretti et al., 2013.

3.2.5.4 Hypothesis about the production technology

Thanks to the Venetian recipes it has been possible to understand the procedure used to make aventurine glass. Cullet glass (soda-lime-silica type, by using soda plant ash as a fluxing agent) represented the base glass, which was re-melted. Afterward, flakes of iron or steel together with cuprous oxide were added to the molten glass. Using several tests, the glassmaker controlled if opaque red glass was obtained, which indicated that the correct redox conditions were achieved. At this point, the furnace was switched off and left to cool spontaneously very slowly. The molten glass was left to cool inside the furnace for five days (or more) until it had reached room temperature [83]. This phase is the most critical, because the reduction in viscosity was necessary during the cooling phase to encourage the growth of the metallic copper crystals. Moreover, the lack of technological equipment which could help to indicate the range of temperature, useful to understand the nucleation or crystal growth rates, made this phase difficult to control and full of anxiety for the glassmakers. Only when the crucible was broken was it possible to understand if aventurine has been obtained or not.

3.3 Discussion and Conclusions

Throughout the data and information collected from the literature review, it is possible to outline a brief history of the technological development of copper-opaque red glass produced since the 14th century BC. By using the concentration of copper and lead (collected in the literature) and the value range indicated by Freestone [7], the three types of opaque red can be neatly divided. At the same time, as explained by [7], this division is too rigid, and several transition periods highlighted the probable presence of more than one type of opaque red circulating at the same time, maybe with different chemical characteristics.

Fig. 3.19 shows the presence of high copper-no lead in the period (7th – 6th centuries BC) after the Late Bronze Age. It is unknown if they were misdated or maybe re-used. Similar considerations can be advanced for red brown glass, which could be already produced by around the 3rd century BC. However, samples of this period with low copper-low lead should be investigated in more detail, because some of them were coloured by cuprite rather than metallic copper [72], as should be expected with red brown glass.

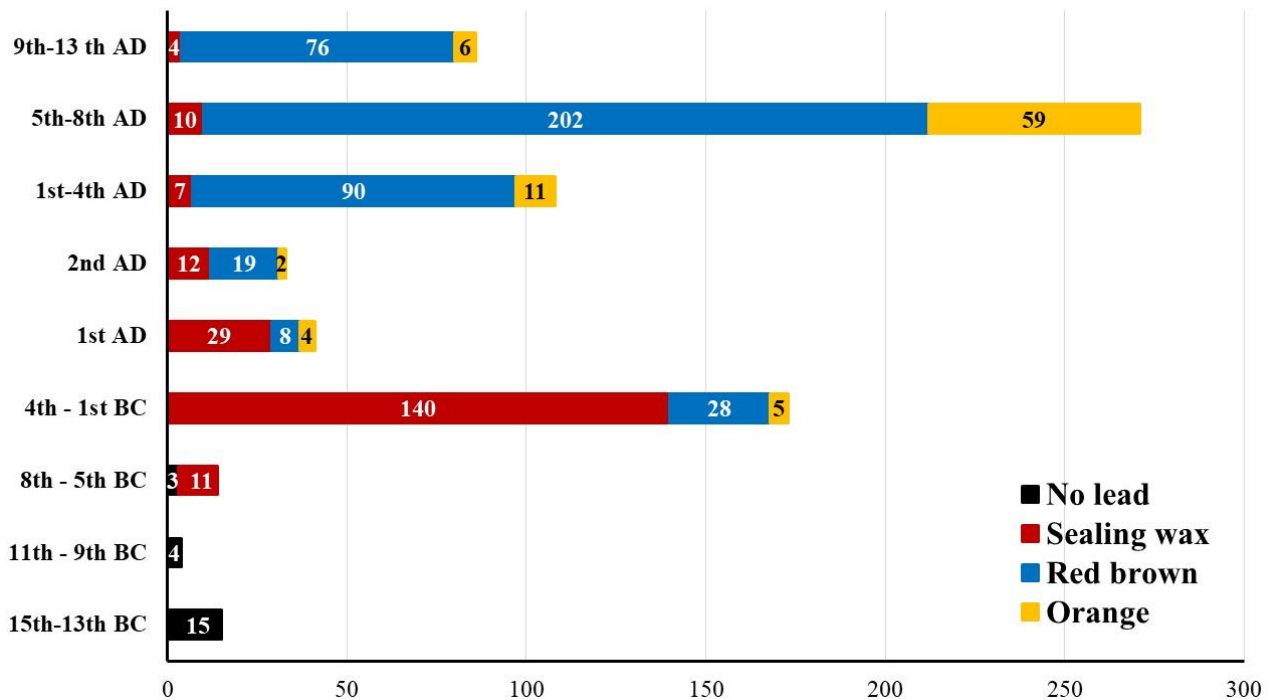


Fig. 3.19 Bar graph with the number of analyses for each red type divided by date.

3.3.1 High copper-no lead - some considerations

A well-established tradition and organised production emerged in Egypt, in which specialised glass factories were devoted to the production of coloured glass ingots. Moreover, an intensive long-distance trade supplying the Eastern Mediterranean basin and probably the Near East developed.

On the other hand, Frattesina was an important centre of production and trade in glass during this phase (1300 – 900 BC) in continental Europe, and a complex colouring technique for opaque red glass (probably still linked with the fayence technique) was used [38].

3.3.2. Sealing wax - some considerations

Although in general, sealing wax has been indicated as high copper-high lead, each period, and each region showed significant compositional differences which could indicate a variety of recipes for making sealing wax. First of all, two distinct glassmaking traditions emerged, in the Near East and the Mediterranean/continental Europe. They can be distinguished not only by the fluxing agent used (soda plant ash in the Near East samples, and natron for the other groups), but also by the amount of copper, lead and antimony, which could indicate different raw materials or recipes used to make sealing wax.

Moreover, even though Hellenistic/Roman, Celtic and La Tène samples have been considered a unique group (in this chapter), the base glass composition and the higher amount of iron in the La Tène samples make them a different sub-group. It is usually accepted that sealing wax found in continental Europe was imported via the Eastern Mediterranean area or Italy. However, some writers have highlighted the possibility that the samples from the La Tène area could represent a local recipe, using raw glass exported via the Levantine area, and then locally coloured [89]; this could explain the higher amount of iron in the La Tène samples (except the samples from Mont-Beuvray – France) which was not found in the others. However, the most widely accepted hypothesis supports the trade of ingots or cake of sealing wax from the Levantine regions or Italy to the workshops located in several regions of Europe, as isotopic analyses have revealed [47].

3.3.3. Red Brown - some considerations

About red brown glass, two points should be underlined.

- a) The period between the 5th and 13th centuries AD has been investigated by more analyses than the Roman Empire. This affects the possibility of having a clear vision of its development in each century (fig. 3.20).
- b) The period from the 3rd to 1st century BC has very few analyses, and has been studied mainly by chemical analyses, while a few archaeometric investigations have explored the nature of the colouring agent. Beyond an average higher amount of lead (PbO 7.8 wt%) in this early red brown than the later red brown (PbO 3.3-4.4 wt%) glasses, in some of the early red brown cuprite crystals have been revealed. At this point, how to define these samples is complex (chemical composition similar to red brown but coloured by cuprite). Perhaps they should be considered a further type of opaque red, resulting from the transition from high copper-no lead to red brown.

The archaeometric analyses have revealed that in the Roman period, undissolved metallic materials were rarely detected, while they have been frequently found in the samples dating from the 5th-8th centuries AD (Early Byzantine, Merovingian, Anglo-Saxon). Some scholars have suggested several tin and iron compounds [18, 28, 63], while others have advanced a probable faster melting procedure, by using high amounts of reducing agents, adopted to make red brown and unable to completely dissolve the metals [25]. Although this is still a

complex point to explain, it could be possible that after the collapse of the Roman Empire, regional recipes used different raw materials and melting procedures. The production of red brown in the transition period from the Roman Empire and the Late antique should be investigated in more detail.

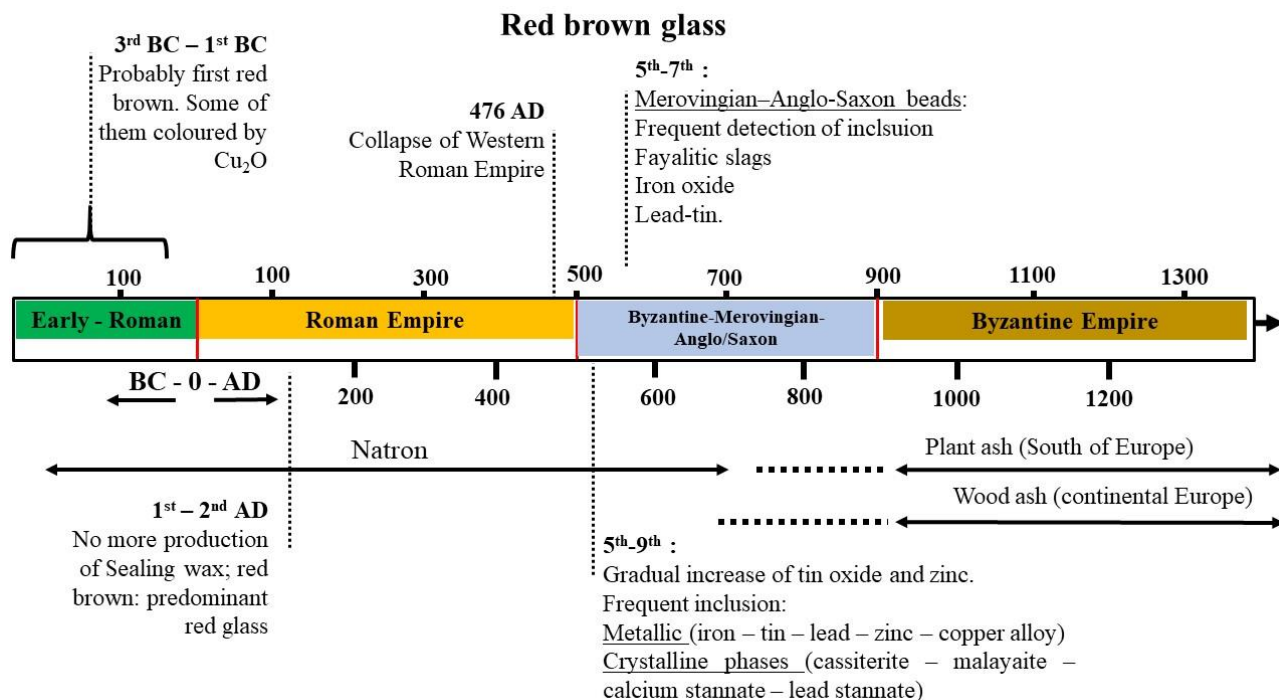


Figure 3.20. Timeline of the main phases of red brown glass.

3.3.4. Orange glass - some considerations

Orange glass is still a less investigated colour, and its production technology seems to be still unknown. However, the compositional differences between the Roman/Byzantine orange glass and the second group of Merovingian orange beads could indicate that orange glass could be produced through distinct procedures. It also suggests the presence of different local recipes spread across continental Europe which probably used the Eastern Mediterranean natron raw glass, and then coloured beads were locally coloured or imported from other sites.

This literature review has provided an overview of the manufacture of opaque copper-red glass in different regions and ages.

Although the three main opaque reds were restricted by a rigid timeframe, the main changes and features of their production were underlined, showing a continue transformation in their chemical composition, probable raw materials, colouring agent and likely melting procedures.

Social-economic aspects were only briefly mentioned, because the main focus was to show the technological changes. However, more studies are required for a deeper understanding of the trade and the organisation of production.

This review may be helpful in identifying the main features of the opaque red produced in different periods, and to discover others still unknown.

References

1. Caley E.R. Early investigation. *Analyses of ancient glassess 1790-1957*. Cornign N.Y., The cornign museum of glass, New Your, USA, 1962, pp. 13-23.
2. Caley E.R. Early investigation. *Analyses of ancient glassess 1790-1957*. Cornign N.Y., The cornign museum of glass, New Your, USA, 1962, pp. 24-66.
3. Bimson, M. Opaque red glass: A review. In Bimson and Freestone. In *Early Vitreous Materials; British Museum Occasional Paper, 56*; Bimson, M., Freestone, I.C., Eds.; British Museum: London, UK, 1987; pp. 165–171; ISBN 978-0861590568.
4. Turner W.E.S. Glass Fragments from Nimrud of the Eighth to the Sixth Century B.C. *Iraq*, **1955**, 17 (1), 57-68.
5. Hughes, M.J. A technology study of opaque red glass of the Iron Age in Britain. *Proc. Prehist. Soc.* **1972**, 38, 98–107.
6. Brill R.H., Wampler, J.M. Isotope Studies of Ancient Lead. *Am. J. Archaeol.* **1967**, 71 (1), 63-77.
7. Freestone, I.C. Composition and microstructure of opaque red glass. In Bimson and Freestone. In *Early Vitreous Materials; British Museum Occasional Paper, 56*; Bimson, M., Freestone, I.C., Eds.; British Museum: London, UK, 1987; pp. 173–191. ISBN 978-0861590568.
8. Brill, R.H.; Cahill, N.D. A Red Opaque Glass from Sardis and Some Thoughts on Red Opaque in General. *J. Glass Stud.* **1988**, 30, 16–27.
9. Moretti, C.; Gratuze, B. Vetri rossi al rame e avventurina. Confronto di analisi e ricette. *Riv. Stn. Sper. Vetro* **1999**, 3, 147–160.
10. Brun, N.; Pernot, M. The Opaque Red Glass of Celtic Enamels from Continental Europe. *Archaeometry* **1992**, 34, 235–252.
11. Brun, N.; Mazerolles, L.; Pernot, M. Microstructure of opaque red glass containing copper. *J. Mater. Sci. Lett.* **1991**, 10, 1418–1420.
12. Rehren, Th. Ramesside glass-colouring crucibles. *Archneomerry* **1997**, 39 (2), 355-368.
13. Barber, D.J.; Freestone, I.C.; Moulding, K.M. Ancient copper red glasses: Investigation and analysis by microbeam techniques. In *From Mine to Microscope. Advances in the Study of Ancient Technology*; Shortland, A.J., Freestone, I.C., Rehren, T., Eds.; Oxbow Books: Oxford, UK, 2009; pp. 115–127; ISBN 978-1-84217-259-9.
14. Henderson, J. Chemical characterization of Roman glass vessels, enamels and tesserae. *Jewel. Stud.* **1991**, 5, 65–77.
15. Stapleton C. P.; Freestone I.C.; Bowman, S.G.E. Composition and Origin of Early Mediaeval Opaque Red Enamel from Britain and Ireland. *J. Archaeol. Scie.* **1999**, 26, 913–921.
16. Arletti, R.; Ciarallo, A., Quartieri, S., Sabatino G., Vezzalini, G. Archaeometric analyses of game counters from Pompeii. In *Geomaterials in Cultural Heritage*. Maggetti & Messiga, Eds-; Geological Society, London, Special Publications, **2006**, 257, pp. 175–186.

17. Silvestri, A., Tonietto, S., Molin, G., and Guerriero, P. The palaeo-Christian glass mosaic of St. Prodocimus (Padova, Italy): Archaeometric characterisation of tesserae with copper- or tin-based opacifiers, *J. Archaeol. Sci.* **2014**, 42(1), 51–67.
18. Shugar, A. Byzantine Opaque Red Glass Tesserae from Beit Shean, Israel. *Archaeometry* **2000**, 42, 375–384.
19. Maltoni, S.; Silvestri, A. A Mosaic of Colors: Investigating Production Technologies of Roman Glass Tesserae from North eastern Italy. *Minerals* **2018**, 8, 255.
20. Maltoni, S.; Silvestri, A.; Molin, G. Opaque red glass tesserae from Roman and early-Byzantine sites of North-Eastern Italy: New light on production technologies. In Proceedings of the *Annales du 20e Congrès de l'Association Internationale pour l'Histoire du Verre, Fribourg, Switzerland, 7–11 September 2015*; Wolf, S., de Pury-Gysel, A., Eds.; Verlag Marie Leidorf GmbH: Rahden, Germany, 2017; pp. 280–287.
21. Arletti, R. Roman coloured and opaque glass: A chemical and spectroscopic study. *Appl. Phys. A* **2006**, 83, 239–245.
22. Guido, M.; Henderson, J.; Cable, M.; Bayley, J.; Biek, L. A bronze age glass bead from Wilsford Whilshire: Barrow G.42 in the Lake group. In *Proceedings of the Prehistoric Society*, **1984**, 50, pp. 245-254
23. Cable, M.; Smedley, J.W. The Replication of an opaque red glass from Nimrud. In *Early Vitreous Materials*; British Museum Occasional Paper 56; Bimson, M., Freestone, I.C., Eds.; British Museum: London, UK, 1987; pp. 151–164. ISBN 978-0861590568.
24. Welham, K.; Jackson, C. M.; Smedley, J.M. Colour formation in sealing wax red glass, In Proceedings of the *Annales du 14e Congrès de l'Association Internationale pour l'Histoire du Verre, Venzia-Milano*, 1998, pp. 11–15.
25. Peake, J.R.; Freestone, I.C. Cross-Craft Interactions between Metal and Glass Working: Slag Additions to Early Anglo-Saxon Red Glass. In *Integrated Approaches to the Study of Historical Glass—IAS12*; Meulebroeck, W., Nys, K., Vanclooster, D., Thienpont, H., Eds.; Proceedings of SPIE: Cergy, France, 2012; Volume 8422, p. 842204.
26. Verità, M.; Arena, M.S.; Carruba, A.M.; Santopadre, P.. Materiali vitrei nell'opus sectile di Porta Marina (Ostia antica), *BOLL. ICR* **2008**, 16-17, pp. 78-94.
27. Verità, M.; Santopadre, P. Unusual Glass Tesserae from a Third-century Mosaic in Rome. *J. Glass. Stud.* **2015**, 57, 287–292.
28. Fiori, C. Production technology of Byzantine red mosaic glasses. *Ceram. Int.* **2015**, 41, 3152–3157.
29. Boschetti, C.; Henderson, J.; Evans, J.; Leonelli, C. Mosaic tesserae from Italy and the production of Mediterranean coloured glass (4th century BCE–4th century CE). Part I: Chemical composition and technology. *J. Archaeol. Sci. Rep.* **2016**, 7, 303–311.
30. Heck, M., Hoffmann, P. Analysis of the early Medieval glass beads – The raw materials to produce green, orange and brown colours. *Mikrochim. acta* **2002**, 139, 71-76,.
31. Heck m., Hoffmann, P. Coloured opaque glass beads of the Merovingians. *Archaeometry*, 42 (2), **2000**, 341-357.
32. Freestone, I.C.; Stapleton, C.P.; Rigby, V. The production of red glass and enamel in the Late Iron Age. Roman and Byzantine periods. In *Through a Glass Brightly: Studies in Byzantine and Medieval Art and Archaeology*; Presented to David, Buckton; Entwistle, C., Buckton, D., Eds.; Oxbow Books: Oxford, UK, 2003; pp. 142–154. ISBN 978-1785702518.
33. Silvestri, A.; Tonietto, S.; D'Acapito, F.; Molin, G. The role of copper on colour of palaeo-Christian glass mosaic tesserae: An XAS study. *J. Cult. Herit.* **2012**, 13, 137–144.
34. Schibille, N.; Boschetti, C.; Valero, M.A.; Veron, E.; Juan, J. The Color Palette of the Mosaics in the Roman Villa of Noheda (Spain). *Minerals* **2020**, 10, 272.

35. Arletti, R.; Fiori, C.; Vandini, M. A study of glass tesserae from mosaics in the monasteries of Daphni and Hosios Loukas (Greece). *Archaeometry* **2010**, 52, 5, 796–815.
36. Shortland, A.J., Eremin, K. The analysis of second millennium glass From Egypt and Mesopotamia, part 1: new WDS analyses, *Archaeometry* **2006**, 48 (4), 581–603.
37. Brill, R.H. Chemical analyses of some glasses from Frattesina, *J. Glass Stu.* **1992**, 34, 11–22
38. Santopadre, P.; Verità, M. Analyses of the production technologies of Italian vitreous materials of the Bronze Age. *J. Glass Stu* **2000**, 42, 25–41.
39. Angelini, I.; Artiolia, G.; Bellintani, P.; Diella, V.; Gemmi, M.; Polla, A.; Rossi, A. Chemical analyses of Bronze Age glasses from Frattesina di Rovigo, Northern Italy. *J. Archaeol. Sci.* **2004**, 31, 1175–1184.
40. Lilyquist, C.; Brill, R.H. Analytical procedure. In *Studies in Early Egyptian Glass*; Metropolitan Museum of Art: New York, NY, USA, 1993, pp. 47-58; ISBN 978-0300200195.
41. Henderson, J. Electron probe microanalysis of mixed-alkali glasses, *Archaeometry*, **1988**, 30, 77-91.
42. Rehren, Th. New aspect of the Egyptian glassmaking. *J. Glass Stu.* **2000**, 42, 13-24.
43. Rehren, Th.; Pusch, E.B. Late Bronze Age glass production at Qantir-Piramesses, Egypt. *Science* **2005**, 308, 1756–1758.
44. Jackson, C.M.; Nicholson, P.T. The provenance of some glass ingots from the Uluburun shipwreck. *J. Archaeol. Sci.* **2010**, 37, 295–301.
45. Boschetti, C. Vitreous Materials in Early Mosaics in Italy: Faience, Egyptian Blue, and Glass. *J. Glass Stu.* **2011**, 53, 59-91.
46. Bayley, J. Roman enamel and enamelling: new finds from Castelford, Yorkshire, In *Proceeding of the Annales du 16e Congrès de l'Association Internationale pour l'Histoire du verre, Vol. London 2003 (Nottingham, 2005)*, pp. 72–75.
47. Boschetti, C.; Henderson, J.; Evans, J. Mosaic tesserae from Italy and the production of Mediterranean coloured glass (4th century BCE–4th century CE). Part II: Isotopic provenance. *J. Archaeol. Sci. Rep.* **2017**, 11, 647–657.
48. E. Marianne Stern, “Hellenistic Glass from Kush (Modern Sudan),” In *Proceeding 8eAnnales de l'Association Internationale pour l'Histoire du Verre, v. 8, London/Liverpool, 1979 (Liège, 1981)*, pp. 35–59.
49. Weinberg, G.D. *Glass Vessels in Ancient Greece. Their History Illustrated from the Collection of the National Archaeological Museum, Athens*; Archaeological Receipt Fund: Athens, Greece, 1992; pp. 112–115.
50. Ignatiadou, D. A Haematinon bowl from Pydna. In *Proceedings of the Annales du 18e Congrès de l'Association Internationale pour l'Histoire du Verre, Thessaloniki, Greece, 20–25 September 2009*; Ignatiadou, D., Antonaras, A., Eds.; ZITI Publishing: Thessaloniki, Greece, 2012; pp. 69–74.
51. Davis, M.; Freestone I.C. Trading North: Glass-working beyond the edge of the empire. In *Things that travelled- Mediterranean Glass in the First Millennium CE*. Rosenow, D., Phelps, M., Meek, A., Freestone I., Eds.; Publisher: UCL Press University College London, UK, 2018, pp. 107-133.
52. Brill, R.H. *Chemical Analyses of Early Glasses. Volume 2 Tables of Analyses*; The Corning Museum of Glass: Corning, NY, USA, 1999; ISBN 0-872900-143-2.

53. Shortland, A.; Schachner, L.; Freestone, I.; Tite, M. Natron as a flux in the early vitreous materials industry: sources, beginnings and reasons for decline. *J. Archaeol. Sci.* **2006**, *33*, 521-530.
54. Ahmed, A.A.; Ashour, G.M. Effect of heat treatment on the crystallisation of cuprous oxide in glass. *Glass Technol.* **1981**, *22*, 24-33.
55. Nenna, M.D.; Gratuze, B. Etude diachronique des compositions de verres employés dans les vases mosaïques antiques: Resultats preliminaires. In *Proceedings of the Annales du 17e Congrès de l'Association Internationale pour l'Histoire du Verre, Antwerp, Belgium, 4-8 September 2006*; Janssens, K., Degryse, P., Cosyns, P., Caen, J., Van't dack, L., Eds.; University Press Antwerp: Antwerp, Belgium, 2009; pp. 199-205.
56. Freestone, I.; Stapleton, P.C. Composition, technology and production of coloured glasses from mosaic vessels of the early Roman Empire. In *Glass of the Roman Empire*; Bayley, J., Freestone, I., Jackson, C., Eds.; Oxbow: Oxford, UK, 2013, pp. 61-76.
57. Neri, E.; Jackson, M.; O'Hea, M.; Gregory T.; Blet-Lemarquand M.; Schibille, N. Analyses of glass tesserae from Kilise Tepe: New insights into an early Byzantine production technology. *J. Archaeol. Sci. Report* **2017**, *11*, 600-612.
58. Santagostino Barbone, A.; Gliozzo, E.; D'acapito, F.; Memmi Turbanti, I.; Turchiano, M.; Volpe, G. The sectilia panels of faragola (Ascoli Satriano, southern Italy): A multi-analytical study of the red, orange and yellow glass slabs. *Archaeometry* **2008**, *50*, 451-473.
59. Brill, R.H.; Whitehouse, D. The Thomas Panel. *J. Glass Stu.* **1988**, *30*, 34-50.
60. Wypyski, M.T. Technical Analysis of Glass Mosaic Tesserae from Amorium. *Dumbarton Oaks Papers*, **2005** ,*59*, 183-192.
61. Verità M. Perle vitree dalle necropoli longobarde in Italia. In *Natura dei materiali e tecniche di lavorazione. Archeologia medievale a trezzo sull'adda il sepolcreto longobardo e l'oratorio di san martino le chiese di santo stefano e san michele in sallianense*, Lusuardi Siena S. e Giostra. C., Eds; Milano, 2012, pp. 355-379.
62. Lazar, I.; Willmott, H. *The glass from the Gnalčić wreck*. Univerza na Primorskem, Znanstveno-raziskovalno središče Koper, Inštitut za dediščino Sredozemlja, Koper, Založba Annaleskoper 2006 pp. 62, 64.
63. Schibille, N.; Degryse, P.; Corremans, M.; Specht, C.G. Chemical characterisation of glass mosaic tesserae from sixth-century Sagalassos (south-west Turkey): chronology and production techniques. *J. Archaeol. Sci.* **2012**, *39*, 1480-1492.
64. Barca, D.; Basso, E.; Bersani, D.; Galli, G.; Invernizzi, C.; La Russa, M.F.; Lottici, P.P.; Malagodi, M.; Ruffolo, S.A. Vitreous tesserae from the calidarium mosaics of the Villa dei Quintili, Rome. Chemical composition and production technology. *Microchem. J.* **2016**, *124*, 726-735.
65. Verità, M. Le tessere vitree dei mosaici Medievali a Roma. Tecnologia e degrado. In *Mosaici Medievali a Roma Attraverso il Restauro Dell'icr 1991-2004*; Andaloro, M., D'Angelo, C., Eds.; Publisher: Gangemi, Rome, Italy, 2017, pp. 437-477.
66. Arletti R.; Quartieri, S.; Vezzalini, G.; Sabatino, G.; Triscari, M.; Mastelloni, M.A. Archaeometrical analyses of glass cakes and vitreous mosaic tesserae from Messina (Sicily, Italy). *J. Non-Cryst. Sol.* **2008**, *354*, 4962-4969.
67. Schibille, N.; McKenzie, J. Glass tesserae from Hagios Polyuktos, Constantinople: Their early Byzantine affiliations. In *Neighbours and Successors of Rome. Tradition of Glass Production and Use in Europe and the Middle East in the Later 1st Millennium AD*; Keller, D., Price, J., Jackson, C.M., Eds.; Oxbow Books: Oxford, UK, 2014; pp. 114-127, ISBN 978178297397.
68. Paynter, S.; Kearns, T.; Cool, H.; Chenery, S. Roman coloured glass in the Western provinces: The glass cakes and tesserae from West Clacton in England. *J. Archaeol. Sci.* **2015**, *62*, 66-81.

69. Van der Werf, I.; Mangone, A.; Giannossa, L.C.; Traini, A.; Laviano, R.; Coralini, A.; Sabbatini, L. Archaeometric investigation of Roman tesserae from Herculaneum (Italy) by the combined use of complementary micro-destructive analytical techniques. *J. Archaeol. Sci.* **2009**, *36*, 2625–2634.
70. Ricciardi, P.; Colombari, P.; Tournié, A.; Macchiarola, M.; Ayed, N. A non-invasive study of Roman Age mosaic glass tesserae by means of Raman spectroscopy. *J. Archaeol. Sci.* **2009**, *36*, 2551–2559.
71. Verità, M. Analisi di tessere musive vitree del battistero della Basilica di San Marco in Venezia. In Proceedings of the *Scienza e Tecnica del Restauro della Basilica di San Marco: Atti del Convegno Internazionale di Studi, Venezia, Italy, 16–19 May 1995*; Vio, E., Lepschy, A., Eds.; Publisher: Istituto Veneto di Scienze, Lettere ed Arti, Venezia, Italy, 1999; pp. 567–585, ISBN 8886166796.
72. Gedzeviciute, V.; Welter, N.; Schüssler, U.; Weiss, C. Chemical composition and colouring agents of Roman mosaic and millefiori glass, studied by electron microprobe analysis and Raman microspectroscopy. *Archaeol. Anthropol. Sci.* **2009**, *1*, 15–29.
73. Basso, E.; Invernizzi, C.; Malagodi, M.; La Russa, M.F.; Bersani, D.; Lottici, P.P. Characterization of colorants and opacifiers in roman glass mosaic tesserae through spectroscopic and spectrometric techniques. *J. Raman Spectrosc.* **2014**, *45*, 238–245.
74. Schibille, N.; Neri, E.; Ebanista, C.; Ammar, M.R.; Bisconti, F. Something old, something new: The late antique mosaics from the catacomb of San Gennaro (Naples). *J. Archaeol. Sci. Rep.* **2018**, *20*, 411–422.
75. Neri, E.; Biron, I.; Verità, M. New insights into Byzantine glass technology from loose mosaic tesserae from Hierapolis (Turkey): PIXE/PIGE and EPMA analyses. *Archaeol. Anthropol. Sci.* **2018**, *10*, 1751–1768.
76. Verità, M.; Rapisarda, S. Studio analitico di materiali musivi vitrei del XII-XIII secolo dalla Basilica di Monreale a Palermo. *Riv. Staz. Sper. Vet.* **2008**, *2*, 15-29.
77. Freestone, I.C.; Bimson M.; Buckton D. Compositional categories of Byzantine glass tesserae, in *Annales du 11e Congrès de l'Association Internationale pour l'Histoire du Verre*, Bâle, 29 agosto – 3 settembre 1988, AIHV, Amsterdam, 1990, pp. 271–278.
78. Andreescu-Treadgold, I.; Henderson J.; ROE, M., Glass from the mosaics on the west wall of Torcello's basilica, in *Arte Medievale*, 2006, *2*, pp. 87-140.
79. Fiorentino, S.; Chinni T.; Vandini, M. Ravenna, its mosaics and the contribution of archaeometry. A systematic reassessment on literature data related to glass tesserae and new considerations. *J. Cult. Heri.*, **2020**, *46*, 335-349.
80. Cholakova, A.; Rehren, T. Producing black glass during the Roman period—notes on a crucible fragment from Serdica, Bulgaria. In *Proceedings of the 39th International Symposium for Archaeometry, Leuven, Belgium, 28 May–1 June 2012*; Scott, R., Braekmans, M., Degryse, P., Eds.; Centre for Archaeological Sciences: Leuven, Belgium, 2014; pp. 261–267.
81. Rehren, T.; Cholakova, A.; Zivanovi, C.M. The making of black glass in Late Roman Doclea. In *New Antiq. Doclea, Ju Muzeji I Galerije Rodgorice*, 2012, *3*, 71–90.
82. Beyersdorfer, P., Studien ueber das Aventuringlas. *Glastechnische Berichte*, **1943**, *21*, 1-7.
83. Moretti, C.; Gratuze, B.; Hreglich, S. Il vetro Aventurina: (II parte) La tecnologia, le analisi. *Staz. Sper. Vet.* **2010**, *6*, 29-47.
84. Zecchin L. Avventurina, lattimo e altri vetri. In *Vetro e vetrai di Murano*. Publisher: Arsenale, Venezia, Italy, 1987, Volume 2, pp. 327-336.
85. Zecchin, P. La pasta venturina, vetro speciale muranese, *J. Glass Stu.* **2005**, *47*, 93-106.

86. Quaranta, A., Ceccato, R.; Menato, C.; Pederiva, L.; Capra, N.; Dal Maschio R. Formation of copper nanocrystals in alkali-lime silica glass by means of different reducing agents. *J. Non Cryst. Solids* **2004**, 345-346, 671-675
87. Shcheglova M.D.; Babenko, T.V.; Polonzhai, S.G.; Svistun, V.M. Mechanism of aventurine formation in copper-containing alkali-lead silicate glass. *J. Glass and Ceramic* **1996**, 53 (1-2), 14-17.
88. Moretti, C.; Gratuze, B.; Hreglich, S. Le verre aventurine (avventurina): son histoire, les recettes, les analyses, sa fabrication. *ArcheoSciences* **2013**, 37, 135-154.
89. Davis, M. The glass: its composition and manufacture. In *Technology at the transition: relationships between culture, style and function in the Late Iron Age determined through the analysis of artefacts*. 2014, PhD Thesis, Cardiff University, pp. 54-78.

**Section Two –
Opaque red glass *sectilia* from the *Lucius Verus* villa. Archaeometric
study**

*Villam praeterea extruxit in via Clodia famosissimam,
in qua per multos dies et ipse ingenti
luxuria debacchatus est cum libertis suis et amicis imparibus*
[*Historia Augusta, Ver. 8*]

4. Archaeological context: sites and materials

4.1 The history of the archaeological site

The Lucius Verus villa is located on the top of the hill in Acquatraversa five miles along the *Via Cassia/Clodia*, northwest of Rome (fig. 4.1). Only the remains of the wall foundations and the pavements of the numerous settings are visible today. However, in the same place in which the villa was located, there is now the 19th century Villa Manzoni which is the headquarters of the Kazakhstan embassy; the government of Kazakhstan acquired this building for its embassy in 2003 [1].



Figure 4.1. City of modern Rome, to identify the position of the *Lucius Verus* villa.

The first mention of the *Lucius Verus* villa is attested in the 12th century AD by a small inscription on the wall of the St. Lorenzo in Lucina church. The villa was reinhabited, at least according to the documentation, at the beginning of the 17th century AD, when the entire complex was bought by Marcantonio Borghese in 1609 [1]. In this period several busts of *Lucius Verus*, and of Marco Aurelio, were recovered thanks to the excavation carried out by the Borghese family and commissioned by Pope Clemente X (1674). From these excavations numerous sculptures and other objects dating back to the Roman Age were uncovered. Unfortunately, most of the properties of the Borghese family were sold; for example several busts of *Lucius Verus* and Marcus Aurelius were sold to Napoleon in the 1807. Now all of these finds are on display in the Louvre Museum [1].

In the 19th century the villa was subjected to the predatory activities of unscrupulous antique dealers who removed all the decorative materials which adorned the villa's numerous rooms. In the 1923 the villa was acquired by Count Manzoni, who obtained permission to construct a new building (the villa still stands today as the Villa Manzoni) using the foundation of the ancient Roman villa. The structural archaeological evidence of the Lucius Verus villa has been heavily damaged by these building works. In the 1953 the villa built by Count Manzoni was sold to NPDAL and this location fell into irreversible decay [1].

At the end of the 1980s, two archaeological excavations were performed (1987-1988), directed by the *Soprintendenza Archeologica di Roma*, which discovered parts of the original Roman villa [1].

In 2003, the Kazakhstan government bought Villa Manzoni in order to establish its embassy (as mentioned above), and between 2005 and 2009 new archaeological excavations were conducted in the same area, enriching the previous data and shedding light on the decoration in some settings of the Roman villa [1].

4.1.2 The Roman villa from the 1st century BC to the 4th century AD

Two hectares of the garden around the Villa Manzoni were involved in the archaeological excavation and investigation, which occurred in 1987 and 1988. The Roman villa extends down the slope of the hill with several terraces, including constructions dating from different ages. For this reason, the archaeologists decided to divide the archaeological evidence into five sectors labelled A, B, C, D and E (fig.4.2). In each sector several rooms or settings, indicated by normal numeration, have been identified.

Using the scheme elaborated by Caserta [1] in which the main steps of the villa from the late Republican period until the 4th century AD are summarised, the sectors can be divided chronologically:

- Republican Age to 1st century AD
 - Hydraulic system, subterranean cistern (sector D)
 - Opus incertum* and *opus reticulatum* (sector C, D; subterranean A, B, D)
 - Tank for collecting water
- Imperial villa (*Lucius Verus*, 2nd century AD)
 - Monumental fountain (sector A)
 - Settings 16-19 (sector C, subterranean Villa Manzoni)
 - Reconstruction works in the cistern in settings 21-23 and 28 (sector D)
 - Settings 25-53 and wall with niches (sector D)
- Changes occurring in the 3rd century AD
 - Settings 17-19 (sector C)
 - Setting 24-25 restoration (sector D, E)
 - Settings 32-45 (sector D)
 - Mosaic decoration, setting 32 (sector D)
- Traces of the 4th century AD
 - Setting 24 – *doliarium* – (sector D)
 - Setting 48, 51-53 *calcara* (sector E)

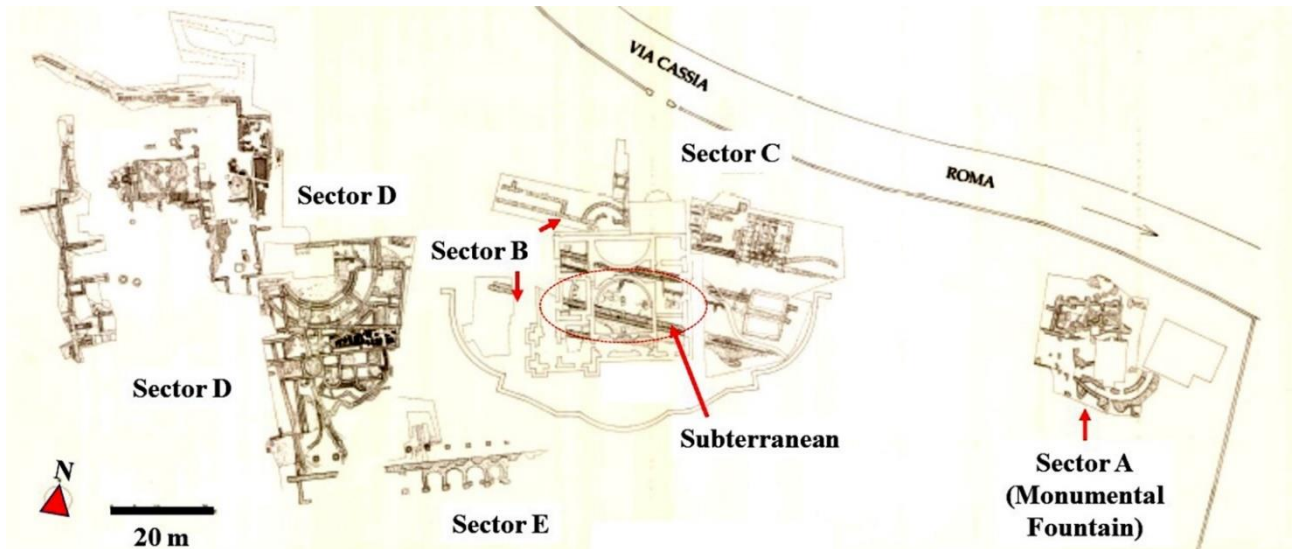


Figure 4.2. Planimetry of the Lucius Verus villa. Picture taken from Caserta et al. 2012.

4.1.2.1 Before being an Imperial villa (2nd century BC – 1st century AD)

The first area to be inhabited was sector D, as revealed by the recovery of hydraulic system devoted to collecting water and avoiding the formation of backwater. The wall made by *opus incertum* technique (sector D) dates from the same period. These data support the hypothesis advanced by Lugli in 1923 which established that this area was used for agriculture activities since the 2nd century BC [1].

This place continued to be inhabited until the 1st century AD as attested by the presence of fragmentary walls in sector C, measuring about 36 m and indicating the existence of housing nucleus, made by *opus reticulatum* (sector C) and a tank and other drainage channel made by the same technique [1].

4.1.2.2 The Imperial villa of Lucius Verus (2nd century AD)

Lucius Ceionius Commodus Verus was born in 130 AD and was adopted by the Emperor Antonino Pio together with Marcus Aurelius. The two brothers were co-Emperors from 161 until 169 AD, when *Lucius Verus* died [1].

They conducted a war against the Parthian Empire in the Near East (near modern-day Syria) between 162 and 166, achieving an important victory. It was probably around 166 AD, when the two Emperors came back from the war, that *Lucius Verus* decided to build his *otium* villa on the top of the hill five miles along the *Via Cassia* (at modern-day Acquatraversa).

Between 166 and 169 the villa was the Imperial residence of the emperor, and as mentioned in the *Historia Augusta*, the Emperor (*Lucius Verus*) lived in a dissolute way, probably with frequent luxury banquets and long parties [1].

In 169 ad, *Lucius Verus* and *Marco Aurelio* moved toward the northern border of the Empire in a new war against the Quadi and Marcomanni. However, *Lucius Verus* had to leave the battle very early, and some days after he died in Altino, some kilometres north of modern-day Venice. The real cause of *Verus*' death is still

unknown; however, his body was brought to Rome by Marcus Aurelius, and was then deified by the Roman Senate.

Focusing more on the villa, it emerged from the archaeological findings that during the 2nd century AD new edifices were constructed to host rich and luxury rooms, fountains, a thermal complex and other facilities. Moreover, many parts of this villa would have been decorated by precious marbles, mosaics (glass tesserae and lithic tesserae) and the *opus sectile* technique using both marbles and glass *sectilia* to increase the beauty of the villa [1].

The villa was located on the highest part of the hill, and it was possible to reach it by walking from the entrance which was down in the valley. On the east side (sector A) a monumental fountain of 700 square meters was built, which would have been decorated with precious marbles. On the West side (sector D) a small thermal complex, with *frigidarium*, *tepidarium* and *caldarium*, which were collocated at slightly different height in order to take advantage of the sun light until the sunset. On the top of this little thermal system, there were several rooms decorated by pavements with lithic mosaic black and white, using specific geometrical motifs [1].

In sector C (fig. 4.3; 4.4) there were some rooms in which a precious decoration in *opus sectile* technique (both stone and glass *sectilia*) and a spectacular view from the hill toward the south (hence to Rome) should impress the guest of the Emperor for its beauty and luxury. All these sectors are dated to the 2nd century AD, due to the similarities of the construction technique, the coeval developments of the structures which follow (almost always) a similar orientation, and also for the recovery of anepigraphic stamps dated to the period of *Lucius Verus* [1].

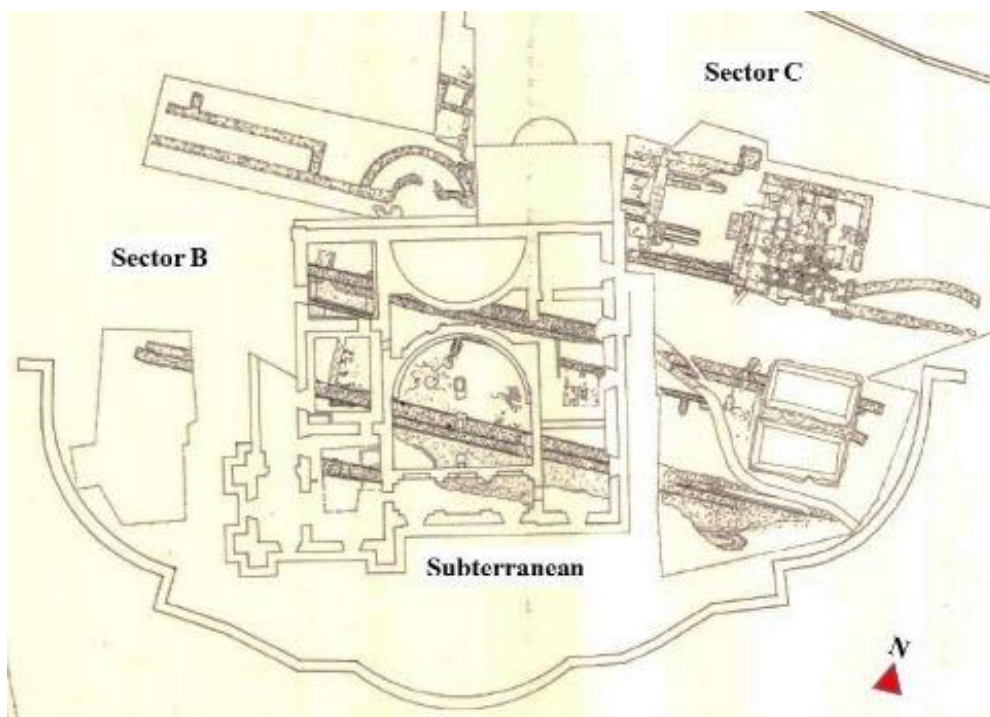


Figure 4.3. Planimetry of the sector B and C. Picture taken from Caserta et al. 2012.

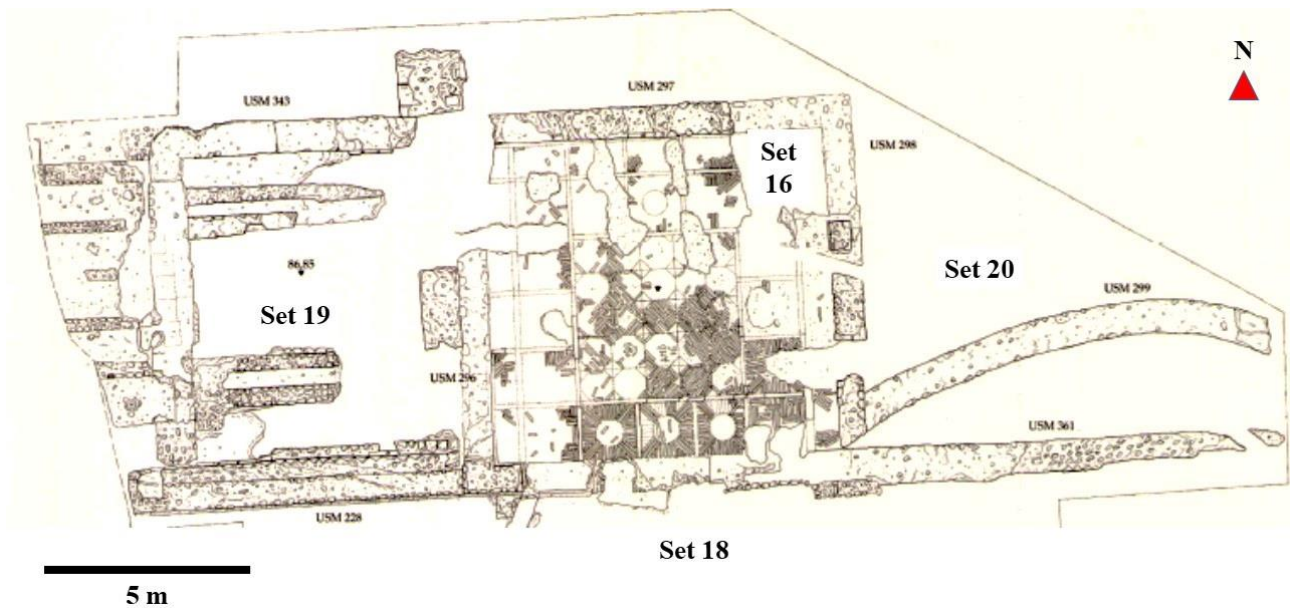


Figure 4.4. Planimetry of the sector C showing the presence of pavement preparation for the opus sectile decoration. Picture taken from Caserta et al. 2012.

Room 16 is of particular interest for this research. It is 9.5 x 8.7 m in size, and the pavement still exhibited the preparation to receive the *opus sectile* decoration (fig. 4.5a, b, c, d). The preparation was composed of two layers: the first was a pozzolana mortar with fragments of tuff 25 cm in size and the second was made by mortar with fragment of potsherds or earthenware (African production) cut in rectangular shape of 7 cm of length. The central area (4.4 m x 4.4 m) is composed of several squares with 90 cm x 90 cm each side, in which the potsherds were collocated to create regular geometrical shapes such as: hexagonal (with side of 36 cm) and triangles. Each square is divided into fragments of white marble with 8 cm of length.

Between the preparation of the pavement and the wall an empty space of about 5 mm divided the two structures. This could be due to the fact, that also the walls were decorated by *opus sectile* technique, and that empty space would have been the thickness of the glass *sectilia* [1].

In other parts of the villa, such as in room 19 (sector C), and in rooms 21, 23 and 28 (sector D), several findings connected to the preparation for *opus sectile* decoration were uncovered. However, most of the *sectilia* used to decorate the rooms have not been found in the villa, except 806 glass *sectilia* in the last excavation in 2005-2009 [1].

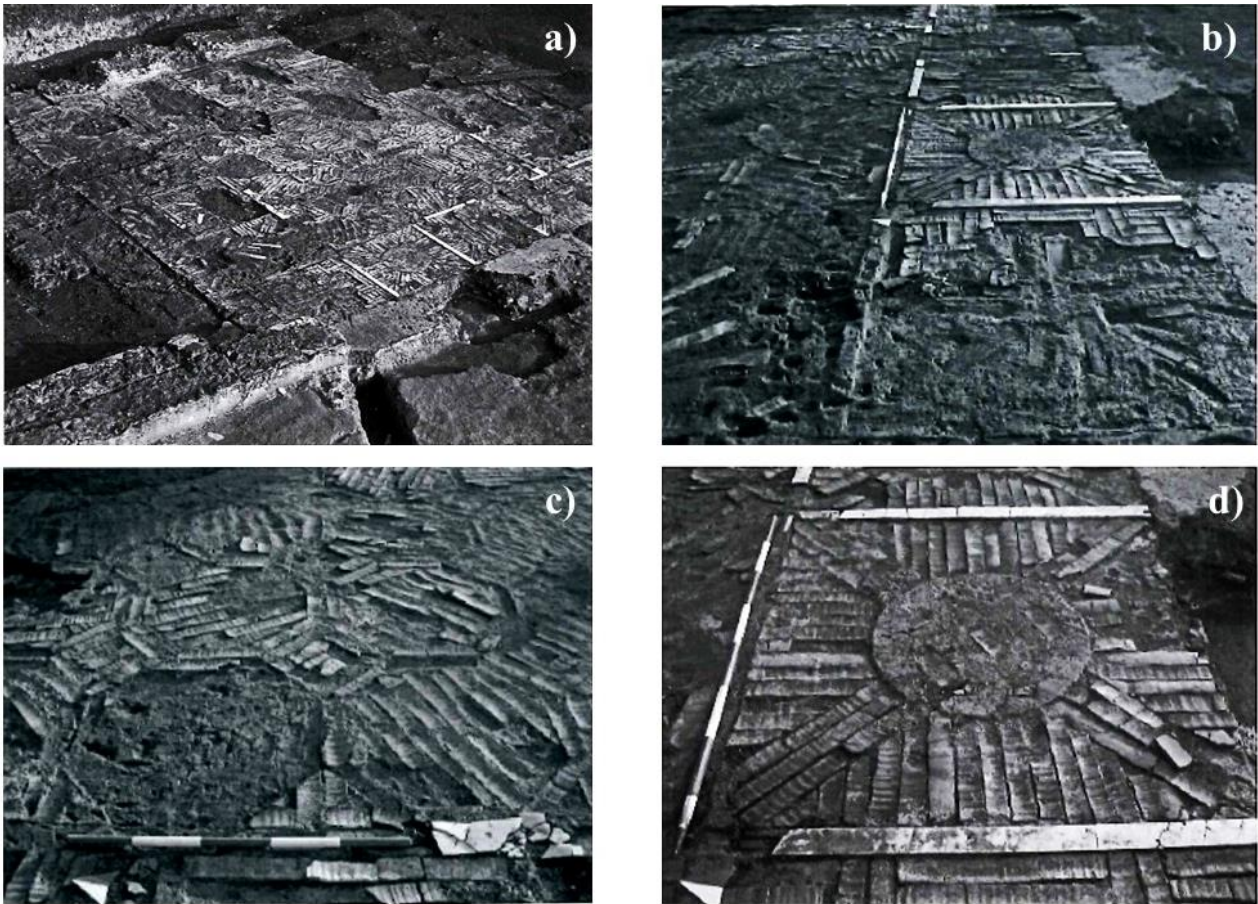


Figure 4.5. The preparation layer for *opus sectile* decoration of the Lucius Verus villa uncovered in sector C (room 16) revealed by the archaeological excavations in 1988-1989. Picture taken from Caserta et al. 2012.

4.1.2.3 The villa from 3rd to 4th century AD

After Lucius Verus died, it is likely that his daughter Lucilla lived in the villa before being imprisoned and sent into exile to the Island of Capri where she died. After Lucilla's death, the villa was acquired by a rich aristocratic family, which used it at least until the beginning of the 4th century AD. There are no documents which attest to the name of the new owner. The structure of the villa can be considered almost the same, and the archaeological excavation revealed only some maintenance work to the main structures, and some structural changes. Of artistic interest is the mosaic decoration over the thermal complex, in white and black lithic *tesserae* representing human figures with a specific iconographic meaning [1].

4.2 The Gorga collection and the *opus sectile* decoration from the Lucius Verus villa

4.2.1 The Gorga collection

The Italian tenor Evangelista Gennaro Gorga (1865 – 1957) was an impressive collector, who between the 19th – 20th century AD collected every type of ancient object and artefact of different materials: ceramic, metal, sculpture and glass. To give an idea of the number of objects that he collected, ten apartments in Rome were rented by him to store the acquired artefacts. However, during the 1950s Gorga had financial problems and so was forced to sell part of his collection to other collectors and the rest to the Italian government, which obtained greater part of his collection [2]. The glassware from the collection is stored in the storehouse of *Soprintendenza Archeologica di Roma*, in St. Croce in Gerusalemme square.

The study of the glass objects in the Gorga collection was commissioned to Professor L. Saguì and her co-workers by the director of the *Soprintendenza Archeologica di Roma* Dr. Mariarosa Barbera, in 1993.

The collection is comprised of 160,000 glass fragments dating from the 4th century BC until the 19th century AD, and all were recovered from excavations in Rome between the 19th and 20th centuries [3]. After several years of study, Saguì and co-workers grouped 26,000 pieces (Table 4.1) of glass which showed similar characteristic: shapes, thickness, and how they were cut. The homogeneity of these pieces suggested the same provenance, probably from a Roman Imperial villa.

Table 4.1. Number of *sectilia* pieces divided by colour. Data taken from Saguì et al., 2009.

Monochrome	N. of pieces	Thickness (mm)	Colour hues
Red	8183	1.8-10	3-4
orange	223	2-10	2
yellow	1362	1.7-7	3-4
green	1138	1.7-13	8.10
Light blue	2531		4
blue	911	1.7-9	2-3
black	10		
white	120		
Polychrome	N. of boxes	Thickness (mm)	Colour hues
Red with white dots	0.5	1.7 - 7	4
Serpentine type 1	2	4-5 rare 20-30	Yellow strips on one side
Serpentine type 2	11	Slabs 1-10 Strips 11-12	White, yellow or green strips

Through the comparison of the Gorga *sectilia* with other glass *sectilia* found in the *Museo del Vetro di Murano*, British Museum and the Victoria and Albert Museum which were attested to come from Lucius Verus villa, it was possible to assume the same provenance. Indeed, the *sectilia* studied by Saguì exhibit the same thickness, shapes and colours and they form the same decorative panel reconstructed and exhibited in the Museums mentioned above.

In the archive of the *Museo del Vetro di Murano*, the scholar Nesbitt is named as the donor of these *sectilia*. Furthermore, in his manuscript (1880), Nesbitt described the excavations and the *opus sectile* decoration of the Lucius Verus villa, mentioning the presence of thousands of glass fragments which adorned the pavements of the villa (probably room 16, mentioned in the previous paragraph). Nesbitt was not the only visitor in this historical site, indeed he mentioned the presence of numerous other people who gathered and broke the glass

sectilia into several fragments, hampering a future reconstruction of the original decorative motif. Moreover, he noted that the numerous *sectilia* found on the floor, which had clearly fallen from the walls [4]. Nesbitt was able to save only “a few thousand” *sectilia* from this predatory practise. These *sectilia* were offered by Nesbitt to the *Museo del Vetro Murano*, to the British Museum (which has six panels), and to the Victoria and Albert Museum (fig.4.6b) [1,2,4,5].

Tomassetti was another important source for Professor Saguì’s research, because, as well as Nesbitt, he visited the historical site in 1879 and mentioned that several thousands of coloured sheets glass were recovered from the pavements of the Lucius Verus villa and boxes full of these glass pieces were sold to a rich Roman collector, most likely Evangelista Gorga.

The panels formed a decorative motif called *cancellum*, comprised of the following elements: a rectangular bar including transparent green glass and a yellow border (H. 1.55 cm, W. 1.9 cm); two or four rectangular bars (L. 2.8 cm, W. 1.05 cm) with rows of four yellow ring-and-dot motifs, overlapping and incomplete, in a red matrix; at each end, a circular piece made by canes (D. 1.75 cm) consisting of a yellow rosette with eight petals in the red matrix with a yellow border. Inside the border, at each corner, red triangles of two different sizes (L. of base 4.3 cm; L. 6.9 cm); rectangular bars (L. 4.4. cm, W. 0.6 cm) with a row of five solid yellow circles in a red matrix; the ends of the bars touch the corners of the rectangular base at the midpoints of the sides; some components are trimmed at the points of contact with circular canes and green and yellow bars [4].

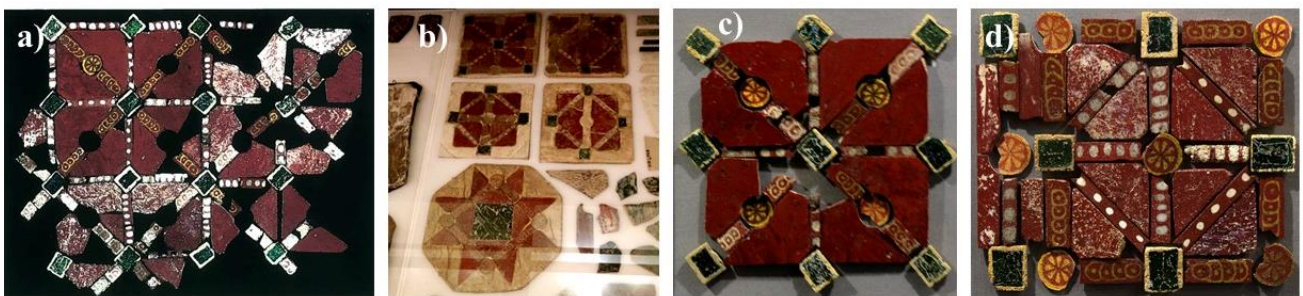


Figure 4.6. Panels of the *opus sectile* decoration from the Lucius Verus villa, with *cancellum* motif. They exhibit the round rosette with 8 yellow petals which suggested a common provenance. **a)** Picture taken from Saguì et al., 2005; **b)** picture taken from the Victoria and Albert Museum, London; **c)-d)** picture taken from the *Palazzo Altemps* Rome.

Today, panels with identical characteristics are attested in the British Museum, Victoria and Albert Museum, Collection Sangiorgi, Metropolitan Museum, Corning Museum (previously owned by the Victoria and Albert Museum), *Palazzo Altemps* and the *Museo del Vetro di Murano*.

All these panels have some or all the same six elements mentioned above, so it is reasonable to suppose that they were found in the same place and originally formed part of a single decorative scheme [4].

However, the last excavation and studies on the Lucius Verus villa, occurred between 2005 and 2009 provided evidence which confirm the date and establish the provenance of the Gorga *sectilia*. Indeed, Messineo and co-workers found 806 monochrome and polychrome glass *sectilia* showing a wide range of colours, as shown in the table 4.2, which match very well with those in the Gorga collection. Indeed, as well as the *sectilia* found in the *Museo del Vetro di Murano*, the *sectilia* uncovered by Messineo showed the same yellow rosette and

translucent green tesserae; moreover, the shapes and thickness are identical with those stored in the Gorga collection.

Establishing a definite date was debated for several years, but most of the scholars agreed to date them to the 2nd century AD. Whitehouse (as well as Prof. Sagui), used the round glass with yellow rosette as a “fossil guide”. According to Whitehouse, the round glass with the yellow rosette is a typical pattern of the Ptolemaic period (around the 1st century AD), showing close parallels with Ptolemaic glass production of the first century AD [4]. However, Whitehouse did not have any hesitation in dating the glass *sectilia* to the Lucius Verus villa period (166-169 AD). It is possible to claim that the 26,000 glass *sectilia* stored in the Gorga collection come from the Lucius Verus villa *opus sectile* decoration, and they can be dated to the 2nd century AD.

Table 4.2. Number of monochrome and polychrome glass *sectilia* uncovered in the last excavation in 2005 by Messineo (data reported from Caserta et al. 2012).

Monochrome	N. of pieces	Polychrome <i>sectilia</i>	N. of pieces
White	28	Colourless with white and yellow layer	1
Yellow	138	White with grey layer	1
Yellow/grey	9	White with flower of ametistas and yellow dots	1
Orange	23	Yellow with white bands	8
Red	115	Yellow/grey with white dots	1
Dark red	2	Yellow with ametista flower	2
Light green	115	Red with white bands	1
Dark green	4	Red with white dots	2
Light blue	147	Red with dark bands	12
Blue	35	Red with yellow and whit dots	1
Ametista	18	Red with orange layer	1
		Serpentine	44
		Light blue with white bands	3
		Light blu with red flower	3
		Blue with light bule bands	2
		Ametistas with white bandes	8
		Ametista with white dots	20
		Ametista with yellow flower and light blue dots	5
		Mixed with yellow – white and ametista bands	23
		Mixed with yellow – white – ametista - green bands	1
		Frame with yellow and ametista bands	18
		Frams with white and ametista bands	4
		Frame with white, blue and light blue bands	1
		Mixed colour	7

4.2.2 The *opus sectile* technique

The use of pieces of marble cut into geometrical shapes to create geometrical or figurative motifs is a decoration technique which probably started around the 1st century BC in the Western part of the Mediterranean Sea and spread across the Roman empire during the 4th century AD [3, 6]. Glass was cheaper to produce, easier to polish, to cut and trade, and it was shinier than marbles. Furthermore, the advanced technical skills reached by the Roman glassmakers enabled them to imitate the precious marble commonly used in architectural adornment. Hence, when some details such as petals, the pupils of eyes, or flowers were required in the decoration, the marble was frequently substituted for glass *sectilia*.

There are examples, discovered in the last few decades, in which glass *sectilia* was the main material used in this technique; unfortunately, only a few cases have been chemically studied by archaeometry investigations: Aiano-Torraccia di Chiusi [6], Ostia, Porta Marina [7], the Lucius Verus villa [8, 9], Kenchreai [10, 11], Villa di Faragola [12] and the Thomas panel, found in Fayum [13]. These cases (ranging between the 2nd and 6th

century AD) attest to the spread of this decorative technique, from the Roman period to the Late Antique [12] in the houses of the Roman aristocracy, to display their wealth.

Saguì [3] has suggested that the glass *sectilia* could have been manufactured by using different techniques. The thicker *sectilia* were made by first preparing monochrome or polychrome glass canes which were placed together on a plate or plane and re-heated in a kiln or furnace. They were heated at a low temperature (about 800°C) and the glass was softened enough to be pressed from the top and on the edge so that canes could adhere to each other and make a slab.

The manufacturing of the thin *sectilia* is still unclear; however, the molten glass was probably poured into a mould and stretched in order to form a flat and thin glass sheet. The shape was probably formed using a tool such as a *grossarium* [2], or as suggested by [3] an iron rod heated on the point and used to mark the glass. Marks of the use of *grossarium* are visible by careful observation on the thin edges of the samples; other marks of other tools (such as a pinch or *rastrello*) are present.

Other *sectilia* were probably obtained by pouring the molten glass into a mould, and then drawn. These are techniques that were well mastered during the Hellenistic period, and several examples were recovered from Ptolemaic Egypt [3].

According to Brill and Whitehouse, the panels with the *sectilia* were previously prepared in the workshop and then applied on the pavement or on the wall [13, 14]. The panels could be prepared following two procedures:

- The first hypothesis points to the initial preparation of a tray of potsherds, composed of amphorae fragments cut into rectangular shapes, which were covered by a softened coating (probably made of pine resin and powdered marble). When the coating was still hot the artist applied the glass *sectilia* following his decorative project. Once the resin was cooled, the glass was glued to the support.
- The second hypothesis suggests first preparing the glass *sectilia* face down and creating the decorative motif; when the artist had finished the composition, the coating was poured down onto the glass *sectilia*, and the potsherds were pressed onto the still softened coating.

Brill and Whitehouse have suggested the last procedure as the most probable and convenient, since the artist could create his composition with less restriction due to the cooling of the resin [13].

Where these panels were manufactured has not been still solved. Brill and Whitehouse suggested the existence of specialised workshops which made the panels. This hypothesis is based on a comparison of the Thomas panels [13] and the Kenchreai. The iconography and the stylistic similarities led scholars to support this hypothesis [4]. During the investigation of glass *sectilia* in Faragola [12], Egyptian manufacture was also posited.

At this moment these are only hypotheses; more detailed analyses, both scientific and iconographic, are required before indicating a probable manufacturing location.

References

1. Caserta, E. Roma (via Cassia). La villa di Lucio Vero alla luce delle recenti indagini archeologiche. In *Atti della accademia Nazionale dei Lincei: Notizie degli scavi di Antichità*; vol. XXI-XXII, 2010-2011, Scienze e Lettere Eds, Roma 2012; pp. 53-191.
2. Bacchelli, B.; Barbera, M.; Pasqualucci, R.; Saguì, L. Nuove scoperte sulla provenienza dei pannelli in opus sectile vitreo della Collezione Gorga. In *Proceeding of conference: Atti del II Colloquio AISCOM, Roma, Italy, 5-7 Dicembre 1994*; Bragantini, I., Guidobaldi, F., Eds.; Istituto Internazionale di Studi Liguri, Bordighera, Italy 1995; pp. 447-466.
3. Saguì, L.; Santopadre, P.; Verità, M. Technology. Colours, Forms, and Shapes in the 2nd Century Glass Opus Sectile Materials from the Villa of Lucius Verus in Rome. In *Proceedings of the Annales du 18e Congrès de l'Association Internationale pour l'Histoire du Verre, Thessaloniki, Greece, 20-25 September 2009*; Ignatiadou, D., Antonaras, A. Eds.; ZITI Publishing: Thessaloniki, Greece, 2012; pp. 133-138.
4. Whitehouse D. Opus sectile panels. *Roman Glass in the Corning Museum of Glass*, Herson, R., Price, R.W. Eds.; Publisher: The Corning Museum of Glass, New York, USA, 1997, pp. 32-38.
5. Saguì, L. La villa di Lucio Vero sulla via Clodia e le sue decorazioni in vetro. In *Emergenze storico-archeologiche di un settore del suburbio di Roma: la Tenuta dell'Acqua Traversa*, atti della giornata di Studio, Roma, 7 giugno, 2003. Roma, 2005, 211-229
6. Cavalieri, M.; Landi, S.; Manna, D.; Giamello, M.; Fornacelli C.; Bracci, S.; Palma, G.; Siotto, E.; Scopigno R. Analisi dei frammenti di sectilia vitrei dalla villa romana di Aiano-Torraccia di Chiusi (si) e studio della tecnica d'esecuzione. In *Proceeding Atti del XXIV colloquio dell'associazione italiana per lo studio e la conservazione del mosaico (AISCOM). este, 14-17 marzo 2018*. Michele Bueno, Chiara Cecalupo, Marco Emilio Erba, Daniela Massara, Federica Rinaldi Eds.; Publishing: Quasar, Tivoli, Italy, 2019, pp. 605-617.
7. Marco Verità, Maria Stella Arena, Anna Maria Carruba, Paola Santopadre. Materiali vitrei nell'opus sectile di Porta Marina (Ostia antica), *BOLL. ICR* **2008**, 16-17, 78-94.
8. Verità, M.; Maggetti, M.; Saguì, L.; Santopadre, P. Colors of Roman Glass: An Investigation of the Yellow Sectilia in the Gorga Collection. *J. Glass Stud.* **2013**, 55, 21-34.
9. Tesser, E.; Verità, M.; Lazzarini, L.; Falcone, R.; Saguì, L.; Antonelli, F. Glass in imitation of exotic marbles: An analytical investigation of 2nd century AD Roman sectilia from the Gorga collection. *J. Cult. Herit.* **2020**, 42, 202-212.
10. Brill, R.H. Kenchreai Panel Revisited. *The Corning Glass NewsLetter*, summer **1996**, 1-2.
11. Brill, R.H. *Chemical Analyses of Early Glasses*; Volume 2 Tables of Analyses; The Corning Museum of Glass: Corning, NY, USA, 1999; ISBN 0-872900-143-2.
12. Santagostino Barbone, A.; Gliozzo, E.; D'acapito, F.; Memmi Turbanti, I.; Turchiano, M.; Volpe, G. The sectilia panels of Faragola (Ascoli Satriano, southern Italy): a multi-analytical study of the red, orange and yellow glass slabs. *Archaeometry.* **2008**, 50 (3), 451-473.
13. Brill R.H.; Whitehouse, D. The Thomas Panel. *J. Glass Stu.* **1988**, 30, 34-50.
14. Davidson, S. Technology of glass production. *Conservation and Restoration of Glass*, 2nd ed.; Butterworth-Heinemann Eds.; Publisher: Oxford UK, 1997, pp. 124-125.

5. Sampling

5.1 Methodology of sampling

Sampling involved the collaboration of several professionals. Firstly, Professor Lucia Saguì who gave us access to the storehouse of the *Soprintendenza Archeologica di Roma* and then indicated and explained which boxes were devoted to the Lucius Verus villa excavations. There are 250 boxes containing glass *sectilia* from the Lucius Verus villa currently stored in the deposit, and our attention was focused on the nine boxes in which opaque red glass *sectilia* were collected [1]. In each box, other smaller boxes were placed in which the samples were divided according to their thickness, red hues, shapes and polychrome glass (fig.5.1).



Figure 5.1. Boxes containing opaque red glass *sectilia* (both monochrome and polychrome) from the Lucius Verus villa excavations, and stored in the storehouse of the *Soprintendenza Archeologica di Roma*. Picture of single boxes was taken in the storehouse of *Soprintendenza Archeologica di Roma*, in St. Croce in Gerusalemme square (Rome), and then assembled by me in this picture.

Together with Dr. Verità, Dr. Santopadre and Professor Saguì, and according to the limit imposed by the *Soprintendenza Archaeologica di Roma*, 40 samples were gathered. Two criteria were used to proceed with the collection of the samples: red hues and the thickness. Due to the presence in most of the samples of black, green, or white corrosion layers on the surface, recognising the red hues was difficult. Indeed, only where the inner side was visible or a fresh fracture were present, showing the uncorroded glass, it was possible to observe and identify the red shades. In some cases, it was hard to distinguish between the front and the back of the

samples, and only through careful observation they were recognised. However, three main red hues were identified, varying from red, brownish, and very dark red. Moreover, a slightly different red hue was observed which constituted the fourth of the red tints. Orange samples were added to the red hues and selected following the same procedure previously described.

Once the red hues were identified, the sampling continued to obtain at least two samples for each red hue, in order to observe if there were some distinct chemical or mineralogical differences to each red tone.

Thickness and shape represented a further criterion to select the samples. The glass *sectilia* showed a wide variety of thickness which could indicate different manufacturing technique and probably distinct chemical and mineralogical features. Hence, where it was possible, samples with different thicknesses and shapes were selected to be representative of each of the red and orange hues.

5.2 Grouping and description of the samples

The samples, based on their red hue, were divided into five groups. The first group comprises samples showing a brick red colour (20 samples), and it is called Gr-1. In the Gr-1 group the thickness of the samples varies between the 1 and the 11 mm. This group is very heterogeneous, and the thicker samples are often broken, fragmentary and their original shape could be considered lost (fig. 5.2a-c). In contrast, some thinner samples exhibit geometrical shapes (rectangular, round or rhomboid) (fig. 5.2d).

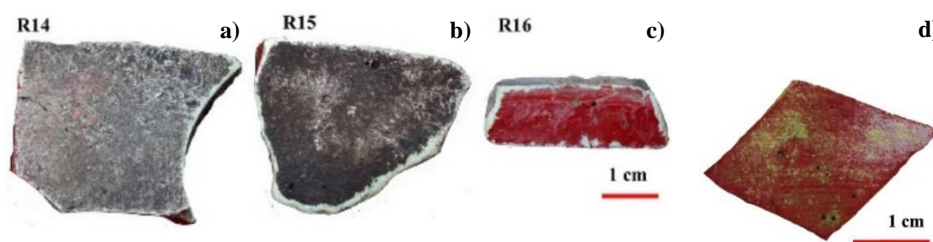


Fig. 5.2. Fragmentary samples, and thin samples in geometrical shapes.

Fig.5.3 shows some samples in which it is possible to see the marks of the tools used to cut the glass sheets (fig. 5.3a) or to stretch the molten glass (fig. 5.3b); others exhibited a particular edge known as “becco di civetta” (fig. 5.3c). Most of the thicker samples are characterised by the presence of canes on the reverse side, which indicate the technique used to manufacture them (fig.5.3d).

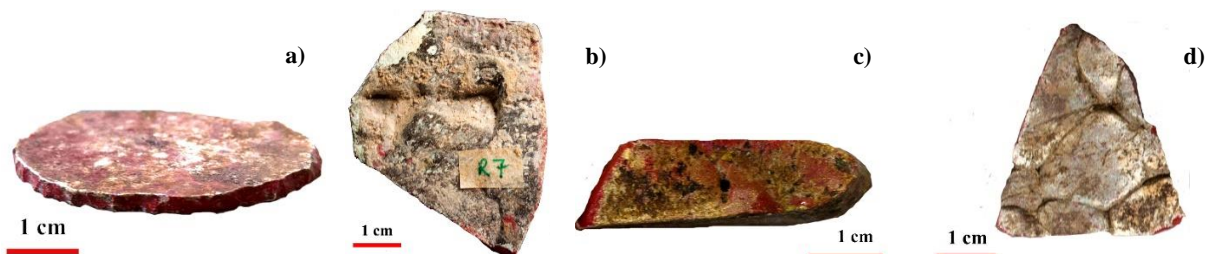


Figure 5.3. a) round *sectilia* with the visible marks of the tools used to cut the glass in order to create the rounded shape; b) maker of the tool (likely) to stretch the molten glass; c) sample with the “becco di civetta” edge; d) front of a thicker sample of the Gr-1 group, composed of the juxtaposition of several canes.

Some polychrome glass was recovered (not studied in this research) which exhibited a red matrix with white dots (formed by the juxtaposition of canes), while another revealed a red matrix with yellow circles (fig. 5.4).

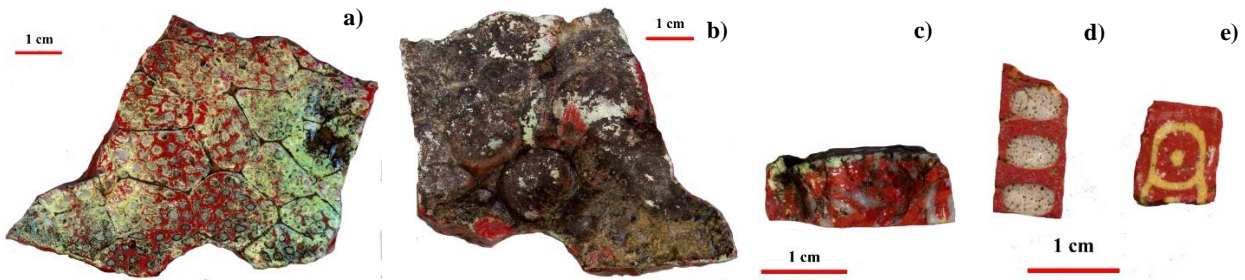


Figure 5.4. Polychrome sectilia a)-b) red with white dots; c) cross section; d)-e) fragment of the framework

Moreover, it was observed that some thicker samples with geometrical shapes, probably used to make a frame, showed a slightly different red hue (which will constitute the Gr-4 group), which was very difficult to distinguish in the first observation (fig. 5.5).

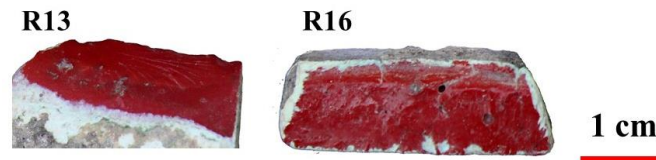


Figure 5.5. Comparison between R13 (Gr-4 group) and R16 (Gr-1 group). The samples of Gr-4 group were excluded from the Gr-1 group after several visual examinations.

The second group (Gr-2) included six samples showing a reddish brown tone fig. 5.6. They are thin, ranging between 2 and 3 mm, and usually exhibit a geometrical shape, which could be due to intentional cutting of the glass sheets into geometrical forms; however, it is not possible to obtain the original decorative pattern. Some of them reveal signs of tools, such as shown in fig. 5.7.

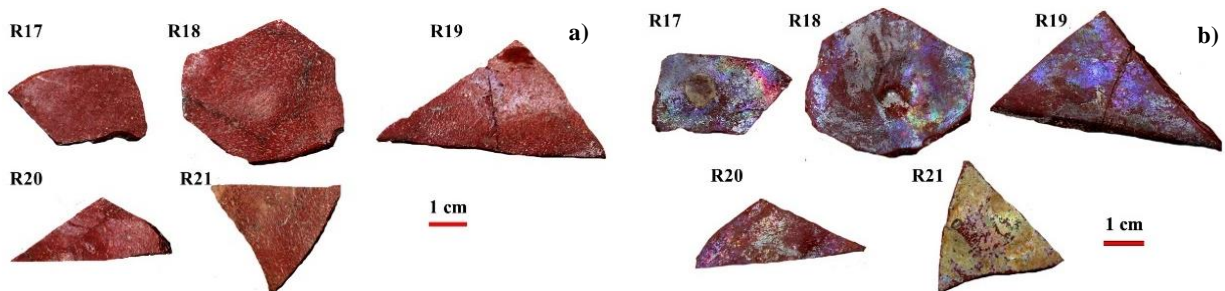


Figure 5.6. Five of the brownish samples (Gr-2 group) front (a) and back (b).



Figure 5.7. Markers of the tool.

The third group (Gr-3) is composed of four samples a few millimetres thick between 2-4 mm, and showing that originally they were cut into a specific shape. The colour is a very dark red, obtained by extreme heterogeneity in which countless red and black layers alternate (fig.5.8). They constitute a small group and most of them are broken into very small fragments.



Figure 5.8. Samples of the Gr-3 group

The fourth group (Gr-4) is composed of four red samples which formed rods and *sectilia* with geometrical shape, and thickness varies between 3 - 6.5 mm (fig. 5.9). They are extremely corroded, with a white - green layer of corrosion covering their entire external surface. However, some of them were already broken showing their true colour. Most of them were already collected and located in a specific box, while others were found in some boxes in which Gr-1 samples were stored. In this case, it was very difficult to distinguish them because the red hues were very close; however, the Gr-4 samples exhibit a very intense opaque red colour, that after careful observation is possible to recognise. Among them different shapes and thickness were found, such as dissimilar tones of red.

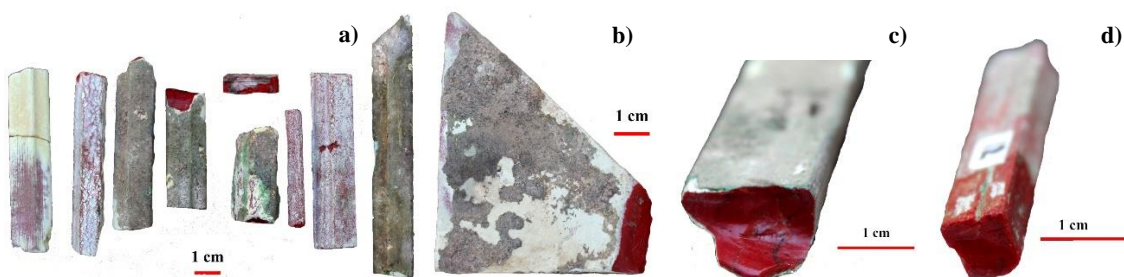







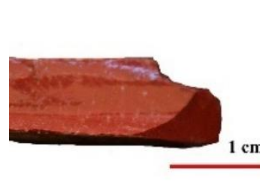
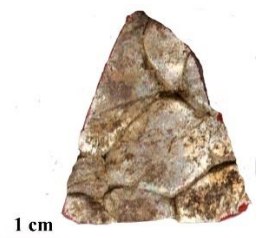

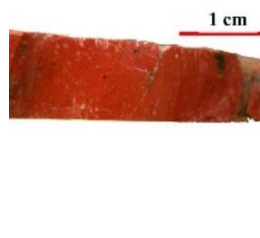
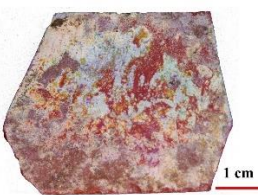

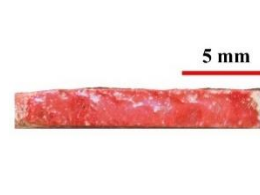

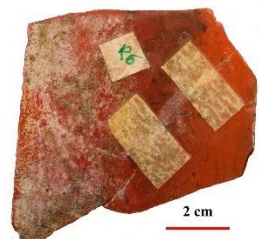
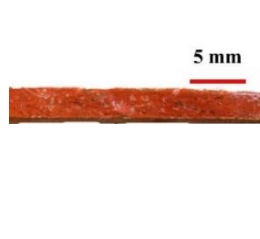
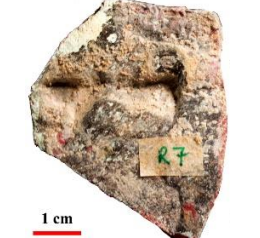
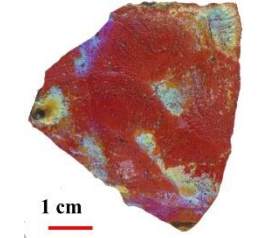

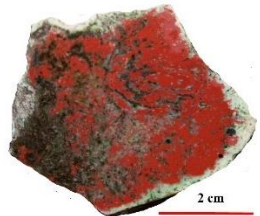


Figure 5.9. a) rods of Gr-4 samples with the visible corrosion layer; b) geometrical *sectilia* with fresh fractures; c)- d) rods with fresh fractures.

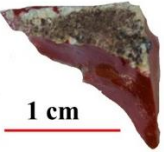


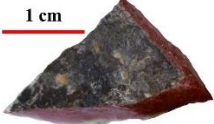
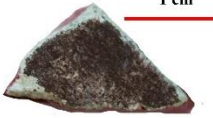

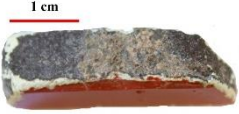



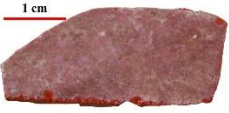




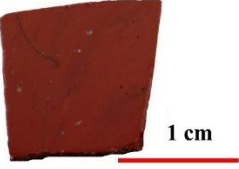
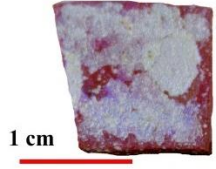

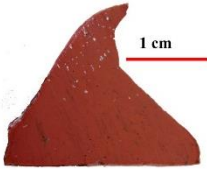
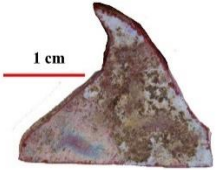

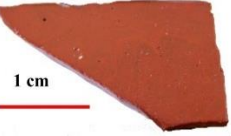


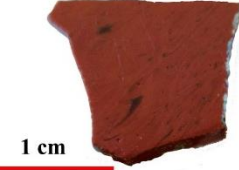
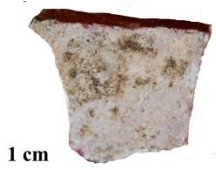

The Gr-5 is a very small group (fig. 5.10), composed of a few orange samples, most of them in fragments; moreover, they have been covered by a layer of white-green corrosion. Where fresh fractures were present, it was possible to observe the original colour and six of them were chosen. They have slightly different orange hues from lighter to reddish, and some are more heterogeneous than others. Only in a few samples was it possible to observe the probable original geometrical shapes. Their thickness ranges between 2.7 and 8 mm.

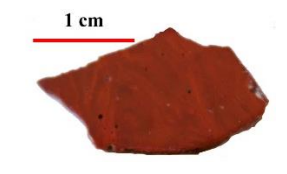
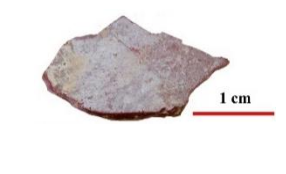
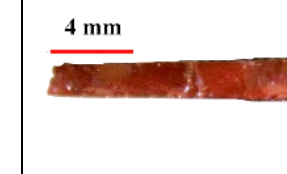

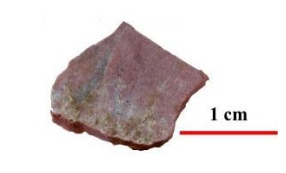
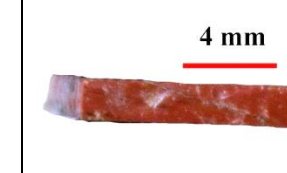
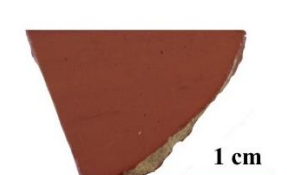
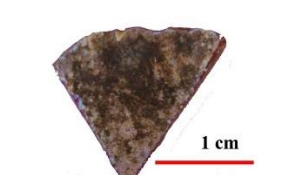
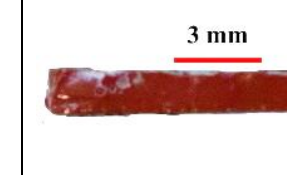
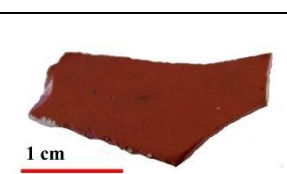
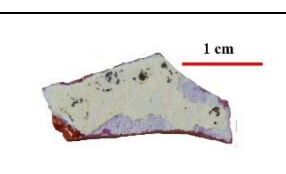







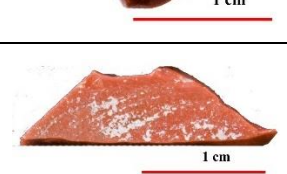
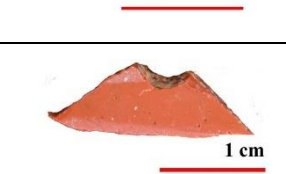
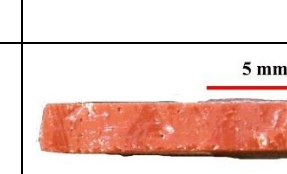
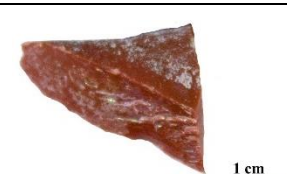
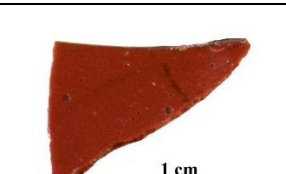
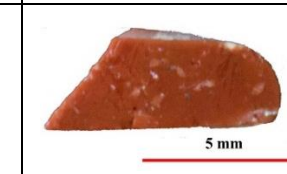
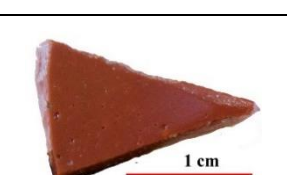
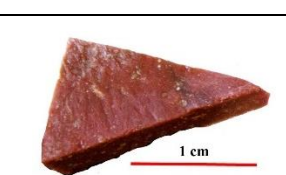
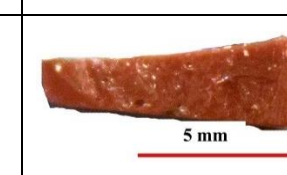


Figure 5.10. Orange samples, Gr-5 group.



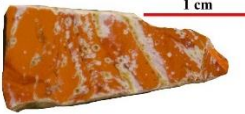


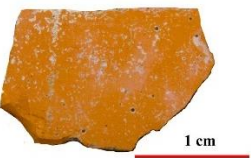
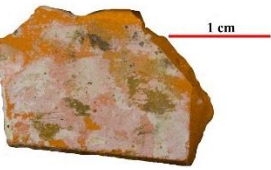


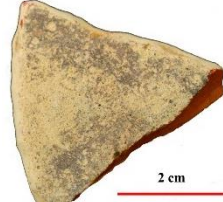







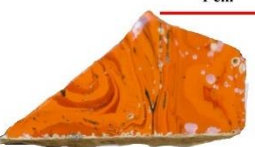

Table 5.1. Samples collected from the *Soprintenza Archeologica of Rome*. Fragments representing the different red hues, they are showed through their retro-verso and cross-section. **L:** length; **W:** width; **Th:** thickness. * **Fragments, without regular shape, difficult to measure and understand their side.**

Sample	L cm	W cm	Th mm	Retro	Verso	Cross section	Group
R2	2.3	1.0	1.7				GR-1
R3	4.0	2.6	9-11				GR-1
R4	4.0	3.5	8				GR-1
R5	4.6	3.8	2				GR-1
R6	7.1	7.1	3				GR-1
R7	5.6	4.9	9				GR-1
R8	4.4	4.9	9				GR-1

R14	0.9	0.8	7				GR-1
R15	1.7	1.3	7				GR-1
R16	3.0	1.0	5				GR-1
R25	3	1.3	2				GR-1
R26	3.0	1.0	2				GR-1
R27	1.2	1.1	1				GR-1
R28	2.2	1.7	1.5				GR-1
R29	2.1	1.2	2				GR-1
R30	1.3	1.5	2				GR-1

R31	1.7	1.2	2				GR-1
R32							GR-1
R33	1.6	1.5	1.5				GR-1
R34	2.1	1.0	1				GR-1
R10	7.8	4.8	3.3				GR-2
R17	1.5	1.0	2				GR-2
R18	2.0	1.0	3.0				GR-2
R19	1.6	1.0	3.5				GR-2
R20	1.5	1.0	3				GR-2

R21	0.7	1.0	3				GR-2
R1	4.3	5.3	3-4				Gr-3
R22	2.0	1.2	4				Gr-3
R23	0.8	1.0	4.0				Gr-3
R24	2.4	1.1	4.0				Gr-3
R9	5.7	4.3	6.5				GR-4
R11*	1	0.5	2.5				GR-4
R12	0.3	0.7	0.8				GR-4

R13*	2.2	0.6	3				GR-4
AR1	2.0	0.9	4.5				GR-5
AR2	2.1	1.4	2.7				GR-5
AR4	3.8	3.8	8.0				GR-5
AR6*	1.7	1.8	3.0				GR-5
AR7	2.1	0.8	7.0				GR-5
AR8	1.9	1.0	3.5				GR-5

References

1. Bacchelli, B.; Barbera, M.; Pasqualucci, R.; Saguì, L. Nuove scoperte sulla provenienza dei pannelli in opus sectile vitreo della Collezione Gorga. In *Proceeding of conference: Atti del II Colloquio AISCOM, Roma, Italy, 5-7 Dicembre 1994*; Bragantini, I., Guidobaldi, F., Eds.; Istituto Internazionale di Studi Liguri, Bordighera, Italy 1995; pp. 447-466.

6. Analytical Method

6.1 Identification of the colour

6.1.1 OM (Optical Microscope)

Cross-section of the selected samples were cut, mounted and embedded in epoxy resin blocks, afterwards they were ground and polished to a flat, mirror-like surface down to 1 μ m following standard procedure. Images were collected using a Zeiss Axioplan 2 Imaging system (HAL 100) attached to a Nikon DXM1200F digital camera and ACT-1 software. Different illumination modes (bright field and dark field) were used.

6.1.2 FORS (Fiber Optics Reflectance Spectroscopy)

Cross-section of the selected samples were cut, mounted and embedded in epoxy resin blocks, afterwards they were ground and polished to a flat, mirror-like surface down to 1 μ m following standard procedure. MAYA 200 PRO from Ocean Optics spectrophotometer with a single beam dispersive optical fiber was used, at the scientific laboratory in DCR Lisbon, together with a 2048 CCD Si detector that operates in the 200–1050 nm range. The light source was a HL-200-HP 20 W halogen from Ocean Optics, with a single optical path between 360 and 2500 nm. The spectra were taken directly onto the glass surface of the objects, in reflectance (R) mode, with a 45°/45° configuration (illumination angle/acquisition) and ca. a 2 mm diameter of the area analysed. Spectra were obtained between 380 and 1050 nm, with an integration time of 8 ms per scan and 15 scans. A Spectralon® surface was used as a reference for calibration.

By means of the reflectance spectra, it is possible to calculate the band gap energies of semiconductor materials using the following equation proposed in the literature [1-5]:

$$(\alpha h\nu)^n = A(h\nu - E_g)$$

where α is the absorption coefficient, $h\nu$ is the energy of incident photon, E_g is the band gap energy, A is a proportionality constant and n is an exponent which is related to the optical transition. As mentioned by Rosi [1], it was necessary to convert the FORS spectra into Kubelka-Munk values which are proportional to the absorption coefficient. Afterwards, a band gap energy was calculated by extrapolating the linear region of a plot of $(\alpha h\nu)^2$ vs. $h\nu$ [1-5].

6.1.3 Colorimetric measurements

Cross-section of the selected samples were cut, mounted and embedded in epoxy resin blocks, afterwards they were ground and polished to a flat, mirror-like surface down to 1 μ m following standard procedure. Colorimetric measurements were made at the Stazione Sperimentale del Vetro (SSV), Murano Venice, with a UV-VIS-NIR spectrophotometer Perkin-Elmer Lambda 900 with a Spectralon 15 mm diameter integrating sphere Pela1000. Ceramic tile certificate NIST (SRM2019) was used as standard for the measurements in reflection.

Because of the small sizes of the samples, a specific protocol was adopted. An area of 3x3 mm was measured by applying a mask on the sample, made of carbon paper, to avoid any interference.

These analyses were taken and elaborated by the procedure outlined in Publication CIE n°15:2004 “colorimetrie”, with illuminating D65 (CIE n°15) and observer 2° (CIE 1931) - 5 nm.

6.2 Chemical analyses

6.2.1 EPMA (Electron Probe Micro Analyses)

Cross-section of the selected samples were cut, mounted and embedded in epoxy resin blocks, afterwards they were ground and polished to a flat, mirror-like surface down to 1µm following standard procedure. The analysis was performed by Dr. Verità with a Cameca SX-50 from Stazione Sperimentale del Vetro, Murano, Venice, Italy, equipped with three wavelength-dispersive spectrometers (PET, LiF and TAP crystals). The operating conditions used in the first microprobe were: accelerating potential 15 kV, beam current 20 nA for major and minor components or 100 nA for trace elements, respectively. A 40 x 50 mm scanning electron beam and limited counting time (10 s for major and minor elements, 20e30 s for trace elements) were used to ensure that no significant alkali drift (ion migration) occurred during the irradiation [6].

6.2.2 LA-ICP-MS (Laser Ablation Inductively Couple Plasma Mass Spectroscopy)

Laser Ablation Inductively Coupled Plasma Mass Spectrometry (LA-ICP-MS) was performed at IRAMAT-Centre-Ernest-Babelon (Orléans). The analyses of the red glass embedded polished sections were carried out by Laser Ablation-Inductively Coupled Plasma-Mass Spectrometry (LA-ICP-MS). Cross-section of the selected samples were cut, mounted and embedded in epoxy resin blocks, afterwards they were ground and polished to a flat, mirror-like surface down to 1µm following standard procedure. The instrumentation consisted of a Resolution M50E UV laser probe from Resonetics/ASI (Eximer ArF laser working at 193 nm equipped with the S155 cell) coupled with a Thermo Fisher Scientific ELEMENT XR mass spectrometer [7]. LA-ICP-MS allows a nearly non-destructive analysis, invisible to the naked eye, of the glass objects. Analytical parameters were as follow: the excimer laser was operated at 5.5 mJ with a repetition rate of 10 Hz, ablation time was set to 40 seconds: 10 seconds pre-ablation, so that transient signal could be removed, and 30 seconds collection time corresponding to 9 mass scans from lithium to uranium. The signal was measured in counts/second, in low resolution mode for 58 different isotopes. The fifty-eight elements include all major, minor (except sulphur) and trace elements which are usually present in glass samples [7]. Blanks were run periodically between series of 20 analyses. Spot sizes were set to 100 µm (although reduced down to 70 µm when saturation occurred for element such as manganese or copper). During analysis live counts were continuously observed: when element spikes signifying the presence of inclusions were observed, results were

discarded, and a new site selected. From two to six areas were analysed per sample; homogeneity and agreement between runs was consistently good.

Calibration was performed using five reference standards: NIST610, Corning B, C and D, and APL1 (an in-house reference glass used for chlorine determination), were run periodically (every 15 to 20 samples) to correct for eventual drifts. The standards are used to calculate the response coefficient (k) of each element. The measured values were normalised against ^{28}Si , the internal standard. Concentrations are calculated assuming that the sum of the concentrations of the measured elements is equal to 100 weight percent. In total, 58 elements were recorded. For the major and minor elements accuracy and precision were within 5 % relative and within 10 % for most trace elements.

6.2.3 FEG-SEM (Field Emission Gun Scanning Electron Microscope)

Cross-section of the selected samples were cut, mounted and embedded in epoxy resin blocks, afterwards they were ground and polished to a flat, mirror-like surface down to $1\mu\text{m}$ following standard procedure. A field emission electron Gun Scanning Electron Microscope (FEG-SEM, JEOL 7800F), at C2RMF (Centre de Recherche et de Restauration des Musées de France, Paris), was used for the analysis. To limit the charge effects on the surface, a platinum coating of about 1 nm was deposited to make the glass surface conductive and moderate accelerating tensions were used (2–15 kV). For the platinum coating and the SEM observation, samples were submitted to a vacuum of about 1Pa and 5.10^{-5}Pa respectively. At the same time as SEM observations, EDS analysis was carried out on the glass samples, using a BRUKER Quantax 400 system. The intensity of the electronic beam current was 1 nA during the analysis. It was scanned on a surface area, larger than $2\mu\text{m}$, to prevent alkali drift.

6.3 Crystalline phases

6.3.1 μ -Raman microscopy

Cross-section of the selected samples were cut, mounted and embedded in epoxy resin blocks, afterwards they were ground and polished to a flat, mirror-like surface down to $1\mu\text{m}$ following standard procedure. Raman microscopy was carried out at a scientific laboratory in DCR Lisbon using a Labram 300 Jobin Yvon spectrometer, equipped with a solid state 50-mW laser operating at 532 nm. Spectra were recorded as an extended scan. The system was calibrated using a silicon standard. The laser beam was focused either with a $50\times$ or a $100\times$ Olympus objective lens. The laser power at the surface of the samples was controlled with neutral density filters (optical densities 0.3 and 0.6). Raman data analysis was performed using LabSpec 5 software. All spectra are presented as acquired without any baseline correction or other treatment.

6.3.2 XRD (X-ray diffraction)

X-ray diffraction was used in some samples where Raman spectroscopy did not allow the identification of the colouring agent, and in the orange samples, to understand whether other opacifying agents were used. The measurements were performed by X'Pert PRO MPD (PANalytical B.V., Almelo, Netherlands), equipped with an X-ray tube with Cu anode (1.54059 Å, K α , 45 kV, 40 mA) and an X'Celerator detector (ultra-set X-ray 1D detector based on Real Time Multi Steps-RTMS-technology). The scans were collected in the angular range of 3°–89° 2 θ with a 0.03° virtual step size and 30 sec/step counting time. The XRD data were processed by the X'Pert HighScore (PANalytical B.V., Almelo, Netherlands). In order to avoid any contamination of resin peaks, the analyses were performed on bulk samples.

References

1. Rosi, F.; Grazia, C.; Gabrieli, F.; Romani, A.; Paolantoni, M.; Vivani, R.; Brunetti, B.G.; Colomban, P.; Miliani, C. UV–Vis-NIR and micro-Raman spectroscopies for the non-destructive identification of Cd_{1-x}Zn_xS solid solutions in cadmium yellow pigments. *Microchem. J.* **2016**, 124, 856–867.
2. Tauc, J.; Grigorovici, R.; Vancu, A. Optical properties and electronic structure of amorphous germanium. *Phys. Status Solidi* **1966**, 15, 627–637.
3. Jiang X., Zhang M., Shi S., He G., Song X. and Sun Z. Microstructure and optical properties of nanocrystalline Cu₂O thin films prepared by electrodeposition, *Nanoscale Res. Lett.* **2014**, 9:219
4. Murphy, A.B. Band-gap determination from diffuse reflectance measurements of semiconductor films. and application to photoelectrochemical water-splitting. *Sol. Energy Mater. Sol. Cells* **2007**, 91, 1326–1337.
5. Theja, G.S.; Lawrence, R.C.; Ravi, V.; Nagarajan, S.; Anthony, S.P. Synthesis of Cu₂O micro/nanocrystals with tunable morphologies using coordinating ligands as structure controlling agents and antimicrobial studies. *CrystEngComm* **2014**, 16, 9866–9872.
6. Verità, M.; Basso, R.; Wypyski, M.T.; Koestler, R.J. X-ray microanalysis of ancient glassy materials: A comparative study of wavelength dispersive and energy dispersive technique. *Archaeometry* **1994**, 36, 241–251.
7. Gratuze, B. *Glass Characterization Using Laser Ablation-Inductively Coupled Plasma-Mass Spectrometry Methods*. In L. Dussubieux, M. Goltzko B. Gratuze (Ed.), *Recent Advances in Laser Ablation ICP-MS for Archaeology*. Springer-Verlag, **2016** Ltd. pp. 179-196.

7. Results

7.1 Optical microscope observation

The samples of the Gr-1 group are characterised by heterogeneity due to the presence of a layer with different red hues (from orange to red) and a dark transparent layer. In [fig. 7.1](#), two types of heterogeneity are observed. In the first, a gradual variation of red hue occurred, also visible at high magnifications. In contrast, sample R31, a thin sample, exhibits layers closer to the orange-brown hues.

The samples made by canes (R7, R8, R14, R15 and R16) showed a similar colour to each other, while the red hue of R3 and R4 is slightly darker. The red hue in the thinner *sectilia* varies from brick red to a brownish colour, and the texture is characterised from high heterogeneity to less evident heterogeneity.

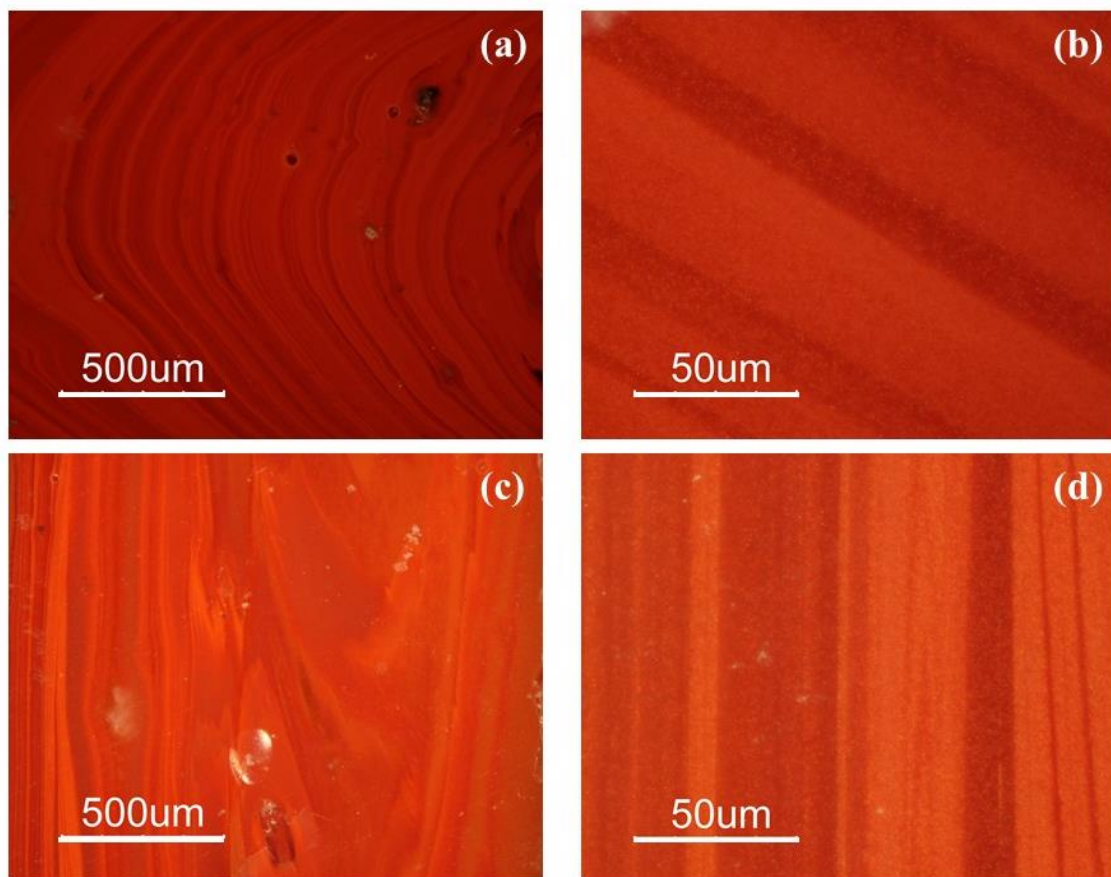


Figure 7.1. Optical micrographs: **a)** sample R4 and its magnification **b)**; **c)** sample R31 with pronounced orange-brown heterogeneity, and its magnification **d)**.

In the samples of the Gr-2 group, larger particles widely spread within the glass matrix are observed. In samples R10 and R17 crystals hexagonal and triangular in shape were detected, varying between 20 and 50 µm in size ([fig. 7.2](#)). Moreover, these samples are not characterised by the presence of darker layers or pronounced heterogeneity. However, there are some bands in which smaller particles were grouped and the colour of these areas is orange.

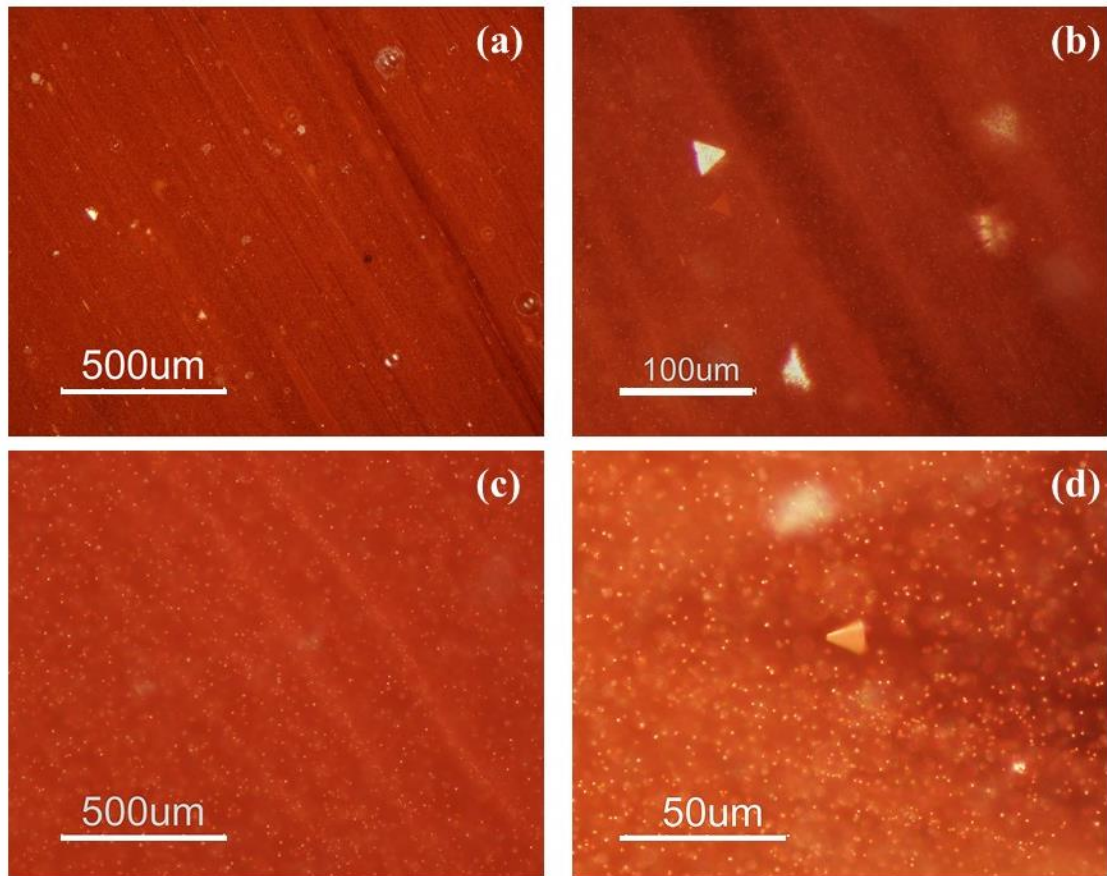


Figure 7.2. Optical micrographs from the Gr-2 group: samples R10 **a-b)** and R17**c-d)**.

The samples comprising the Gr-3 group are very heterogeneous with vast red area in contrast to a large dark transparent area (fig. 7.3). In the red area, layers with different red hues are present, while in the dark transparent area no particles were observed. In sample R22 in the edge between the red and black areas several spherical black/grey inclusions can be observed.

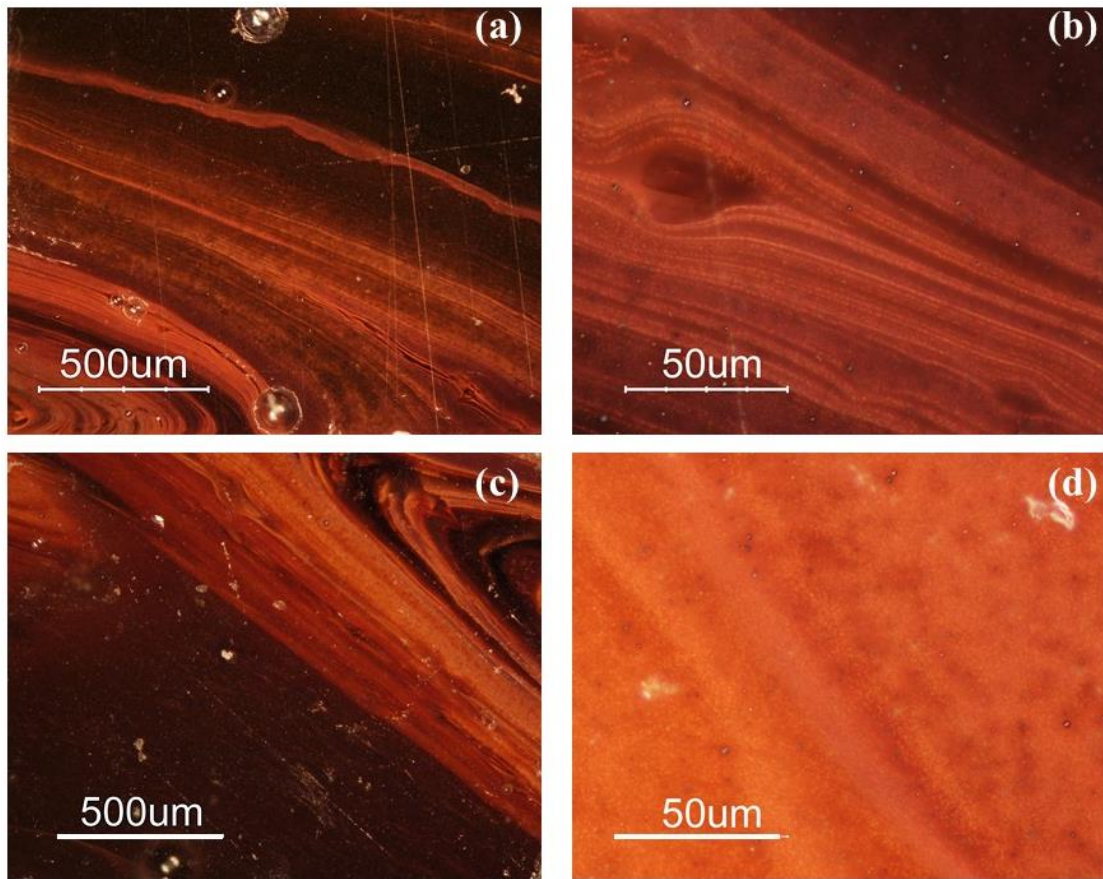


Figure 7.3. Optical micrographs from the Gr-3 group: samples R1 (a, b) and R22 (c, d) showing the different red layers and the presence of a large dark transparent area.

In the Gr-4 group the samples are characterised by large dendritic crystals with several branches and embedded in a colourless glass matrix. The number and the size of these crystals are slightly different in each sample, forming darker (R12) (fig. 7.4a-b) and lighter hues (R13) (fig. 7.4c-d) within this group. These features are comparable with red type sealing wax. No inclusions were observed except a little aggregation of particles in sample R11.

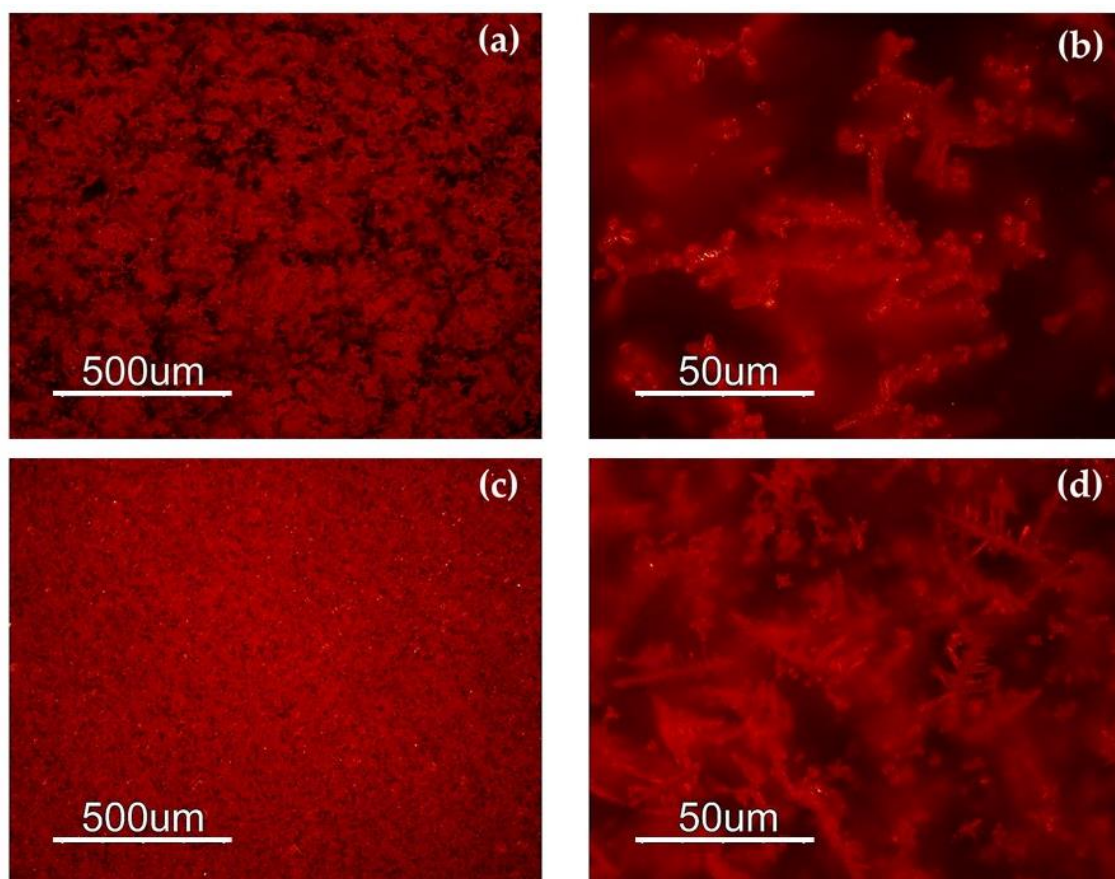


Figure 7.4. Optical micrographs from Gr-4: a)-b) sample R12; c)-d) sample R13.

The orange samples (Gr-5 group) are a heterogeneous group in which three different orange hues were identified (fig. 7.5 a, b, c, d). Samples AR4 and AR6 look more orange reddish, while samples AR1 and especially sample AR2 tend more towards a yellowish orange hue. Samples AR1, AR4, AR6, AR7 and AR8 are very heterogeneous with the presence of several red layers in which dendritic crystals or larger particles are often observed. In the orange layers the crystals are very small and their shapes are difficult to understand with any precision. Sample AR2 exhibits a homogenous colour, without the presence of red or orange bands, and only rarely are there small dark areas including dendritic red crystals (fig. 7.5d).

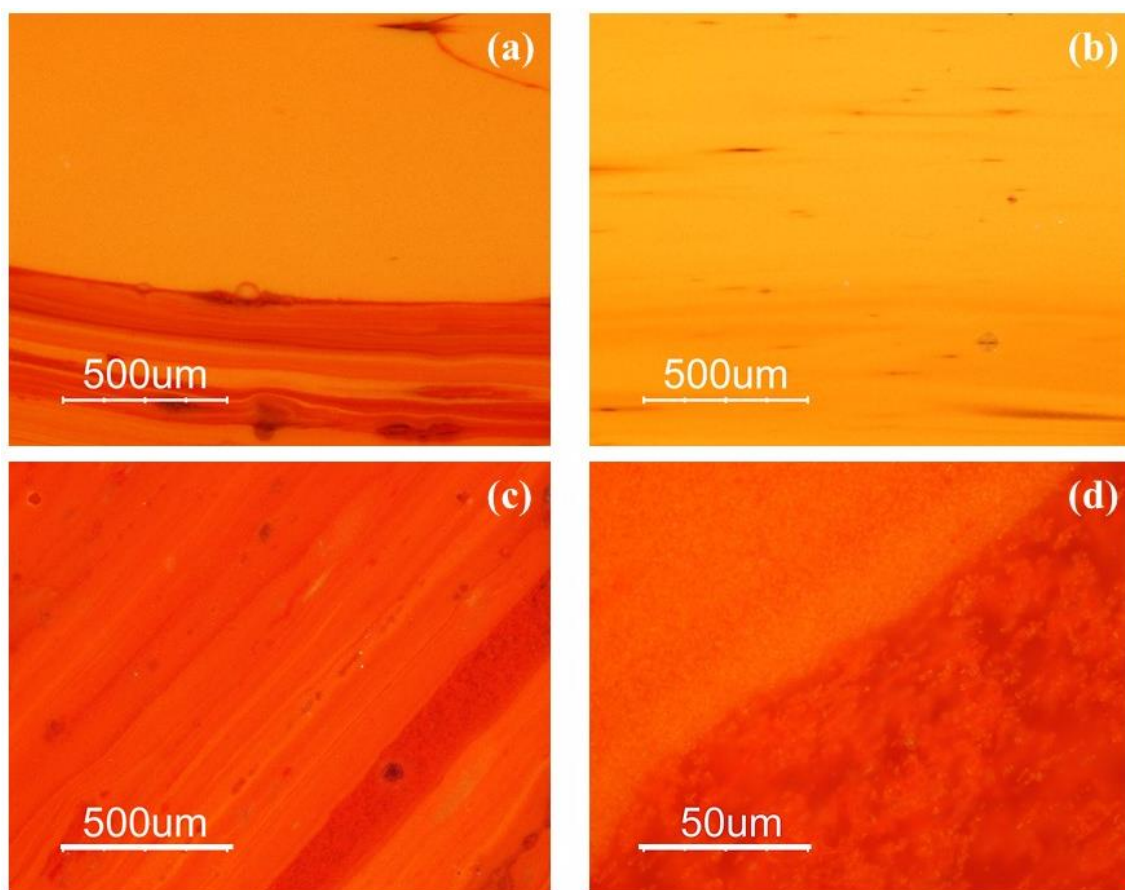


Figure 7.5. Optical micrographs from Gr-5 group: samples **a)** AR1; **b)** AR2; **c)-d)** AR4.

7.2 UV-Vis reflectance spectroscopy with optical fibers (FORS)

The FORS spectroscopy helped to discriminate the red hues by the reflectance percentage and the calculation of the inflection points, which correspond to the maximum of the first derivative in the reflectance spectra [1, 2].

The samples of Gr-1 group (fig. 7.6a) showed an inflection point between 579 and 588 nm (fig. 7.6b) which is typical of a red colour, and the different reflectance percentage observed in the range between 650 and 780 nm makes some of them slightly lighter than others. The value of the inflection point could be attributed to the presence of metallic copper [2-7].

In the Gr-2 group, the reflectance spectra exhibit a different shape (fig. 7.6c), while the value of the first derivative is in a narrower range between 582 and 586 nm (fig.7.6d), probably due to metallic copper nanoparticles. Moreover, the shape of the spectra, as well as the first derivative, showed a shoulder centred around 660 nm which could be indicative of several iron oxides present in the samples [8]. The Gr-2 group has a lower reflectance percentage than the Gr-1 group, which leads to a darker hue. Moreover, two different sub-groups emerged, observing a range between 650 and 780 nm, which move R18-R19-R20-R21 toward lighter tonality while R10 and R17 are darker than the previous samples.

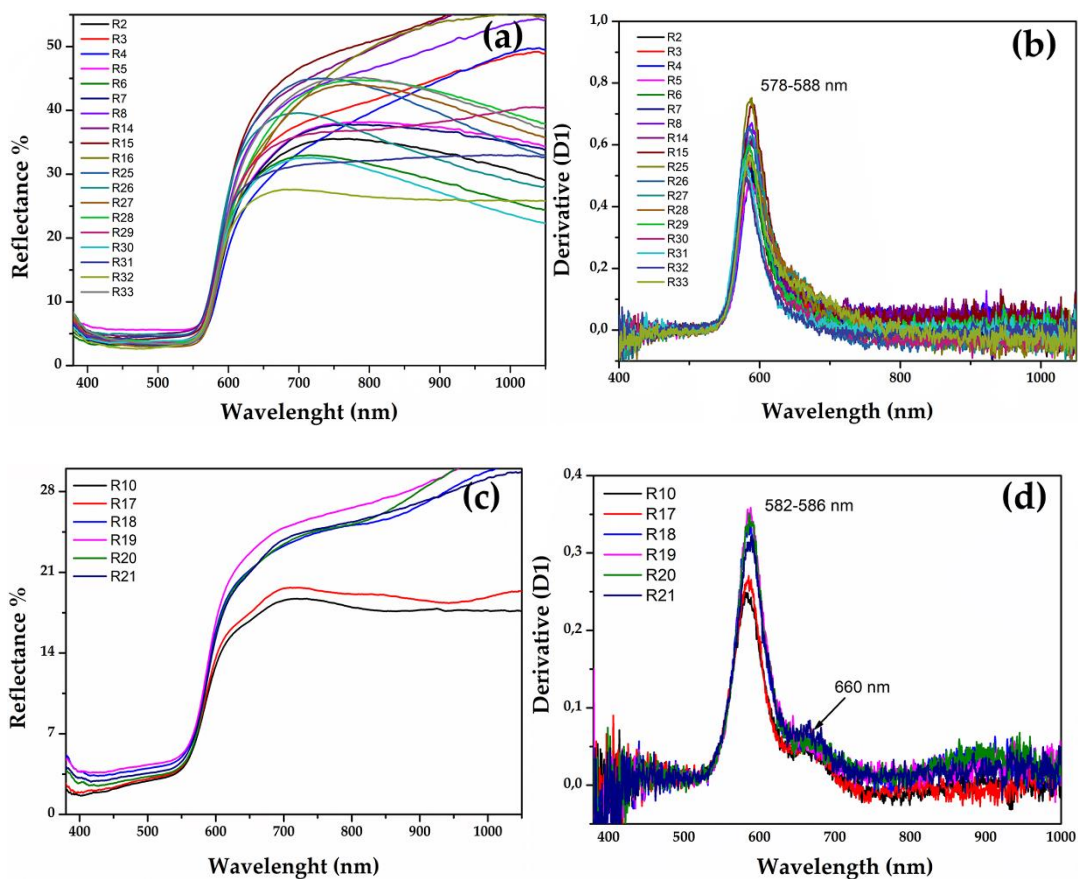


Figure 7.6. a) reflectance spectra of Gr-1 samples and b) the calculated first derivative; reflectance spectra of Gr-2 samples c) and d) their first derivative.

Gr-3 samples (fig. 7.7) are very dark with extremely low reflectance values; however, by means of fiber optics it was possible to discriminate the reflectance spectra of opaque red and dark transparent layers in samples R1 and R22. In the opaque red layer, the first derivative exhibited an inflection point at *ca* 575 nm, suggesting the presence of metallic copper nanoparticles (fig. 7.7b). An extremely weak inflection point at the same position was detected in the dark transparent layer, suggesting the presence of a few copper nanoparticles (fig.7.7d).

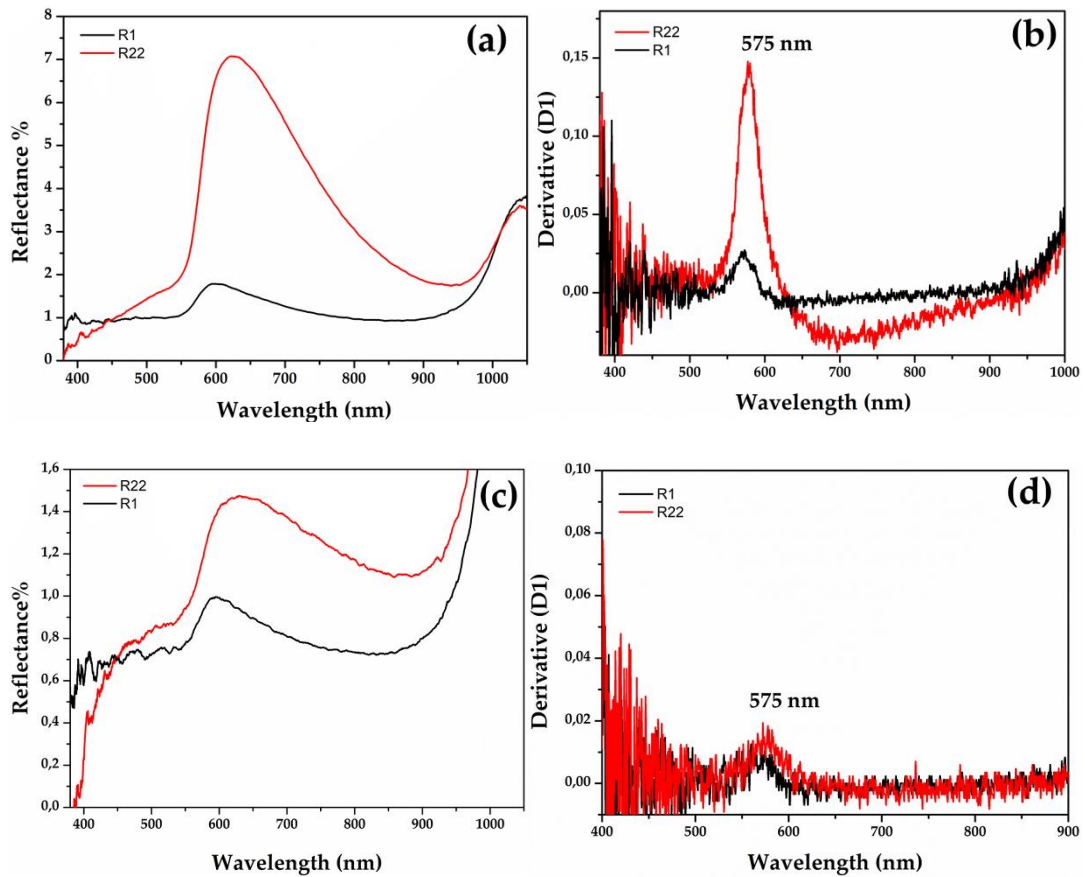


Figure 7.7. Reflectance spectra of Gr-3 groups with **a)** red and **c)** dark transparent layer. **b)** The first derivative of the red and **d)** dark transparent layers.

The sigmoid shapes with a steeper rise around the inflection point (fig. 7.8a), may indicate the presence of a semiconductor such as cuprous oxide in the Gr-4 group. This group exhibits reflectance values close to the Gr-1 group. The optical band gap was calculated extrapolating the plot of formula [9-11], and two values were obtained for the four samples, at *ca* 1.98 and 2.08 eV. corresponding to an inflection point at 625 nm and 595 nm, respectively (fig.7.8b) [12, 13]. Furthermore, these values are related to the presence of a cuprous oxide, which could be affected by the presence of some impurity.

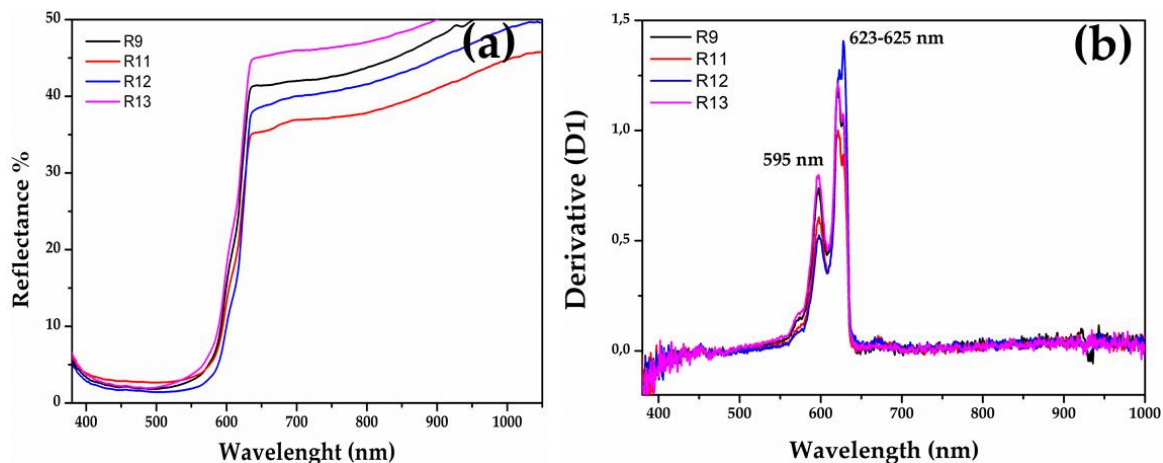


Figure 7.8. a) FORS spectra of Gr-4 samples, in which cuprous oxide could be present as a colouring agent with b) their respective first derivative.

The spectra of the Gr-5 group (orange samples) show two different hues, one more yellowish-orange (fig. 7.9a) and the second one reddish orange (fig. 7.9b). Sample AR4 exhibits a broad absorption band between 400 and 620 nm, while the rest of the samples show a narrow absorption before 500 nm. The interpretation of these spectra is complicated. The energy band gaps of all samples revealed four values: 2.56-2.13-2.08 and 1.98 eV corresponding to absorption band a 482-583-595-623 nm (fig. 7.9c). They could suggest the presence of nanocrystals of cuprite with different sizes and shapes [12, 13] and probably lead oxide [14].

The probable presence of metallic copper and cuprite crystals could correspond to two different colouring techniques.

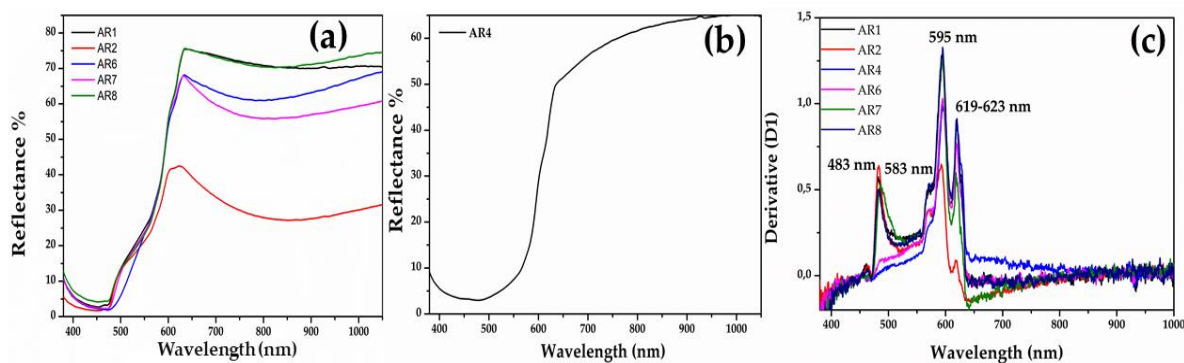


Figure 7.9. FORS spectra of orange samples. a) yellowish orange samples; b) reddish orange sample (AR4); c) first derivative of the orange samples

7.3 Colorimetry

Through the colorimetric measurements the samples and the groups are clearly identifiable by the chromatic coordinate a^* and b^* (fig. 7.10) and in the 3D chart (fig.7.11); however, in some cases they are divided by only slight chromatic differences (table 7.1).

Some of the Gr-1 group samples (R31, R32), as observed through the FORS analyses, move toward more brownish coordinate with a slight decrease of the a^* (20 and 21, respectively) and b^* (10.7-12 respectively) coordinate.

In the samples of Gr-2 group, the values of colorimetric coordinates decreased, especially a^* (13.3-16.8) and b^* (9.2-10.6) leading them towards a reddish-brown hue.

Samples from the Gr-3 group showed a significant reduction of both colorimetric coordinate a^* and b^* , in which the red and yellow part is almost absent. An increase in the contribution of green and blue part was observed, while the lowest brightness values move these samples toward an extremely dark colour, almost black. Because of the small size of sample R1 it was not possible to measure the red and black layers separately. Consequently, it seems almost black (L^* : 24.3; a^* : 1.3; b^* : 1.2). In sample R22 the red and black part were analysed showing an increase of the a^* (6.1 and 5.3 respectively) coordinate while the brightness is almost the same (L^* : 26.5 and 24.3 respectively).

As was observed by the naked eye and by the reflectance values, the samples from the Gr-4 group are very close to those of Gr-1, making them almost identical. Samples R9 and R13 are clearly distinct from R12 and showed higher contribution of a^* (23.5 and 26 respectively) and b^* (10.8 and 11.2 respectively) chromatic coordinates. Probably the more intense red is due to the low values of b^* coordinate, which is higher in the Gr-1 group samples.

Orange (Gr-5) samples split into two hues: reddish orange samples characterised by an increase of the red component (coordinate a^* : 30.3-32.4); while yellowish orange samples exhibit high brightness values (L^* : 49.3-50.1) and higher values of b^* coordinate (29.4-34).

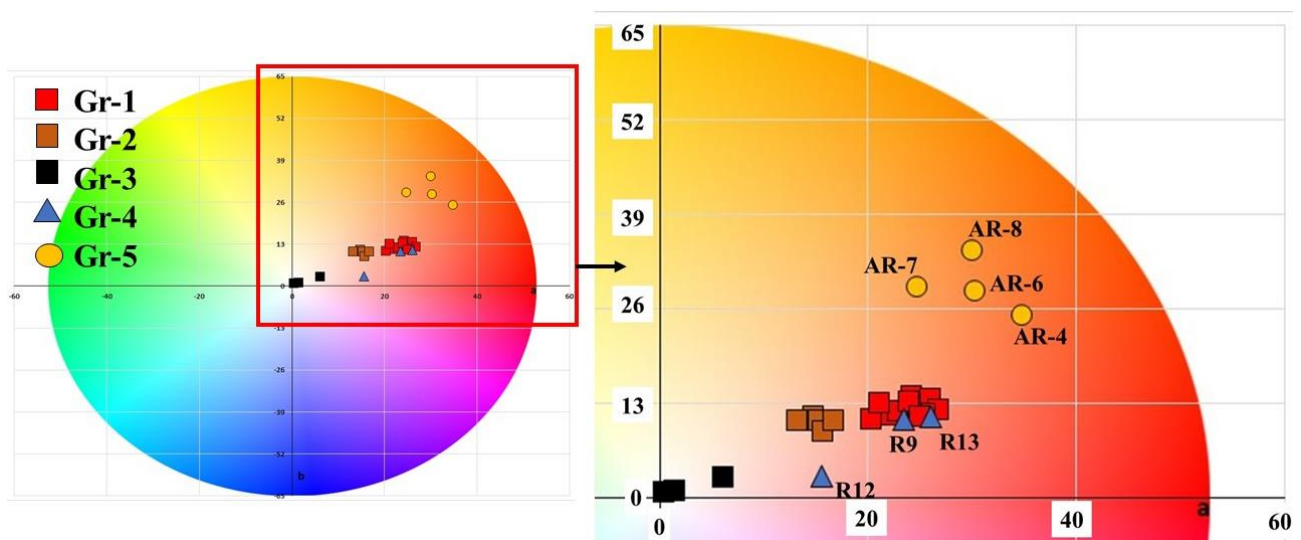


Figure 7.10. CIE Lab graphic representation composed of the chromatic coordinate a^* (x axis) and b^* (y axis).

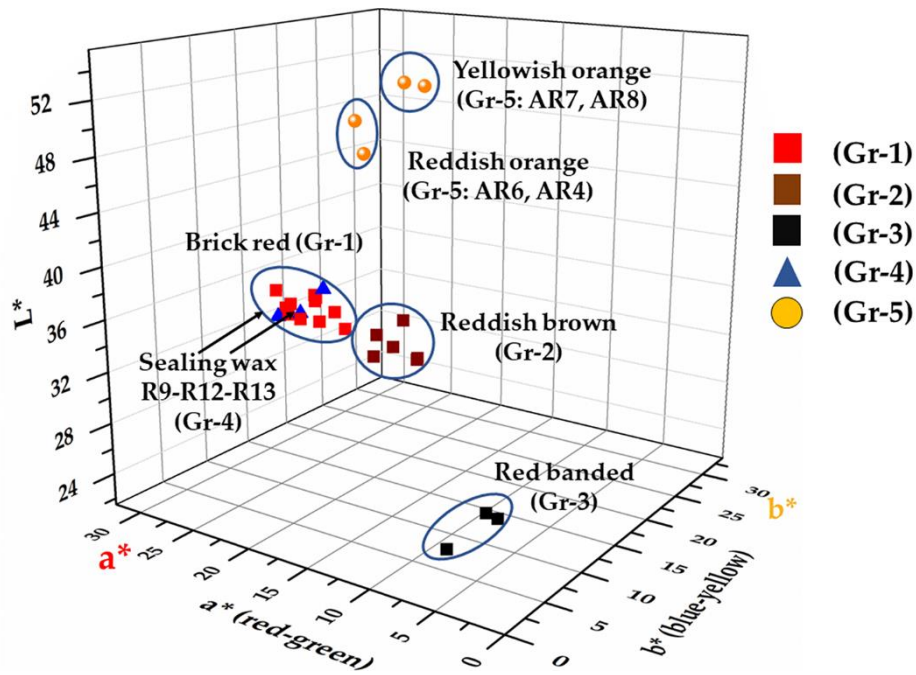


Figure 7.11. CIE Lab graphic representation: $L^* a^* b^*$ chromatic coordinates of the samples projected on the $L^* a^* b^*$ space.

Table 7.1. Average chromatic and colorimetric coordinates of the five groups.

Group	Colour	Colorimetric coordinates CIE $L^* a^* b^*$		
		L^*	a^*	b^*
Gr-1	Brick red	34-36.3	20.4-26.7	10.7-13.3
Gr-2	Reddish-brown	33.7-36	13.3-16.8	9.2-10.6
Gr-3	Red banded	24-28	1.3-6.3	1.2-5.3
Gr-4	Sealing wax	34.6-40.5	15.6-26	7-11.2
Gr-5	Yellowish orange	49.3-50.1	24.7-29	29-34
Gr-5	Reddish orange	43.8-46.2	30.3-32.4	28.4-30.2

7.4. Chemical analyses

The major and minor elements and the trace elements of the five groups samples are reported in [table 7.2](#) and [table 7.3](#) respectively.

Based on the concentration of copper and lead, the five groups can be divided into two main categories:

- high copper ($\text{CuO} > 5 \text{ wt\%}$) high lead ($\text{PbO} > 15 \text{ wt\%}$) which includes Gr-4 (CuO 7.7 – 11.7 wt%; PbO 28 – 30.4wt%) and Gr-5 groups (CuO 7.2 – 11.0 wt%; PbO 8.0 – 22.4wt%);
- low copper ($\text{CuO} < 5 \text{ wt\%}$) low lead ($\text{PbO} < 15 \text{ wt\%}$) composed of Gr-1 (CuO 1.5 – 3.0 wt%; PbO 0.31 – 2.0 wt%), Gr-2 (CuO 2.6– 3.4 wt%; PbO 0.86 – 1.3 wt%) and Gr-3 groups (CuO about 0.30 wt%; PbO 0.31 – 0.39 wt%).

More compositional differences were revealed within the low copper – low lead. In the GR-1 group the iron concentration is very similar in each sample, varying between 1.1 – 1.6 wt%; however, only R29 and R31 samples are distinct for their higher iron content (Fe_2O_3 3.4 wt%). The concentration of iron is considerably higher in the Gr-2 (Fe_2O_3 4.4-5.0 wt%) and Gr-3 (Fe_2O_3 4.2 wt%).

The quantities of SiO_2 , Na_2O and CaO detected in the Gr-1 (SiO_2 57.8 - 60.4 wt%; Na_2O 10.3 - 14.4 wt%; CaO 7.9- 12.6 wt%), Gr-2 (SiO_2 60.2 – 62.1 wt%; Na_2O 15.8 – 18.0 wt%; CaO 5.8 – 6.4 wt%) and Gr-3 (SiO_2 64.6 – 65.7 wt%; Na_2O 15.4 – 16.2wt%; CaO 7.9 – 8.1 wt%) group samples suggest the use of soda-lime-silica glass as the base glass. Due to the high concentration of lead in the Gr-4 and Gr-5 groups, their samples can be considered soda-lime-high lead-silica glass. Indeed, the ratio $\text{PbO}/(\text{SiO}_2 + \text{Na}_2\text{O} + \text{CaO})$, ranging between 0.12 and 0.60, indicates a soda-lime-high lead silica glass as the base glass [15].

To better understand the base glass composition of the five red hues, avoiding the effect that the deliberate addition of a colourant or reducing agent can bring to the final composition, a reduced composition was calculated (table 7.4). The base glass composition was calculated according to the method outlined by Brill [16]. The colouring or opacifying agents (PbO , CuO , SnO_2 , Sb_2O_3 , ZnO), added to the raw glass, were subtracted from the total of the composition of each sample, leaving only the elements incorporated in the silica source (sand) and the fluxing agent. The chemical composition was re-calculated and normalised. Iron, as well manganese content were included in the base glass composition (because they could enter as contaminants from the sand). However, it is probable that they were intentionally added to the base glass.

R19²	Gr-2	Br	N	60.5	2.1	17.0	0.73	6.12	0.58	0.72	0.13	0.89	0.10	5.0	0.38	3.3	1.1	0.22	0.66
			<i>Std. dev.</i>	0.049	0.019	0.042	0.003	0.037	0.004		0.040	0.040	0.040	0.025	0.001	0.001	0.004	0.040	0.002
R20*	Gr-2	Br	N	62.1	2.6	15.8	0.74	6.43	0.67	n.d	0.22	0.92	0.11	4.9	0.33	2.7	1.3	0.22	0.66
			<i>Std. dev.</i>	0.042	0.127	0.063	0.007	0.066	0.005		0.003	0.004	0.005	0.019	0.003	0.049	0.022	0.001	0.001
R21*	Gr-2	Br	N	61.4	2.6	17.4	0.73	6.21	0.84	n.d	0.22	1.1	0.13	4.4	0.53	2.7	0.86	0.22	0.35
			<i>Std. dev.</i>	0.017	0.020	0.012	0.004	0.022	0.002		0.000	0.002	0.000	0.010	0.000	0.074	0.006	0.040	0.040
R1¹	Gr-3	BdR	N	64.6	2.8	15.5	0.74	8.0	0.80	0.17	0.16	0.72	0.10	4.5	0.60	0.27	0.45	0.03	0.39
			<i>Std. dev.</i>	0.217	0.036	0.102	0.023	0.037	0.004		0.004	0.005	0.040	0.151	0.057	0.057	0.012	0.040	0.007
R22²	Gr-3	BdR	N	64.9	2.5	16.2	0.68	7.9	0.6	0.51	0.19	0.91	0.10	3.9	0.68	0.31	0.20	0.03	0.38
			<i>Std. dev.</i>	0.039	0.012	0.034	0.007	0.018	0.002		0.001	0.006	0.001	0.016	0.001	0.037	0.001	0.040	0.001
R23*	Gr-3	BdR	N	65.2	2.9	15.4	0.66	7.9	0.70	n.d	0.14	0.87	0.10	4.1	0.59	0.31	0.40	0.03	0.38
			<i>Std. dev.</i>	0.137	0.011	0.106	0.004	0.211	0.008		0.002	0.010	0.001	0.118	0.016	0.046	0.003	0.000	0.003
R24*	Gr-3	BdR	N	65.7	2.8	15.9	0.80	8.1	0.83	n.d	0.19	0.91	0.10	2.1	0.47	1.32	0.19	0.11	0.31
			<i>Std. dev.</i>	0.194	0.028	0.030	0.007	0.045	0.006		0.005	0.004	0.040	0.020	0.005	0.143	0.002	0.006	0.001
R9¹	Gr-4	SW	N	43.5	1.6	9.5	0.52	5.0	0.40	0.40	0.09	0.45	0.05	0.45	0.13	7.7	28.5	0.21	1.4
			<i>Std. dev.</i>	0.131	0.005	0.030	0.002	0.038	0.002		0.040	0.005	0.001	0.009	0.002	0.499	0.296	0.002	0.029
R11²	Gr-4	SW	N	41.1	1.2	9.2	0.23	2.9	0.39	n.d	0.10	0.67	0.23	0.69	0.05	11.7	30.4	0.18	1.4
			<i>Std. dev.</i>	0.284	0.015	0.050	0.005	0.041	0.004		0.001	0.006	0.003	0.010	0.001	0.428	0.289	0.001	0.011
R12²	Gr-4	SW	N	42.8	1.5	10.7	0.37	3.9	0.35	n.d	0.06	0.57	0.08	0.63	0.17	9.6	28	0.28	1.5
			<i>Std. dev.</i>	0.248	0.013	0.102	0.005	0.060	0.003		0.040	0.003	0.001	0.013	0.001	0.440	0.092	0.001	0.027
R13*	Gr-4	SW	N	44.4	1.4	8.6	0.32	3.2	0.35	n.d	0.03	0.50	0.07	0.56	0.02	9.4	29.0	0.21	1.6
			<i>Std. dev.</i>	0.051	0.008	0.058	0.040	0.032	0.006		0.000	0.005	0.001	0.006	0.040	0.394	0.240	0.001	0.013
AR1¹	Gr-5	Or	N	44.8	2.8	10.9	0.71	6.8	0.80	0.28	0.19	0.50	0.14	1.5	0.20	8.5	20.0	0.69	0.74
			<i>Std. dev.</i>	0.984	0.007	0.393	0.007	0.179	0.003		0.007	0.078	0.001	0.016	0.004	0.170	1.106	0.011	0.012
AR2¹	Gr-5	Or	N	46.0	1.8	9.5	0.74	4.2	0.70	0.42	0.21	0.50	0.10	0.70	0.35	9.8	22.4	0.87	1.7
			<i>Std. dev.</i>	2.478	0.134	0.275	0.002	0.472	0.075		0.007	0.019	0.005	2.847	0.031	1.879	1.192	0.065	0.082
AR4¹	Gr-5	Or	N	50.8	1.9	13.0	1.2	6.7	1.3	0.57	0.40	0.60	0.12	1.5	0.27	11.0	8.0	0.87	1.4
			<i>Std. dev.</i>	0.268	0.015	0.072	0.008	0.167	0.012		0.022	0.209	0.003	0.004	0.004	0.332	0.121	0.006	0.010
AR6*	Gr-5	Or	N	41.9	3.7	9.7	0.83	7.9	1.4	n.d	0.60	0.72	0.31	3.8	0.27	7.2	19.6	1.2	0.29
			<i>Std. dev.</i>	0.020	0.013	0.017	0.001	0.075	0.000		0.003	0.003	0.000	0.013	0.001	0.076	0.061	0.042	0.003
AR7*	Gr-5	Or	N	43.7	3.0	10.9	0.75	6.8	1.1	n.d	0.34	0.66	0.25	1.7	0.25	8.6	19.4	0.85	1.1
			<i>Std. dev.</i>	0.473	0.026	0.037	0.085	0.129	0.007		0.004	0.008	0.003	0.020	0.001	0.534	0.051	0.010	0.015
AR8²	Gr-5	Or	N	45.7	2.6	10.7	0.79	7.3	0.6	n.d	0.22	0.96	0.15	1.7	0.25	7.9	19.4	0.68	0.82
			<i>Std. dev.</i>	0.965	0.014	0.399	0.010	0.209	0.004		0.008	0.096	0.001	0.019	0.004	0.184	1.047	0.010	0.008

12.7	23.3	2.6	9.9	1.9	0.43	1.50	0.22	1.2	0.25	0.66	0.09	0.65	0.09	1.6	0.19	0.67	0.03	0.40	8.4	3.9	1.2
0.04	0.09	0.02	0.07	0.02	0.01	0.02	0.01	0.03	0.04	0.04	0.04	0.01	0.04	0.02	0.04	0.01	0.03	0.10	0.53	0.01	0.02
5.8	11.6	1.2	5.0	1.0	0.24	0.85	0.14	0.80	0.16	0.43	0.06	0.41	0.06	1.2	0.11	0.28	n.d.	1.4	75.5	1.0	0.96
0.53	3.01	0.12	0.45	0.11	0.03	0.09	0.01	0.08	0.01	0.04	0.01	0.04	0.04	0.09	0.01	0.02		0.21	1.65	0.11	0.18
5.7	10.4	1.2	5.0	1.0	0.25	0.86	0.14	0.84	0.17	0.48	0.07	0.47	0.07	1.3	0.12	0.31	n.d.	8.3	7.3	1.0	0.83
0.15	0.34	0.04	0.17	0.06	0.01	0.06	0.00	0.01	0.01	0.00	0.04	0.01	0.04	0.05	0.00	0.05		10.84	0.10	0.04	0.04
10.2	17.7	2.1	8.3	1.7	0.43	1.5	0.25	1.5	0.30	0.82	0.12	0.83	0.12	2.3	0.40	0.68	0.16	0.35	9.2	2.0	0.97
0.02	0.04	0.01	0.07	0.01	0.07	0.02	0.01	0.02	0.01	0.01	0.04	0.01	0.04	0.05	0.01	0.01	0.08	0.01	0.01	0.04	0.01
8.1	15.1	1.7	7.1	1.5	0.38	1.3	0.21	1.2	0.25	0.69	0.10	0.66	0.10	1.9	0.21	0.14	0.12	0.42	8.3	1.5	0.92
0.11	0.19	0.03	0.07	0.01	0.01	0.03	0.00	0.03	0.04	0.04	0.04	0.01	0.01	0.04	0.00	0.08	0.07	0.01	0.08	0.01	0.07
13.0	23.4	2.6	10.0	1.9	0.42	1.5	0.22	1.2	0.24	0.64	0.09	0.64	0.09	1.6	0.19	0.67	0.02	0.38	8.2	3.9	1.2
0.11	0.07	0.01	0.13	0.01	0.01	0.02	0.00	0.02	0.01	0.01	0.04	0.02	0.04	0.01	0.00	0.01	0.01	0.11	0.41	0.01	0.01

Table 7.4 Data of major and minor elements [wt%] obtained by the reduced composition. Colour description: **BrR**: brick red; **Br**: brown; **BdR**: banded red; **SW**: Sealing wax; **Or**: orange. Type of base glass: **PA**: plant ash; **INT**: intermediate; **N**: natron. ¹ EPMA analyses; ² FEG-SEM analyses; *samples analysed by LA-ICP-MS. Sr, Ba and Zr detected by LA-ICP-MS

Sample	Group	Colour	Type of glass	SiO ₂	Al ₂ O ₃	Na ₂ O	K ₂ O	CaO	MgO	SO ₃	P ₂ O ₅	Cl	TiO ₂	Fe ₂ O ₃	MnO	ppm	Sr	Ba	Zr
R2 ¹	Gr-1	BrR	PA	61.9	1.8	13.5	3.3	12.1	3.1	0.24	1.2	0.77	0.13	1.4	0.4		893	305	41.9
R3 ¹	Gr-1	BrR	INT	65.2	2.7	14.8	2.1	8.9	1.9	0.23	0.77	0.85	0.21	1.8	0.5		570	241	68.0
R4 ¹	Gr-1	BrR	PA	60.2	1.5	14.7	3.8	12.1	3.3	0.26	1.5	0.83	0.11	1.2	0.4		871	330	36.5
R5 ¹	Gr-1	BrR	PA	62.0	2.0	13.4	3.2	12.3	3.1	0.19	1.2	0.84	0.13	1.3	0.4		887	300	42.1
R6 ¹	Gr-1	BrR	PA	61.9	1.7	12.6	3.8	12.7	3.0	0.22	1.6	0.78	0.11	1.1	0.4		905	295	36.9
R7 ¹	Gr-1	BrR	PA	60.8	1.9	14.2	3.1	12.8	3.0	0.24	1.3	0.79	0.13	1.3	0.4		923	302	45.5
R8 ¹	Gr-1	BrR	PA	60.2	1.6	14.5	3.8	12.5	3.2	0.24	1.4	0.83	0.11	1.2	0.4		859	332	36.1
R14 ²	Gr-1	BrR	PA	61.3	1.5	14.9	3.5	11.9	2.7	0.33	1.2	0.87	0.12	1.3	0.4		873	316	37.5
R15*	Gr-1	BrR	PA	61.4	1.6	13.8	3.6	12.5	3.0	0.00	1.4	1.06	0.11	1.2	0.4		847	324	37.2
R16 ²	Gr-1	BrR	PA	62.1	1.5	14.3	3.6	11.9	2.7	0.37	1.1	0.81	0.12	1.3	0.3		776	351	38.9
R25*	Gr-1	BrR	PA	63.3	1.9	12.6	3.2	12.2	2.9	0.00	1.2	0.90	0.13	1.3	0.4		879	298	41.7
R26 ²	Gr-1	BrR	PA	63.0	1.5	13.6	3.5	11.9	2.5	0.26	1.2	0.85	0.11	1.2	0.4		884	281	39.2
R27 ²	Gr-1	BrR	PA	63.0	1.6	13.6	3.1	12.0	2.6	0.31	1.0	0.83	0.14	1.4	0.4		880	297	42.0
R28*	Gr-1	BrR	PA	63.0	1.9	12.6	3.2	12.4	2.9	n.d.	1.1	0.90	0.13	1.3	0.4		897	304	42.8
R29*	Gr-1	BrR	PA	61.0	1.9	10.8	3.8	13.1	3.0	n.d.	1.6	0.74	0.14	3.4	0.5		962	346	46.8
R30*	Gr-1	BrR	PA	63.0	1.7	11.9	3.7	12.7	2.9	n.d.	1.6	0.88	0.11	1.1	0.4		911	296	37.3
R31 ²	Gr-1	BrR	PA	60.9	1.7	11.7	3.7	12.8	2.8	0.16	1.3	0.68	0.14	3.5	0.6		966	345	47.4
R32*	Gr-1	BrR	PA	63.0	1.9	12.6	3.2	12.4	3.0	n.d.	1.1	0.89	0.14	1.3	0.4		895	305	42.4
R33 ²	Gr-1	BrR	PA	62.1	1.5	12.1	3.9	12.6	3.2	0.37	1.5	0.69	0.14	1.4	0.4		919	336	38.8
R34*	Gr-1	BrR	PA	63.1	1.9	12.6	3.2	12.4	2.9	n.d.	1.1	0.89	0.13	1.3	0.4		891	303	42.1
R10 ¹	Gr-2	Br	N	63.3	2.6	18.8	0.78	6.2	1.0	0.26	0.24	1.1	0.13	5.0	0.55		377	261	69.9
R17 ²	Gr-2	Br	N	63.4	2.3	19.3	0.76	6.1	0.63	0.52	0.18	1.1	0.14	5.0	0.53		385	268	73.3
R18*	Gr-2	Br	N	65.2	3.1	16.7	0.80	6.7	0.70	n.d.	0.22	0.96	0.11	5.2	0.35		380	215	66.2
R19 ²	Gr-2	Br	N	64.2	2.2	18.0	0.77	6.5	0.62	0.76	0.14	0.94	0.11	5.3	0.40		388	219	53.7
R20*	Gr-2	Br	N	65.4	2.8	16.7	0.78	6.8	0.71	n.d.	0.23	0.97	0.11	5.3	0.35		379	219	55.0
R21*	Gr-2	Br	N	64.2	2.7	18.2	0.76	6.5	0.87	n.d.	0.23	1.2	0.14	4.7	0.55		384	269	72.3
R1 ¹	Gr-3	BdR	N	65.4	2.9	15.7	0.75	8.1	0.81	0.17	0.16	0.73	0.10	4.5	0.61		451	271	48.3
R22 ²	Gr-3	BdR	N	65.5	2.5	16.3	0.69	7.9	0.61	0.51	0.19	0.92	0.10	3.9	0.69		445	263	48.9
R23*	Gr-3	BdR	N	66.1	3.0	15.6	0.67	8.0	0.71	n.d.	0.14	0.88	0.10	4.2	0.60		448	259	48.6
R24*	Gr-3	BdR	N	67.2	2.8	16.3	0.82	8.2	0.85	n.d.	0.20	0.93	0.10	2.1	0.49		482	244	45.5
R9 ¹	Gr-4	SW	N	70.1	2.5	15.3	0.84	8.1	0.64	0.64	0.14	0.72	0.09	0.72	0.21		299	128	27.4
R11 ²	Gr-4	SW	N	72.3	2.2	16.2	0.40	5.2	0.69	n.d.	0.18	1.2	0.41	1.2	0.09		210	85	150.9
R12 ²	Gr-4	SW	N	69.9	2.5	17.5	0.60	6.5	0.57	n.d.	0.10	0.93	0.14	1.0	0.28		261	126	42.2
R13*	Gr-4	SW	N	74.7	2.3	14.4	0.54	5.5	0.60	n.d.	0.05	0.85	0.11	0.94	0.03		169	82	36.6
AR1 ¹	Gr-5	Or	N	64.3	4.1	15.6	1.0	9.8	1.1	0.40	0.27	0.72	0.21	2.2	0.29		360	247	67.8
AR2 ¹	Gr-5	Or	N	70.4	2.8	14.5	1.1	6.5	1.1	0.64	0.32	0.77	0.15	1.1	0.54		284	135	48.0
AR4 ¹	Gr-5	Or	N	64.8	2.5	16.6	1.6	8.5	1.7	0.73	0.51	0.77	0.15	1.9	0.34		516	190	52.8
AR6*	Gr-5	Or	N	58.9	5.2	13.6	1.2	11.1	2.1	n.d.	0.84	1.0	0.43	5.3	0.38		636	181	97.6
AR7*	Gr-5	Or	N	62.9	4.3	15.8	1.1	9.8	1.5	n.d.	0.49	0.96	0.36	2.4	0.36		525	155	77.7
AR8 ²	Gr-5	Or	N	64.4	3.6	15.1	1.1	10.3	0.85	n.d.	0.31	1.4	0.21	2.4	0.35		361	247	69.0

7.4.1 The base glass composition

The samples from Gr-1 group are characterised by amounts of magnesia, potash ranging between 2.7 – 3.5 wt% and 2.9 – 3.8 wt% respectively. On the other hand, the samples of the Gr-2, Gr-3, Gr-4 and Gr-5 showed concentrations of potash and magnesia lower than 1wt%, except the orange samples AR-4 (MgO 1.7 wt%; K₂O 1.6 wt%), AR6 (MgO 2.1 wt%; K₂O 1.1 wt%) and AR7 (MgO 1.1 wt%; K₂O 1.52 wt%) (Gr-5 group).

Plotting the values of potash versus magnesia (fig. 7.12a), the samples from Gr-1 group are cluster on the right-hand side of the graphs suggesting the use of a soda-plant ash to melt the glass, while the samples of the other groups cluster down to the left part of the graph which indicate the use of natron as a fluxing agent [17]. The samples R3, AR-4, AR-6 and AR-7 showed intermediate composition. They will be named intermediate (INT) in the text.

Taking into account the P₂O₅ content against the K₂O concentration, two groups formed among the five red hues. The samples of Gr-2, Gr-3 and Gr-4 showed phosphorus amounts lower than 0.30 wt%, confirming the use of natron as a fluxing agent, while P₂O₅ between 0.77 and 1.6 wt% were detected in the Gr-1 group samples, suggesting the use of some kind of vegetable ash. Orange samples exhibit concentrations of P₂O₅ higher than the typical natron glass, maybe due to the addition of some rich-phosphorus compound (Fig. 7.12b).

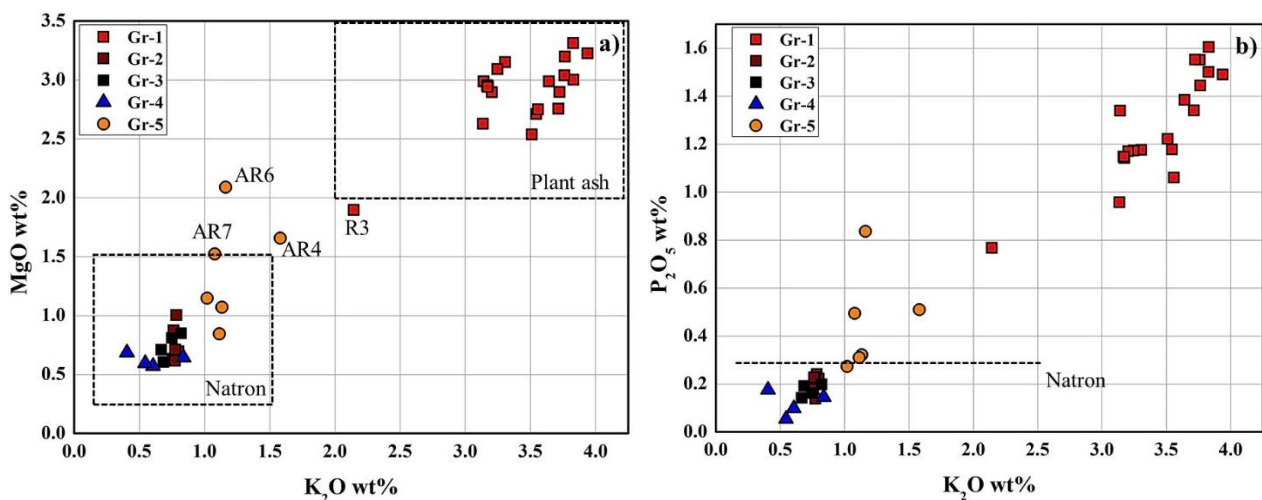


Figure 7.12. Binary graph: **a)** magnesia concentration (MgO) against potash (K₂O) concentration (reduced composition); **b)** phosphorus concentration (P₂O₅) versus potash concentration (K₂O) (reduced composition).

The lowest concentrations of sodium were revealed in the Gr-1 group which ranges between 10.8 and 14.8 wt%, while in the Gr-2 group sodium is much higher, between 16.7 and 18.3 wt%. In the Gr-3, Gr-4 and Gr-5 groups it varies between 15.8 and 18 wt%.

The amount of calcium revealed in the Gr-2 and Gr-4 groups ranges between 5.2 and 6.5 wt%, while it increased in the samples from the Gr-3 and Gr-5 groups in which it was detected between 5.2 and 11.1 wt%. The Gr-1, group samples exhibit the highest CaO content, varying between 8.9 and 13.4 wt%.

The samples from the Gr-1 group exhibited the highest strontium content (Sr ppm) ranging between 776 – 966 (ppm). The Gr-3 group showed higher concentrations of Sr (445 – 482 ppm) than the Gr-2 samples (377 – 388 ppm), Gr-4 samples (169 – 299 ppm) and Gr-5 samples (284 - 636 ppm).

By plotting the concentration of Sr (ppm) versus CaO (fig. 7.13), the Gr-1 group samples are a homogeneous cluster, and Sr and CaO are correlated, suggesting a provenance from the same compound, maybe due to the use of vegetable ash. In the other samples, the positive tendency between two elements could be related to the carbonate fraction present in the sand [18].

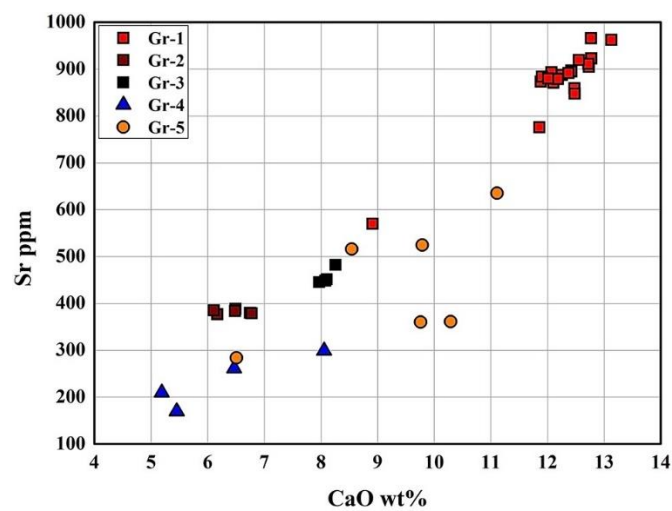


Figure 7.13. Binary graphs: strontium (Sr ppm) concentration versus calcium oxide concentration (CaOwt%) (reduced composition).

Rubidium is usually related to the k-feldspars present in the sand or to the use of wood ash. However, Gr-1 group samples showed values of Rb slightly higher than the samples from the Gr-4 and Gr-5 groups. In contrast, the highest values of Rb (Rb 16.6 – 25.5 ppm) were detected in the samples from the Gr-2 and Gr-3 groups (and AR1, AR8 – Gr-5 group). Moreover, a positive tendency is observed when rubidium is plotted against potash content (fig.7.14a) and a negative tendency when rubidium is plotted against sodium (fig. 7.14b); on the other hand, the samples from the Gr-2 and Gr-3 did not exhibit any tendency.

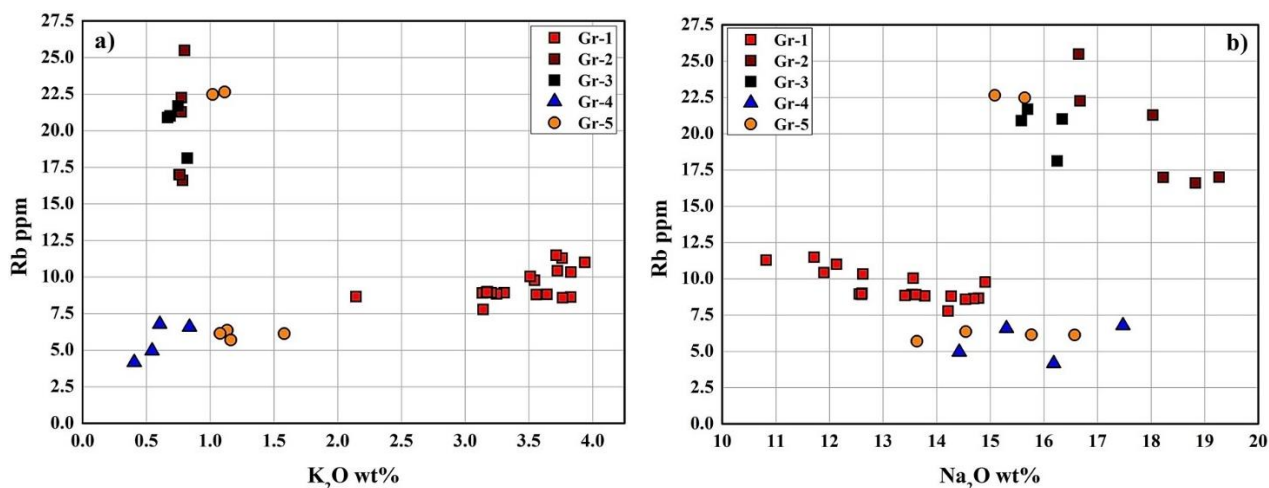


Figure. 7.14 Binary graph: **a)** Rubidium content (Rb) in ppm versus potash concentration (K₂O wt%) (reduced composition); **b)** Rubidium content (Rb) in ppm versus sodium concentration (Na₂O wt%) (reduced composition).

Among the natron base glass samples, those with high Rb content (Gr-2 and Gr-3 groups) are richer in Ba (215 – 271 ppm) than the other samples (Gr-4 and Gr-5: 82-247 ppm) (fig. 7.15). However, the highest barium content was detected in the Gr-1 group samples (Ba 281 – 351 ppm).

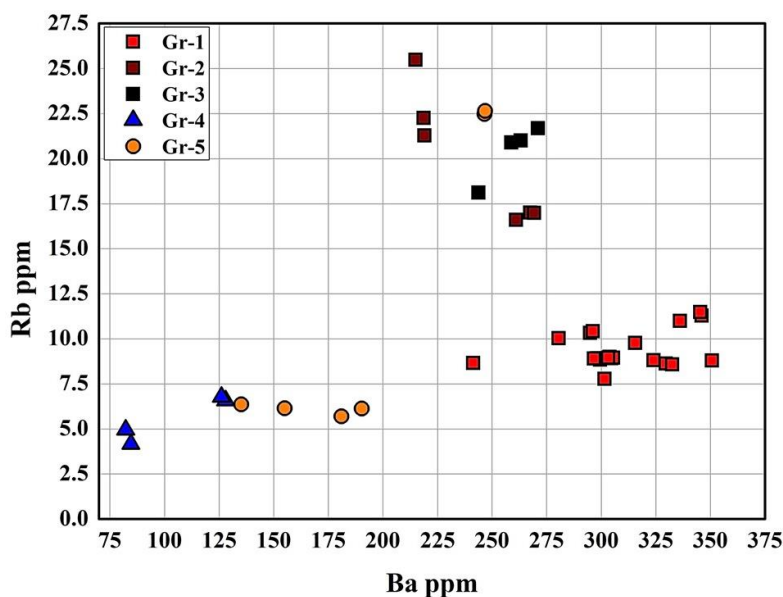


Figure. 7.15 Binary graph: Rubidium content (Rb) in ppm versus barium content (Ba) in ppm (reduced composition).

By plotting the content of Ba versus K₂O and Ba versus P₂O₅, the samples from Gr-1, Gr-4 and Gr-5 groups show a positive tendency while the samples of Gr-2, Gr-3 groups, and the samples AR-1 and AR-8 exhibit a clearly different trend (fig. 7.16a-b).

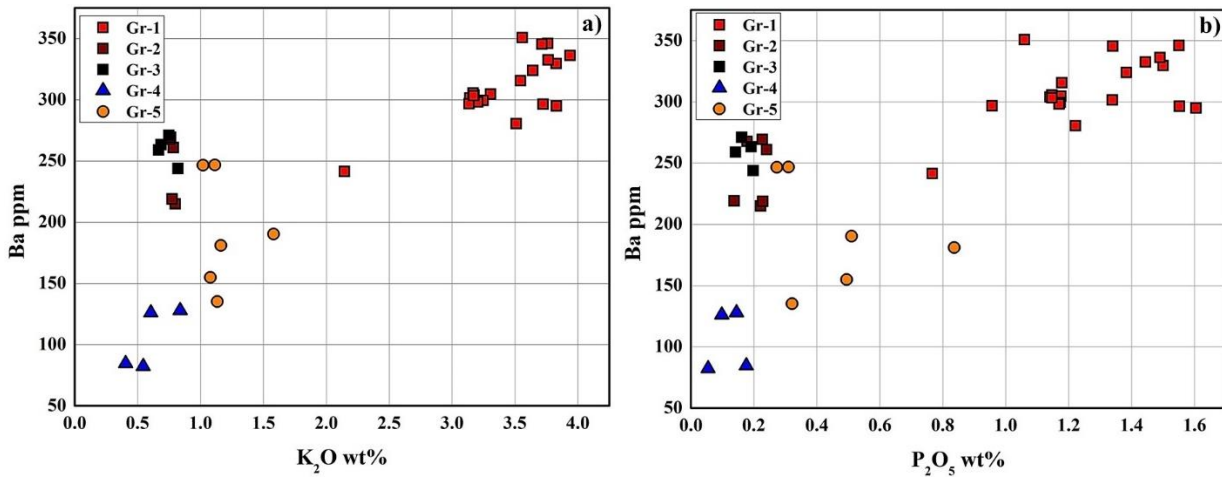


Figure 7.16. Binary graph: **a)** Barium content in ppm (Ba) against the weight percentage (wt%) of potash (K₂O) (reduced composition). **b)** Barium content in Ba ppm content against P₂O₅ wt% (reduced composition).

By plotting the concentration of SiO₂ (silica) against Zr, and Al₂O₃, three main groups are formed (fig. 7.17a-b). The Gr-1 group formed a cluster with low content of Al₂O₃ (< 2wt%), Zr (35-45 ppm) and SiO₂ (< 64 wt%). The samples from Gr-2, Gr-3 and the orange samples (Gr-5) showed higher amount of Zr (45.5 – 97.6 ppm). Based on the amount of alumina, three ranges can be identified: the Gr-1 group with Al₂O₃ < 2 wt% (except R3 samples – 2.7 wt%); the Gr-2, Gr-3 and Gr-4 groups with alumina ranges between 2.2 and 3.1 wt%; and orange samples (Gr-5) with alumina higher than 3.0 wt% (3.6 – 5.2 wt%), except AR2 and AR4 samples with Al₂O₃ values between 2.4 and 2.8 wt%.

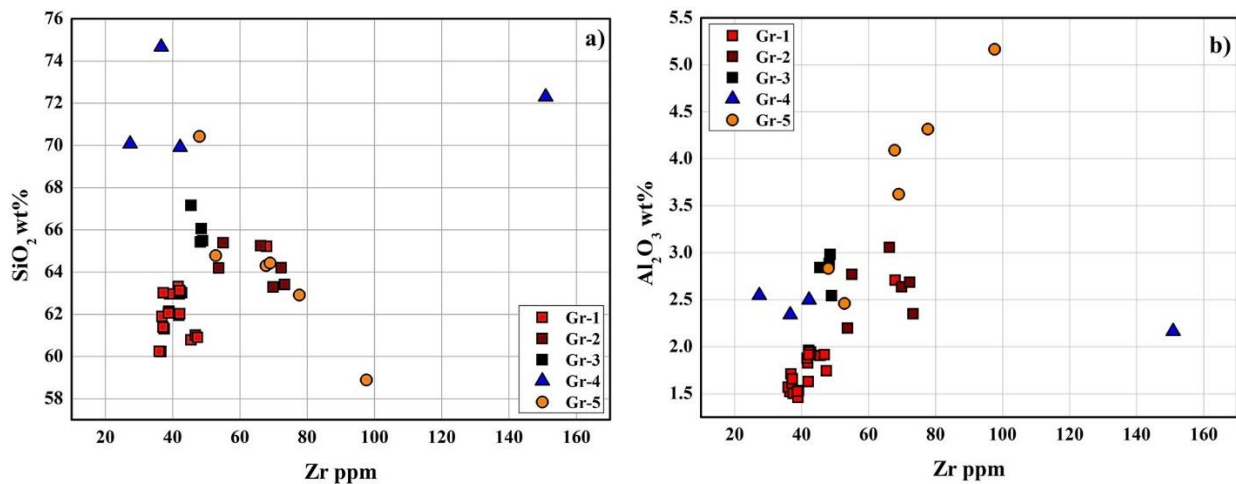


Figure 7.17. Binary graphs: **a)** silica (SiO₂) content against zirconium (Zr) content (ppm) (reduced composition); **b)** silica (SiO₂) content against alumina content (Al₂O₃ wt%) (reduced composition).

The three clusters also formed when TiO₂ and Al₂O₃ are plotted (fig. 7.18a). Beyond the previous differences in the alumina content, Gr-1, Gr-2, Gr-3 and Gr-4 exhibit similar concentrations of TiO₂ (0.09 – 0.14 wt%; except sample R11 TiO₂ 0.39 wt%), while in the orange samples (Gr-5 group) the amounts of TiO₂ vary between 0.15 and 0.46 wt%.

When the Zr content is plotted against the TiO_2 concentration, two different tendencies are observed (fig. 7.18a). The samples from the Gr-2 and Gr-3 groups have a different tendency compared with the samples from the Gr-1 and Gr-4 groups in which Zr and TiO_2 could be correlated; AR-2 and AR-4 samples are close to the Gr-1 and Gr-4 groups. AR-1, AR-8, AR-6 and AR-7 (Gr-5), R3 (Gr-1) and R11 (Gr-4) samples showed higher values of Zr and TiO_2 and are completely separate from the other groups.

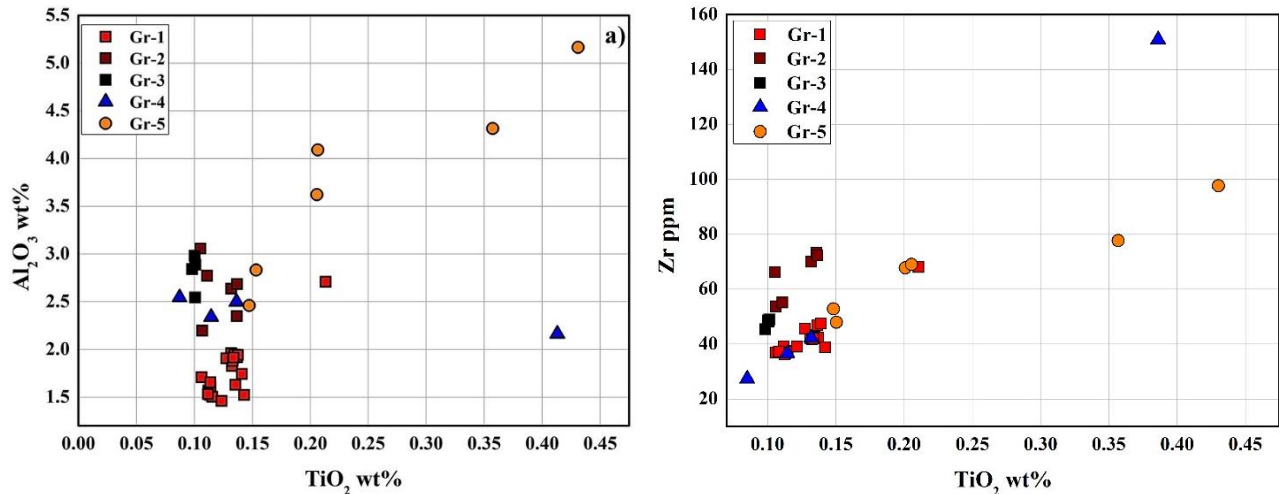


Figure 7.18. a) titanium (TiO_2) content against alumina concentration (Al_2O_3) (reduced composition); b) titanium (TiO_2) content against zirconium (Zr) content (ppm) (reduced composition).

Vanadium and chromium are positively correlated (fig. 7.19). The Gr-1, Gr-2 (R18, R19, R20), Gr-3 groups and AR-2 and AR-4 samples (Gr-5 group) formed a cluster with vanadium content ranging between 16-22 ppm; the Gr-4 group samples made another group with lower V content (7-14 ppm). The samples R10, R17, R21 (Gr-2 group), R3 (Gr-1 group) and the other orange samples showed higher V content (V 24-44 ppm).

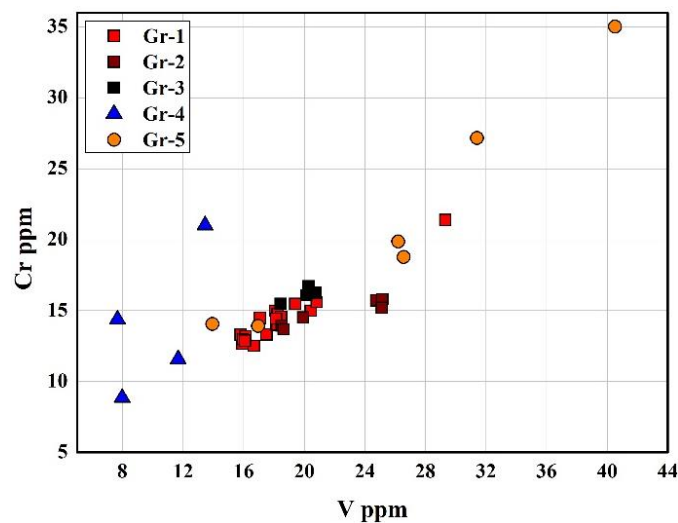


Figure 7.19. Binary graph: chromium content (Cr ppm) versus vanadium content (V ppm) (reduced composition).

The concentration of iron in groups Gr-2, Gr-3 and Gr-5 is high, and this would be due to the intentional addition of iron-bearing compounds as a reducing agent.

In the samples of Gr-1 and Gr-4, iron ($\text{Fe}_2\text{O}_3 < 1.5 \text{ wt}\%$) shows a positive tendency with the titanium concentration which could indicate that it entered the glass through minerals present in the sand (fig. 7.20) rather than as an intentional addition. The samples R29 and R31 have higher concentration of iron ($\text{Fe}_2\text{O}_3 3.4 \text{ wt}\%$), probably due to a deliberate addition of iron-bearing material. Conversely, the samples of the Gr-2, Gr-3 and Gr-5 did not show any correlation, confirming the voluntary addition of iron.

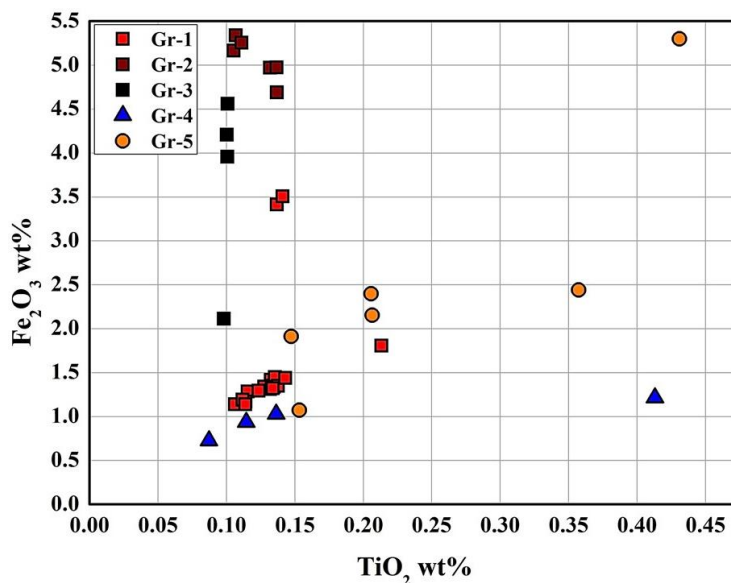


Figure 7.20. Binary graph iron concentration (Fe_2O_3) against titanium content (TiO_2) (reduced composition).

The samples of Gr-1 and Gr-4 (except sample R11) have comparable values of Ce, Hf, Zr (fig. 7.21a-b) which showed a positive tendency, probably originating from a common compound, and they are lower than those revealed in the samples from Gr-2, Gr-3 and Gr-5 (except samples AR-2 and AR-4), which do not seem to be correlated.

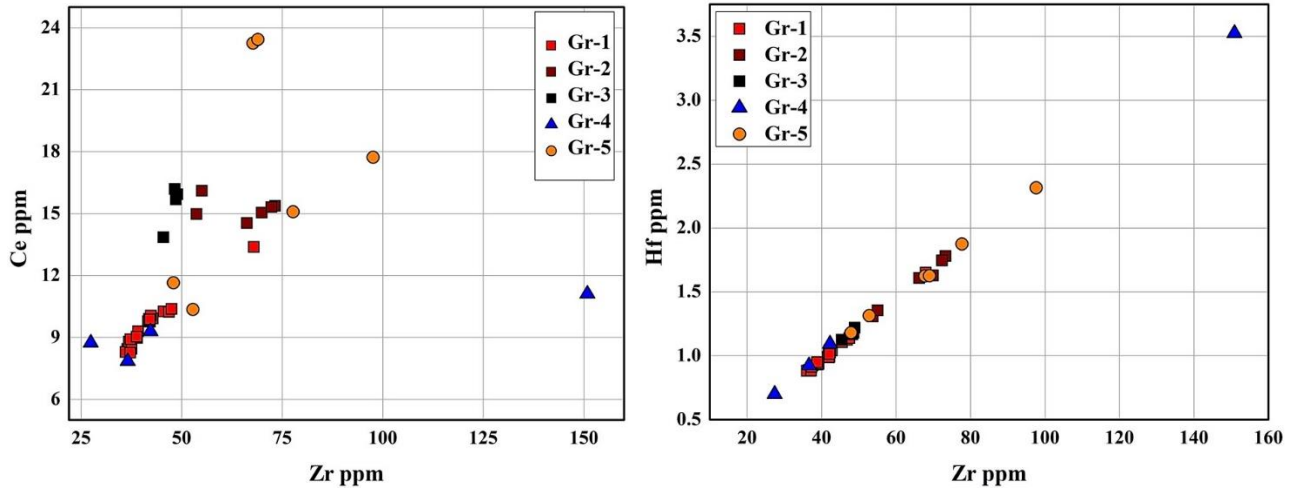


Figure 7.21. Binary graphs **a)** Caesium (Ce ppm) concentration against zircon content (Zr ppm) (reduced composition); **b)** hafnium (Hf ppm) concentration against zircon content (Zr ppm) (reduced composition).

7.4.2 Colouring and reducing agents

Table 7.5. Concentration of the colouring and reducing agents, major and minor elements [wt%], trace elements in ppm (by LA-ICP-MS). PA: plant ash; INT: intermediate; N: natron. ¹ EPMA analyses; ² FEG-SEM analyses; *samples analysed by LA-ICP-MS.

	Group	Colour	Base Glass	Type of glass	Fe ₂ O ₃	CuO	PbO	SnO ₂	Sb ₂ O ₅	ppm	Zn	Ag	Ni	As
R2 ¹	Gr-1a	BrR	PA	Sheet	1.4	2.0	1.4	0.86	0.14		379	18.4	27	51
R5 ¹	Gr-1a	BrR	PA	Sheet	1.3	2.0	1.3	0.87	0.14		377	19.8	27	51
R25*	Gr-1a	BrR	PA	Sheet	1.3	2.0	1.1	0.85	0.13		369	16.3	27	50
R27 ²	Gr-1a	BrR	PA	Sheet	1.4	3.0	1.1	0.84	0.13		362	18.6	26	49
R28*	Gr-1a	BrR	PA	Sheet	1.3	2.0	1.1	0.87	0.14		372	19.3	27	49
R29*	Gr-1a	BrR	PA	Sheet	3.3	1.5	1.8	0.58	0.11		179	9.6	27	43
R31 ²	Gr-1a	BrR	PA	Sheet	3.3	1.8	2.0	0.56	0.11		179	11.3	28	43
R32*	Gr-1a	BrR	PA	Sheet	1.3	2.0	1.1	0.86	0.13		369	18.8	27	49
R33 ²	Gr-1a	BrR	PA	Sheet	1.4	2.8	1.6	0.96	0.32		1232	16.4	45	103
R34*	Gr-1a	BrR	PA	Sheet	1.3	2.0	1.1	0.86	0.13		368	19.1	27	49
R6 ¹	Gr-1b	BrR	PA	Sheet	1.1	2.2	0.65	0.21	0.15		229	12.7	19	34
R26 ²	Gr-1b	BrR	PA	Sheet	1.2	2.3	0.31	0.23	0.19		221	12.4	17	33
R30*	Gr-1b	BrR	PA	Sheet	1.1	2.1	0.57	0.21	0.15		228	12.9	20	34
R3 ¹	Gr-1	BrR	INT	Cane	1.6	2.0	8.3	0.21	0.66		444	15.6	21	56
R4 ¹	Gr-1b	BrR	PA	Cane	1.2	2.2	0.53	0.30	0.12		291	23.2	18	31
R7 ¹	Gr-1b	BrR	PA	Cane	1.3	1.8	0.55	0.21	0.13		168	8.9	21	35
R8 ¹	Gr-1b	BrR	PA	Cane	1.2	2.1	0.40	0.30	0.12		301	22.5	19	32
R14 ²	Gr-1b	BrR	PA	Cane	1.2	2.8	0.26	0.31	0.12		276	21.4	19	30
R15*	Gr-1b	BrR	PA	Cane	1.1	2.4	0.43	0.30	0.12		286	23.6	18	31
R16 ²	Gr-1b	BrR	PA	Cane	1.2	2.8	0.67	0.16	0.08		431	15.0	19	27
R10 ¹	Gr-2	Br	N	Sheet	4.8	2.6	1.1	0.22	0.35		196	10.7	38	57
R17 ²	Gr-2	Br	N	Sheet	4.7	3.3	1.0	0.22	0.35		194	9.5	39	55
R18*	Gr-2	Br	N	Sheet	4.9	2.8	1.3	0.22	0.65		180	10.1	41	98
R19 ²	Gr-2	Br	N	Sheet	5.0	3.3	1.1	0.22	0.66		183	10.1	42	97
R20*	Gr-2	Br	N	Sheet	4.9	2.7	1.3	0.22	0.66		183	10.0	42	98
R21*	Gr-2	Br	N	Sheet	4.4	2.7	0.86	0.22	0.35		192	9.4	38	55
R1 ¹	Gr-3	BdR	N	Sheet	4.5	0.27	0.45	0.03	0.39		53	3.1	13	18
R22 ²	Gr-3	BdR	N	Sheet	3.9	0.31	0.20	0.03	0.38		53	1.9	12	17
R23*	Gr-3	BdR	N	Sheet	4.1	0.31	0.40	0.03	0.38		53	1.7	12	17
R24*	Gr-3	BdR	N	Sheet	2.1	1.32	0.19	0.11	0.31		116	9.8	14	23
R9 ¹	Gr-4	SW	N	Listel	0.45	7.7	28.5	0.21	1.4		40	47.6	76	160
R11 ²	Gr-4	SW	N	Listel	0.69	11.7	30.4	0.18	1.4		18	38.8	16	81
R12 ²	Gr-4	SW	N	Listel	0.63	9.6	28	0.28	1.5		50	40.0	79	156
R13*	Gr-4	SW	N	Listel	0.56	9.4	29.0	0.21	1.6		59	49.2	59	412
AR1 ¹	Gr-5	Or	N	Fragment	1.5	8.5	20.0	0.69	0.74		1678	25.1	37	82
AR2 ¹	Gr-5	Or	N	Fragment	0.70	9.8	22.4	0.87	1.7		55	55.3	39	194
AR4 ¹	Gr-5	Or	INT	Cane	1.5	11.0	8.0	0.87	1.4		593	56.7	53	160
AR6*	Gr-5	Or	INT	Cane	3.8	7.2	19.6	1.2	0.29		2934	35.3	38	85
AR7*	Gr-5	Or	INT	Cane	1.7	8.6	19.4	0.85	1.1		1783	31.4	35	138
AR8 ²	Gr-5	Or	N	Fragment	1.7	7.9	19.4	0.68	0.82		1690	26.3	37	83

Compositional differences among the Gr-1 samples are related to the concentration of lead and tin forming two sub-groups (table 7.5): Gr-1a is composed mainly of thin *sectilia* and Gr-1b which includes mainly the *sectilia* made by canes.

In the Gr-1a samples the concentrations of PbO (0.89 and 1.8 wt%) and SnO₂ (0.56 – 0.96 wt%; except sample R26 with SnO₂ 0.23 wt%) are usually higher than Gr-1b (PbO < 0.60 wt%; SnO₂ < 0.30 wt%). The Gr-1a group is richer in Zn (average values of Zn 400 ppm) than Gr-1b samples (average Zn 294 ppm).

In contrast, both the two sub-groups showed comparable concentration of MnO (varying between 0.32-0.47 wt%) and Sb₂O₃ (varying between 0.11-0.19 wt%), which are not enough to consider them deliberate addition.

Taking into account the trace elements, the two sub-groups showed slight differences in the concentrations of Co (Gr-1a Co 23-32 ppm; Gr-1b Co 10-23 ppm), Ni (Gr-1a Ni 27-45 ppm; Gr-1b Ni 18-20ppm) and As (Gr-1a 49-103 ppm; Gr-1b As 27-35).

The Gr-2 group samples can be divided into two sub-groups. The first sub-group is composed of R10, R17 and R21 which exhibited higher manganese (MnO 0.51-0.53 wt%) and zinc (Zn about 196 ppm), and lower lead (PbO 0.86 wt%) and antimony (Sb₂O₃ 0.35 wt%) than samples R18, R19 and R20 (MnO 0.34 wt%; Zn 180 ppm; PbO 1.8 wt%; Sb₂O₃ 0.65 wt%). Moreover, samples R10, R17 and R21 showed higher concentrations of cobalt (Co 67 ppm) and lower arsenic content (As 55 ppm) than R18, R19 and R20 (Co 33 ppm; As 98 ppm).

The Gr-3 group samples are very similar each other, and only R24 samples are distinct due to the lower iron content (Fe₂O₃ 2.1 wt%) and higher amount of copper (CuO 1.3 wt%). Despite the Gr-1 and Gr-2 groups, manganese content is about 0.60-0.62 wt%, while antimony is about 0.30 wt% which is similar to the Gr-2 samples and higher than the Gr-1 group.

The samples from the Gr-4 group are characterised by high antimony content (Sb₂O₃ 1.4-1.6 wt%), low iron (Fe₂O₃ 0.51-0.78 wt%), manganese (MnO 0.02-0.22 wt%) and tin (SnO₂ 0.18-0.28 wt%). The concentration of Zn is lower than the other groups, varying between 28 and 58 ppm, while the amounts of arsenic (As 81-412 ppm) and nickel (Ni 59-79 ppm) are higher than the other groups.

Increased quantities of iron were observed (Fe₂O₃ 0.74-3.8 wt%) in the Gr-5 group, as well as the tin content (SnO₂ 0.68-1.2 wt%), while antimony showed comparable values (Sb₂O₃ 0.29-1.7 wt%) with the Gr-4 group. High Zn content was detected, ranging between 593 and 2934 ppm, as well arsenic (As 82-160 ppm). The concentration of Co and Ni detected in the orange samples (Gr-5 group) are comparable with the samples from the Gr-1, Gr-2 and Gr-3 groups.

7.5 Crystalline phase

7.5.1 Low copper – low lead (Gr-1, Gr-2, Gr-3 groups)

7.5.1.1 FEG-SEM analyses

Copper-rich particles were detected in the Gr-1 samples. The particles are rich in copper, and it is likely that they are metallic copper nanoparticles. However, small amounts of lead, tin and zinc were detected in their chemical composition. If the concentrations of tin are plotted against the copper content, as well lead against tin, two tendencies are observed. In the graph in [fig. 7.22a](#), the tin content decreases with the increase in the amounts of copper showing a negative tendency. In contrast two groups are formed by plotting lead and tin content ([fig. 7.22b](#)), and the group on the upper half of the graph is composed of the analyses performed on the copper-rich particles in the R3 sample. However, the two oxides seem to be positively correlated in both cases.

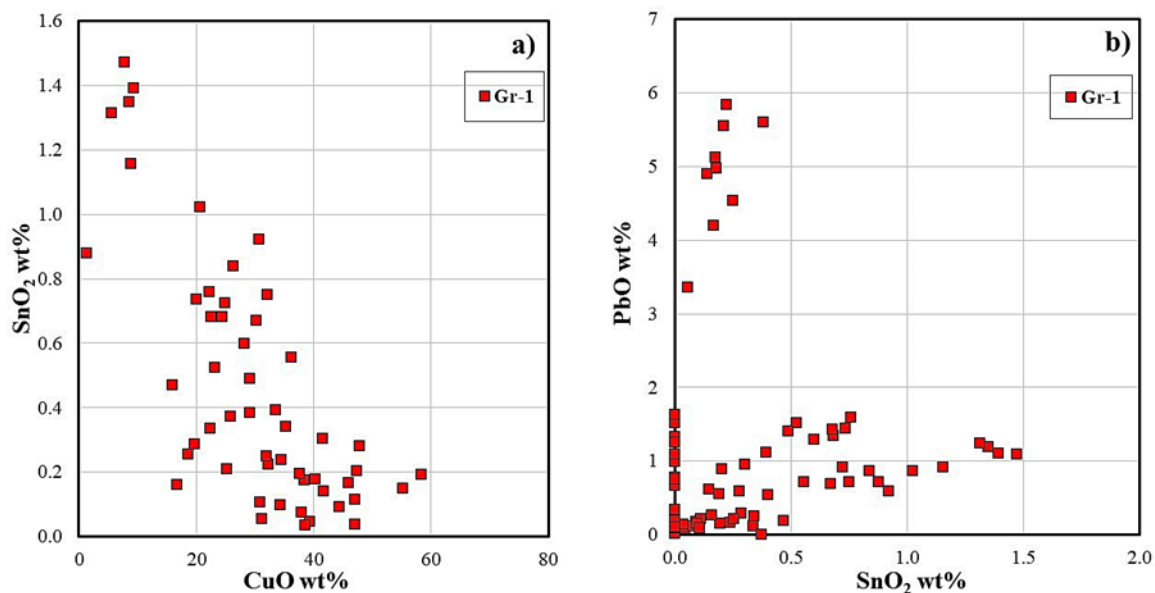


Figure 7.22. Binary graph: **a)** The concentration of tin oxide (SnO₂) against copper oxide (Cu). **b)** concentration of lead oxide (PbO) against tin oxide (SnO₂). The squares are representative of the analyses performed on the Cu-metal particles identified by FEG-SEM analyses in the Gr-1 group samples.

It was noted that usually the thin samples (R2, R5, R6, R26, R27, R31 and R33) exhibit particles varying between 40 and 300 nm and are spherical in shape. The samples made by canes (R3, R4, R7, R8, R14, R16), showed particles with a larger range of dimensions, from 70 nm up to 500 nm. Particles of 100 nm in size were frequently spherical in shape ([fig. 7.23a](#)). In contrast, when they are larger than 100 nm they often assume cubic shapes. However, the two forms can both be present in the same samples, and detected in samples R4, R7 and R8 ([fig. 7.23b](#)).

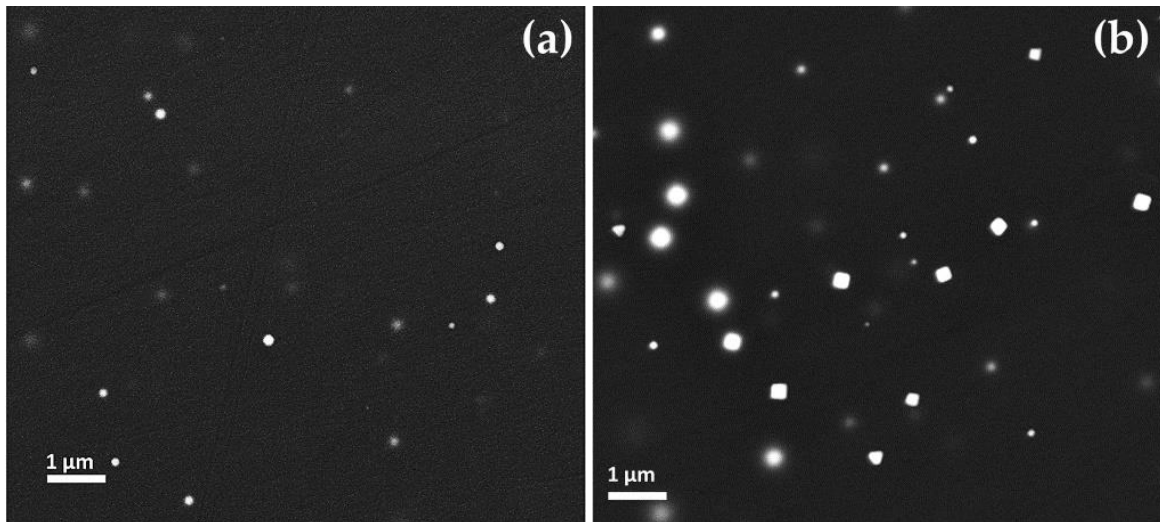


Figure 7.23. FEG-SEM micrographs of Gr-1 samples: **a)** sample R2, copper spherical nanoparticles; **b)** copper spherical and cubic nanoparticles in sample R4.

As observed through the optical microscope, a heterogeneous texture characterises the samples of the Gr-1 group. Two factors cause the heterogeneity in these samples: the number and sizes of the particles, and the presence of black bands.

The number and sizes of the copper-rich particles cause the formation of several layers with different red tonality. In the several thin samples, the colour of the layers varies from orange to dark red. In sample R31, for example, there is a high concentration of copper-rich particles with sizes ranging between 50 and 130 nm (fig. 7.24). In the red layers, the number of particles decreases while the sizes increase, varying between 100 and 500 nm. The transition from orange layer to the dark one is gradual, and it is composed of numerous thin intermediate bands with slightly different numbers and sizes of the particles, which makes the texture of this sample extremely heterogeneous. The colour is also different, resulting in a brownish orange hue.

In the samples made by canes the heterogeneity is less pronounced; however, the same phenomenon was observed. In the light red layer, high numbers of particles varying between 80 and 130 nm were observed, while in the dark layer low numbers of larger particles (200 – 400 nm) were detected.

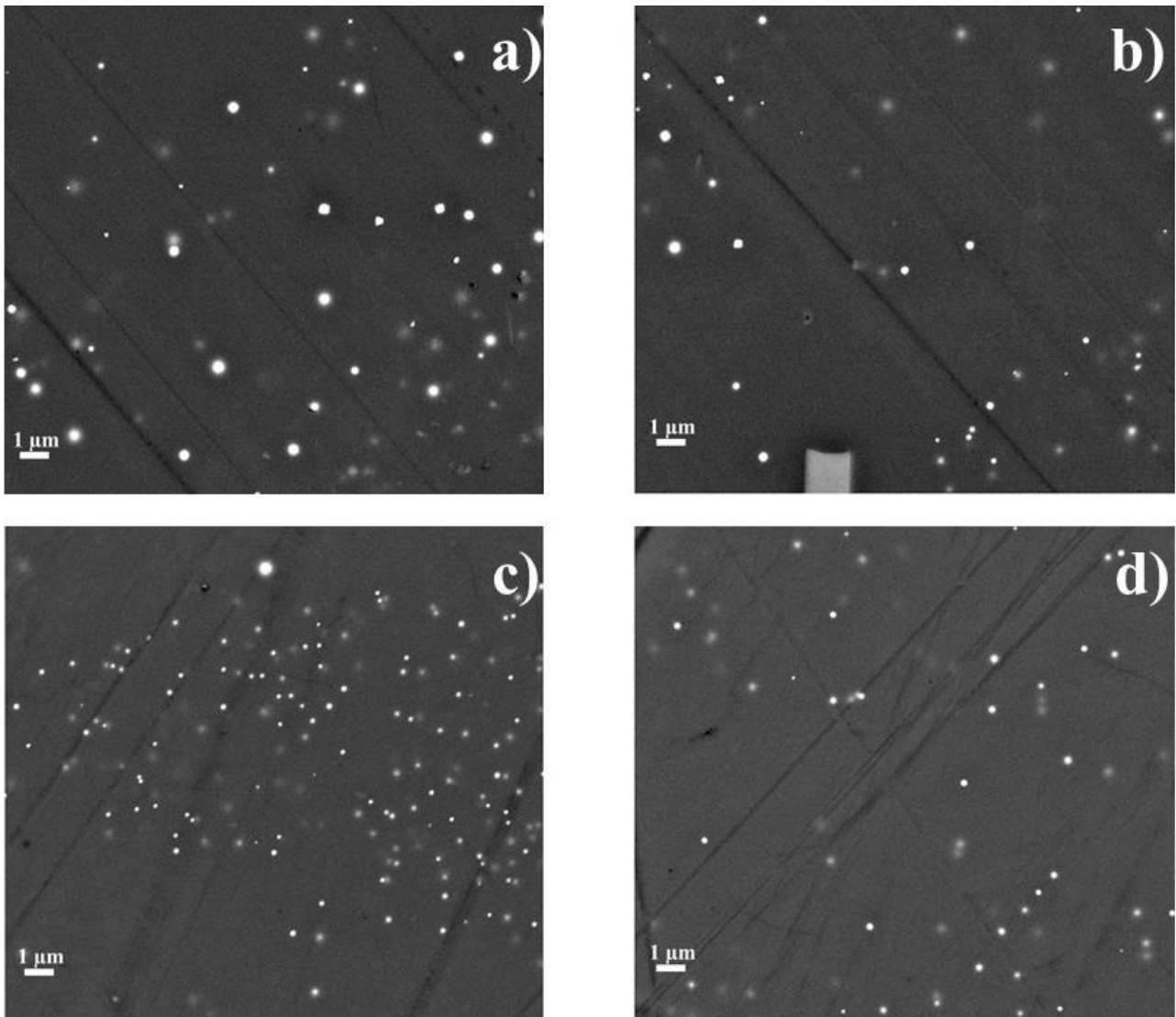


Figure 7.24. FEG-SEM micrographs of Gr-1 samples. Different red layer with different number and size of particles in sample R14: a) light red layer and b) dark red layer; sample R31 c) orange layer and d) red layer.

The presence of black layers was frequently observed in this group, especially in the thin samples (fig. 7.25). This is a green dark transparent glass, in which no particles precipitated, and no compositional differences were revealed between the red and the green dark transparent layer. They could have different dimensions, and devitrification products were frequently detected within these layers.

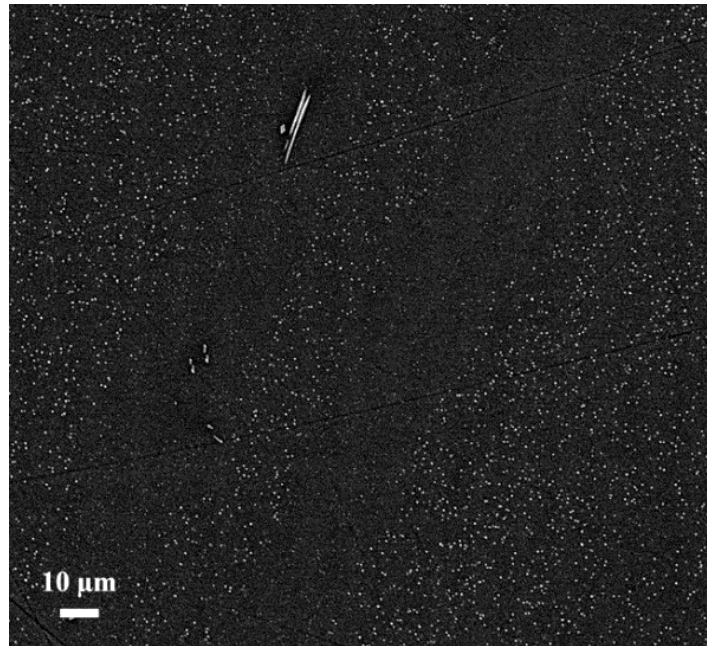


Figure 7.25. FEG-SEM micrographs: presence of black layers in sample R5.

In the samples from the Gr-2 groups, euhedral copper-rich particles with hexagonal, triangular, and cubic shapes, varying between 500 nm and 1 μm, were detected (fig. 7.26a-b). In samples R10 and R17, crystals appearing as a white line, larger than 10 μm, were frequently detected, which correspond to their vertical section or their thickness (fig. 7.26a). The number of crystals is reduced, and the heterogeneity is drastically diminished, if compared with the Gr-1 samples; only in the proximity of some inclusions was a high aggregation of very small copper-rich particles observed.

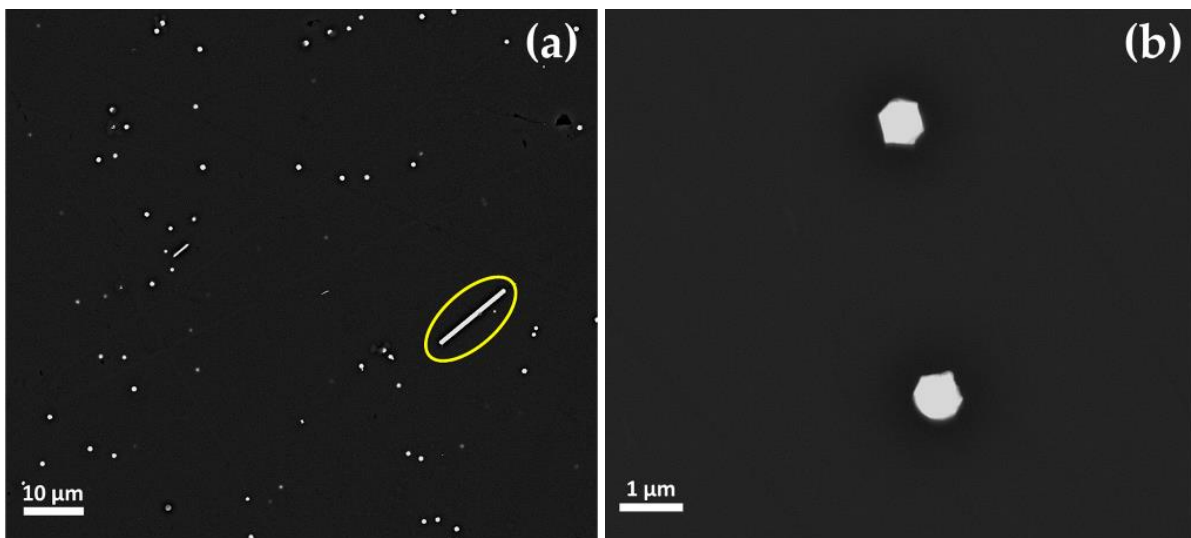


Figure 7.26. FEG-SEM micrographs of Gr-2 group samples: **a)** hexagonal and triangular crystals of metallic copper in sample R10; **b)** hexagonal crystals of metallic copper in sample R10.

The dark transparent and the opaque red layers of the samples from the Gr-3 group were analysed separately by FEG-SEM. No significant compositional differences were detected between the two layers; only in the red layers (R1: 5.4 wt%; R22: 4.5 wt%) was there a higher amount of iron than the dark transparent areas (R1: 4.6 wt%; R22: 3.3 wt%).

A high number of copper-rich particles, in the range between 50 and 100 nm, were observed in the red layers (fig-7.27a-b). Particles rich in copper and sulphur (probably Cu_2S), slightly larger than $1\mu\text{m}$ in size, were observed constantly in both the red and in the dark transparent layers (fig. 7.27b).

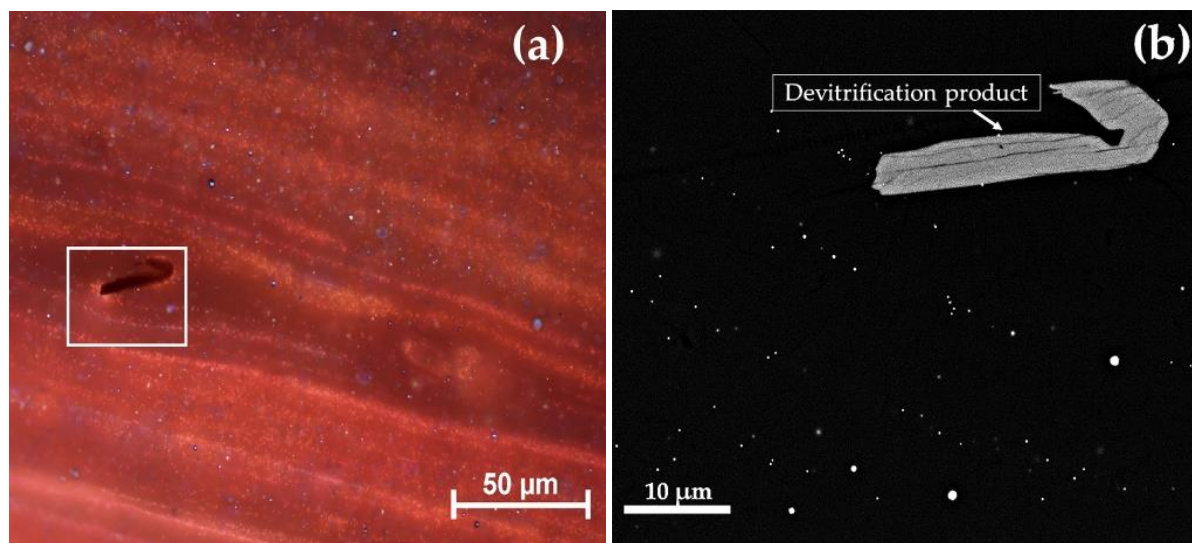


Figure 7.27. Gr-3 group sample: a) R22 at optical micrograph and b) FEG-SEM micrographs of R22.

In order to estimate the quantity of copper which remains in the glassy phase and the amount of copper precipitate to form copper rich particles, mean measurements were performed on the samples from the five groups. Through EDS analyses two different areas of the samples were investigated: a) in a large mean area including the glassy phase and the nanoparticles; b) in a much smaller area covering only the glassy phase close to the edge of the particles⁵.

The results are reported in table 7.6. It was observed that the differences in copper content between the average area and the glassy phases are very low. In the samples coloured by Cu^0 particles (R16 and R19), the compositional differences are minimal, ranging between 0.2 wt% (Gr-1) or 0.6 wt% (Gr-2). This evidence suggests that it is likely that only a low percentage of copper precipitated as Cu^0 [19].

⁵ Dr. Patrice Lehuédé (responsible for the FEG-SEM analyses at the C2RMF) performed several points out of the particles, so that we can be confident that the influence of nanoparticles below the surface can be neglected. Moreover, when performing BSE pictures it is possible to see particles below the surface (they appear blurred, but visible), and only the areas without such particles were selected.

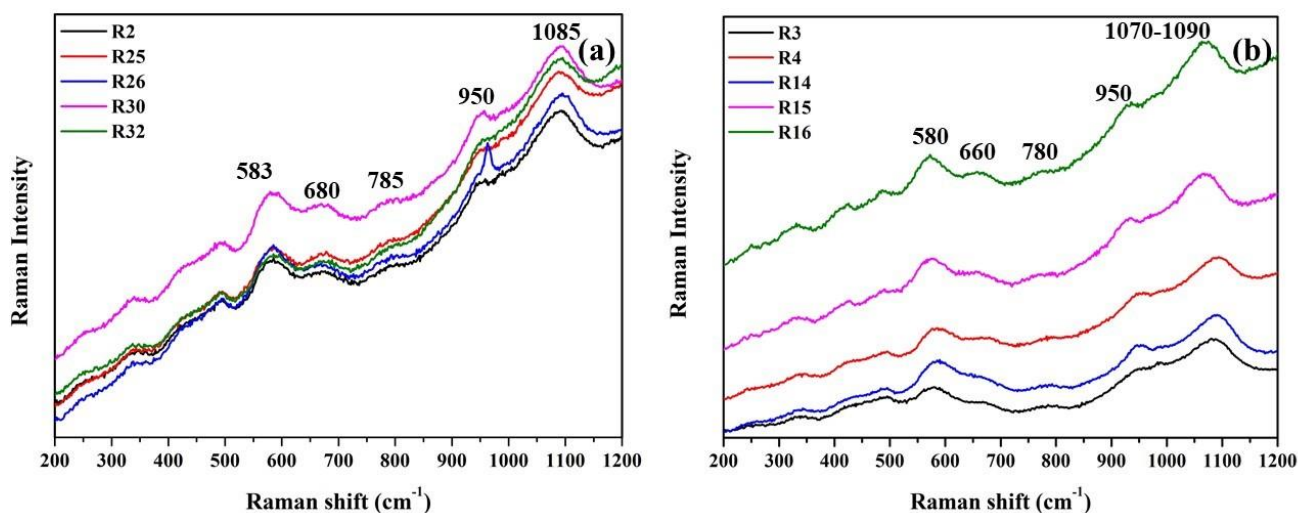
Throughout the program STATAGEM the depth at which the influence of any Cu particle is negligible, was calculated. The curves obtained give the intensity collected for Cu $K\alpha$ as a function of the glass layer thickness (intensity is 1 for a thickness $0.0\mu\text{m}$, and decreases as the thickness increases). It can be seen that the contribution of a copper particle located at $2.0\mu\text{m}$ below the surface is 98 - 99 % attenuated as compared to a particle at the surface. And at $1\mu\text{m}$, the signal is 85 - 88 % attenuated.

Table 7.6. Average (crystals + glassy phase) and regular (glassy phase) EDS analyses performed on the Gr-1 and Gr-2 groups. S.D.: Standard Deviation; five measurements were performed (at least) for the area investigated.

Oxide	Average	Glassy phase	Average	Glassy phase
Groups	R16 (Gr-1)		R19 (Gr-2)	
Al₂O₃	1.4	1.4	2.1	2.1
<i>S.D.</i>	0.09	0.06	0.05	0.05
Na₂O	13.6	13.6	17.0	17.0
<i>S.D.</i>	0.24	0.12	0.06	0.07
K₂O	3.4	3.4	0.73	0.72
<i>S.D.</i>	0.09	0.03	0.02	0.02
P₂O₅	1.0	1.1	0.13	0.20
<i>S.D.</i>	0.08	0.07	0.06	0.05
Fe₂O₃	1.2	1.2	5.0	4.9
<i>S.D.</i>	0.09	0.11	0.08	0.09
MnO	0.30	0.33	0.40	0.40
<i>S.D.</i>	0.08	0.12	0.07	0.07
CuO	2.8	2.6	3.3	2.8
<i>S.D.</i>	0.32	0.10	0.27	0.13
PbO	0.67	0.82	1.1	1.2
<i>S.D.</i>	0.09	0.07	0.07	0.06
SnO₂	0.51	0.47	0.46	0.46
<i>S.D.</i>	0.13	0.17	0.09	0.11

7.5.1.2 μ -Raman spectroscopy

By using Raman spectroscopy to analyse the samples from the Gr-1, Gr-2 and Gr-3 groups, no representative peaks of colouring particles were obtained. In the case of the Gr-1 group samples, the spectra were characterised by high fluorescence which also make it impossible to correctly interpret the peaks of the glassy phase (the subtraction of the base line was avoided). However, in samples R29 and R31, which are richer in iron, the typical peaks of a soda-lime-silicate glass appeared (fig. 7.28). They showed two main regions attributable to the bending mode (400-500 cm^{-1}) and stretching modes (900-1000 cm^{-1}) of the Si-O [20-22].



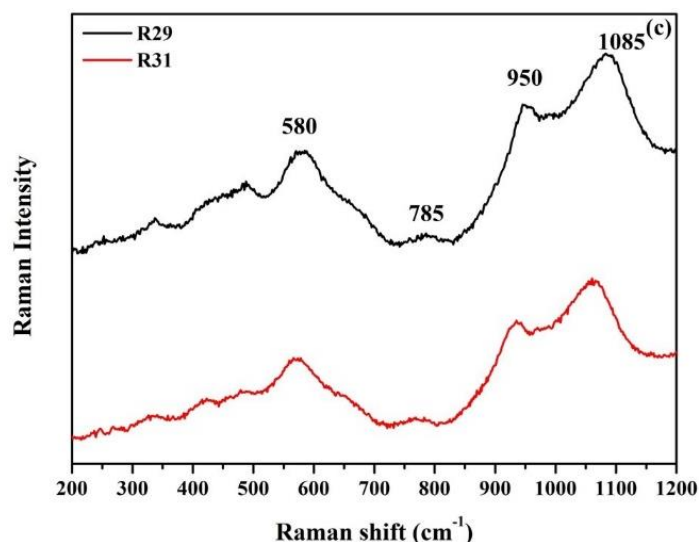


Figure 7.28. Raman spectra of the samples in the Gr-1a group **a**), and in the Gr-1b group **b**); samples R29 and R31 richer in iron **(c)**.

Spectra similar to those from the R29 and R31 samples were obtained from the samples from the Gr-2 and Gr-3 groups, which did not exhibit fluorescence (fig. 7.29a-b). The spectra of these are slightly different from those from the R29 and R31 samples. Indeed, in the Gr-2 samples well-defined peaks are observed at 990 and 1090 cm^{-1} , while in the samples from the Gr-3 group there are two weak peaks at 950 cm^{-1} (as well as in the R29 and R31 samples) and 990 cm^{-1} (very weak). Nevertheless, no cuprite peaks were detected in the samples from the Gr-1, Gr-2 and Gr-3 groups.

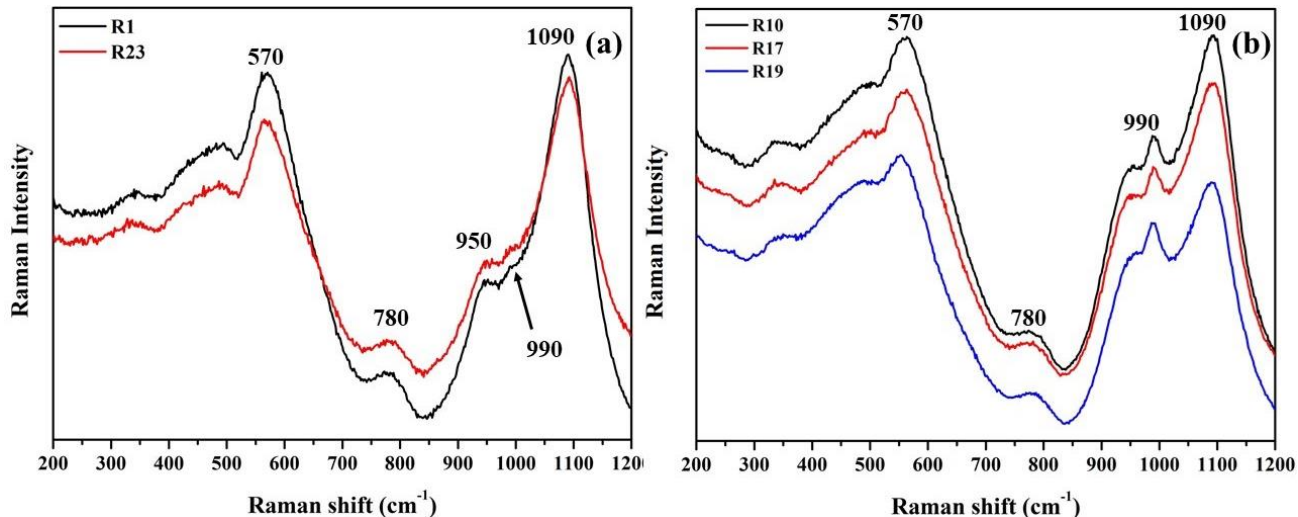


Figure 7.29. Raman spectra of the samples in the Gr-3 group **a**), and in the Gr-2 group **b**).

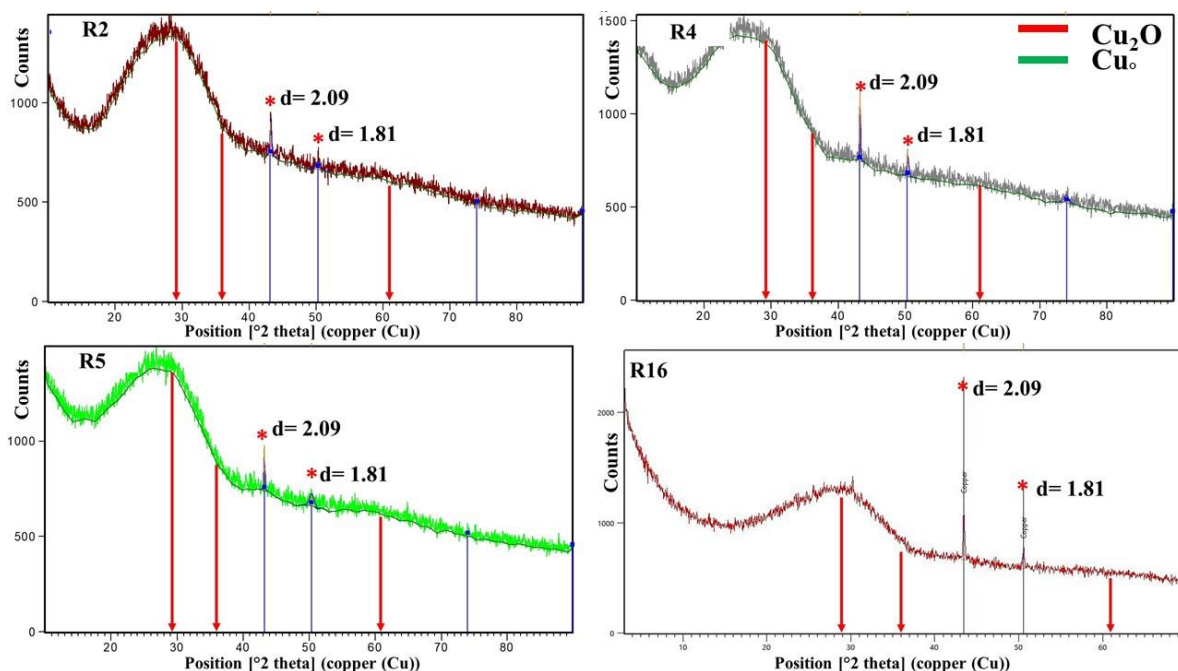
The differences revealed in the spectra of the three groups are probably linked to a different degree of glassy structure polymerisation, which could be affected by the distinct chemical composition of the base glass (high potash and magnesia, and on the other hand natron base glass), and the size and number of the colouring particles observed by FEG-SEM analyses. Although it is very interesting, this aspect was not studied because

it was not considered the main goal of these analyses, which were focused on identifying the nature of the colouring particles.

Nevertheless, as noted by Colombari, when only the characteristic peaks of the glassy phase are obtained by Raman spectroscopy on opaque red glass, it could indicate the presence of metallic copper nanoparticles [20, 21]. Indeed, the 532 nm laser (used in these analyses) is very close to the surface plasmonic resonance of metallic copper, which is strongly absorbed at this energy, and only the signature of the Si-O bonds interacting with Cu^0 particles are observed. Fluorescence is very common when copper-containing glass is analysed by Raman spectroscopy, as a result of the strong absorption of Cu^0 mentioned above [20, 21]; however, it is interesting that this phenomenon is not present in the samples with high iron content (R29, R31, Gr-2 and Gr-3). Iron is mentioned only because it seems to be the only common factor found in these samples, but other causes could generate this evidence.

7.5.1.3 X-ray diffraction analyses

X-ray diffraction were performed on the selected samples from Gr-1, Gr-2, Gr-4 and Gr-5 groups, while, due to the small size of the Gr-3 they were not analysed. Four samples of the Gr-1 group representative of the two types of manufacture (2 for the thin and 2 for the thicker) were analysed. They showed a broad peak of between 20° and 30° (2Theta), typical of vitreous material, and two weak peaks at $d=2.09$, $d=1.81$ which were assigned to metallic copper with cubic symmetry (fig. 7.30). The R10 and R17 samples (representative of the Gr-2 groups) are characterised by the same peaks, which were attributed to metallic copper particles. In the diffractogram of the R10 sample, the intensity of the peaks observed is higher, which could be due to the size of the particles (larger than in the Gr-1 groups) and their concentration, observed through the FEG-SEM analyses.



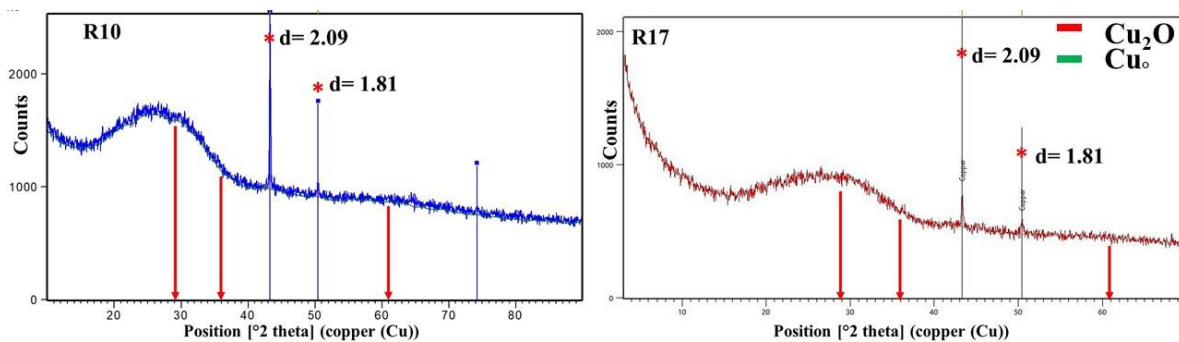


Figure 7.30. X-ray diffraction on the samples of Gr-1 (R2- R4-R5) and Gr-2 (R10), showing the typical peaks of metallic copper. No cuprite crystals were detected.

7.5.1.4 Other crystalline phases

Euhedral crystals rich in Ca-Si or Na-Ca-Si, classical devitrification products [23], were detected in several samples from the Gr-1, Gr-2, and Gr-3 groups. The crystalline phase, devitrification products and other inclusion are reported in table 7.7, in order to provide a general view of the results obtained in the different red hues.

Inclusions of different types were detected in the samples from Gr-1 group. In sample R8, a large metallic inclusion (black at the OM) was observed (fig. 7.31a). The inclusion is composed of two parts: the white part is rich in lead and sulphur (PbO 72.4 wt%; SO₃ 21.6 wt%), while copper and sulphur were revealed as the main components (CuO 67.1 wt%; SO₃ 30.4 wt%) in the grey part (fig. 7.31b-c).

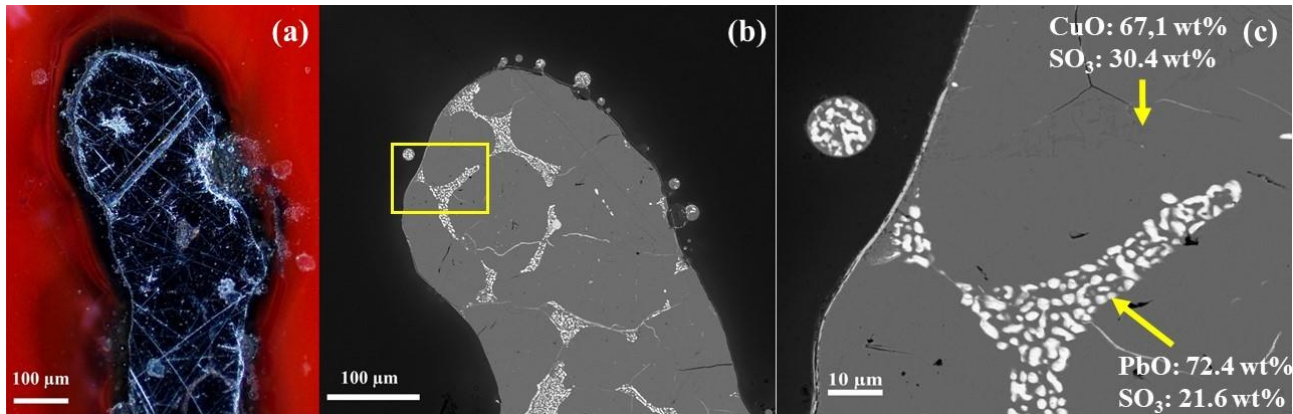


Figure 7.31. a) metallic inclusion in sample R8, observed by OM; b)-c) FEG-SEM micrographs and chemical characterisation of the inclusion by EDS.

Sample R16 showed another large spherical inclusion rich in copper, silver and sulphur. This inclusion is surrounded by particles rich in silver, copper and antimony, measuring 10 μm (fig. 7.32a).

Inclusions rich in iron, whose chemical composition could be comparable with magnetite, were detected in samples R6 and R8 (fig. 7.32b). Moreover, in samples R6 and R26, particles rich in phosphorus and calcium, with spherical or elongated shapes, were detected (fig. 7.32c).

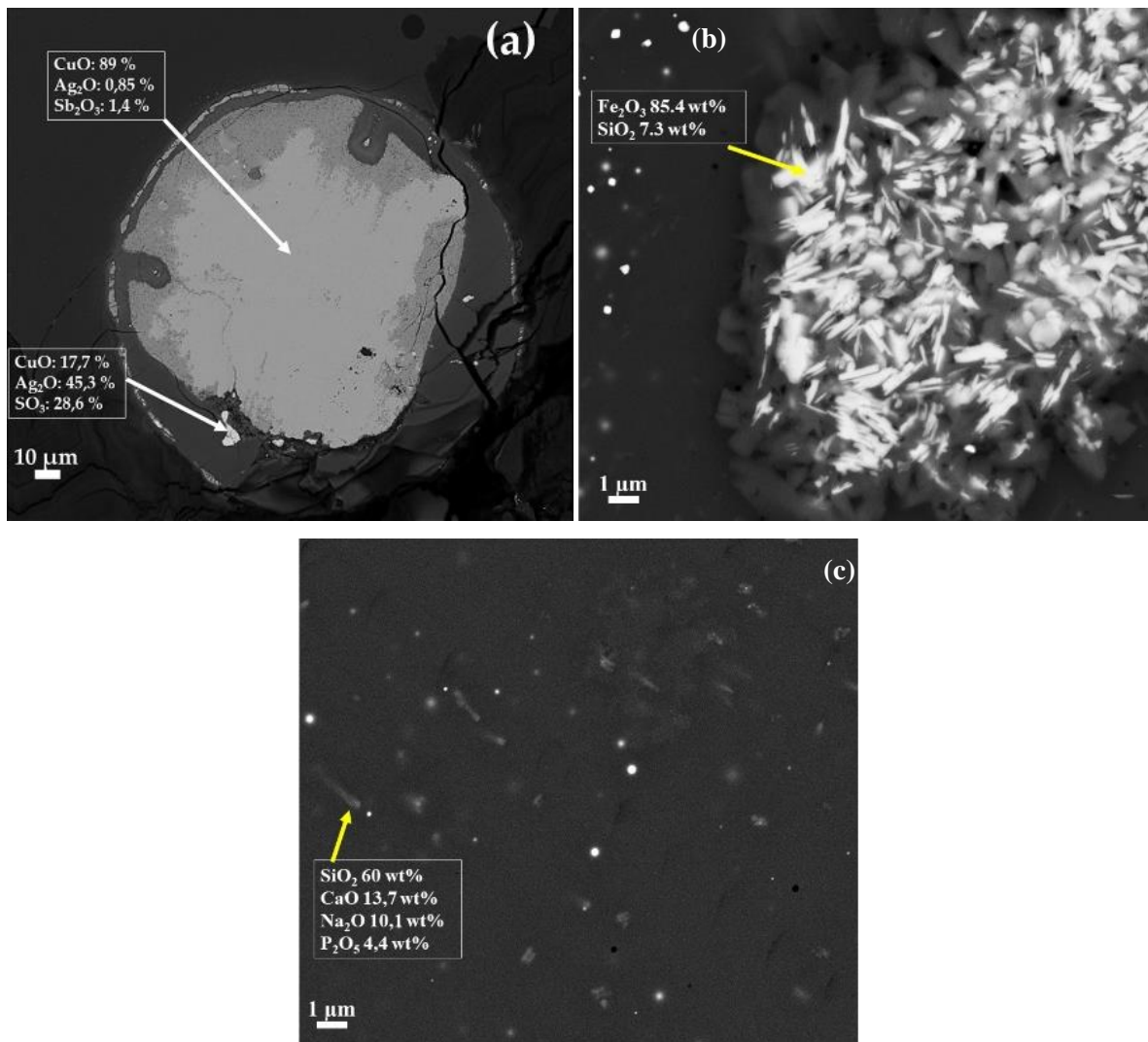


Figure 7.32 FEG-SEM micrographs a) metallic inclusion in sample R16 with particles rich in Ag; b) iron rich inclusion probably magnetite in sample R6; c) calcium and phosphate particles in sample R6 and R26.

In the sample R17 (Gr-2 group) a large metallic inclusion (black at the OM) was observed, and by EDS analyses they turned out to be rich in copper and sulphur, probably Cu_2S (fig. 7.33a). Around these inclusions numerous bubbles were formed in the glass. Moreover, a large copper-rich inclusion (probably metallic copper) was detected, in which around it a high concentration of small copper-rich particles (200 nm) was noted.

In several samples of the Gr-2 group, inclusions rich in Si-Al-Fe-K-Na were frequently revealed in sample R10, R19 and R17 (fig. 7.33b), which could be clay fragments coming from the wall of the crucible or furnace, or some inclusions from the sand. However, close to these inclusions, a high number of smaller crystals were observed.

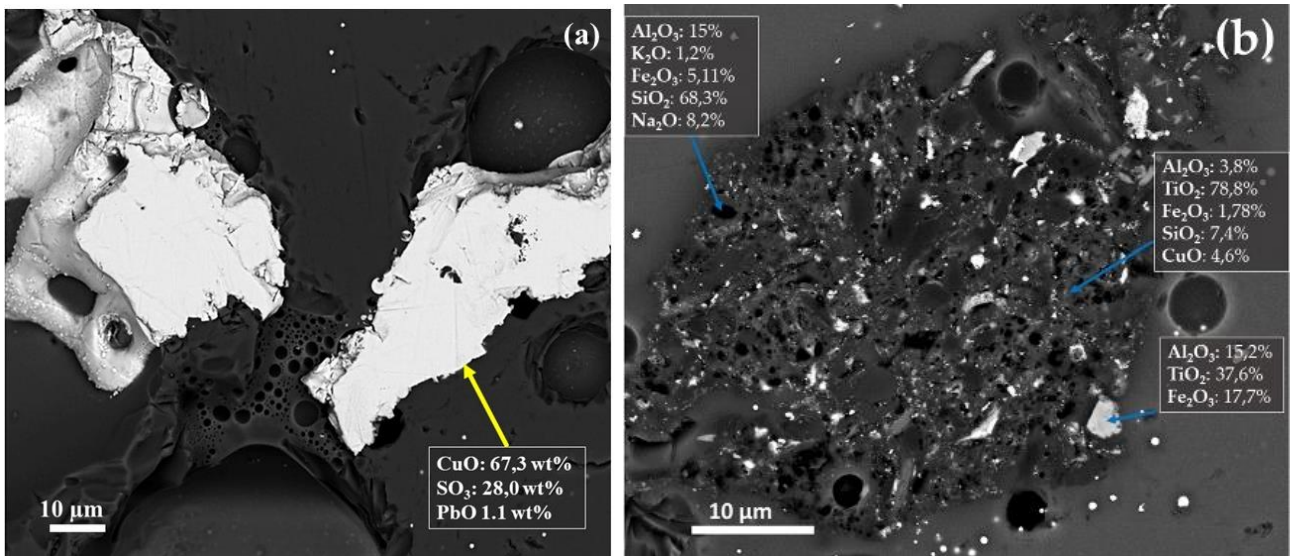


Figure 7.33. FEG-SEM micrographs: **a)** metallic inclusion rich in copper and sulphur, likely Cu_2S , detected in the R17 sample; **b)** inclusions rich in Si-Al-Fe-K-Na detected in sample R10.

In the red banded samples (Gr-3), spherical particles composed of copper and sulphur (fig. 7.34) were found in both of the layers, while in sample R1 (in the dark transparent layer) a large inclusion of haematite (Fe_2O_3) was detected together with a devitrification product (wollastonite).

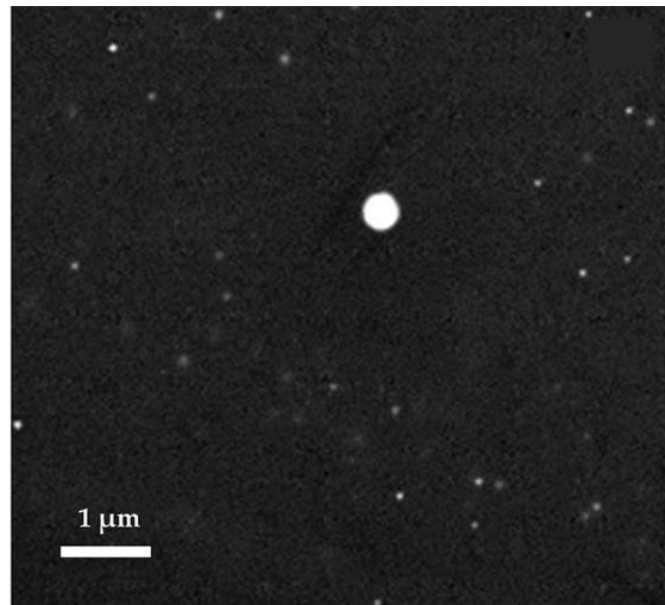


Figure 7.34. FEG-SEM micrographs: inclusion rich in copper and sulphur, likely Cu_2S , detected in the R22 sample.

7.5.2 High copper – high lead, (groups Gr-4 and Gr-5)

7.5.2.1 FEG-SEM analyses

The samples from the Gr-4 group are characterised by large dendritic-shape crystals, rich in copper and oxygen, likely cuprous oxide (fig. 7.35).

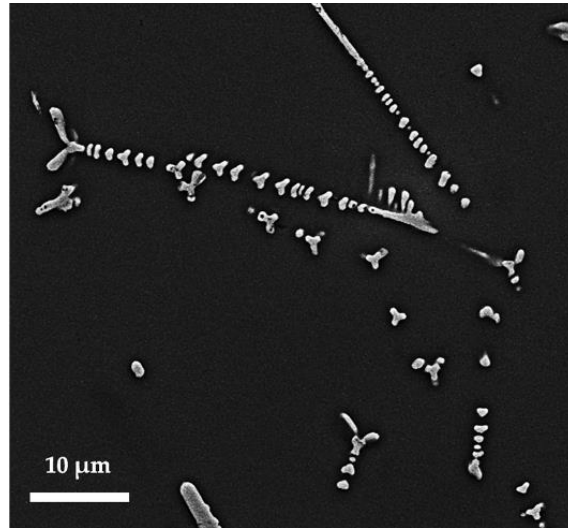


Figure 7.35. FEG-SEM micrographs cuprite crystal in sample R9 (Gr-4).

The crystals are slightly larger in sample R11 than in samples R9 and R13. The number and the size of the cuprous oxide crystals could cause the formation of different red hues: a few large crystals in the darkest sealing wax (R11-R12) and a high number of small dendritic cuprite crystals in the lightest (R9-R13).

Moreover, sample R11 showed more heterogeneity than the other samples. Indeed, it featured the presence of lighter layers, which are richer in lead oxide than the darker layer. This characteristic was not detected in the other samples (fig. 7.36a-b).

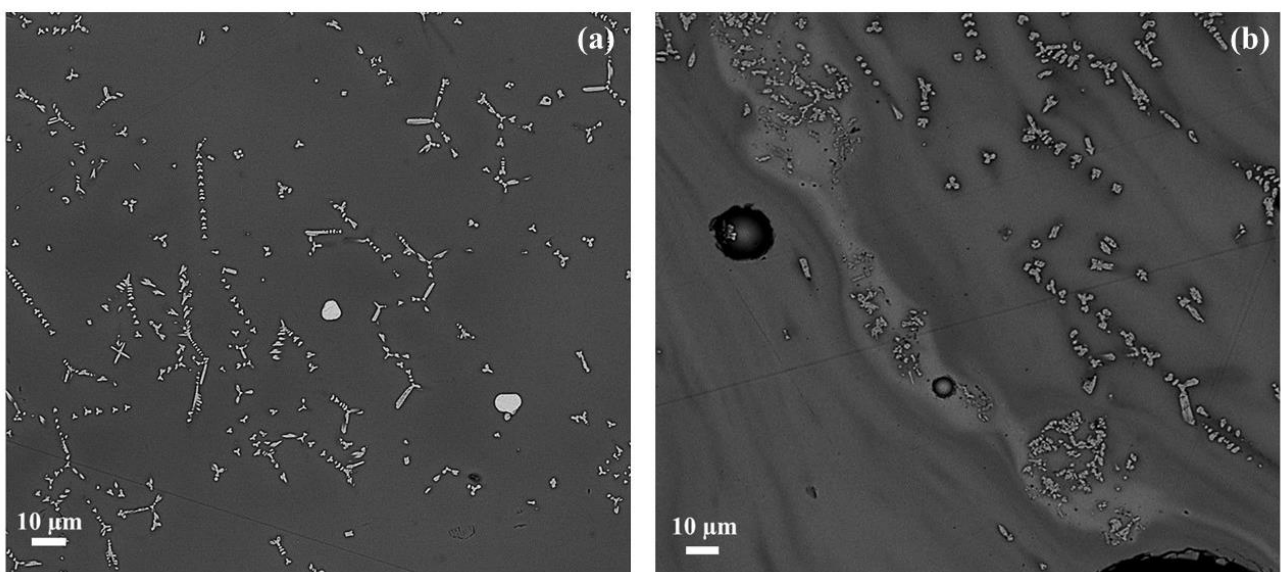


Figure 7.36. FEG-SEM micrographs: (a) sample R9 which is more homogeneous than sample R11 (b) in which lighter layers formed.

Crystals rich in Cu and O, likely cuprous oxide, were observed in all the orange samples (Gr-5 group). Each orange hue from the Gr-5 group is characterised by the distinct abundance and size of the crystals. The yellowish orange samples exhibited a high number of crystalline particles, which hexagonal or cubic in shape. In sample AR1 (fig. 7.37a), the crystals vary between 100 and 300 nm, while in sample AR2 (fig. 7.36b) the number of the particles increased, and their sizes are slightly lower (200nm). In the reddish orange hue, the concentration of crystals seems to be reduced while they are enlarged in size. Sample AR8 (fig. 7.37c) exhibits large copper-rich particles reaching approximately 1µm which are mainly hexagonal in shape, while in sample AR4 (fig. 7.37d) the sizes are included in the range between 200 and 800 nm and are hexagonal in shape.

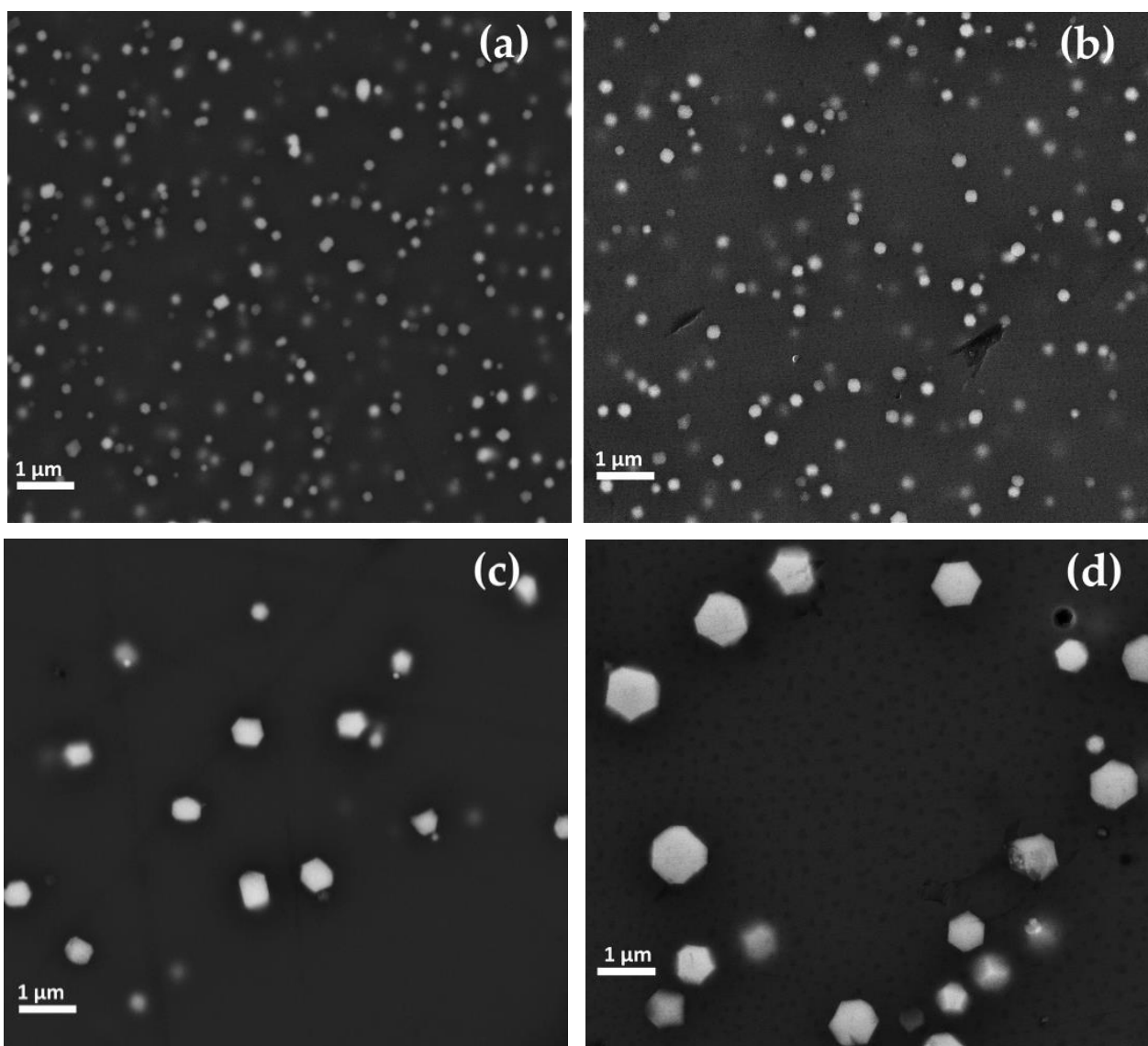


Figure 7.37. FEG-SEM micrographics of Gr-5 group samples: cuprite crystals observed in sample AR1 **a)** and AR2 **b)**; AR8 **c)** and AR4 **d)**.

The heterogeneity of the samples composed of red and orange layers (AR1, AR4, AR8), is not characterised by compositional differences. On the contrary, the abundance and the sizes of the particles distinguish the two

layers. Indeed, a high number of small crystals were detected in the yellow layer, while a few large crystals were revealed in the red layer (sometime dendritic in shape) (fig. 7.38a-b).

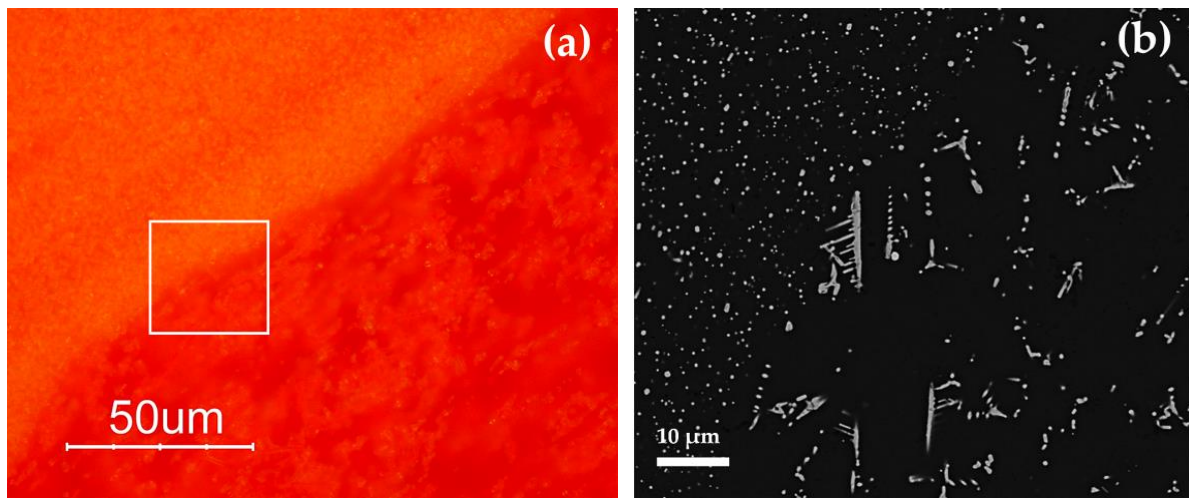


Figure 7.38. Optical **a)** and FEG-SEM micrographs **b)** of the red layer and orange layer in sample AR4 (Gr-5).

As for the low copper -low lead samples, to estimate the quantity of copper which remains in the glassy phase and the amount of copper precipitate to form copper rich particles, mean measurements were performed in the samples from the Gr-4 and Gr-5. Through EDS analyses two different areas of the samples were investigated: a) in a large mean area including the glassy phase and the nanoparticles; b) in a much smaller area covering only the glassy phase close to the edge of the particles.

The results are reported in [table 7.7](#). In the samples coloured by Cu_2O these compositional differences are more evident varying between 3.4 wt% (Gr-4) and 4.3 wt% (Gr-5). This evidence suggests that it is likely that only a low percentage of copper precipitated as Cu_2O [19].

Table 7.7. Average (crystals + glassy phase) and punctual (glassy phase) EDS analyses performed on the Gr-4 and Gr-5 groups. S.D.: Standard Deviation; five measurements were performed (at least) for the area investigated.

Oxide Group	Average	Glassy phase	Average	Glassy phase
	R12 (Gr-4)		AR4 (Gr-5)	
Al₂O₃	1.5	1.6	1.9	1.7
S.D.	0.06	0.03	0.12	0.07
Na₂O	10.7	10.8	13.0	14.3
S.D.	0.12	0.05	0.34	0.49
K₂O	0.37	0.33	1.2	1.1
S.D.	0.04	0.03	0.07	0.02
P₂O₅	0.06	0.10	0.40	0.32
S.D.	0.05	0.05	0.04	0.02
Fe₂O₃	0.63	0.67	1.5	1.7
S.D.	0.08	0.10	0.10	0.01
MnO	0.17	0.30	0.27	0.35
S.D.	0.10	0.09	0.08	0.07
CuO	9.6	6.2	11.0	6.7
S.D.	0.64	0.19	0.39	0.35
PbO	28.0	29.2	7.8	8.5
S.D.	0.64	0.23	0.39	0.12
SnO₂	0.24	0.14	1.2	1.2
S.D.	0.09	0.09	0.07	0.08

7.5.2.2 μ -Raman spectroscopy

The spectra obtained by focusing a red μ -Raman laser (532 nm) on the dendritic crystals in samples from Gr-4 and Gr-5 groups are very different from those of the previous groups: no fluorescence was found and peaks indicating the probable colouring agent were detected.

The spectra are characterised (both Gr-4 and Gr-5) by an intense peak at 218 cm^{-1} (fig. 7.39a-b), and other weak bands at 416 and 630 cm^{-1} (Gr-4) and at 409 and 624 cm^{-1} (Gr-5). These features are in good agreement with the Raman spectra of cuprite (Cu_2O) present in the literature, belonging to the Pn3m space group [24]. The peaks at 140 and 160 cm^{-1} , and 630 cm^{-1} are due to a lattice mode, while the peaks at 215-218 cm^{-1} and between 400 and 490 cm^{-1} are attributed to multiphonon Raman scattering [25]. The peak at 142 and 145 cm^{-1} could be related to the crystal lattice vibration of Pb-O [24].

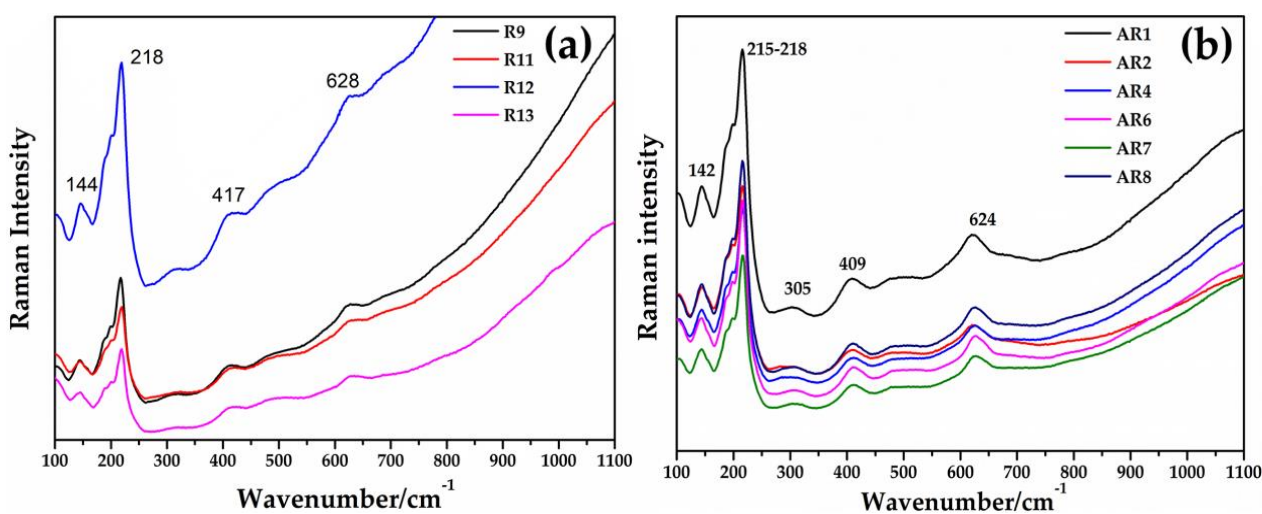


Figure 7.39. Raman spectrum of cuprite (Cu_2O) detected in Gr-4 (a) and Gr-5 (b) groups.

7.5.2.3 X-ray diffraction

XRD analyses in the Gr-4 (Fig. 7.40) groups, show intense peaks at $d=2.46$, $d=2.13$, $d=1.51$, while the Gr-5 samples (fig. 7.41) exhibited weak peaks at $d=3.01$, and $d=1.28$ and $d=1.23$. They were attributed to cuprite crystals. No other crystalline phases were detected in orange samples by mean of XRD analyses.

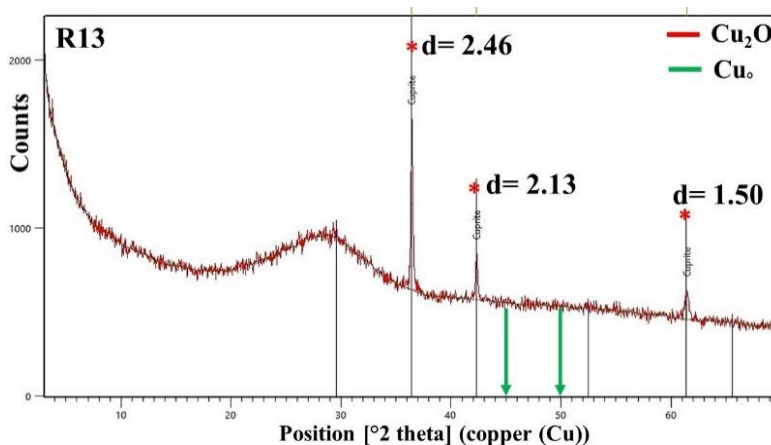


Figure 7.40. X-ray diffraction of the R13 (Gr-4 group), showing the fingerprint of cuprite crystals.

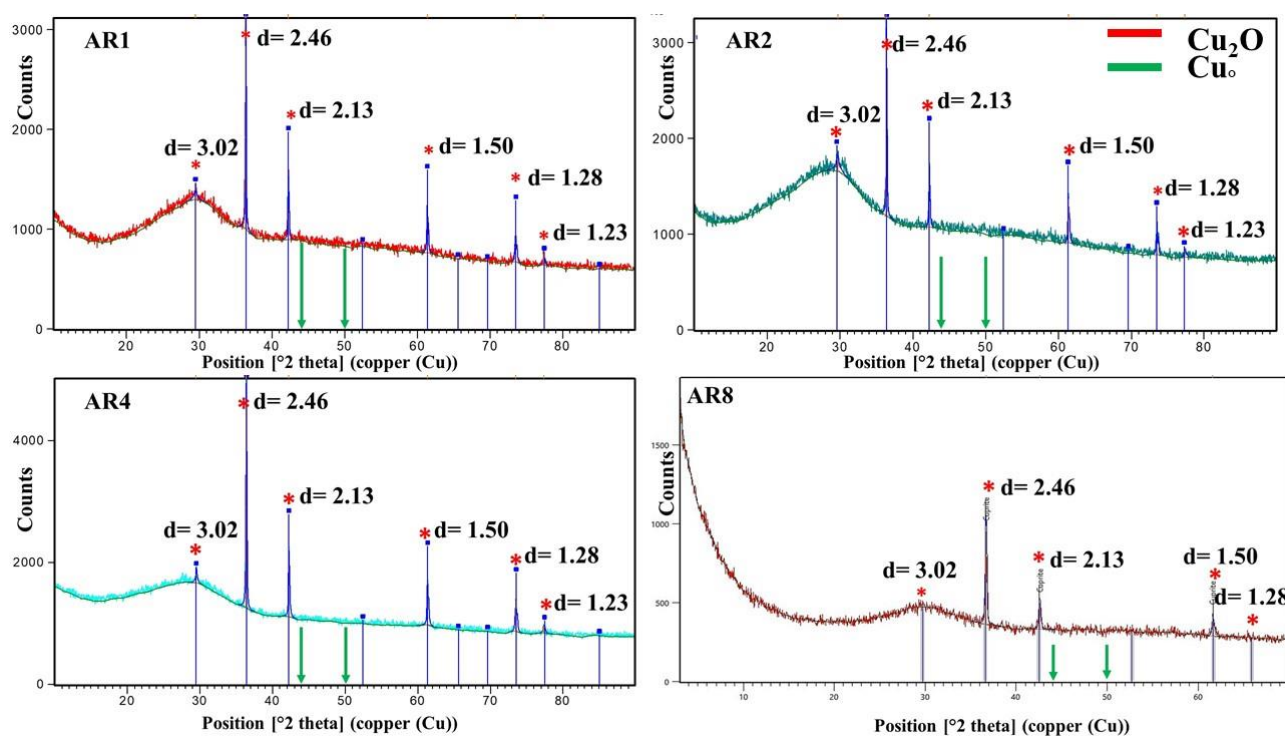


Figure 7.41. X-ray diffraction for the three orange samples of Gr-5 group. The diffractograms show the typical peaks of cubic cuprite crystals. No metallic copper crystals were detected.

7.5.2.5 Other crystalline phases

A few copper-rich particles (comparable with metallic copper) were detected in the Gr-4 group samples, ranging between 500 nm and 1 μm . They were detected in geometrical shapes, such as nodules, in sample R9 (fig. 7.42).

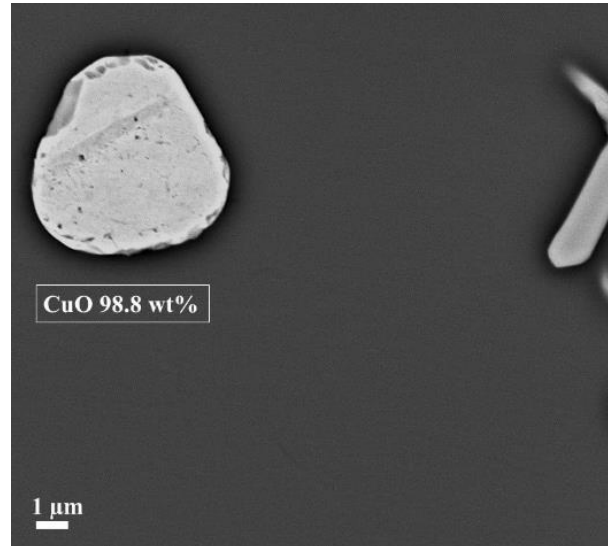


Figure 7.42. FEG-SEM micrographs: metallic inclusion rich in copper revealed in sample R9.

In sample R11, several black inclusions of rounded and irregular shape were observed. As in sample R9, these inclusions are comparable with metallic copper. However, it is interesting to note that branching dendritic crystals (rich in copper and oxygen – probably Cu_2O -) were formed around or from these metallic copper inclusions (fig. 7.43a-b). No devitrification products were revealed in these samples.

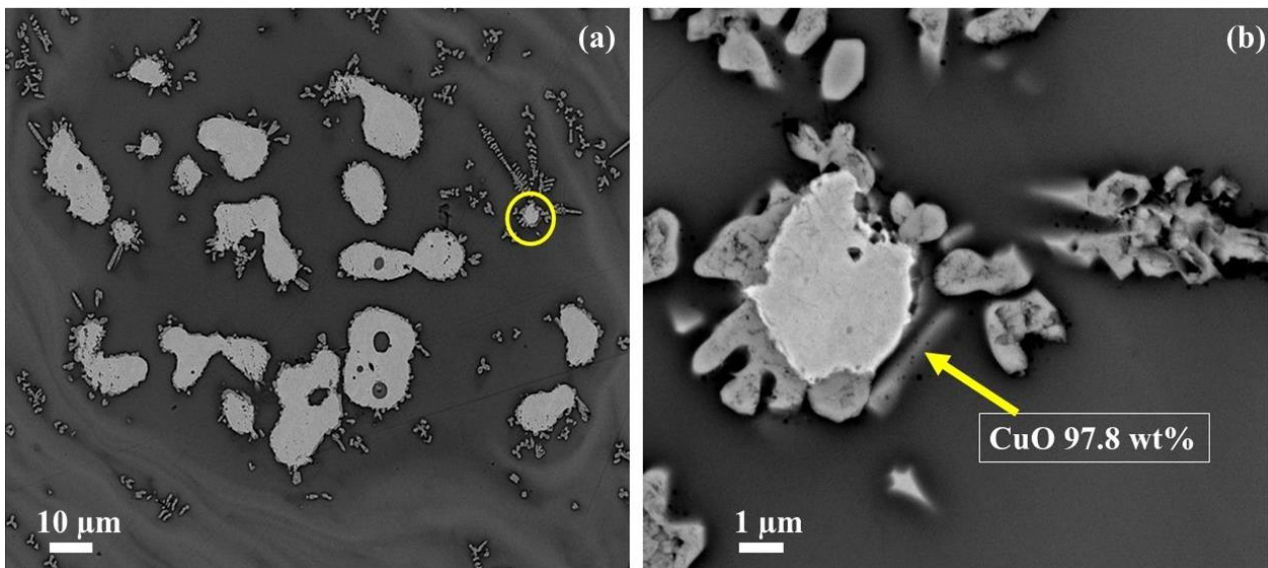


Figure 7.43. FEG-SEM micrographs: a) metallic inclusion rich in copper revealed in sample R11; b) same inclusion observed at higher magnification.

Among the samples from the Gr-5 group, only in the AR2 sample were aggregates of euhedral crystals spread across different zones of the sample detected. They are irregular in shape, and form long aggregation larger than 10 μm (fig. 7.44a-b). High concentrations of antimony (Sb_2O_3 36.3 - 43.2 wt%), tin (SnO_2 7.1 – 26.4 wt%), calcium (CaO 12.6 - 15.3 wt%) and lead (PbO 14.1 – 21.9 wt%) oxides were revealed through EDS analyses. Moreover, they contained moderate concentrations of iron oxide, varying between 0.50 wt% and 5.2 wt%.

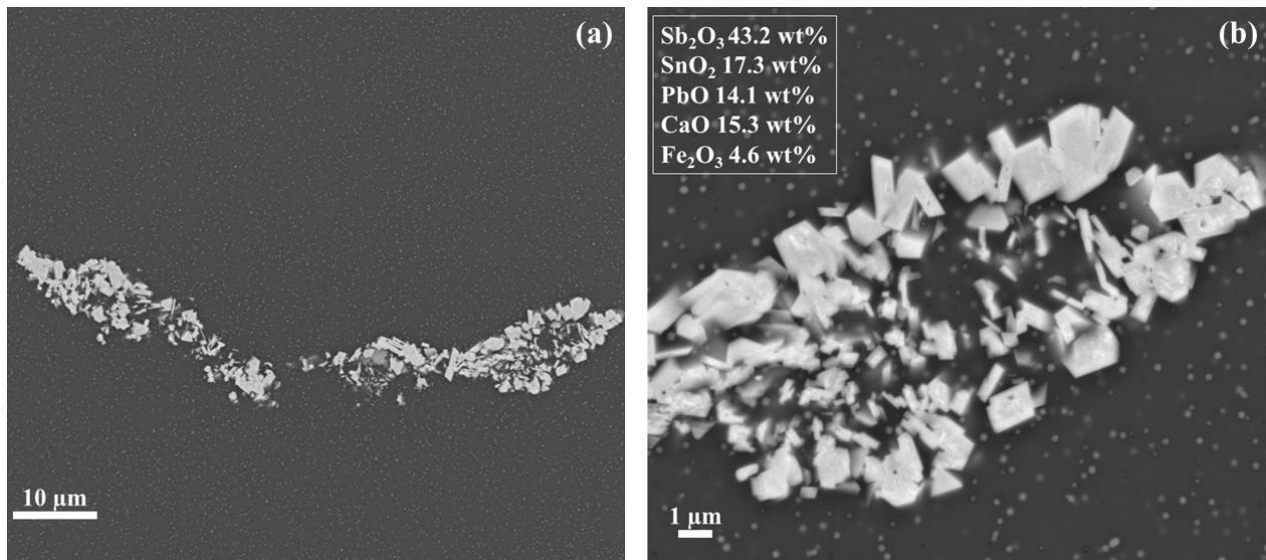


Figure 7.44. FEG-SEM micrographs: a) inclusion rich antimony, tin and calcium; b) same inclusion observed at higher magnification.

Plotting the concentration of calcium against the antimony content (fig. 7.45a) and tin oxide against the antimony content (fig. 7.45b) detected in these crystalline phases, two different tendencies were obtained. Calcium and antimony showed a positive trend. In contrast tin and antimony seemed negatively correlated. No correlations or noteworthy trend were observed between antimony and lead, and between antimony and iron; tin and lead did not correlate either.

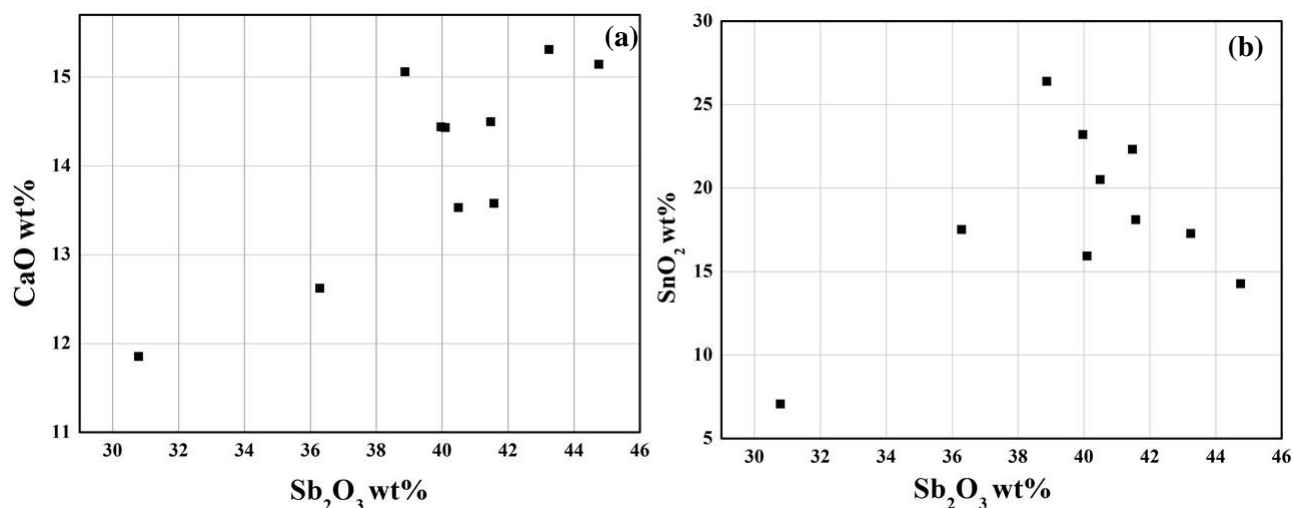


Figure 7.45. Biplot graphs of **a)** the calcium concentration (CaO) against antimony content (Sb₂O₃); **b)** tin oxide (SnO₂) versus antimony content (Sb₂O₃) – EDS analyses.

Using Raman spectroscopy, these crystalline phases were identified as calcium antimony (fig. 7.46). The sharp peaks situated at 478 and 631 cm⁻¹ are the typical fingerprint of orthorhombic calcium antimonate (Ca₂Sb₂O₇) [24, 26]; the weak peaks at 320 and 372 cm⁻¹ are due to the bending mode of the O-Sb-O, while the other weak peaks at 785 and 823 cm⁻¹ are combinations of overtone [24, 26].

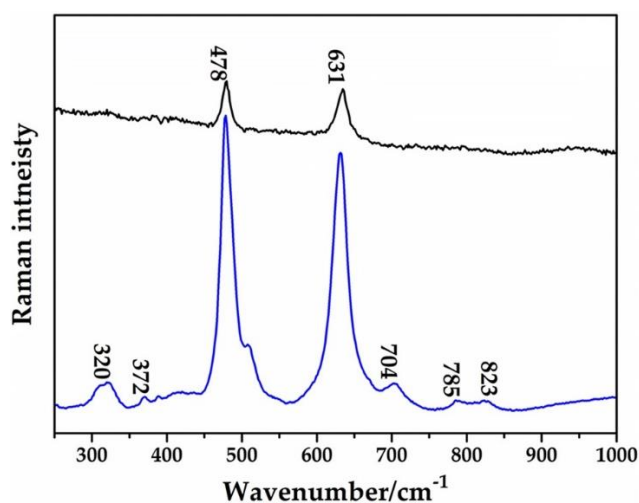


Figure 7.46. Raman spectra of two crystalline phase detected in the sample AR-2 and identified as Ca₂Sb₂O₇ (calcium antimonate).

Table 7.8. Colouring, metallic and devitrification particles investigated by FEG-SEM, Raman spectroscopy and X-ray diffraction. **Cu^o**: metallic copper; **Cu₂O**: cuprite; **W**: wollastonite (CaOSiO₂); **Dt**: Devitrite (Na₂O.3CaO.6SiO₂), **Dp**: diopside (CaO.MgO.2SiO₂). **Pol.**: polyphase (Al-Si-Na-Fe-Ca); **C**: Chalcocite (Cu₂S); **CP**: calcium phosphate; **CA**: calcium antimonate (Ca₂Sb₂O₇); **Mgn**: magnetite (Fe₃O₄); **Hem**: Haematite (Fe₂O₃); **Inc.A**: inclusions composed of Cu-Ag-Sb; **Inc.B**: PbS-Cu₂S; **Inc.C**: inclusions rich in Fe₂O₃, SiO₂, Al₂O₃ and TiO₂.

Group	Sub-group	Base Glass	Colour Hues	FEG-SEM (particles)			Raman (particles)		XRD Colouring	
				Colouring (µm)	Devitrification	Others	Metallic (µm)	colouring		Others
Gr-1		Soda-lime-Silica (PA)	Brick red	Cu ^o 0.04 – 0.7	W; Dt; Dp.	Pol. (R3, R14); CP (R6, R26)	Mgn (R6, R8); C(R26); Inc.A (R16); Inc.B (R8)	-	Inc.C (R26)	Cu ^o
Gr-2		Soda-lime-Silica (NA)	Reddish Brown	Cu ^o > 1	Dt (R10)	Inc. C(R10); Pol. (R17)	C. (R17)	-	-	Cu ^o
Gr-3	Average	Soda-lime-Silica (NA)	Dark red	-	-	-	-	-	-	-
	Gr-3cBK		Black layer	-	W; Dt;	-	C (0.1); Hem	-	-	-
	Gr-3cR		Red layer	Cu ^o (0.02 – 0.1)	W; Dt;	-	C (0.1);	-	-	-
Gr-4		Soda-Lime-high lead (NA)	Sealing wax	Cu ₂ O (dendritic crystals)			Cu ^o (R9, R11)	Cu ₂ O	-	Cu ₂ O
Gr-5	Gr-5dOr	Soda-Lime-high lead (NA)	Yellowish orange	Cu ₂ O (0.1 – 0.3)	W; Dt (AR1)	CA		Cu ₂ O		Cu ₂ O
	Gr-5dR		Reddish orange	AR4: Cu ₂ O (0.3-1)	W; Dt (AR4)			Cu ₂ O	CA	Cu ₂ O

References

1. Picollo, M.; Aceto, M.; Vittorino, T. UV-Vis spectroscopy. *Phys. Sci. Rev.* **2018**, *4*, 1–14.
2. Aceto, M.; Agostino, A.; Fenogli, G.; Idone, A.; Gulmini, M.; Picollo, M.; Ricciardi, P.; Delaney, J.K. Characterisation of colourants on illuminated manuscripts by portable fibre optic UV-visible-NIR. Reflectance spectrophotometry. *Anal. Method* **2014**, *6*, 1488–1500.
3. Bacci, M.; Corallini, A.; Orlando, A.; Picollo, M.; Radicati, B. The ancient stained windows by Nicolò di Pietro Gerini in Florence. A novel diagnostic tool for non-invasive in situ diagnosis. *J. Cult. Herit.* **2007**, *8*, 235–241.
4. Drünert, F.; Blanz, M.; Pollok, K.; Pan, Z.; Wondraczek, L.; Möncke, D. Copper-based opaque red glasses e Understanding the colouring. *Opt. Mater.* **2018**, *76*, 375–381.
5. Nagao, H.; Misonou, M.; Kawahara, H. Mechanism of Coloration in Copper-Stained Float Glass. *J. Non Cryst. Solids* **1990**, *120*, 199–206.
6. Capatina, C. The study of copper ruby glass. *Ceram. Silik.* **2005**, *49*, 283–286.
7. Möncke, D.; Palles, D.; Palamara, E.; Papageorgiou, M.; Kamitsos, E.I.; Zacharias, N. Coloring Vitreous Materials: Pigments. Colloids and Ions in Glasses and Glazes from the Mycenaean to Medieval Periods—probed by Spectroscopic Techniques. In *Proceedings of the Conference: 3rd ARCH_RNT Archaeological Research and New Technologies, Kalamata, Greece, 22–23 October 2010*; pp. 153–164.
8. Bacci, M.; Baldini, F.; Carla, R.; Linari, R. Color Analysis of the Brancacci Chapel Frescoes. *Appl. Spectrosc.* **1991**, *45*, 26–31. 68.
9. Rosi, F.; Grazia, C.; Gabrieli, F.; Romani, A.; Paolantoni, M.; Vivani, R.; Brunetti, B.G.; Colomban, P.; Miliari, C. UV–Vis–NIR and micro-Raman spectroscopies for the non-destructive identification of Cd¹⁺—xZn^xS solid solutions in cadmium yellow pigments. *Microchem. J.* **2016**, *124*, 856–867.
10. Tauc, J.; Grigorovici, R.; Vancu, A. Optical properties and electronic structure of amorphous germanium. *Phys. Status Solid* **1966**, *15*, 627–637.
11. Murphy, A.B. Band-gap determination from diffuse reflectance measurements of semiconductor films. and application to photoelectrochemical water-splitting. *Sol. Energy Mater. Sol. Cells* **2007**, *91*, 1326–1337.
12. Theja, G.S.; Lawrence, R.C.; Ravi, V.; Nagarajan, S.; Anthony, S.P. Synthesis of Cu₂O micro/nanocrystals with tunable morphologies using coordinating ligands as structure controlling agents and antimicrobial studies. *CrystEngComm* **2014**, *16*, 9866–9872.
13. Banerjee, S.; Chakravorty, D. Optical absorption by nanoparticles of Cu₂O. *Europhys. Lett.* **2000**, *52*, 468–473.
14. Vratny, F.; Kokalas, J.J. The Reflectance Spectra of Metallic Oxides in the 300 to 1000 Millimicron Region. *Appl. Spectrosc.* **1962**, *16*, 176–184.
15. Silvestri, A.; Tonietto, S.; Molin, G.; Guerriero, P. The palaeo-Christian glass mosaic of St. Prosdocimus (Padova, Italy): Archaeometric characterisation of tesserae with copper- or tin-based opacifiers. *J. Archaeol. Sci.* **2014**, *42*, 51–67.
16. Brill, R.H. Chemical Analyses of Early Glasses; Volume 2 Tables of Analyses; The Corning Museum of Glass: Corning, NY, USA, 1999; ISBN 0-872900-143-2.
17. Lilyquist, C.; Brill, R.H. Analytical procedure. In *Studies in Early Egyptian Glass*; Metropolitan Museum of Art: New York, NY, USA, 1993, pp. 47–58; ISBN 978-0300200195.

18. Silvestri, A.; Molin, G.; Salviulo, G. The colourless glass of Iulia Felix. *J. Archaeol. Sci.* **2008**, *35*, 331-341.
19. Moretti, C.; Gratuze, B. Vetri rossi al rame e avventurina. Confronto di analisi e ricette. *Riv. Stn. Sper. Vetro* **1999**, *3*, 147–160.
20. Colomban, P.; Schreiber, H.D. Raman signature modification induced by copper nanoparticles in silicate glass. *J. Raman Spectrosc.* **2005**, *36*, 884–890.
21. Colomban, P.; Tourniè, A.; Ricciardi, P. Raman spectroscopy of copper nanoparticle-containing glass matrices: Ancient red stained-glass windows. *J. Raman Spectrosc.* **2009**, *40*, 1949–1955.
22. Cesaratto, A.; Sichel, P.; Bersani, D.; Lottici, P.P.; Montenero, A.; Salvioli-Mariani, E.; Catarsi, M. Characterization of archeological glasses by micro-Raman spectroscopy. *J. Raman Spectrosc.* **2010**, *41*, 1682–1687.
23. Navarro J.M.F. Desvitrificaciones. *El vidrio: constitución, fabricación, propiedades*, 3rd ed.; Consejo Superior de Investigaciones Científicas, Instituto de Cerámica y Vidrio, Madrid, 2003, pp. 264-272.
24. Basso, E.; Invernizzi, C.; Malagodi, M.; La Russa, M.F.; Bersani, D.; Lottici, P.P. Characterization of colorants and opacifiers in roman glass mosaic tesserae through spectroscopic and spectrometric techniques. *J. Raman Spectrosc.* **2014**, *45*, 238–245.
25. Meyer, B.K.; Polity, A.; Reppin, D.; Becker, M.; Hering, P.; Kramm, B.; Klar, P.J.; Sander, T.; Reindl, C.; Heiliger, C.; et al. The physics of copper oxide (Cu₂O). *Semicond. Semimet.* **2013**, *88*, 201–226.
26. Gedzevičiute V.; Welter, N.; Schüssler, U.; Weiss, C. Chemical composition and colouring agents of Roman mosaic and millefiori glass, studied by electron microprobe analysis and Raman micro spectroscopy. *Archaeol. Anthropol. Sci.* **2009**, *1*, 15–29.

8. Discussion

8.1 Presence of two colouring techniques: Cu° and Cu_2O

Through the FEG-SEM, μ Raman spectroscopy and XRD analyses, two main colouring agents were revealed which are considered the main colouring and opacifying agents: metallic copper (Cu°) and cuprite crystals (Cu_2O). Based on the colouring agents, the copper-red glass *sectilia* studied in the Gorga collection can be divided into two main categories, which represent two distinct glassmaking technologies.

The samples from the Gr-1, Gr-2 and Gr-3 group are coloured by metallic copper particles which represent one technology, while the samples from the Gr-4 and Gr-5 groups are coloured by cuprite crystals representing another technology. They are characterised by dissimilar chemical compositions, as well as the concentration of copper and lead oxide, or the presence of iron, tin and antimony oxides.

The way they were manufactured (melting condition, heat-treatments) would have been distinct in the two technologies, and in some case each hue required a specific method. The features of each technology will be shown individually later in the text; however, it is possible to highlight two aspects that are common in both categories.

a) The red and orange hues are affected by the number and the size of the colouring particles (fig. 8.1). In the Cu° technology a high number of Cu° particles ranging between 50 nm and 500 nm coloured the brick red glass (Gr-1 group), while larger Cu° particles ($> 1 \mu\text{m}$, and reaching in some case $50 \mu\text{m}$ in sizes) produced the reddish brown glass (Gr-2 group). The red banded samples (Gr-3 group), showed Cu° particles only in the red layers, varying between 50 nm and 100 nm.

Similar phenomenon occurred in the category of the cuprite crystals (Gr-4 and Gr-5). With the presence of a high number of cuprite particles, ranging between 200 nm and 800 nm, an orange glass (Gr-5) is produced. They could have been cubic, hexagonal or in some case also octagonal in shape. The number and the size of the particles is the cause of the different orange hues. Indeed, in the yellowish orange, the concentration of cuprite crystals is higher than the reddish orange, and they showed cuprite crystals smaller ($< 300 \text{ nm}$) than reddish orange (300 – 800 nm). In contrast, when cuprite crystals develop into dendritic shapes, measuring tens of μm in magnitude, an intense red glass is obtained which corresponds with sealing wax red glass.

It is possible to conclude that in the Cu° technology, the higher the number of the particles the smaller their size, and the colour is red. In contrast, by increasing the dimensions of the colouring particles their concentration goes down, and the glass moves towards a more brownish tone.

In the Cu_2O technology, the colour of the glass changes from yellowish to orange by increasing the crystal sizes and diminishing their number, up to the red glass when the crystals' dimensions are larger than tens of μm and the particles are dendritic in shape.

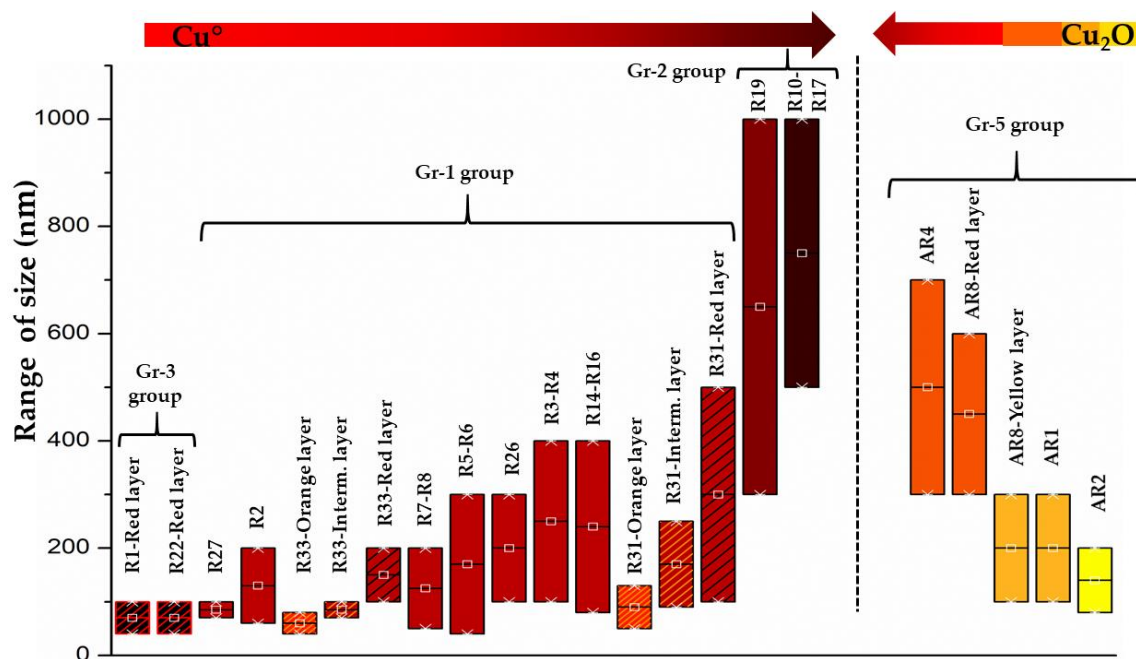


Figure 8.1. The colour changes with the increase in the size of the colouring agent (Cu° on the right; Cu_2O on the left). The samples of Gr-4 group were not reported, because it was difficult to correctly establish the dimensions of the dendritic crystals.

b) Small differences in copper concentration were detected, in both technologies, between the bulk chemical composition (glassy phase + crystals) and the glassy phase (among the copper rich particles).

Indeed, the regular EDS analyses on (only) the glassy phase revealed that a small percentage of copper precipitated to form Cu° or Cu_2O , while the majority remained in the form of Cu^+ or Cu^{2+} ions. Moreover, in the Gr-4 and Gr-5 groups the amount of Cu^+ which precipitated contributing to the formation of cuprite crystals is higher than that of Cu° . This highlights the strong colouring power of metallic copper.

This was also observed in the literature, when analysing reproduction of ruby glass or lustre glaze. By EXAFS measurements only a very small portion (20 wt%) of the entire copper content present in the bulk composition precipitated in the form of metallic copper [1-3]. However, this means that the mild reducing conditions mentioned by Brown [4] and Wakamatsu [5] were reached and allowed enough colouring particles to precipitate; otherwise too much reducing condition would lead to an increase in the precipitated metallic copper, which would produce a grey or black colour.

8.1.1 Base glass, raw materials

8.1.1.1 Fluxing agent

Two main types of base glass were identified by chemical analyses: soda-lime-silica glass (Gr-1, Gr-2 and Gr-3 groups) and soda-lime-high lead silica (Gr-4 and Gr-5). Although in the Gr-2 and Gr-3 groups, natron was used as the fluxing agent to melt the glass, showing low K_2O , MgO ($< 1wt\%$) and P_2O_5 ($< 0.3wt\%$) typical of Roman natron composition, in the samples from the Gr-1 group the values of magnesia and potash are higher than 2 wt%, and P_2O_5 is higher than 1wt%.

In the literature, Roman glass with these concentrations of magnesia, potash and phosphorus have been usually treated with suspicion, and to explain these anomalies two main branches were formed in the literature supporting two theses, sometimes in contrast each other:

a) Some of the writers interpreted the content of K_2O and MgO being higher than 1.5 wt% (the maximum limit for natron base glass) as the result of adding fuel ash to the molten natron glass in order to reach the reducing conditions necessary to facilitate the precipitation of metallic copper (Cu^0). Due to the presence of carbon or charcoal (strong reductant [6]) in the fuel ash, its addition could bring some technical advantage in manipulating the internal redox conditions. Furthermore, the values of K_2O and MgO are often slightly higher than 1.5 wt%, while the unambiguous values for the use of soda plant ash glass have to be higher than 2 or 2.5 wt% [7]. Moreover, the concentration of P_2O_5 is higher than the common values detected in the typical soda-plant ash of the medieval period. This theory has been supported by Freestone [8] analysing opaque red canes present in mosaic glass fragments from the 1st century BC/AD, Fiori [9], Maltoni [10], Paynter [11], and Fiorentino [12] studying mosaic tesserae in Ravenna, Aquileia, Padova, Trento, and West Clacton from the 2nd century AD to 5th/6th century AD.

According to Schibille, the high values of K_2O , MgO and P_2O_5 are due to the intensive recycling of the glass (cullet glass, waste glass) [13, 14]. The prolonged melting period used in the secondary furnace to manufacture opaque red glass could favour pollution by contaminants from the fuel ash [13]. This hypothesis is supported by Paynter [15], who highlighted that the glass during the melting process (in a secondary furnace, thought to be smaller than the primary furnace) was contaminated by the vapour or gases released from the wood fuel which are mainly rich in calcium and potash. The experiments showed that the concentration of K_2O in the glass increased after 54 hours of melting. However, the P_2O_5 content was not revealed by the analyses, while the MgO concentration seemed not to be affected by the prolonged melting period.

In continental Europe during the medieval period, trees such as beech, bracken and oak were the main fuel for glass furnaces [16, 17]. During the Roman period, it is difficult to identify which type of tree was used. Barford recently proposed the use of nuts from olive oil, produced during the extraction of olive oil. Indeed, several of these residues were uncovered close to the glass furnace evidence [18]. These compounds are rich in potash, calcium, manganese, phosphorus, and poorer in sodium, and showed concentrations similar to those detected in the wood ash used in continental and Northern Europe since the medieval period. In this case, the chemical composition of these ashes is also extremely variable and affected by the nature of the soil, the season in which

the trees are harvested, the type of tree, and how they were burnt (temperature, oxidation state of the furnace atmosphere, timing) [16, 17].

These hypotheses support the idea that coloured glass production took place “locally” in secondary workshops spread in the Empire, in which raw glass was re-melted (or recycled) and colourant or opacifier agents were added.

b) other writers advanced an alternative theory which supports the manufacture of specific colour by using soda plant ash as a fluxing agent. Emerald green, black, opaque red and orange glass are the main colours in which these anomalous values have been observed. All these colours require a careful manipulation of the redox conditions and are coloured by copper. Jackson [19] analysed emerald green glass in depth and suggested that they were manufactured by soda plant ash fluxing agents, probably because they were technically beneficial. High K_2O , MgO and P_2O_5 in emerald green glasses were detected in Adria, Pompei and Bastanis, showing almost the same compositional characteristics [20-22].

Nenna and Gratuze analysed several *millefiori* glass samples from the 3rd century BC to 3rd century AD, which were sampled in several parts of the Roman Empire and Mediterranean basin, and they detected a considerable amount of opaque red glass with values of MgO and K_2O ranging between 1.6 wt% to 3 wt% and P_2O_5 0.72-2.50 wt% [23]. Nenna suggested that they are soda-plant ash base glasses and due to the high glassmaking knowledge and skills required by this colour, opaque red glass was produced in specialised workshops.

Verità, studying mosaic *tesserae* and glass *opus sectile* dating from 3rd-4th century AD in Rome, found the coexistence of opaque red glass *tesserae* with high MgO and K_2O (both > 2wt%, P_2O_5 0.60-1.2 wt%) and other *tesserae* with the typical Roman natron glass (MgO and K_2O < 1.5 wt%, P_2O_5 0.10-0.20 wt%) [24, 25]. He suggested that the high MgO and K_2O contents were due to the use of soda plant ash, which by containing carbonaceous residues would help to reduce the partial pressure of the oxygen inside the melt, necessary to obtain the metallic copper nanoparticles. Indeed, Verità noted that in the “anomalous” red brown *tesserae*, the concentration of iron (the main reducing agent in red brown) is usually lower than those detected in the typical natron opaque red glass.

These hypotheses imply that specific coloured glass was probably produced by using a different raw glass. The coloured glass (in this case opaque red) would be produced in the form of canes/rods, cakes or ingots and traded [19, 24, 25].

Cagno detected concentrations of MgO and K_2O higher than 1.5 wt% in black glass from the 2nd century AD. He proposed that the glass with these anomalous values was probably manufactured in specific workshops located on the edge of the Roman Empire, which were affected by the glassmaking tradition of the neighbouring empires (such as the Sassanian Kingdom) that used to melt the glass by adding soda-plant ash [26].

The debate between these contrasting hypotheses it is still unresolved, and it underlines that the understanding of coloured glass production in the Roman Age (especially between 1st-4th century AD) is still far from being completely understood.

Through a comparison between the Gr-1 group samples and common soda plant ash (Islamic glass), it is possible to observe that the magnesia and potash content of the Gr-1 group samples match very well with the common soda-plant ash glass (fig. 8.2). Moreover, the concentration of Na_2O is very close to that revealed in the soda-plant ash glass of the 3rd century to 12th century AD.

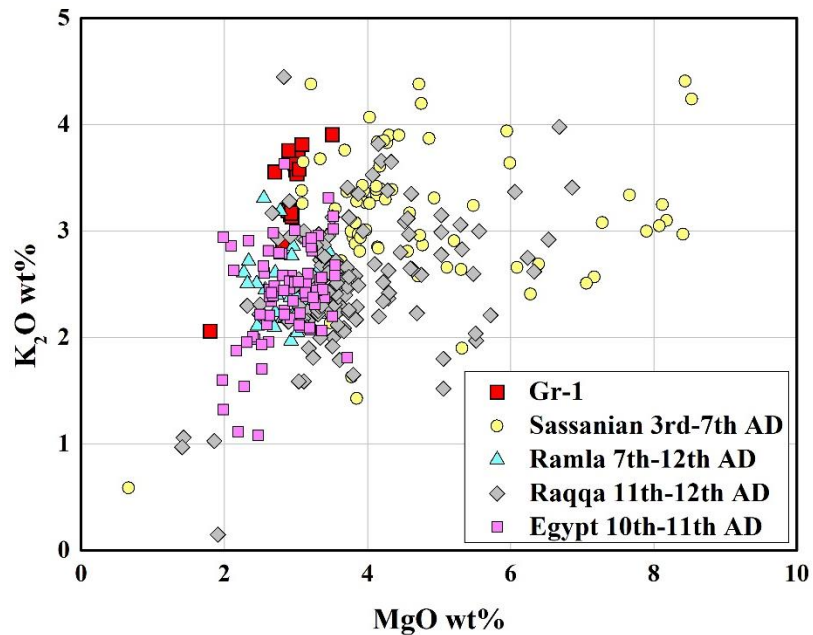


Figure 8.2. Binary graph showing the concentration of potash (K_2O wt%) against magnesia (MgO wt%) content (reduced composition). The samples from the literature were taken from [27-32].

Nevertheless, the P_2O_5 content, ranging about the 1 wt%, is much higher than the common values found in soda-plant ash (Fig. 8.3).

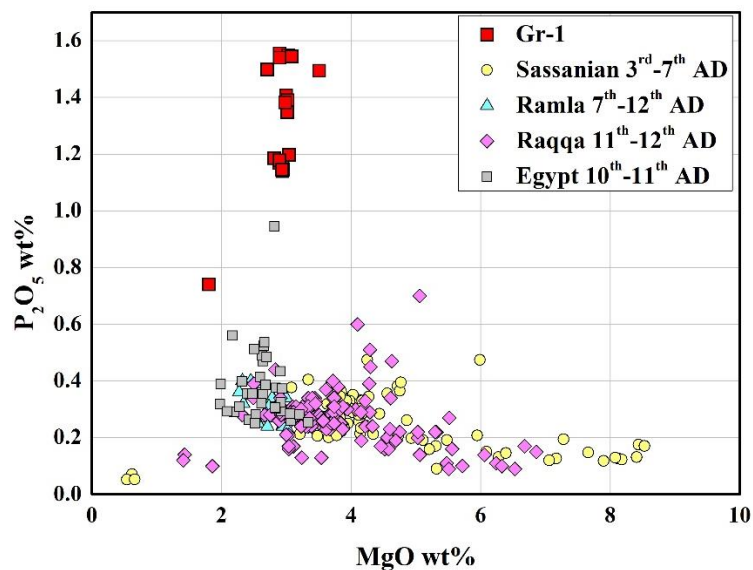
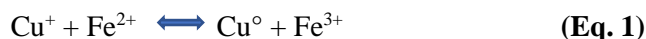


Figure 8.3. Binary graph showing the concentration of phosphorus (P_2O_5 wt%) against magnesia (MgO wt%) content (reduced composition). The samples from the literature were taken from [27-32].

This P₂O₅ content could be due to several factors: a) the high variable composition of the plant ash, which depends on the nature of the substrate and how specific elements are synthesised in their tissue [33]; b) how the ashes were prepared or burned; c) the possibility that ashes of different plants were mixed together and used as a fluxing agent (this is not to be ruled out), altering the composition of the typical soda-plant ash; d) the addition of fuel ash to a soda plant ash base glass; e) a contamination from the fuel ash or vapour present in the furnace.

However, the important question is “*why different recipes should be employed, instead of the natron glass recipe?*” (detailed study in appendix A). They have been frequently found in Roman (1st-4th century AD) opaque red glass, as has emerged in several studies of Roman and Late antique opaque red [8, 22-25, 34-36]. This recipe could have been engineered to solve the most crucial aspect of opaque red glass production, the correct oxidation state in the melt. The addition of an internal reductant is fundamental to reducing copper to its elemental state (Cu⁰). It is well known that iron interacts with copper according to the redox equation (Eq.1).



The proportion of Cu⁺/Cu⁰ and Fe²⁺/Fe³⁺ depends on several factors during cooling and the equilibrium (Eq.1) is displaced toward the right, inducing the formation of Cu⁰ and Fe³⁺ [37, 38].

In the samples from Gr-1 group, the iron content is slightly higher than 1 wt %, which seems to indicate a minimal addition of iron, probably not enough to promote the precipitation of Cu⁰ particles. Moreover, a positive tendency between iron and titanium (TiO₂), suggests that the iron could come from the silica source, or minimal amounts were necessary to be added. In contrast, a deliberate addition of iron is evident in samples R29 and R31 in which the iron content is about 3 wt%.

The hypothesis could be advanced that in these red glass *sectilia*, the use of partially burned soda ashes, containing carbonaceous compounds would create the correct reducing conditions which would lead to the formation of Cu⁰ nanoparticles [24-39].

It is still difficult to establish if soda plant ash was used or not as a fluxing agent. It may be that fuel ashes were added to a soda-plant ash glass. This hypothesis could explain the P₂O₅ and Sr content being higher than the typical soda-plant ash (see appendix B).

However, this evidence could prove the existence of an alternative recipe involving a different preparation of the batch, or different raw materials to achieve the necessary reducing condition to facilitate the precipitation of the Cu⁰ particles.

Natron was used as a fluxing agent in the high lead Gr-4 and Gr-5 groups, as it is possible to deduce from the magnesia and potash content lower than 1.5 wt%, except for AR-4, AR-6 and AR-7 samples (Gr-5 group). They showed a concentration of magnesia varying between 1.5 wt% and 2 wt%, together with an increased amount of P₂O₅ (0.50 – 0.83 wt%) and strontium (Sr 516-636 ppm).

8.1.1.2 Silica source

The elements related to the silica source (Al, Zr, Ti, Hf) exhibited evident compositional differences which could indicate the supply of a different silica source. This point could be considered crucial since a distinct silica source could be indicative of a distinct location where the glass was manufactured.

A purer silica source was used for the Gr-1 group samples which showed the lowest values of alumina (Al_2O_3 1.9-2.0 wt%, except R3 sample with 2.9 wt%) if compared with the other groups. On the other hand, the concentration of TiO_2 detected in the Gr-1 group is comparable with the Gr-2, Gr-3 and Gr-4 group samples. The concentrations of alumina and titanium detected in the Gr-5 group samples are higher than the other groups.

Fig. 8.4. plots the concentration of TiO_2 vs Zr detected in the *Lucius Verus* samples and those revealed in several naturally transparent coloured glass samples dating from the 1st to the 4th century AD. It should be noted that Gr-2 and Gr-3 match well with the samples from the literature showing a positive tendency. In contrast, although the samples from Gr-1, Gr-4 and Gr-5 exhibited a positive tendency too, their trend is different from that showed by the samples from the literature and from the Gr-2 and Gr-3 groups.

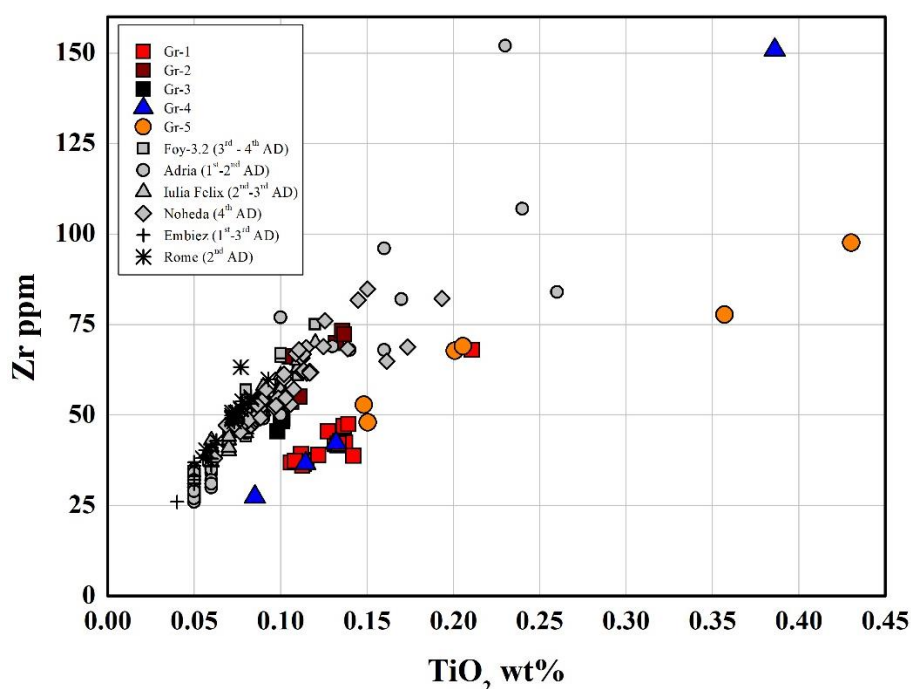


Figure 8.4. Biplot of the concentration of zirconium concentration (Zr ppm) and titanium content (TiO_2 wt%) of the typical Roman natron glass dating from the 1st c. AD to 4th c. AD and the *Lucius Verus* copper-red glass (reduced composition). Roman natron glass taken from [20, 36, 40-43].

The samples from the Gr-2 and Gr-3 generally fit well with the natural-coloured glass from Noheda, Adria and Iulia Felix. In contrast, the samples from the Gr-1 and Gr-4 and Gr-5 groups showed several compositional differences, which are not comparable with the colourless or naturally coloured samples found in the literature. Although the precise location where the samples from Noheda, Adria, Rome and Iulia Felix were manufactured has not been established, the Levantine Coast (probably the Syro-Palestinian coast) is considered a very likely

production centre. Hence, it is possible to advance the hypothesis that the samples from the Gr-2 and Gr-3 groups were produced by re-melting/recycling the same raw glass used to manufacture these colourless or naturally coloured glass.

The different trends exhibited by the Gr-1 and Gr-4 groups could indicate a different provenance, maybe Egypt, or as some writers have suggested, Western Europe (such as Gaul, Spain or Italy), but there are not enough archaeological or archaeometric data to establish this.

8.1.2 Colouring, reducing agent and other compounds

8.1.2.1 Cu⁰ group

Iron is considered the main reducing agent for copper-red glass, but it is still unknown which iron-bearing material was used. In the Gr-2 and Gr-3 groups, iron was abundantly used; however, no metallic inclusions are revealed, except some inclusions comparable with the chemical composition of magnetite and haematite (detected by FEG-SEM analyses). The use of magnetite minerals is unlikely because it presents both the oxidation states of iron which make it a weak reducing agent. Haematite can also be ruled out due to its oxidising action. The use of hammer-scales from the hammering of incandescent iron could be an hypothesis. It was already observed in the previous studies on Roman black glass from the 2nd century AD that metallic iron compounds were used as a colouring agent. This metallurgical by-product could contain wüstite (FeO), magnetite and metallic iron, supplying enough reducing agents [44-46]. Additionally, this is commonly indicated in the Venetian manuscripts for making red brown glass.

Due to the low amount of iron detected in the samples from Gr-1, it is unclear if some iron-bearing was deliberately added as a reducing agent, or maybe, small amounts of iron were enough to cause the precipitation of the Cu⁰ particles.

Copper compounds

The copper-bearing material used in the production of opaque red glass is usually considered to be pure copper or some copper-alloy roasted in air and powdered [47]. Some complex metal slags from the silver-refining process containing lead, copper, silica, tin and zinc and other trace elements are also suggested [48, 49].

In the Gr-1 samples, compositional differences related to the amount of tin, lead and zinc were revealed between the thin *sectilia* (Gr-1a) and the *sectilia* composed of canes (Gr-1b), indicating two different copper-bearing materials. Normalising the chemical composition of the samples for copper, tin and zinc in the three groups of the Cu⁰ technology, it is possible to get some indication of the copper-bearing used as a raw material [table 8.1](#).

Table 8.1. Average composition (wt%) of a hypothetical copper-alloy used in the three red hues produced by Cu^o particles.

Group	CuO		SnO ₂		ZnO	
	Av.	S.D.	Av.	S.D.	Av.	S.D.
Gr-1a	69.0	1.6	29.2	0.86	1.8	1.0
Gr-1b	88.5	1.1	10.0	1.4	1.5	0.44
Gr-2	92.0	0.25	7.2	0.25	0.77	0.02
Gr-3	90.1	0.82	8.3	0.51	1.6	0.35

The concentration of Zn reported in [table 8.1](#) is lower than 5 wt% in each group, suggesting the use of a bronze material similar to that reported in the literature and dated to the same period [50]. In [fig. 8.5a](#), tin and copper exhibit a positive tendency in the Gr-1a group, indicating a probable common provenance, while the other groups do not show any relationship.

It is likely that zinc entered through the copper-bearing material. In [fig. 8.5b](#) the three groups exhibit a positive tendency between Zn and CuO, which could indicate the same provenance such as brass or bronze.

Lead, as well as tin, is present in concentrations higher than 1000 ppm; however, in this case it is also less probable that it entered through a deliberate addition. In contrast, lead could represent a contaminant from the copper-bearing material. In [fig. 8.5c](#), most of the thin *sectilia* exhibits a positive tendency between lead and copper, which could indicate that lead and copper entered through the same raw material.

Moreover, plotting the amounts of lead against tin content, a positive tendency links the samples from the Gr-1a subgroup, suggesting a common raw material provenance. By contrast, zinc and lead did not show any tendency or grouping.

On the other hand, no evidence of a tendency was found in the other samples from the Gr-1b, Gr-2 and Gr-3 groups.

These data seem to indicate that a bronze scale was probably used in the samples from the Gr-1b, Gr-2 and Gr-3 groups. Indeed, in the compositions reported in [table 8.1](#), the copper content is above 70 wt% while tin is lower than 10 wt% and zinc lower than 5 wt%.

The same elements are present in different concentrations in the samples from the Gr-1a subgroup, which could be due to the use of a complex metallurgical by-product containing lead, tin, copper and zinc or maybe a leaded-bronze scale.

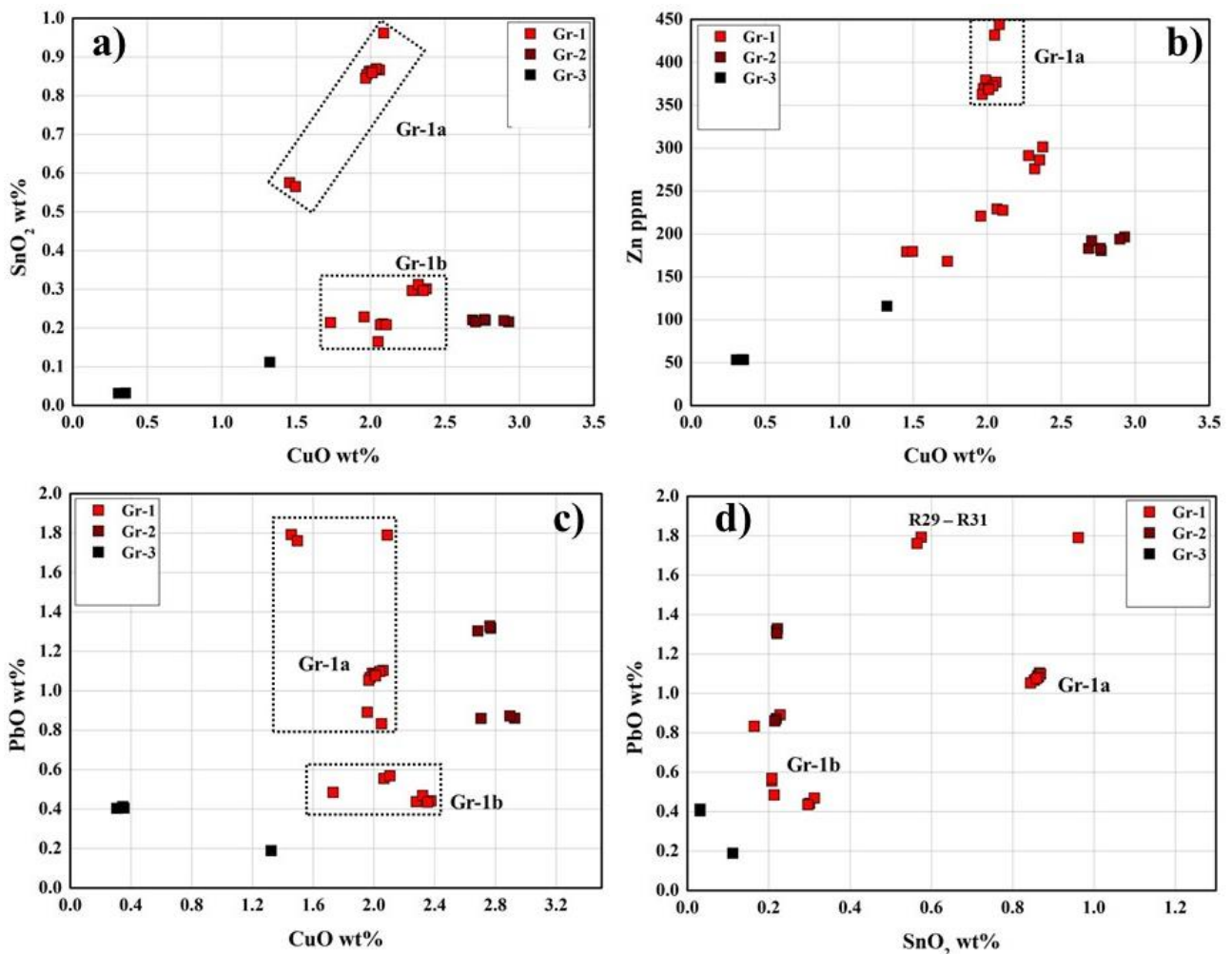


Figure 8.5. Biplot graphs: **a)** Tin content (SnO_2) against copper concentration (CuO); **b)** zinc content (ZnO) against copper concentration (CuO); **c)** lead content (PbO) against copper concentration (CuO); **d)** lead content (PbO) against tin concentration (SnO_2).

As mentioned by Brill [47], the use of one raw material rather than another one is not always related to a specific technological advantage. On the contrary, it is possible that it represents an available raw material in a specific region.

Several writers have mentioned that the composition of copper-alloys could vary depending on the purpose for which it was used, and different regions produced copper-alloys by different compositions and techniques [51, 52]. The inclusion detected in samples R16, composed of silver-copper-antimony, could indicate the use of litharge or slags obtained from a silver-refining process, such as a copper-bearing, as reported by Freestone [49].

Use of the decolourants or recycling of glass

It is established that concentrations of MnO higher than 0.025 wt% and Sb_2O_3 higher than 0.03 wt% point to a deliberate addition of some Mn- or Sb-bearing as decolouriser [53]. In the samples of the Gr-1, Gr-2 and Gr-3 groups MnO varies between 0.30 and 0.68 wt%, while Sb_2O_3 ranges between 0.11-0.66 wt%. These values suggests that MnO and Sb_2O_3 were deliberately added during the lifecycle of the glass. It could imply

the use of recycled glass such as Mn-Sb colourless glass. This practise was common in the Roman Age (1st-3rd century AD) as suggested by some authors [53]. Nevertheless, in this case, it is complex to explain exactly the presence of MnO and Sb₂O₃ concentrations. Indeed, antimony could be a contaminant of the copper-bearing. However, the amount of MnO are still unsolved. In the samples of the Gr-2 and Gr-3 the use of recycled glass is not to rule out, while in the Gr-1 group samples more studies are required.

8.1.2.2 Cuprite (Cu₂O) group

Copper and lead

Contrary to the Cu⁰ colouring technique, the production of cuprite crystals (sealing wax red -Gr-4- and orange -Gr-5- groups) required high concentrations of copper and lead oxide. Strong reducing conditions would have been avoided to prevent the precipitation of Cu⁰ particles and metallic lead (Pb⁰). Since Cu⁺ is more soluble than Cu⁰, high percentages of copper (Cu⁺) would have been used for the formation of cuprite crystals. Lead oxide plays a key role in this technology because: a) it decreases the working temperature, reducing the viscosity and giving enough time for the copper ions to aggregate in dendritic form and grow; b) it shifts the Cu²⁺/Cu⁺ towards Cu₂O [37, 38, 49].

Although modern laboratory reproduction obtained opaque red and orange glass only by managing the heat treatment [54], it cannot be excluded that Roman glassmakers would also have controlled the colour by manipulating the chemical composition of the glass.

The concentration of lead oxide is different in the two groups, which could be related to controlling the number and the size of the particles. It was observed that the higher the concentration of lead, the larger the sizes of the cuprite crystals. In contrast, a cut in the lead content could help to increase the number of Cu₂O particles which were smaller in size [38]. Therefore, the lead content could explain why there were higher concentrations in the sealing wax red (PbO 28-30.4 wt%) than in the orange samples (PbO 8-22.4 wt%).

The lead-bearing compounds used in the Cu₂O technology are not completely understood, however, it is less probable that it was added by the same material which introduced copper. Indeed, the high amount of lead suggests a deliberate addition of some lead material, maybe litharge as suggested in the literature [49, 55].

The identification of the probable copper-bearing raw materials used to manufacture sealing wax red and orange glass is still unclear. Table 8.2 shows the average normalised concentrations for Cu, Sn and Zn from these samples.

Table 8.2. Average composition (wt%) of the hypothetical copper-alloy used in the sealing wax (Gr-4) and orange (Gr-5) glass. They were obtained by normalising the chemical composition for copper, tin and zinc.

Group	CuO		SnO ₂		ZnO	
	Av.	S.D.	Av.	S.D.	Av.	S.D.
Gr-4	97.6	0.4	2.3	0.4	0.05	0.02
Gr-5	89.8	3.6	8.3	2.4	1.9	1.3

From the normalised composition, it could be possible that bronze scales of two different compositions were used. The compositional differences are complex to explain.

The low number of samples does not make it possible to note any specific tendency between these elements (fig. 8.6.). However, it emerged that a rich Zn copper-bearing was used in the orange samples, but not in all (AR-2 sample).

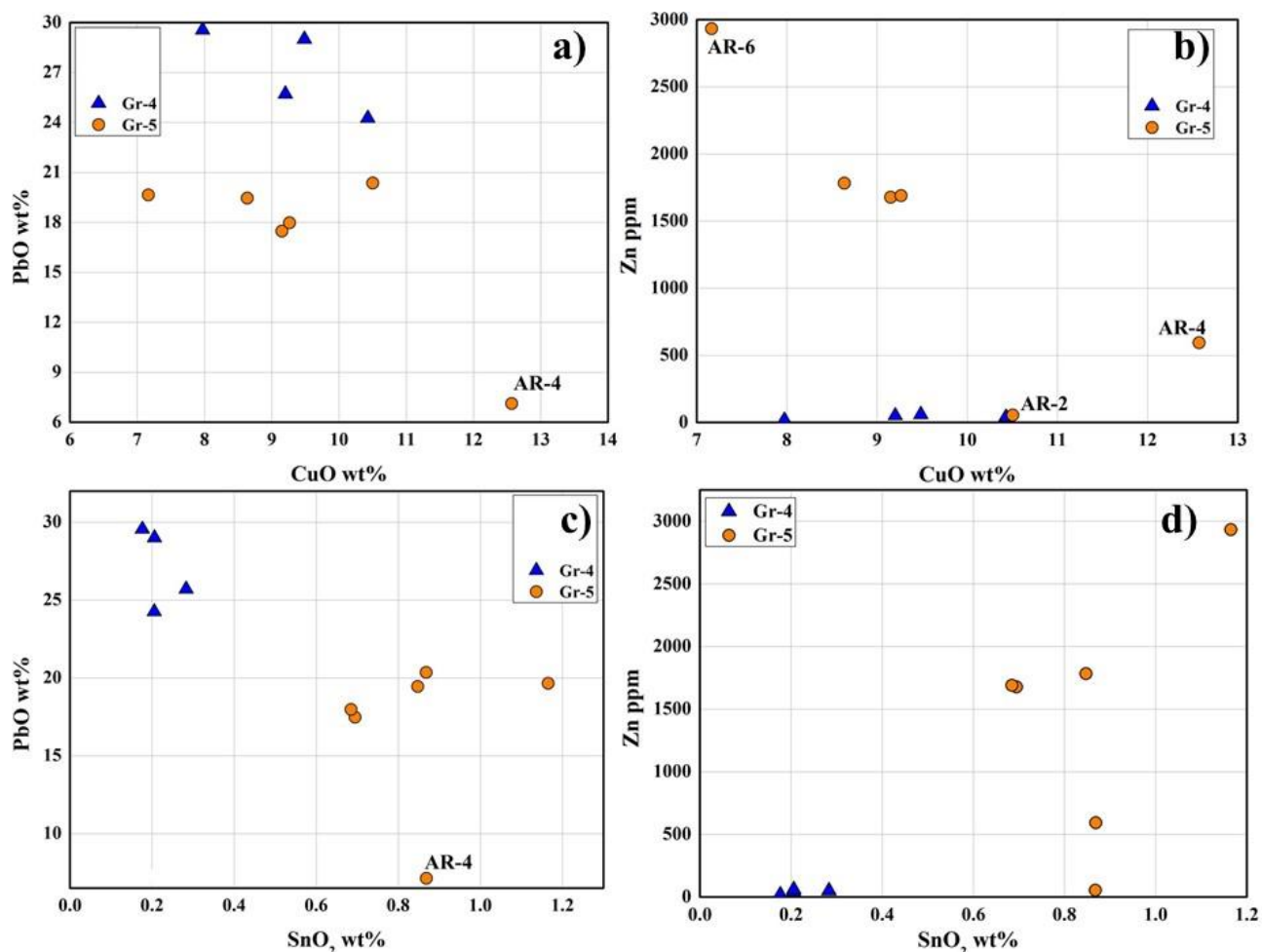


Figure 8.6. Biplot graphs: a) lead content (PbO) against copper concentration (CuO); b) zinc content (ZnO) against copper concentration (CuO); c) lead content (PbO) against tin concentration (SnO₂); d) zinc content (ZnO) against copper concentration (CuO).

Antimony and manganese

It is difficult to understand the precise role played by the antimony. According to the literature it was usually used as a reducing agent in sealing wax technology. However, it could also act as a nucleant agent favouring the aggregation of cuprous ions, rather than as a reducing agent [55]. In Roman sealing wax, the antimony oxide content is usually lower than 2 wt%, while it was higher than 4 wt% in the sealing wax red produced in the Near East between the 8th and the 6th centuries BC [47, 49, 56]. It is still unclear if the low concentration revealed in Roman sealing wax is enough to bring technological benefit for the formation of the red colour, or if they entered as contaminants from the lead-bearing or were already present in the base glass.

The same question occurred for the orange samples (Gr-5), in which antimony is often higher than 1 wt%, but its role is still unclear. Beyond antimony, in orange glass, despite the sealing wax red glass, iron and tin are

often higher than 1 wt%, suggesting an intentional addition. Why so many reducing agents? Maybe it is due to the fact that the reduction of Cu^{2+} to Cu^+ is much easier than that of Cu^+ to Cu^0 , hence a moderate amount of reducing agent (such as Fe^{2+} , Sn^{2+} , Sb^{3+}) may hamper the precipitation of metallic copper.

The concentration of MnO detected in these two groups is higher than 0.025 wt%, pointing that they used a raw glass decolorized by MnO or maybe recycled glass. However, it is still difficult to establish with certainty if recycled glass or Sb-colourless glass was used to make the Gr-4 and Gr-5 group samples.

8.1.3. Production technology

8.1.3.1 Cu^0 technology

How the Gr-1 group samples were manufactured is still unclear. As mentioned above, the use of a specific base glass composition could help to obtain the required reducing condition inside the melt. It could be possible that to cause the reduction of Cu^+ to Cu^0 the glassmakers applied a particular melting procedure, involving the cooling rate temperature and control of the oxidation state of the furnace atmosphere. Opaque red glass manufactured in the Late Bronze Age does not show the presence of any reducing agent, but completely opaque ingots were found [57], suggesting the possibility of producing opaque red without the addition of a specific reducing agent.

However, the low iron content could help to achieve a vivid or light red hue. In fact, the higher the iron content the darker or more brownish is the red hue [58], as is clear in sample R31 which shows a higher concentration of iron than the other samples from the Gr-1 group, and its colour moves slightly toward reddish brown hue. It is noteworthy that distinguishing brick red glass (Gr-1) from the sealing wax (Gr-4) with the naked eye was a difficult task (fig. 8.7). This underlines that Roman glassmakers were able to obtain a colour very close to the sealing wax by using Cu^0 . Moreover, the colorimetric measurements showed only a few differences in the chromatic coordinate, making them very similar.



Figure 8.7. Comparison of two fragments of copper red glass: sealing wax (a) and brick red (b).

The heterogeneity, which microscopically characterises the samples of the Gr-1 group, is due to the presence of dark transparent layers in which no particles were detected, because layers with different ratios of number and size of Cu^0 are formed. Identifying the cause which leads to this heterogeneity is complex, and it is

probable that several factors around the melting condition or how the molten glass was cooled, play a crucial role. No significant compositional differences were detected through the chemical analyses. Therefore, it is probable that the glass was not in the correct oxidation state to cause the precipitation of the Cu° particles. Hence, it is likely that the proper redox conditions were not achieved in the dark transparent layers. This could be due to the stirring of the melt. This operation, for instance, is often mentioned in the Venetian recipe manuscripts to prevent the formation of dark transparent layers. This procedure helps to mix the more oxidised upper layer of the molten glass (green transparent) with the inner and more reduced part of the melt (opaque red).

This heterogeneity is almost absent in the samples from the Gr-2 group. This could be due to the higher concentrations of iron and copper which stabilize the glass redox environment through a buffering effect. As observed above, the Gr-2 group samples have lower numbers but larger crystals than the red brick samples (Gr-1). This is the result of a higher concentration of copper and of a specific heat treatment.

The high concentration of copper aids the aggregation of the Cu° atoms in large crystals, while the presence of a high iron content should hamper the formation of cuprous ions [58]. When copper-containing glass is rapidly cooled, metallic copper crystals are chilled in sub-micrometric sizes, caused by the increase in viscosity which prevents crystal growth, creating an opaque red glass [6, 58, 59]. In contrast, the crystal growth is favoured when the molten glass is maintained at a temperature that favours a low viscosity for a prolonged period and is slowly cooled. As result, the copper-containing glass will be brown, or in extreme cases crystals visible to the naked-eye will form [58, 59]. This process is driven by Ostwald ripening, which favours the growth of thermodynamically stable particles of a specific size, while the smaller particles dissolve in the glass matrix [60]. Since this technology is temperature and time-dependent, through specific heat treatment it is possible to control the growth of a few large particles or the high numbers of small crystals.

These samples seem to prove that Roman glassmakers knew these principles, probably in an empirical way. However, they foresaw the technological production of aventurine glass, firstly produced in high amounts by Venetian glassmakers at the end of the 16th century AD. Indeed, in the R10 and R17 samples, a sparkling effect was noted on their surfaces, which is due to the glossy effect of the large Cu° particles (fig. 8.8).

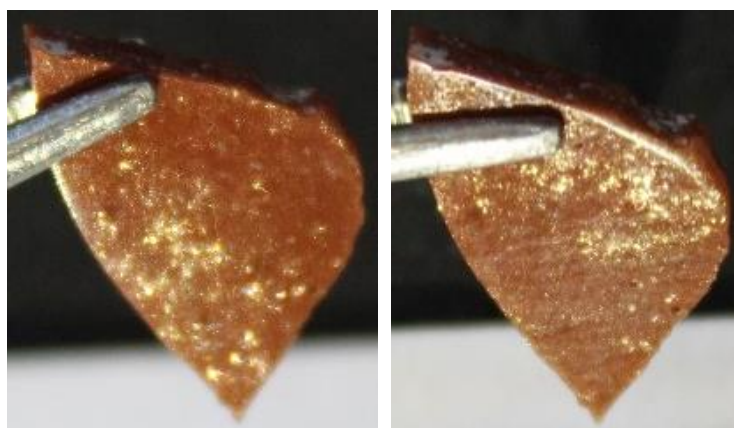


Figure 8.8. Picture of the R17 sample illuminated, generating a shinning and glassy effect on its surface.

Aventurine glass was an extreme consequence of a long and slow cooling phase (some Venetian recipes said that it took one week), through which large crystals produced a clear sparkling effect [61]. The chemical analyses confirmed that the samples from the Gr-2 group are typical of Roman natron glass [62, 63]; however, the concentrations of copper and iron are very close to those detected in Venetian aventurine of the 19th century, although the tin content often detected in Venetian aventurine (SnO₂ 2.0-2.5 wt%) was higher than in the Gr-2 samples, probably due to the addition of lead/tin calx, as suggested in some Venetian recipes [61].

The samples from the Gr-3 group present red bands in a dark transparent glass. The chemical analyses did not highlight any compositional differences. A redox difference can be suspected, originating from the disproportionate amounts of iron (R1: 4.5 wt%; R22: 3.9 wt%) and copper (R1: 0.27 wt%; R22: 0.31 wt%). To obtain this heterogeneity, it is likely that a continuous stirring of the glass was adopted by the glassmakers. This excludes the possibility that Cu₂S particles frequently detected in both layers (red and transparent green) could be the colouring agent. The Cu₂S particles are the result of a first crystallisation in which the two elements reacted below their melting temperatures. Once the sulphur available to react has been consumed, a second crystallisation occurred leading to the formation of metallic copper nanoparticles.

8.1.3.2 Cu₂O technology

The procedure to produce sealing wax (Gr-4) and orange (Gr-5) glass required distinct heat treatments for the formation of Cu₂O crystals of specific dimensions. According to the laboratory reproduction, to produce sealing wax it was important that the molten glass was left at a temperature slightly below the melting temperature (for a long period) to promote the formation of a few nuclei. A second step was probably a gradual and prolonged cooling phase in order to encourage the growth of crystals [54]. In contrast, to produce orange glass, the molten glass would have been maintained at a temperature lower than the sealing wax in order to increase the number of small cuprite crystals [54].

The different orange hues were created by combining specific chemical compositions with mastered heat treatment, which affected the number and the size of the cuprite crystals. Hence, the euhedral calcium antimonate crystals, detected in sample AR2, should not be considered a possible opacifying or a voluntary addition to achieve a specific hue. Most probably they formed as the glass started to cool or was left at a temperature below the melting point for a prolonged period [38]. In sealing wax red glass, no devitrification products were detected. High concentrations of lead probably obstructed the formation of devitrification products, which prevented the development of cuprite [38].

8.2 Conclusion

The opaque red glass from the *opus sectile* decoration in the villa of Lucius Verus has been a good opportunity to investigate in depth the technical aspects of this demanding colour and underlines the main unresolved questions around its production.

The multi-analytical approach used to investigate the copper red glass *sectilia* of the Gorga collection made it possible to analyse several crucial aspects of these glasses, providing precious insights with which to clarify its production technology.

In this research, five red hues from orange to brown through to the red were distinguished. Each hue is characterised by two main factors: the chemical composition and the relationship of the size-number of copper-rich particles. Two main colouring techniques were detected which used two different colouring and opacifying agents: metallic copper and cuprite. They were never found together in the same samples. The nature of the colouring agents is strictly linked with the chemical composition, while the number and the size of the particles are the result of specific heat treatments.

Three recipes were identified within the metallic copper colouring technique which included groups Gr-1, Gr-2 and Gr-3. In this technique, iron plays an important role, and the manipulation of the proportions of iron and copper is a key factor to obtaining the three different red hues. Moderate concentrations of copper and iron were used for the brick red glass (Gr-1), while by increasing their content the colour moved towards reddish brown hue (Gr-2). To produce a dark red (Gr-3) glass, high quantities of iron and small amounts of copper were used, obtaining red banded samples in which extreme heterogeneity was composed of dark green transparent and opaque red layers.

Two different base glass compositions were used, natron glass in the Gr-2 and Gr-3 groups and soda plant ash glass in the Gr-1 group. In order to better control the reducing conditions inside the melt and ensure a light red colour, it is likely that in the recipe for brick red (Gr-1) a soda plant ash glass was used. The high concentrations of potassium and magnesium, and the lower sodium content should be attributed to the use of soda plant ashes as a fluxing agent, rather than the addition of fuel ash to a natron base glass. Moreover, compositional differences involved in the silica source emerged through a comparison with the typical natron glass used for Roman glass vessels. These differences could be clues to the use of a different raw glass from that used to make the vessels. It may be that the Gr-1 samples were not produced by re-melting the same natron glass used for the glass vessels. Indeed, the concentration of MnO and Sb₂O₃ is not enough to establish whether a colourless glass was used or recycled to make Gr-1 samples. All this evidence calls into question the organisation of the glassmaking industry proposed in the literature. Specific coloured glass may have been produced in specialised workshops by using different recipes and their own raw glass.

However, it is still not possible to establish whether there were specific production centres in the Roman Age which manufactured soda plant ash glass, and more analyses are necessary to shed light on this intriguing question.

The compositional differences of tin and lead, detected between the Gr-1a and Gr-1b samples, suggest the use of two different copper-bearing. Gr-1a samples are the thinnest *sectilia*, while most of the Gr-1b samples are made by canes. The production of these two types of *sectilia* may have required two different batches. However, the base glass composition does not show any marked chemical differences.

The red colour of some of the Gr-1 group samples is very close to sealing wax red, making it very difficult to distinguish them. The typical heterogeneity observed by the naked eye (Gr-3) and microscopically (Gr-1) in the metallic copper colouring technique could be due to the continued stirring of the glass, which was included in their recipe. Conversely, the reddish brown samples (Gr-2) are not affected by heterogeneity. They were probably produced through a specific heat treatment, in which a slow and prolonged cooling phase was employed in order to favour the crystal growth of metallic copper. The features and the chemical composition of the reddish brown samples are very close to Venetian aventurine glass. This seems to suggest that this technology, up to now only attributed to late 16th century AD Venetian glassmakers, was known to Roman glassmakers.

In the cuprite technology, high concentrations of lead and copper were used. The chemical compositional differences detected in the two groups (Gr-4 and Gr-5), highlighted the extraordinary attention to the proportion of specific elements. The production of orange glass showed the incredible skill needed to manipulate the chemical composition and control the melting process, which at that time may have been challenging. An engineered chemical composition made it possible to increase the number of small cuprite crystals, while a mastered heat treatment made it possible to control the size. As result of the control of this technique, four different orange hues were produced.

Sealing wax red glass seems to possess a different chemical composition when compared to those produced before the Roman Age. It is likely that a change in the raw material or an improvement in the heat treatment occurred. However, sealing wax red glass is an unexpected guest in the glass of the 2nd century AD, since it is generally accepted that its production stopped around the 1st century AD. The presence of sealing wax among the *sectilia* of the villa of Lucius Verus could open a new path in defining the correct chronology of its production. Other writers found sealing wax in Roman mosaic tesserae and enamels but only until the 1st century AD [22, 34]. In our case, sealing wax is abundantly present, which could suggest that during the 2nd century AD this technology had not been abandoned, but was still well known. Its production may not have been replaced by red brown, but continued to be used exclusively for specific requirements.

References

1. Nakai, I.; Numako, C.; Hosono, H.; Yamasaki, K. Origin of the red colour of Satsuma copper-ruby glass as determined by EXAFS and optical absorption Spectroscopy. *J. Am. Ceram. Soc.* **1999**, *82*, 689–784.
2. Padovani, S.; Sada, C.; Mazzoldi, P.; Brunetti, B.; Borgia, I.; Sgamellotti, A.; Giulivi, A.; D’Acapito, F.; Battaglin, G. Copper in glazes of Renaissance luster pottery: Nanoparticles, ions, and local environment. *Appl. Phys.* **2003**, *93*, 10058–10063.
3. Moretti, C.; Gratuze, B. Vetri rossi al rame e aventurina. Confronto di analisi e ricette. *Riv. Stn. Sper. Vetro* **1999**, *3*, 147–160.
4. Brown, S.F.; Norton, F.H. Constitution of copper-red glaze. *J. Am. Ceram. Soc.* **1959**, *42* (11), 499-503.
5. Wakamatsu, M.; Takeuchi, N.; Ishida S. Effect of heating and cooling atmospheres on colors of glazes and glass containing copper. *J. of Non-Crystalline Solids.* **1986**, *80*, 412-421.

6. Weyl, W.A. Copper in copper-ruby glasses (Hematinone and copper aventurine). In *Coloured Glasses*; Society of Glass Technology: Sheffield. UK. 1951, pp. 420-432; ISBN 9780900682063.
7. Lilyquist, C.; Brill, R.H. Analytical procedure. In *Studies in Early Egyptian Glass*; Metropolitan Museum of Art: New York, NY, USA, 1993, pp. 47-58; ISBN 978-0300200195.
8. Freestone, I.; Stapleton, P.C. Composition, technology and production of coloured glasses from mosaic vessels of the early Roman Empire. In *Glass of the Roman Empire*; Bayley, J., Freestone, I., Jackson, C., Eds.; Oxbow: Oxford, UK, 2013, pp. 61-76.
9. Fiori, C. Production technology of Byzantine red mosaic glasses. *Ceram. Int.* **2015**, 41, 3152–3157.
10. Maltoni, S.; Silvestri, A.; Molin, G. Opaque red glass tesserae from Roman and Early-Byzantine sites of north-eastern Italy: New light on production technologies. In Proceedings of the *Annales du 20e Congrès de l'Association Internationale pour l'Histoire du Verre, Fribourg, Switzerland, 7–11 September 2015*; Wolf, S., de Pury-Gysel, A., Eds.; Verlag Marie Leidorf: Rahden, Germany, 2017; pp. 280–287.
11. Paynter, S.; Kearns, T.; Cool, H.; Chenery, S. Roman coloured glass in the Western provinces: The glass cakes and tesserae from West Clacton in England. *J. Archaeol. Sci.* **2015**, 62, 66–81.
12. Fiorentino, S.; Chinni T.; Vandini, M. Ravenna, its mosaics and the contribution of archaeometry. A systematic reassessment on literature data related to glass tesserae and new considerations. *J. Cult. Her.* **2020**, 46, 335-349.
13. Schibille, N.; Degryse, P.; Corremans, M.; Specht, C.G. Chemical characterisation of glass mosaic tesserae from sixth-century Sagalassos (south-west Turkey): chronology and production techniques. *J. Archaeol. Sci.* **2012**, 39, 1480-1492.
14. Schibille, N.; Neri, E.; Ebanista, C.; Ammar, M.R.; Bisconti, F. Something old, something new: The late antique mosaics from the catacomb of San Gennaro (Naples). *J. Archaeol. Sci. Rep.* **2018**, 20, 411–422.
15. Paynter S. Experiments in the reconstruction of Roman wood-fired glassworking furnaces: waste products and their formation processes, *J. Glass Stu.* **2008**, 50, 271-290.
16. Jackson, C.M.; Booth, C.A.; Smedley, J.W. Glass By Design? Raw Materials, Recipes And Compositional Data. *Archaeometry* **2005**, 47 (4), 781–795.
17. Misra, M.K.; Ragland, K.W.; Baker A.J. Wood Ash Composition as a function of furnace temperature *Biomass and Bioenergy* **1993**, 4 (2), 103-116.
18. Barfod, G.H.; Freestone, I.C.; A. Lichtenberger, Rubina Raja¹, Holger Schwarzer⁴. Geochemistry of Byzantine and Early Islamic glass from Jerash, Jordan: Typology, recycling, and provenance. *Geoarchaeology*, **2018**, 3, 623–640.
19. Jackson, C.M.; Cottam, S. ‘A green though in a green shade’; Compositional and typological observation concerning the production of emerald green glass vessels in the 1st century AD. *J. Archaeol. Sci.* **2015**, 61, 139-148.
20. Gallo, F.; Silvestri, A.; Molin G.; Glass from the Archaeological Museum of Adria (North-East Italy): new insights into Early Roman production technologies. *J. Archaeol. Sci.* **2013**, 40, 2589-2605.
21. Rosenow, D.; Rehren, Th. Herding cats e Roman to Late Antique glass groups from Bubastis, northern Egypt. *J. Archaeol. Sci.* **2014**, 49, 170-184.

22. Boschetti, C.; Henderson, J.; Evans, J.; Leonelli, C. Mosaic tesserae from Italy and the production of Mediterranean coloured glass (4rd century BCE–4th century CE). Part I: Chemical composition and technology. *J. Archaeol. Sci. Report.* **2016**, *7*, 303-311.
23. Nenna, M.D.; Gratuze, B. Etude diachronique des compositions de verres employes dans les vases mosaïques antiques: Resultats preliminaires. In Proceedings of the *Annales du 17e Congrès de l'Association Internationale pour l'Histoire du Verre, Antwerp, Belgium, 4–8 September 2006*; Janssens, K., Degryse, P., Cosyns, P., Caen, J., Van't dack, L., Eds.; University Press Antwerp: Antwerp, Belgium, 2009; pp. 199-205.
24. Verità, M.; Santopadre, P. Unusual Glass Tesserae from a Third-century Mosaic in Rome. *J. Glass. Stud.* **2015**, *57*, 287–292.
25. Verità, M.; Arena, M.S.; Carruba, A.M.; Santopadre, P.. Materiali vitrei nell'opus sectile di Porta Marina (Ostia antica), *BOLL. ICR* **2008**, 16-17, pp. 78-94.
26. Cagno, S.; Cosyns, P.; Izmer, A.; Vanhaecke, F.; Nys, K.; Janssens, K.. Deeply colored and black-appearing Roman glass: a continued research. *J. Archaeol. Sci.* **2014**, *42*, 128-139.
27. Mirti, P.; Pace, M.; Negro Ponzi, M.M.; Aceto, M. ICP–MS Analysis of glass fragments of Parthian and Sasanian epoch from Seleucia and Veh Ardasir (Central Iraq). *Archaeometry* **2008**, *50* (3), 429–450.
28. Mirti, P.; Pace, M.; Malandrino, M.; Negro Ponzi, M.M. Sasanian glass from Veh Ardasir: new evidences by ICP-MS analysis. *J. Archaeol. Sci.* **2009**, *36*, 1061–1069.
29. Henderson, J.; Chenery, S.; Faber E.; Kröger, J. The use of electron probe microanalysis and laser ablation-inductively coupled plasma-mass spectrometry for the investigation of 8th–14th century plant ash glasses from the Middle East. *Microch. J.* **2016**, *128*, 134–152
30. Schibille, N.; Gratuze, B.; Ollivier, E.; Blondeauc, É. Chronology of early Islamic glass compositions from Egypt. *J. of Archaeol. Sci.* **2019**, *104*, 10–18.
31. Phelps, M. Glass supply and trade in early Islamic Ramla: An investigation of the plant ash glass. In *Things that travelled-Mediterranean Glass in the First Millennium CE*. Rosenow, D., Phelps, M., Meek, A., Freestone I., Eds.; Publisher: UCL Press University College London, UK, 2018, pp. 236-282.
32. Henderson, J.; Mcloughlin, S.D.; Mcphail, D.S. Radical Changes In Islamic Glass Technology: Evidence For Conservatism And Experimentation With New Glass Recipes From Early And Middle Islamic Raqqa, Syria. *Archaeometry* **2004**, *46* (3), 439–468.
33. Tite, M.S.; Shortland, A.; Maniatis, Y.; Kavoussanaki, D.; Harris S.A. The composition of the soda-rich and mixed alkali plant ashes used in the production of glass. *J. Archaeol. Sci.* **2006**, *33*, 1284-1292.
34. Henderson, J. Chemical characterization of Roman glass vessels, enamels and tesserae. *Jewel. Stud.* **1991**, *5*, 65–77.
35. Santagostino Barbone, A.; Gliozzo, E.; D'acapito, F.; Memmi Turbanti, I.; Turchiano, M.; Volpe, G. The sectilia panels of faragola (Ascoli Satriano, southern Italy): A multi-analytical study of the red, orange and yellow glass slabs. *Archaeometry* **2008**, *50*, 451–473.
36. Schibille, N.; Boschetti, C.; Valero, M.A.; Veron, E.; Juan, J. The Color Palette of the Mosaics in the Roman Villa of Noheda (Spain). *Minerals* **2020**, *10*, 272.

37. Tress, H.J. Ruby glass and related glasses from standpoint of the chemical potential of oxygen in glass. Part 1. Physics and Chemistry of Glasses. *Glass Technol.* **1962**, 3, 28–36.
38. Freestone, I.C. Composition and microstructure of opaque red glass. In Bismon and Freestone. In *Early Vitreous Materials*; British Museum Occasional Paper, 56; Bimson, M., Freestone, I.C., Eds.; British Museum: London, UK, 1987; pp. 173–191. ISBN 978-0861590568.
39. Kunicki-Goldfinger, J.; Freestone, I.C.; McDonald, I.; Hobot, J.A.; Gilderdale-Scott, H.; Ayers, T. Technology, production and chronology of red window glass in the medieval period—Rediscovery of a lost technology. *J. Archaeol. Sci.* **2014**, 41, 89–105.
40. Silvestri, A.; Molin, G.; Salviulo, G. The colourless glass of Iulia Felix. *J. Archaeol. Sci.* **2008**, 35, 331–341.
41. Gliozzo, E. The composition of colourless glass: a review. *Archaeol Anthropol Sci* **2017**, 9, 455–483.
42. Foy, D., Vichy, M., and Thirion-Merle, V. Caractérisation des verres de la fin de l'Antiquité en Méditerranée occidentale: l'émergence de nouveaux courants commerciaux , In *Actes du colloque de l'Association Française pour l'Archéologie du Verre*; D. Foy, M. D. Nenna Eds.; Aix-en-Pro, Monique Mergoil, Montagnac, France, 2003; pp. 41–85.
43. Ganio, M.; Boyen, S.; Fenn, T.; Scott, R.; Vanhoutte, S.; Gimeno, D.; Degryse P. Roman glass across the Empire: an elemental and isotopic characterization. *J. Anal. At. Spectrom.* **2012**, 27, 743–753
44. Cholakova, A.; Rehren, T. Producing black glass during the Roman period—notes on a crucible fragment from Serdica, Bulgaria. In *Proceedings of the 39th International Symposium for Archaeometry, Leuven, Belgium, 28 May–1 June 2012*; Scott, R., Braekmans, M., Degryse, P., Eds.; Centre for Archaeological Sciences: Leuven, Belgium, 2014; pp. 261–267.
45. Rehren, Th., Cholakova, A. The Early Byzantine HIMT Glass From Dichin, Northern Bulgaria. In *Interdisciplinary Research*, 2010, pp. 81–96.
46. Maltoni, S.; Silvestri, A. Innovation and tradition in the fourth century mosaic of the Casa delle Bestie Ferite in Aquileia, Italy: Archaeometric characterisation of the glass tesserae. *Archaeol. Anthropol. Sci.* **2018**, 10, 415–429.
47. Brill, R.H.; Cahill, N.D. A red opaque glass from sardis and some thoughts on red opaque in general. *J. Glass Stud.* **1988**, 30, 16–27.
48. Stapleton C. P.; Freestone I.C.; Bowman, S.G.E. Composition and Origin of Early Mediaeval Opaque Red Enamel from Britain and Ireland. *J. Archaeol. Sci.* **1999**, 26, 913–921.
49. Freestone, I.C.; Stapleton, C.P.; Rigby, V. The production of red glass and enamel in the Late Iron Age. Roman and Byzantine periods. In *Through a Glass Brightly: Studies in Byzantine and Medieval Art and Archaeology*; Presented to David, Buckton; Entwistle, C., Buckton, D., Eds.; Oxbow Books: Oxford, UK, 2003; pp. 142–154. ISBN 978-1785702518.
50. AshkenaziaD.; Taxel I.; Talb, O. Archeometallurgical characterization of Late Roman- and Byzantine-period Samaritan magical objects and jewelry made of copper alloys. *Mater. Character.* **2015**, 102, 195–208

51. Dungworth, D. Roman Copper Alloys: Analysis of Artefacts from Northern Britain. *J. Archaeol. Sci.* **1997**, 24, 901–910.
52. Poinitng, M.J. Roman military copper-alloy artefacts from israel: questions of organization and ethnicity. *Archaeometry* **2002**, 44 (4), 555 – 57.
53. Schibille, N., Sterrett-Krause, A. & Freestone, I.C. Glass groups, glass supply and recycling in late Roman Carthage. *Archaeol Anthropol Sci* **2016**, 9, 1223–1241.
54. Ahmed, A.A.; Ashour, G.M. Effect of heat treatment on the crystallisation of cuprous oxide in glass. *Glass Technol.* **1981**, 22, 24–33.
55. Cable, M.; Smedley, J.W. The Replication of an opaque red glass from Nimrud. In *Early Vitreous Materials; British Museum Occasional Paper 56*; Bimson, M., Freestone, I.C., Eds.; British Museum: London, UK, 1987; pp. 151–164. ISBN 978-0861590568.
56. Brill, R.H. *Chemical Analyses of Early Glasses; Volume 2 Tables of Analyses*; The Corning Museum of Glass: Corning, NY, USA, 1999; ISBN 0-872900-143-2.
57. Rehren, Th. Ramesside glass-colouring crucibles. *Archneomerry* **1997**, 39 (2), 355-368.
58. Ahmed, A.A.; Ashour, G.M.; El-Shamy, T.M. The effect of melting conditions on the crystallization of cuprous oxide and copper in glass. In *Proceedings of the 11th international Congress of Glass, Prague, Czech Republic, 4–8 July 1977*; pp. 177–187.
59. Tress, H.J. Ruby glass and related glasses from standpoint of the chemical potential of oxygen in glass. Part 2. Gold and copper glasses. *Glass Technol.* **1962**, 3, 95–106.
60. Ratke, L.; Vooehees, P.W. Coarsening: Basics and Laws. In *Growth and Coarsening. Ostwald Ripening, in Material Processing*, 1st ed.; Springer: New York, NY, USA, 2002; pp. 117-123 ISBN 978-3-642-07644-2.
61. Moretti, C.; Gratuze, B.; Hreglich, S. L'avventurina: (II parte) la tecnologia e le analisi. *Riv. Stn. Sper. Vetro* **2010**, 6, 29–47.
62. Sayre, E.V.; Smith, R.W. Compositional categories of ancient glass. *Science* **1961**, 133, 1824–1826.
63. Freestone, I.C.; Gorin-Rose, Y.; Hughes, M.J. Primary glass from Israel and the production of glass in Late antiquity and the early Islamic period. In *La Route du Verre, Ateliers Primaires et Secondaries du Second Millenaire av. J.-C. ou Moyen Age (TMO 33)*; Nenna, M.D., Ed.; Maison d'Orient: Lyon, France, 2000; pp. 65–83.

-Section Three-
Recipes and laboratory reproductions

9 Laboratory reproductions

9.1 Introduction

This section aims to investigate some aspects of the production technology of Roman opaque red brown glass through systematic laboratory reproduction, to better understand the raw materials used, the manufacturing process and the control of the final colour.

Based on the bibliographical research, it was decided to test mainly iron compounds in the laboratory experiments. Indeed, in the chemical analyses of red brown reported in the literature, iron is often present in concentrations higher than 2 wt%, suggesting an intentional addition of some iron-bearing material, which should act as a reducing agent. Copper (added through some form of copper-bearing material) is the colouring agent as established by the extensive literature on copper-red glass. Iron and copper compounds have been used in laboratory reproductions in different concentrations, proportions, oxidation states and melting conditions (time, temperature).

Other elements such as antimony, tin and lead have not been tested, because in the analyses reported in the literature, they showed a wide variability, and it is uncertain whether they entered as contaminants or were deliberately added. Tin was tested in only very few experiments in this research, and two examples are reported to show preliminary results. However, this research does not aim to investigate how tin oxides cause the formation of red colour, which requires more specific studies.

The main goals of the laboratory reproductions are to ascertain:

- a) in which oxidation state iron should be used to produce opaque red glass, hence to identify the probable iron-bearing materials.
- b) when copper and iron should be added to the glass, if directly in the batch or to the melt. It aims to identify a probable procedure for making opaque red.
- c) how to control the final colour and obtain several red hues.

In general, the lack of information on the methods and procedures associated with the manufacture of ancient red brown glass does not enable us to discover how it was obtained. The recipes written on the clay Tell-Umar tablet (14th-12th centuries BC), were not considered in this research, since the composition of the glass produced in that period appears to be different from the well-known red brown made in the Roman Age.

In this case, Renaissance Venetian recipes represent a unique source of information, since both analyses and glassmaking information are available. Indeed, although several innovations occurred in glassmaking techniques from the Roman Age to the Venetian period, the production of red brown glass continued almost unaltered. Iron and copper continued to be the main ingredients for this colour. Therefore, with due caution, the information found in Venetian glassmakers' manuscripts could be an important source of suggestions about how to proceed in the laboratory reproduction of red brown glass. The results have provided significant information on some of the secrets to the manufacture of opaque copper-red glass.

9.2 The Venetian recipes: information about raw materials and melting procedures.

9.2.1 The Venetian manuscripts

Some Venetian glassmaking treatises were studied to examine the recipes for the manufacture of opaque red brown glass.

The *Trattatelli* are three booklets in part attributed to the Venetian glassmaking industry and kept in the State Archives of Florence. They have been dated to between the late 14th – early 15th centuries. Published in the 19th century, [1] the recipes have been commented by Luigi Zecchin [2]. Recipes from these treatises are indicated by TR in the text.

The *Montpellier* manuscript dating from 1536 belonged to Venetian glassmakers and entered the Bibliotheque de l'Ecole de Medicine de Montpellier (France) at the end of the 18th c. Before that, it was in the *Libreria* of the Albani family in Rome. It was partially commented on by Luigi Zecchin [3]; recipes are indicated with an M.

The *Anonimo* recipe book written by an unknown Venetian glassmaker around 1560 is probably a copy of two Muranese treatises. The first dates to the second half of the 15th- early 16th c. It was published and commented on in [4]; these recipes are indicated with an A.

The *Darduin* manuscript, dating from 1644, is a collection of recipes on glassmaking and glass colouring drawn up by several family members since the late 15th century. The final part includes some recipes dated to the late 17th- early 18th c. [5]; Recipes are indicated with a D.

The so-called *Brunoro* manuscript is the recipe book of the Venetian glassmaker Gasparo Brunoro found in Gdansk (Poland). Dated 1645, it also includes northern European recipes demonstrating that the Venetian glassmakers working abroad also experimented with other techniques [6]; these recipes are indicated with a B.

The first published book on glassmaking, *L'Arte Vetraria* by Antonio Neri, 1612 [7], includes a number of recipes of Venetian origin with comments by Luigi Zecchin [8]; Recipes indicated with an N.

(Appendix D has a comparison between some chemical analyses of Venetian opaque red glass and Venetian manuscripts, to observe the presence of similarities)

From these manuscripts, 35 recipes for the production of red brown glass used to make mosaic tesserae, enamels for metals and glass rods (beads) were identified. Recipes devoted to translucent red glass were not considered.

The information gathered from these recipes provided important information on the raw materials (base glass, copper- and iron-bearing), the procedure adopted to make opaque red glass, and in some cases how to control or to manufacture several different red hues.

9.2.2 The raw materials in the recipe books

Raw glass - Most of the recipes prescribe the preparation of a crucible with molten transparent glass and the addition of the colouring components to the melt. The melt is made with glass cullet or *cotisso* (molten glass

poured in water, stored and ready to be re-melted). Only recipes M92 and D202 prescribe how to prepare red brown glass starting by melting a batch of raw materials.

The recipes attest the use of common and *vitrum blanchum*⁶ glass, since the use of low-iron, well decolourised *crystallo* glass does not improve the quality of opaque red glass (B126: “low-quality common glass is the best”, and M132: “with *crystallo* red brown glass will be neither beautiful nor good”). Nevertheless, the use of *crystallo* moils (cullet contaminated by iron flakes from the blow pipe) is indicated in recipes D67 and D155, and recipes A42 and D199 recommend *crystallo* glass mixed with lead silicate glass.

Some recipes (TRB2, M92 and A34) use a potash glass and others (TRB11 and TRB20) a mixed alkali glass where tartar, i.e., the deposit of wine barrels, is the K-bearing compound. Different types of tartar are mentioned. It was used as a potash source in a completely calcined form as in M92 or TRB2, also initially purified by leaching to obtain K-carbonate (N11). Tartar in an unprocessed form as in A42 or in a semi-calcined form (N11 black tartar) was used as a reducing agent (carbonaceous particles) in red brown glass [9].

Lead-tin calx is an intermediate product prepared in the glass furnaces to make white opaque glass or to be used as an opacifier (or clarifier) of transparent coloured glass. It is the main white opacifier found in Renaissance Venetian recipes. To prepare the calx, the treatises prescribe heating a mixture of the two metals at a temperature above the melting point until a powder is obtained [10]. In general, these recipes recommend preparing a calx with a Pb/Sn ratio of 1 (for instance recipes B13, D96 and N93) or 0.5 (D97). One very important recipe is D97, which prescribes how to fire the mixture at a high temperature to obtain white calx (probably, fully oxidised lead and tin) and at a lower temperature to obtain grey calx (partially oxidised lead and tin).

Bone ash (the horns or bones of animals burnt and ground to a powder; Ca-phosphate) was also used as a glass opacifier. Nevertheless, it has also a nucleating effect, which can help the separation of the colouring particles from the melt since phosphorus helps the formation of nuclei and the growth of crystalline particles [11].

The use of high amounts of bone ash are reported in three recipes for red brown glass (TR2, TR20, A38).

Copper and iron - Thirty out of the thirty-five opaque red recipes investigated prescribe the use of iron together with copper to obtain the colour. In some recipes other reducing compounds (lead-tin calx, tin calx and tartar) are added together with iron. Finally, in five recipes (A38, B314, D202, M30 and M128) the reducing agent is tin alone.

The copper source is red copper (Cu₂O, cuprous oxide) generally prepared by firing metallic copper sheets in a small furnace or in the annealing area of the furnace. In some cases, sulphur is also added. The firing can take from 3 days up to 20 days (D296) using a high temperature process (TR-C7). At the end of the process, the sheets are covered by a red product which is separated by beating and then ground to a red powder [9].

⁶ Up to the middle of the 15th century, two qualities of glass had been made by Venetian glassmakers: the so-called common glass, and *Vitrum blanchum*. The first had a pale green, blue or yellow natural glass hue, and cullet or recycled glass was used, while *Vitrum blanchum* was a well decolorized glass made at least since the 14th century. Around the middle of the 15th century, *crystallo* glass was invented in Venice, as an important improvement on *vitrum blanchum* by using quartzite pebbles and a purified soda ash. It was completely decolorized, homogenous such as to be compared with rock crystal.

Two sources of iron are indicated: the flakes produced from beating incandescent iron and unprocessed or calcined steel on the anvil. These products are mixtures of metallic iron and different iron oxides. Their undefined reducing power affects their efficiency in the formation of metallic copper in the melt, making it almost impossible to define the exact amounts to be added to obtain red brown glass. This is why most of the recipes are empirical and suggest small additions of iron compounds to improve the final colour.

9.2.3 The Procedures

In general, the process prescribes preparing first a pot of molten glass to which the colouring components are added. The amounts of glass indicated in the recipes vary, depending on the application. For enamels production amounts of the order of one (example B310) to a few pounds (one pound could correspond to 300 or 477 g) of glass are indicated, while for mosaic production amounts of more than 100 (for instance B155) pounds of glass are indicated. Only recipes D155 and B61 recommend mixing glass grit (cullet and *cotisso* respectively) with copper, iron, lead-tin calx and melting the mixture in a crucible.

In fourteen recipes, comparable amounts of copper and iron (or slightly higher iron) are used, in three recipes the iron addition is up to twice copper and in four recipes copper is added in larger amounts, up to four times.

In nine recipes the amounts of the two colourants are not indicated.

In thirteen recipes iron is added first. The addition of copper occurs after a certain time (30 minutes, one hour, eight or sixteen hours) and should be done bit by bit, but not too much. After adding iron, recipe N58 advises checking the colour of the transparent glass, which should result in yellow and not opaque black. Only then does the addition of copper occur. After a few hours from the last addition of copper the melt is ready to be worked (homogeneously red brown coloured and free of bubbles).

Only two recipes prescribe the addition of copper first and then iron, without any other indication; in six recipes iron and copper are first mixed and added together, while in nine recipes the sequence is not specified.

Some recipes report the addition also of other compounds, such as lead silicate glass “for better results” (recipes A34 and M96) or of unprocessed tartar (M120 and B317).

Many recommendations are reported in the recipes including: a continuous monitoring of the melt to work the melt slowly, once the colour is obtained, to avoid the loss of the opaque red colour (M92 and B126). The melt must be mixed frequently and carefully to avoid dark cords (*tortioni neri*). Once copper and iron have entered the melt, the colour might not appear; in this case after a certain time further additions of them are required.

Recipe N58 is the most complete one: ‘A batch made of *crystallo* frit (20 parts), colourless glass cullet (1 part) and lead-tin calx (2 parts) is first melted. Then, a 1 to 1 mixture of powder made from calcined steel and flakes obtained by beating red hot iron is added. The melt will boil terribly; wait five, six hours. Do not add too much iron, the glass must not become black but transparent dark yellow. Then add calcined red copper in three-four times (the quantity is not specified). On mixing, the glass immediately becomes red. Frequent gatherings are recommended to control the colour. Let the melt cool to the working temperature, leaving the mouth of the furnace open. The melt must be worked within about ten hours, otherwise it will lose colour and become black;

in this case, add more iron'. In table 9.1 are the manuscripts with the procedure which describes how to add the reagents, which compounds to use, and the amount (when mentioned) necessary to make opaque red glass.

Table 9.1. Venetian recipes compatible with the analytical data. Amounts of lead-tin calx, iron (flakes or steel) and red copper prescribed in the recipes to be added to 100 parts of translucent glass to obtain opaque red glass.

Recipe	Lead tin calx	Red copper	Iron flakes	Steel	Raw tartar	Notes
D213	5.5	4.1	2.8	2.8		amounts for 100 parts of glass cullet; the sequence is not indicated.
M120, B310, B317	X	X	X		X	To be mixed together and added to the melt (iron and copper in comparable amounts); raw tartar as last addition
B61	8.3	8.3		8.3		amounts mixed with 100 parts of glass cullet and melted together
D155	5.5	5.5	2.8	2.8		amounts mixed with 100 parts of glass cullet and melted together
A62, M110, B173, B174, D129, D131		X	X			iron and copper together in comparable amounts
M74, M132, D67		X	X			iron first, then copper (comparable amounts)
D156		X	X			iron first, then copper (half of the iron amount)
B126		X		X		iron first the amounts are decided by the glassmaker looking at the glass colour

9.2.4 Colour control

Recipe M110 for mosaic tesserae gives instructions about how to obtain a sequence of seven hues from bright red to brown, confirming that Muranese glassmakers could control this colour. The recipe prescribes melting a pot of common glass and adding comparable amounts of powdered iron flakes from the anvil and red copper. The first bright red hue is obtained by keeping the furnace hot. The second, browner hue (*morello*) is obtained by adding more iron and copper and lowering the temperature of the furnace. By successive additions of copper and iron and a progressive lowering of the furnace temperature, it is possible to obtain 6-7 shades from red to brown.

Recipe pairs B173 (red) and B174 (brown) and D129 - D131 are clearly derived from M110.

Recipes B173 and M110 explain how to avoid the formation of a disturbing optical defect called *tortioni neri* (black cords). The recipes claim that black cords can be removed by adding iron or copper. Instead, their formation can be avoided by slow, gradual additions of copper (M74 and M132). It is quite probable that the *tortioni* correspond to the deep green transparent cords that appear black by visual inspection and are frequently present in red brown glass objects.

10. Materials and methods for laboratory reproduction

10.1.1 Glass composition, colouring and reducing agents (reagents)

In all the experiments a soda-lime-silica glass provided by Effe3 Murano glass-factory (Venice, Italy) was used. The chemical composition is not allowed to be divulged due to commercial patent.

Cupric oxide (CuO) and cuprous oxide (Cu₂O) were used as colouring agents, in form of laboratory reagent from the Aldrich company. Ferrous oxide (FeO), haematite (Fe₂O₃), Pyrite (FeS₂), magnetite (Fe₃O₄) and metallic iron (Fe⁰) were used as iron compounds. Stannous oxide (SnO) was used as a source of tin.

10.1.2 Crucibles and furnace

Cylindrical ceramic crucibles type C.101 and C.110 produced by F.lli Fossati (Milan, Italy) with external diameter 82 mm, height 98 mm and a maximum of capacity of 300 ml (fig. 10.1a) were used. The electric furnace used was a Barracha K-9 (Portugal), with thermoelectric thermocouple probe and automatic programmer with digital temperature indicator, which has a programmed start, automatic variation of heating speed and recovery in case of power failure (fig. 10.1b). It has a maximum temperature of about 1300 °C.

For the annealing an electric furnace (muffle furnace in the text) the Barracha E-1 (Portugal) was used, with thermoelectric thermocouple probe and automatic programmer with digital temperature indicator, which has a programmed start, automatic variation of heating speed and recovery in case of power failure. It has a maximum temperature of about 1050 °C.

To take out the crucible, a common iron glassmakers' pinch was used, and a steel rod was used to stir the glass.

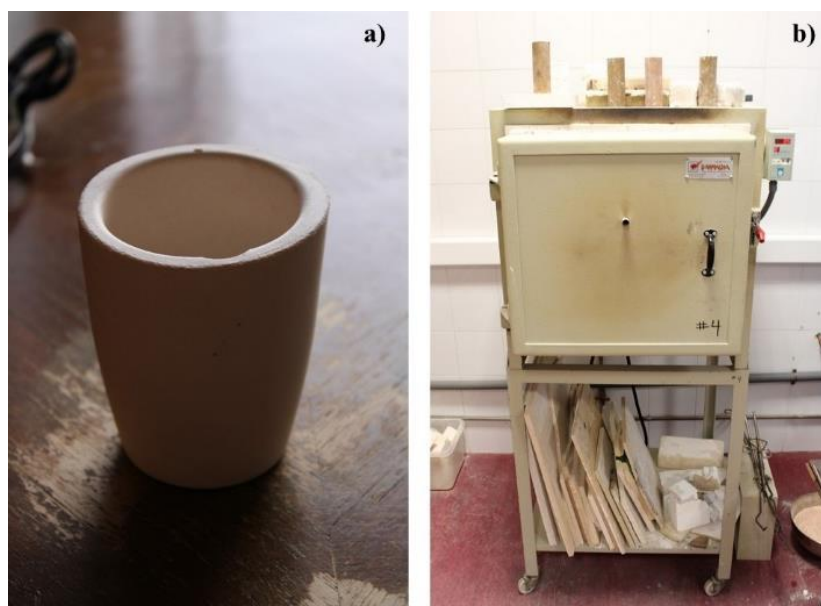


Figure 10.1 a) crucible C.101 Fossati; b) furnace K-9 Barracha;

10.2 Procedure

Defining a standard procedure has been a long process which required several attempts and failures. In this first stage, a considerable number of technical difficulties were encountered. Some results are reported in the [appendix F](#).

At the beginning, the cullet glass was crushed through the use of a steel mortar (fig. 10.2a-b), and iron and copper oxides added to it and mixed. Afterwards, the batch mixture was transferred to the furnace at room temperature; then the furnace was switched on and the melting temperature (1100 °C) was reached in three hours; the melting temperature was then maintained for three hours. The quantities of crushed glass used in these experiments varied between 20-100g. Only two tests are considered and reported here (indicated as V). In the first test, 2 g of cuprous oxide (Cu_2O) and 2 g of metallic iron (Fe°) were mixed with 96 g of raw crushed glass; in the second test 2 g of cuprous oxide (Cu_2O) and 2 g of stannous oxide were mixed with 96 g of raw crushed glass. The batches were melted at 1100 °C, held at this temperature for three hours, and then poured onto a metallic plate.

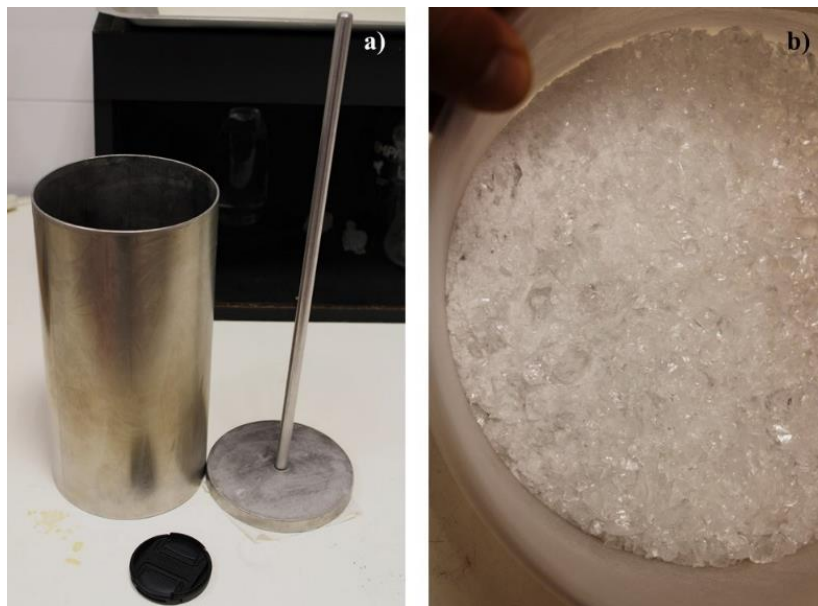


Figure 10.2. a) steel mortar used to crush the raw glass; b) crushed raw glass.

After these first attempts, a definitive procedure was established, called P: crushed glass (from 92 to 97 g) was put in the crucible and transferred to the furnace at room temperature (fig.10.3a-b).



Figure 10.3 a) Crushed glass in the crucible; b) crucible inside the furnace at room temperature.

The glass was melted at 1100°C and held at this temperature for two hours. Iron compounds were successively added to the melt half an hour before the copper. The addition of the reagents took place out of the furnace. The crucible with the molten glass was transferred to a container filled with silica sand in order to avoid the thermal shock to the crucible (fig. 11.4a-b-c). After each addition of the reagents, the melt was mixed, and the crucible was returned to the furnace at 1100 °C (fig. 10.4d-e-f). After the last addition, the melt was left to react for 3 hours at 1100 °C; during this phase, the melt was repeatedly stirred, transferring the crucible out the furnace for at least 1 minute, to perform this operation.



Figure 10.4. Sequence of the definitive procedure: **a)** the crucible was taken out from the furnace; **b)** the crucible was deposited on the container with sand; **c)** addition of the reagents into the molten glass; **d)** stirring the melt; **e)** returning the crucible with the molten glass containing the reagents to the furnace.

Afterward, the molten glass was poured onto a metallic table, pre-heated by metallic bars at 600-700 °C (fig. 10.5a-b-c). When the glass was poured part of the cooled melt was cut by steel scissors, commonly used by glassmakers.

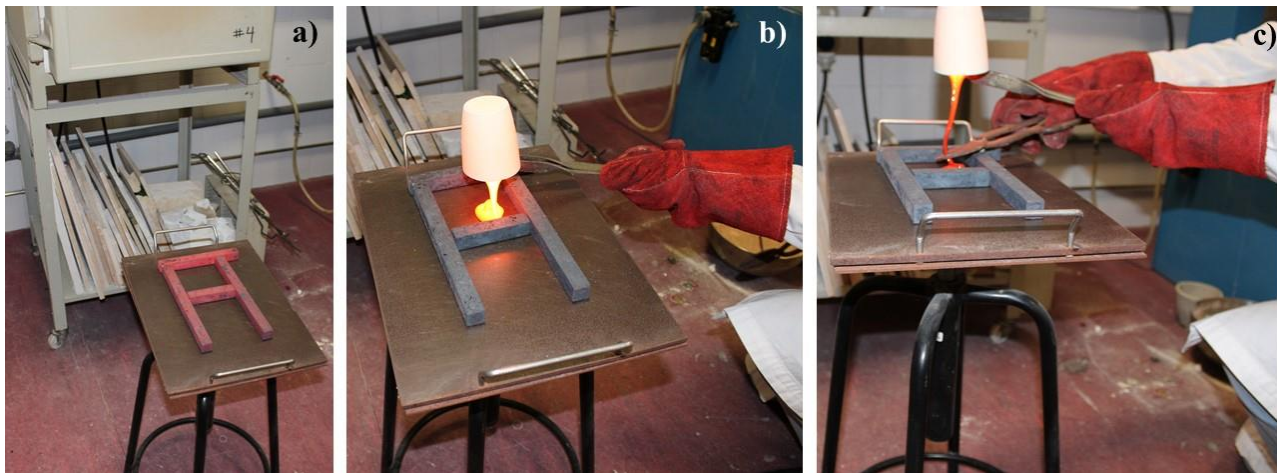


Figure 10.5. a) Warmed iron table with iron bars heated in furnace at about 700°C; b) pouring of the molten glass; c) cutting of the glass to gather the samples which will be transferred into the muffle furnace.

After a few minutes, the pure samples were transferred to the muffle furnace and kept at 550 °C for 1 hour (fig. 10.6a-b), and left to cool spontaneously.

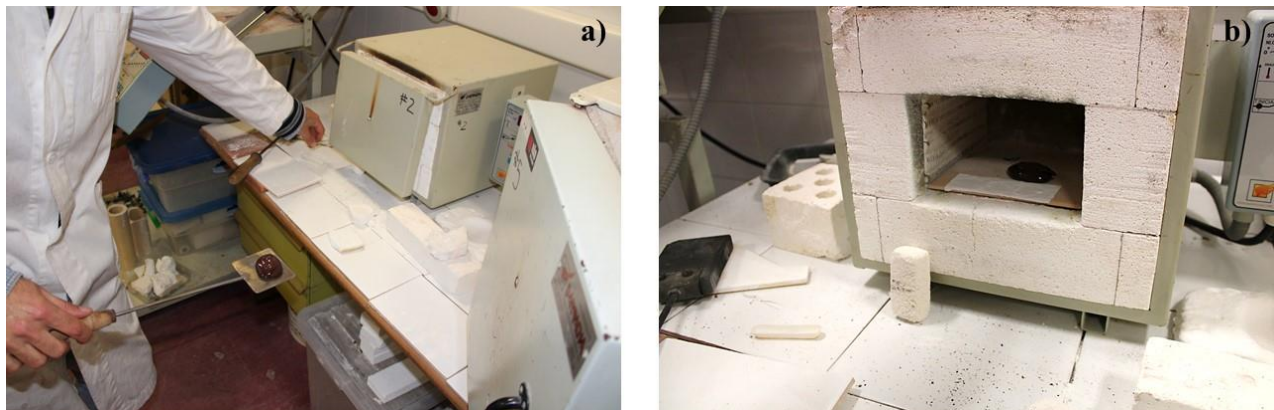


Figure 10.6. a) - b) Transfer of the sample into the muffle furnace at 550 °C, heated for 1h.

After testing the reagents, and observing the results, only metallic iron (Fe^0) and cuprous oxide (Cu_2O) were selected as the main reagent in the next experiments and two compositions were examined called P_F and P_S based on the copper content.

10.2.1 P_F procedure

In the first series of tests, it was decided to use a constant addition of 2g cuprous oxide, based on the average concentration found in the analysis reported in the literature. The cuprous oxide was added to the molten glass through a single addition. The amount of metallic iron varied in each test, ranging from 1 to 6 g. In this case, the quantities of iron have also been added in a single addition. These experiments are indicated as P_F1, P_F2, P_F3, P_F4, P_F5 and P_F6, based on the concentration of iron. However, in some tests using 2 g of Cu_2O and 2 g of Fe^0 , a further addition of Fe^0 or Cu_2O was considered necessary to obtain opaque red. These experiments are indicated as P_FA1, P_FA2 and P_FA3.

10.2.2 P_S procedure

In the second series of tests, 1 g of cuprous oxide was the fixed amount of copper. Metallic iron was added following the same procedure mentioned above and varied from 1 g to 5 g. These are indicated as S_F1, S_F2, S_F3, S_F4 and S_F5. The procedures are reported and summarised in [table 10.1](#).

Table 10.1. The procedures are summarised indicating the reagents with their amounts used in the manufacturing of opaque red.

Procedure		Description	Reagents	Copper amount	Reductant amounts
V	V_1	Preparation of a batch, containing the raw glass and the reagents.	CuO, Cu ₂ O; FeO and Fe [°]	2 g	FeO or Fe [°] 2 g – 4 g;
	V_2		CuO, Cu ₂ O; SnO	2 g	SnO 2 g
P	P	Melting first the raw glass at 1100°C and addition of the reagents. Each reagent added through single addition	CuO, Cu ₂ O; FeO, Fe ₂ O ₃ , FeS ₂ , Fe ₃ O ₄ , Fe [°] ;	2 g	Iron oxides from 2 g – 4 g;
			CuO, Cu ₂ O; SnO	2 g	SnO 2 g
	P_F	Melting, first, the powdered raw glass at 1100°C. Addition to the molten glass of the reagents. Each reagent added through single addition	Cu ₂ O + Fe [°]	2 g	Fe [°] from 1 g to 6 g
		After the addition of 2 g of Cu ₂ O and Fe [°] , further small amount of the reagents were added gradually until the opaque red formed.	Cu ₂ O + Fe [°] (P_FA1, P_FA2 and P_FA3)	From 2 g to 3.5 g	Fe [°] from 2 g to 3.5 g
P_S	Melting, first, the powdered raw glass at 1100°C. Addition to the molten glass of the reagents. Each reagent added through single addition	Cu ₂ O + Fe [°]	1 g	Fe [°] from 1 g to 5 g	

10.3 Heat treatment

For the heat treatments, two compositions were selected. By using the procedure P_F, the first composition was composed of 2 g of metallic iron and 2 g of cuprous oxide (P_F2); in the second composition 4 g of metallic iron and 2 g of cuprous oxide were used (P_F4).

Two types of heat treatments were performed: TT-1 and TT-2 ([fig. 10.7a-b](#)). In the TT-1, the glass was melted at 1100 °C for two hours, and then iron and copper were added, and the melt repeatedly stirred. When opaque red glass was obtained, the temperature was decreased (in 10-15 minutes) to 1000 °C and was maintained for 2 hours. Afterward, the furnace was switched off and the molten glass cooled inside the furnace at room temperature spontaneously for 10-12 hours.

The second heat treatment (TT-2) followed the heat treatment TT-1 until opaque red glass was obtained. Afterward, the temperature was lowered to 1000 °C and held for 2h. Later the temperature was further decreased to 800 °C for 10 minutes and held for another 2h. Finally, the furnace was switched off, and the molten glass cooled inside the furnace until their reached room temperature (about 10 hours).

When the crucibles were at room temperature, they were cut or broken to obtain a vertical section of the glass to be observed microscopically. Then the samples were prepared for OM observation, colorimetric measurement, FORS and Raman spectroscopy.

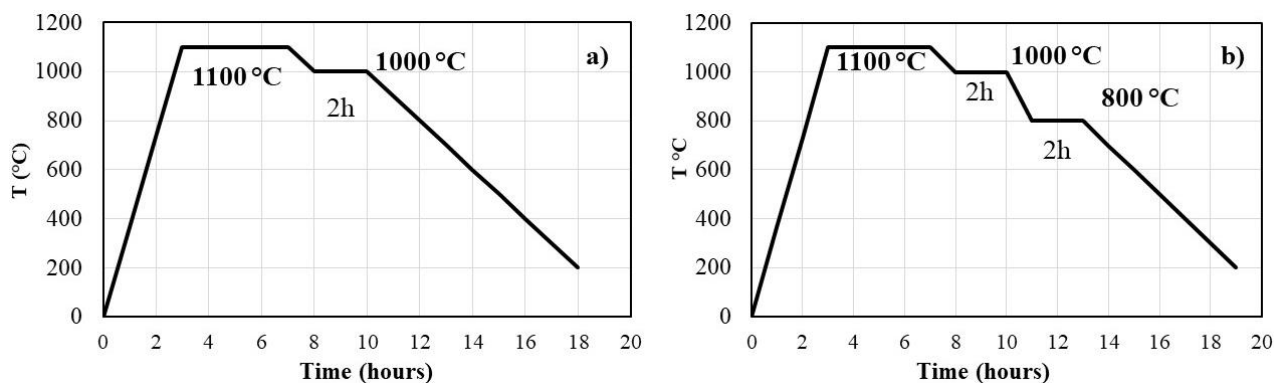




Figure 10.7. a) The set-up for the heat treatment TT-1; b) The set-up for the heat treatment TT-2.

11. Results

11.1 Procedures

The experiments performed by the V procedure turned out to be unsatisfactory and no opaque red glass was produced. By using metallic iron or stannous oxide the resulting glass was green and blue respectively (table 11.1).

Table 11.1. Samples produced by adding to the batch (at room temperature) 2 g of metallic iron (Fe^0) (on the left) or stannous oxide (SnO) (on the right).

2 g Fe^0 (V_1)	2 g SnO (V_2)
	

The addition of the reagents to the molten glass (procedure P) turned out to be satisfactory; indeed, by using the same reducing agents, opaque red glass formed after a few hours. Through this procedure it was possible to control the formation of opaque red step by step.

11.2 The effect of the different iron and copper oxidation states








After having established the standard procedure, several iron and copper compounds were tested. By means of cupric oxide or cuprous oxide opaque red glass is produced; however, cuprous oxide is easier to reduce than cupric oxide.

Through the several experimental reproductions, it has been observed that haematite produced a completely green transparent glass, while magnetite produced a transparent green glass with (sometimes) the presence of small quantity of opaque red (table 11.2). They cannot be considered an efficient reductant. Pyrite produced an extremely heterogenous and dark red glass in only one experiment. In other experiments, it produced a dark amber glass, or a very dark greenish glass.

Ferrous oxide (FeO) and metallic iron (Fe⁰) when used in the correct concentrations causes the redox condition required to facilitate the formation and precipitation of the colouring agent, and opaque red glass is formed.

Few experiments were performed using stannous oxide (SnO) and it led to the formation of a dark opaque red colour. However, more experiments are required to understand how to use it, because its reducing action is stronger than iron, and different concentrations of copper should probably be used.

Table 11.2. Picture of the glass produced by the different reducing agents (using P_F procedure). The concentration of cuprous oxide was fixed at 2 g, as well as the concentration of the reductants used in these experiments.

Hematite (Fe ₂ O ₃)	Magnetite (Fe ₃ O ₄)	Pyrite (FeS ₂)	Pyrite (FeS ₂)	Ferrous oxide (FeO)	Metallic iron (Fe ⁰)	Stannous oxide (SnO)
						

11.3 The effect of different iron and copper content

According to the amount of iron (Fe⁰) added to the molten glass, the colour changes from green to red brown hues (table 11.6). When the iron amount is added in a single addition, the achievement of opaque red is not guaranteed. Indeed, by adding 1 g of Fe⁰ a green glass with opaque red bands is formed (P_F1); while with 3 g or 4 g of Fe⁰ the glass moves towards brownish red or a muddy colour (P_F3, P_F4). In contrast, when the addition of Fe⁰ is 5 g and 6 g the glass turns an orange-brown colour, and considerable undissolved metallic spheres are present (P_F5, P_F6).

The samples containing 2 g of cuprous oxide start to form opaque red glass when at least the same amount of metallic iron is added. Hence the best composition for making opaque red glass by a single addition of the reagents should contain 2 g of metallic iron and 2 g of cuprous oxide. However, this composition is extremely unstable, and it is very easy to fail and obtain a green glass. Approximately eight experiments were conducted using this composition and in three tests opaque red glass was immediately formed, without further addition of metallic iron or copper. The samples in which opaque red did not required any further addition are P_F2a, P_F2b and P_F2c (Table 11.3). On the other hand, by using the same concentration of copper and iron, two samples resulted in green with small red bands (P_F2d, P_F2e – Table 11.4).

Table 11.3. Picture of opaque red glass produced by adding 2 g of metallic iron (Fe°) and 2 g of cuprous oxide (Cu_2O) according to the **P_F** procedure.



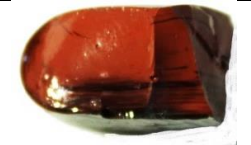
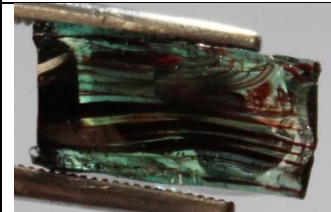




P_F2a	P_F2b	P_F2c
Cu_2O 2 g; Fe° 2 g	Cu_2O 2 g; Fe° 2 g	Cu_2O 2 g; Fe° 2 g
		

Table 11.4. Picture of the unsuccessful results by using 2 g of metallic iron (Fe°) and 2 g of cuprous oxide (Cu_2O) according to the **P_F** procedure.

P_F2d	P_F2e
Cu_2O 2 g; Fe° 2 g	Cu_2O 2 g; Fe° 2 g
	

The last three opaque reds were produced adding small quantities of metallic iron or cuprous oxide when the red colour was still not formed (table 11.5). In the **P_FA1** after the addition of 2 g of Fe° and Cu_2O , a further addition of copper and iron source occurred (1 g) and opaque red formed. In the **P_FA2** two additions were needed: after the ordinary addition of 2 g of both the reagents, the colour did not form, so 0.5 g of both the reagents were added, but opaque red continued not to appear. Hence a further addition of 1 g of both the reagents was necessary to obtain opaque red glass (after some minutes). In the case of the **P_FA3**, the colour did not form after the established amounts of the reagents, but after the addition of 1 g more of cuprous oxide opaque red glass was obtained.

Table 11.5. Picture of opaque red glass produced starting with 2 g of metallic iron (Fe°) and 2 g of cuprous oxide (Cu_2O) according to the **P_F** procedure, and continue with progressive addition of Fe° and Cu_2O until the formation of opaque red.

P_FA1	P_FA2	P_FA3
Cu_2O 3g; Fe° 3g	3.5 g di Fe° + 3.5 g Cu_2O	2 g di Fe° + 3 g Cu_2O
		

With the sets of experiments testing 1 g of cuprous oxide (**S_F**), it turned out to be very difficult to achieve satisfactory results (table 11.7). All the samples appeared very dark on the outer surface, and the colour formed only in the internal part of the glass. The glass was coloured by a few opaque red bands when 1wt% of Fe° was added, but extended areas still appeared to be transparent blue. When 2 g of Fe° was added, the glass still appeared extremely heterogeneous with the formation of numerous thin opaque red bands.

Opaque red glass formed when the addition of Fe⁰ was 3 g or 4 g, however. The colour in the glass was very heterogenous, with the presence of extensive dark areas and in some cases metal particles at the bottom of the samples. A further addition (5 g) of Fe⁰ produced a very dark red glass with several metallic inclusions.

Table 11.6. Results of the composition P_F in which Cu₂O addition was constant at 2 g, and Fe^o varied from 1 to 6 g.


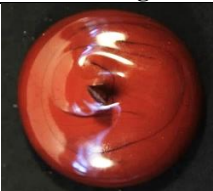















Comp.	P_F1 Fe ^o : 1 g	P_F2a Fe ^o : 2 g	P_F3 Fe ^o : 3 g	P_F4 Fe ^o : 4 g	P_F5 Fe ^o : 5 g	P_F6 Fe ^o : 6 g
Surface						
Cross section						
Colour meas.	L*:	L*: 35; a*: 16; b*: 5.7	L*: 32.7 a*: 7.0; b*: 2.7	L*: 32; a*: 8.0; b*: 2.8	L*: 32.1; a*: 11.2; b*: 7.4	L*: 32.7; a*: 8.3; b*: 7.6

Table 11.7. Results of the second composition (S_F) in which copper content was constant at 1 g, and iron varied from 1 to 5 g.

Composition	S_F1 Fe ^o : 1 g	S_F2 Fe ^o : 2 g	S_F3 Fe ^o : 3 g	S_F4 Fe ^o : 4 g	S_F5 Fe ^o : 5 g
Cross section					
Colour meas.	L*: 26.3; a*: 1.1; b*: -2.7	L*: 24.6; a*: 6.4; b*: 8.7	L*: 30.1; a*: 10.3; b*: 13.5	L*: 30.2; a*: 12.6; b*: 14.1	

11.4 Optical microscope

Tables 11.8 and 11.9 show the OM micrographs of the P_F and S_F composition. As observed microscopically, several opaque red bands embedded in a transparent green glass were observed when only 1 g of iron was added in the P_F1 composition. Afterward, by increasing the addition of iron, from 2 g to 4 g, the colour of the glass turns from a brick red towards a more reddish brown colour, reaching an orange-red-brown colour when 5 g or 6 g of iron was added.

Using the composition S_F, opaque red glass formed only by an addition of 3 g or 4 g. However, a darker red hue was obtained, probably due to the presence of several black bands, more evident in the S_F3 (Fe^o 3 g) than in the S_F4 (Fe^o 4 g). Moreover, the colour was not distributed through the entire sample, but only in the inner part was opaque red formed, while in the external part the colour was very dark.

Table 11.8. Results of the composition P_F in which Cu₂O addition was constant at 2 g, and Fe^o varied from 1 to 6 g.

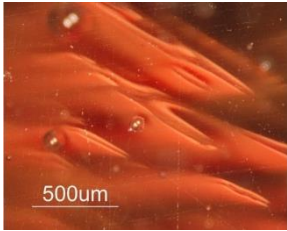
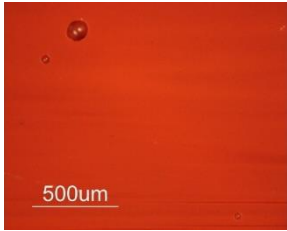
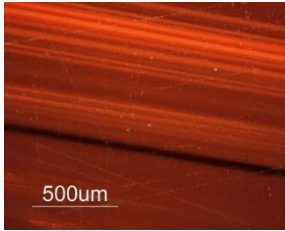
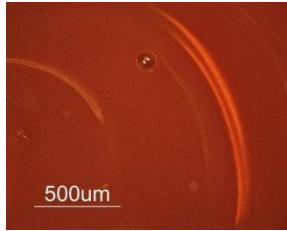
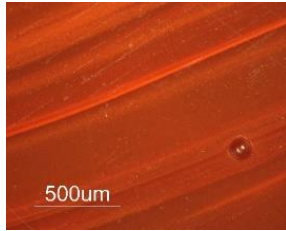
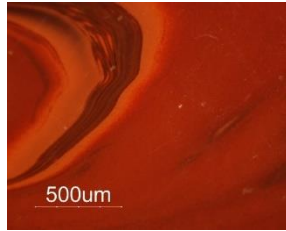
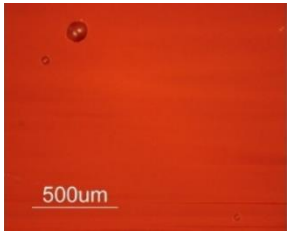
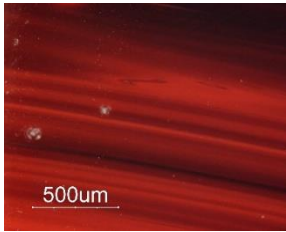
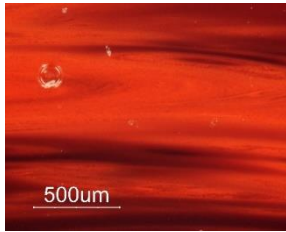
Sample	P_F1	P_F2a	P_F3	P_F4	P_F5	P_F6
Micrographs by OM						
Description	Several opaque red bands embedded in a transparent green glass	Homogenous texture	Heterogenous, composed by numerous layers of different red hues, from light red to brownish	Homogenous brownish glass, only few red layers	Orange-red-brown colour, and the formation of several red bands. Large undissolved metallic inclusion	Orange-red-brown colour, and the formation of several red bands. Large undissolved metallic inclusion

Table 11.9. Results of the composition P_S in which Cu₂O addition was constant at 1 g, and Fe^o varied from 1 to 5 g.

Sample	P_F2a	S_F3	S_F4
Micrographs by OM			
Description		The colour is darker than the samples P_F2a. The colour is not distributed homogeneously in the samples but composed by numerous red layers	Red hue slightly darker than P_F2a, probably due to the presence of several black bands. The colour is not distributed in the entire sample: external part very dark, the inner part red.

11.5 FORS spectroscopy

The FORS analyses exhibited different reflectance percentages, which decrease with the increase in the iron content (fig.11.1a). Indeed, the samples produced by P_FA3 and P_F2a, which are red, showed higher reflectance percentages indicating a lighter red hue than P_F3 (Fe° 3 g) and P_F4(Fe° 4 g). Sample P_F5 (Fe° 5 g) showed a slight increase in the reflectance percentage, suggesting a lighter red hue than P_F3 and P_F4. By calculating the first derivative it was possible to observe the corresponding inflection point of the FORS spectra (fig.11.1b), ranging between 579 and 585 nm in samples P_FA3 and P_F2a, and between 574 and 577 nm in samples P_F3, P_F4 and P_F5. According to the literature, these values can be assigned to the presence of metallic copper particles (Cu°) in the glass [1-3].

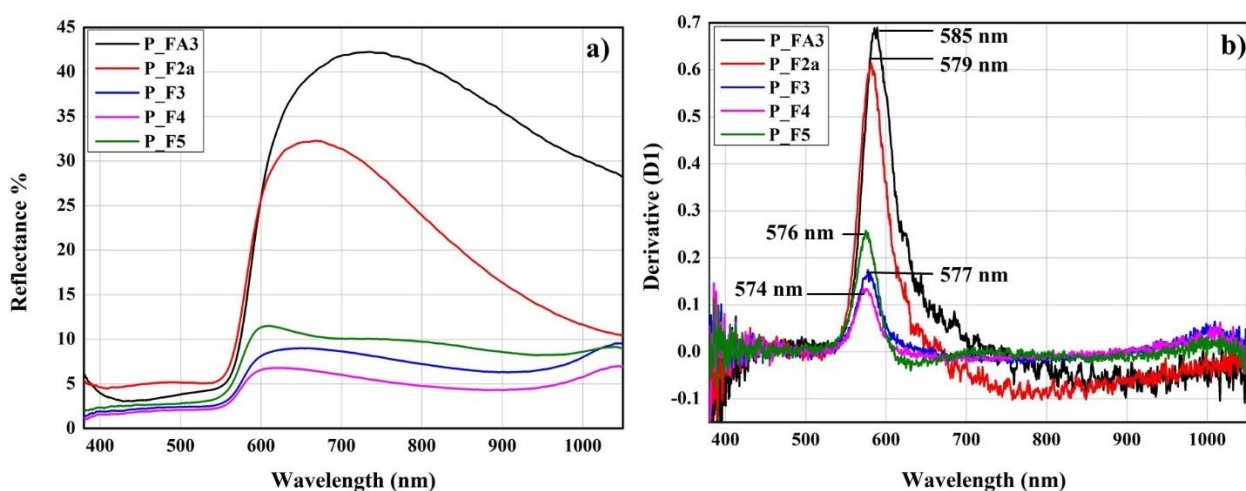


Figure 11.1. a) FORS spectra of samples P_FA3, P_F2a, P_F3, P_F4, P_F5; b) Spectra of the first derivative of samples P_FA3, P_F2a, P_F3, P_F4, P_F5.

11.6 Colorimetric measurements

The variation in the red hues due to the increase in the iron content was also observed through the colorimetric measurements (fig. 11.2a-b; table 11.10). This is clear from sample P_F2a (Fe° 2 g) and samples P_F3 (Fe° 3 g) and P_F4 (Fe° 4wt%) in which the coordinate a^* varied from 16 (P_F2a) to 7 (P_F3) and 8 (P_F4) respectively showing a fall in the red component in the glass. A comparison between P_F2a and samples P_F5 and P_F6 showed a slight decrease in the a^* values in sample P_F5 (a^* 11.2) while P_F6 (a^* 8.3) has values comparable with those of P_F3 and P_F4.

The values of coordinate b^* also varied, indeed in the red sample (P_F2a) it is 5.7 while it decreased in samples P_F3 (b^* 2.7) and P_F4 (b^* 2.8), and increased in samples P_F5 (b^* 7.4) and P_F6 (b^* 7.6) giving them a more orange hue than the red samples.

Sample P_F2a showed the highest brightness values (L^* 35) while in the other samples it decreased by values of about 32 (see table 11.10).

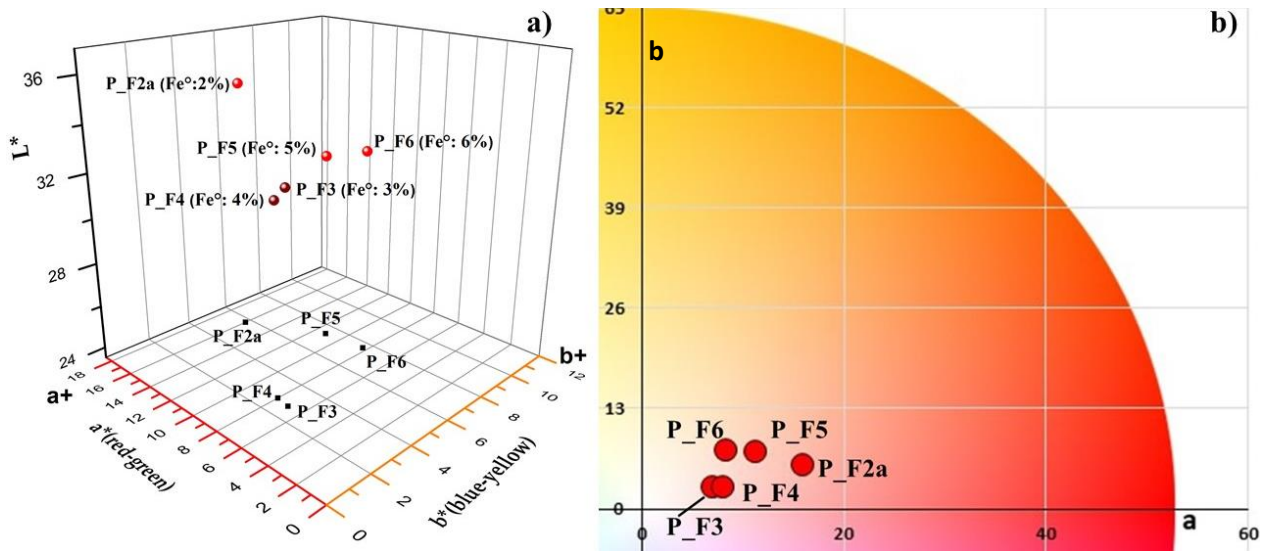


Figure 11.2. a) CIE Lab graphic representation: L^* a^* b^* chromatic coordinates of the samples (P_F) projected on the L^* a^* b^* space; b) CIE Lab graphic representation composed of the chromatic coordinate a^* (x axis) and b^* (y axis).

Table 11.10. Average colorimetric coordinates of the different compositions used in the tests.

Samples	Colorimetric Coordinates CIE $L^*a^*b^*$		
	L^*	a^*	b^*
P_F2a	35	16	5.7
P_F3	32.7	7	2.7
P_F4	32	8	2.8
P_F5	32.1	11.2	7.4
P_F6	32.7	8.3	7.6
S_F1	26.3	1.1	-2.7
S_F2	26.6	6.4	8.7
S_F3	30.1	10.3	13.4
S_F4	30.2	12.6	14.1

The colorimetric measurements in the samples produced by the P_S composition showed that an increase in the iron content raises the values of the b^* (orange component) varying between 8.7 and 14.1, which is higher than the previous composition (P_F the b^* varies between 5.7 and 7.6) (fig. 11.3a-b). The a^* coordinate (red component) is very low in the samples S_F1 (a^* 1.1) and S_F2 (a^* 6.4); while it increases in samples S_F3 (a^* 10.3) and S_F4 (a^* 12.6) which is still lower than the opaque red glass produced by P_F2a (a^* 16). In contrast, it is very close to the colour obtained by the P_F5 (a^* 11.2) composition.

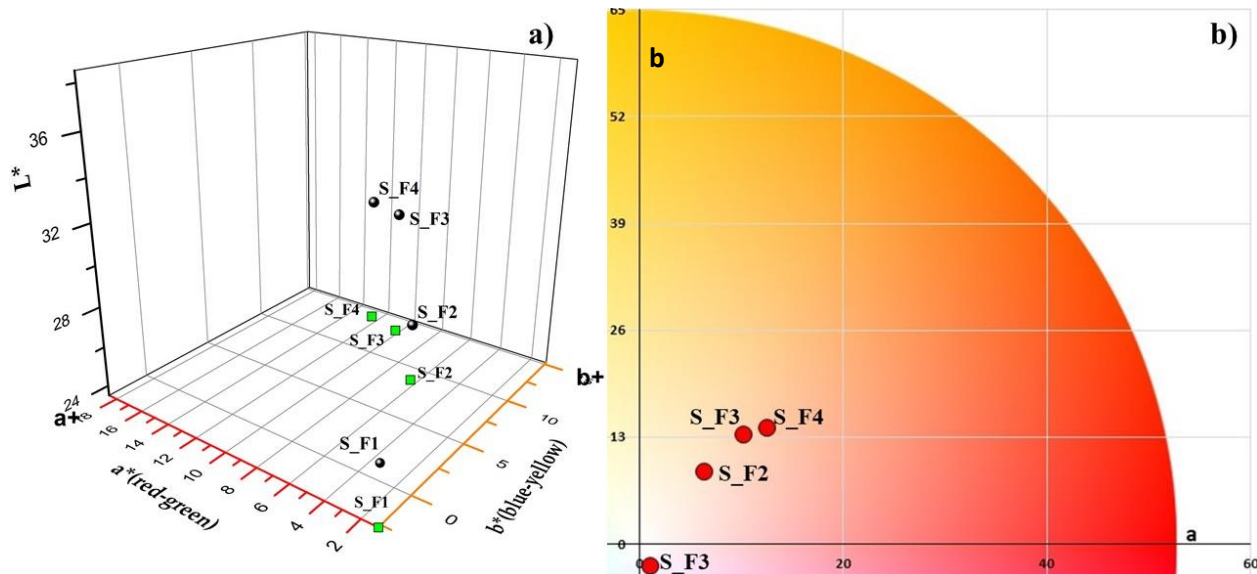


Figure 11.3. a) CIE Lab graphic representation: L^* a^* b^* chromatic coordinates of the samples (S_F) projected on the L^* a^* b^* space; b) CIE Lab graphic representation composed of the chromatic coordinate a^* (x axis) and b^* (y axis).

11.7 Raman spectroscopy and X-ray diffraction

Through Raman spectroscopy no colouring particles were detected. In contrast, only the spectra of the glassy phase were revealed. The spectra of samples P_FA3, P_F2a, P_F3, P_F4 and all the samples produced by S_F composition (with Cu_2O fixed at 1 g) exhibited high fluorescence (fig. 11.4a). Fluorescence is very common when copper-containing glass are analysed by Raman spectroscopy, as a result of the strong absorption of Cu° [4].

However, this fluorescence is not present in samples P_F1 (Fe° 1 g, and no opaque red was produced) and P_F5 (Fe° 5 g). They showed the main regions attributable to the bending mode ($400\text{-}500\text{ cm}^{-1}$) and stretching modes ($900\text{-}1000\text{ cm}^{-1}$) of the Si-O [4-6] (fig.11.5b). Nevertheless, as noted by Colomban, when only the characteristic peaks of the glassy phase are obtained by Raman spectroscopy on opaque red glass, it could indicate the presence of metallic copper nanoparticles. Indeed, the 532 nm laser (used in these analyses) was very close to the surface plasmonic resonance of metallic copper, which strongly absorbed at this energy, and only the signature of the Si-O bonds interacting with Cu° particles were observed [4].

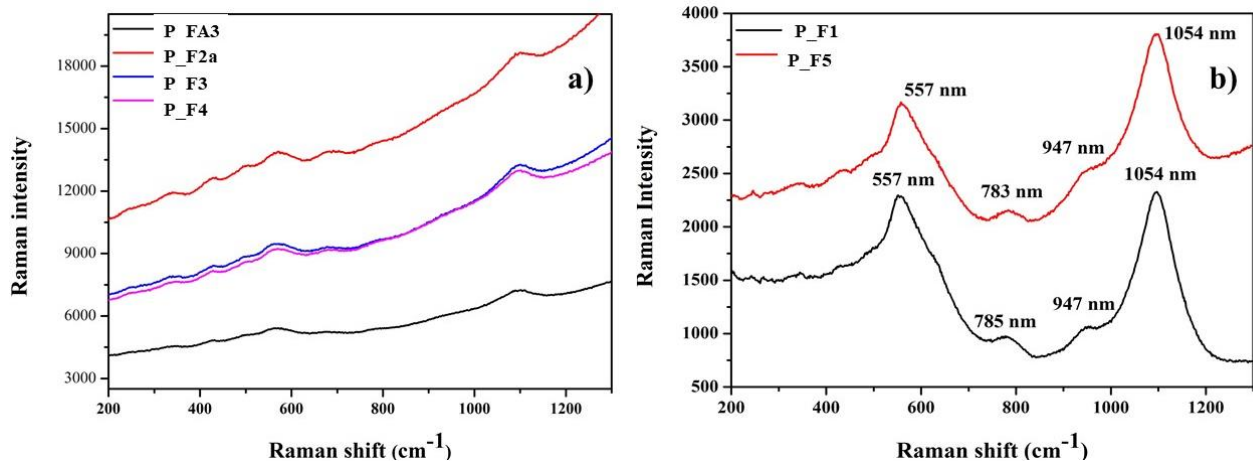


Figure 11.4. a) Raman spectra of the samples P_FA3, P_F2a, P_F3 and P_F4; b) Raman spectra of the samples P_F1 and P_F6.

Throughout the X-ray diffraction, it was possible to detect in samples P_FA3, P_F2a and P_F3 a broad peak between 20° and 30° (2Theta), typical of vitreous material, and two weak peaks at $d=2.09$, $d=1.81$ which were assigned to metallic copper (Cu^0) with cubic symmetry (fig. 11.5a-b).

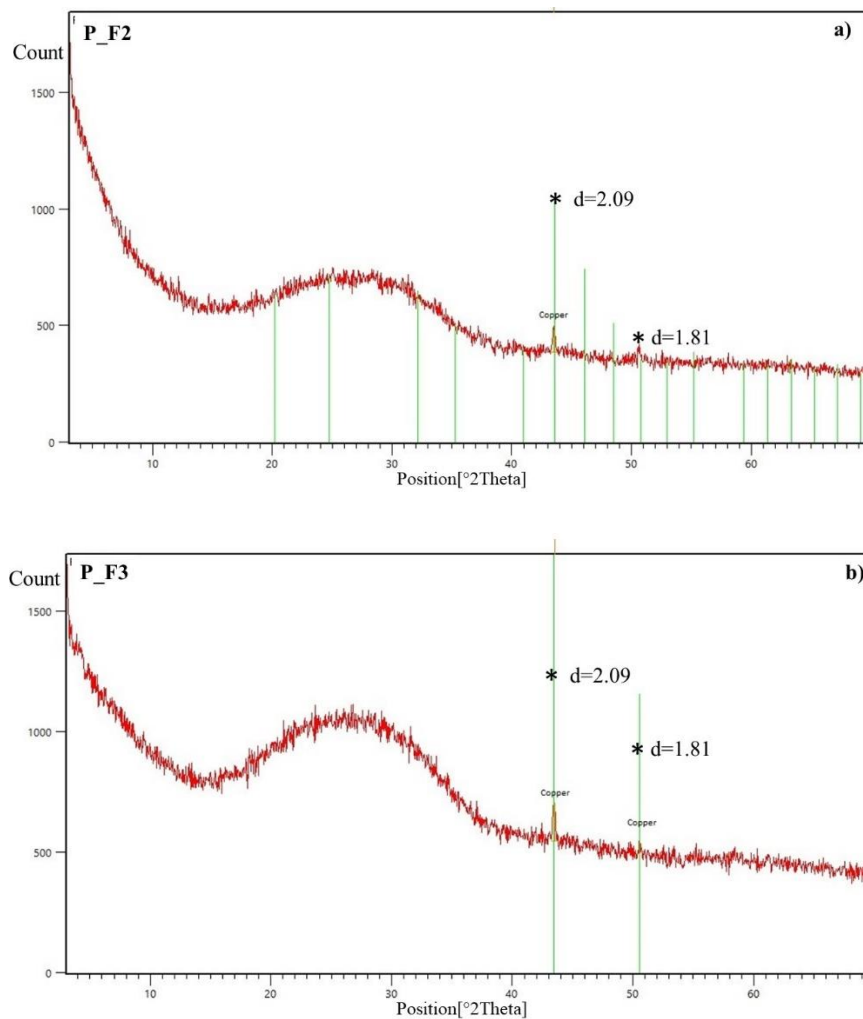


Figure 11.5. X-ray diffraction on the samples a) P_F2a and b) P_F3, showing typical peaks of metallic copper particles. No cuprite crystals were revealed.

11.8 Heat treatment

Through the TT-1 procedure, the P_F2 composition moved toward a brownish red hue, appearing more homogeneous without the presence of black layers or with different red hues (fig. 11.6a). By means of the TT-2 treatments, the colour continued to move towards darker brown hues (fig. 11.6b).

When the TT-1 treatment was applied to the P_F4 composition, an orange-brown colour was obtained (TT-1_P_F4) (fig. 11.6c), while by using the TT-2 treatment the sample moved toward a darker brown (TT-2_P_F4) (fig. 11.6d). However, the colour appeared very homogenous, and no bands of different red or brownish tones were observed. In samples TT-1_P_F4 and TT-2_P_F4, large amounts of undissolved metals on the bottom of the crucible were observed.

A comparison between samples P_F2 and P_F4 not subjected to heat treatments with the corresponding samples produced by the two heat treatments are reported in table 11.11.

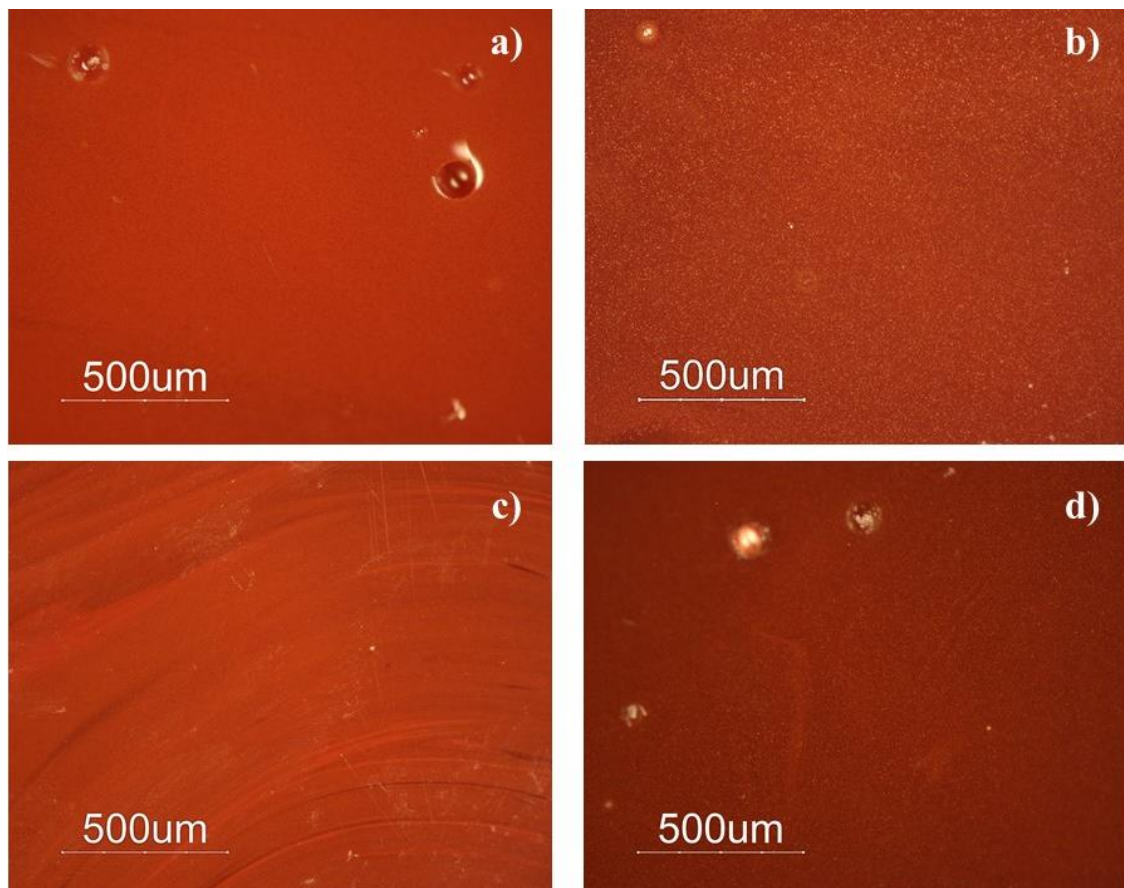
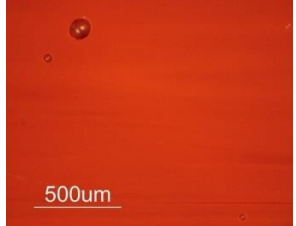
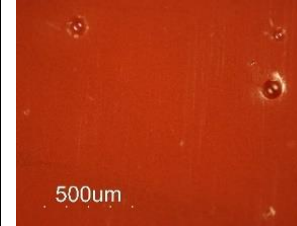
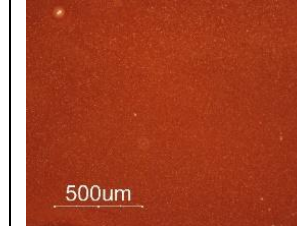
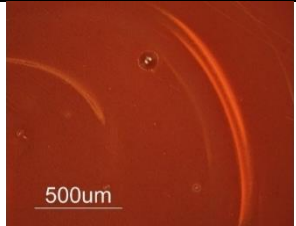
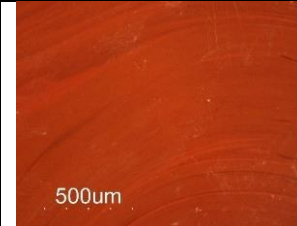
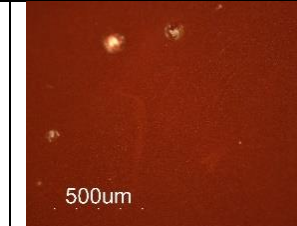


Figure 11.6. Optical microscope picture of **a)** TT-1 P_F2; **b)** TT-2 P_F2; **c)** TT-1 P_F4; **d)** TT-2 P_F4.

Table 11.11. Comparison of the optical microscope observation of the polished section of the samples obtained by the different heat treatments, using two different chemical compositions (P_F2: Cu₂O 2 g and Fe° 2 g; P_F4 Cu₂O 2 g and Fe° 4 g).

Trattamento termico	NT (non trattato termicamente)	TT-1	TT-2
Composizione chimica	Fe° 2 g; Cu ₂ O 2 g		
			
Coordinate colorimetriche	P_F2 - L*: 35; a*: 16; b*:5.7	TT-1_P_F2 - L*: 33.2; a*: 13.9; b*:9	TT-2_P_F2 - L*: 31.8; a*: 7.8; b*: 6.7
Composizione chimica	Fe° 4 g; Cu ₂ O 2 g		
			
Coordinate colorimetriche	P_F4 - L*: 32; a*: 8; b*: 2.8	TT-1_P_F4 - L*: 31.5; a*: 10.5; b*: 7.5	TT-2_P_F4 - L*: 29.6; a*: 7.2; b*: 5

Observing sample P_F2 at higher magnification and the corresponding samples TT-1_P-F2 and TT-2_P-F2, a gradual increase of the crystal sizes was observed, which became more visible by lowering the temperature of the heat-treatment. Indeed, in the F_P2 sample (not subjected to thermal treatments) it was not possible to distinguish the colouring particles. When the temperature was gradually lowered, the particles started to decrease in number and enlarge in size, and the colour moved towards a more brownish hue (11.7a-b-c).

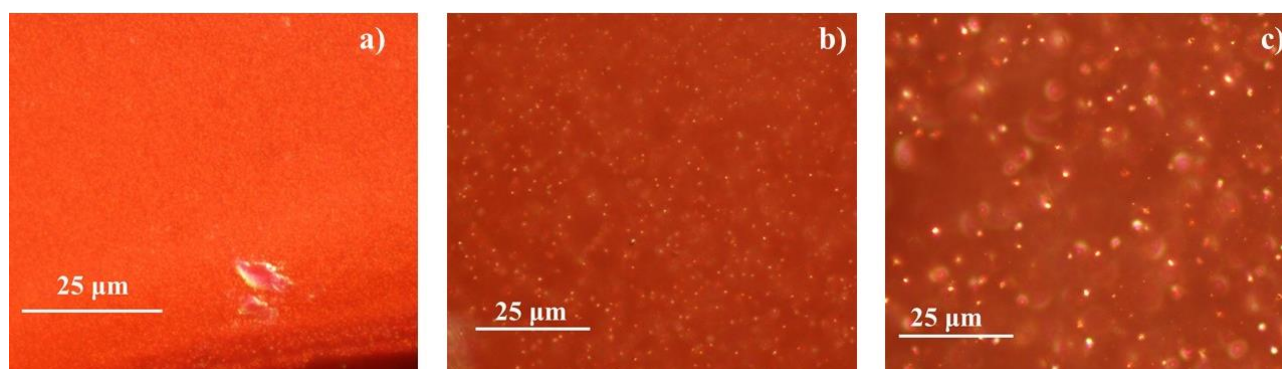


Figure 11.7. Optical microscope micrographs at 50X of magnification of a) P_F2a (no heat treatment); b) TT-1 P_F2; c) TT-2 P_F2.

When the colorimetric coordinates of the P_F2 not subjected to heat treatment were compared with the samples obtained by the TT-1 and TT-2 treatment, it was possible to observe significant differences (fig. 11.8; table 11.11). Although the brightness (L* 33.1) and the red component (a* 13.9) decreased in sample TT-1_P-F2, an increase in the values of the b* (8.7) coordinate was revealed, moving the colour of the TT-1_P-F2 sample toward a more orange-brown tone than the P_F2a.

In contrast, the TT-2_P-F2 composition produced a brown colour in which the colorimetric coordinates decreased (TT-2_P_F2: L^* 31.8; a^* 7.8; b^* 6.7) when compared with the P_F2a.

The TT-1_P-F4 showed an increase in both the a^* (8.6) and the b^* (5.6) coordinates, giving an orange-brown colour to the glass, although the brightness was lower than P_F4, and they appeared slightly darker.

The TT-2_P-F4 sample still exhibited slightly higher values of the orange component (b^* 5). However, both the values for the brightness (L^* 29) and the red component (a^* 7.2) decreased, producing a darker brown glass than TT-1_P-F4.

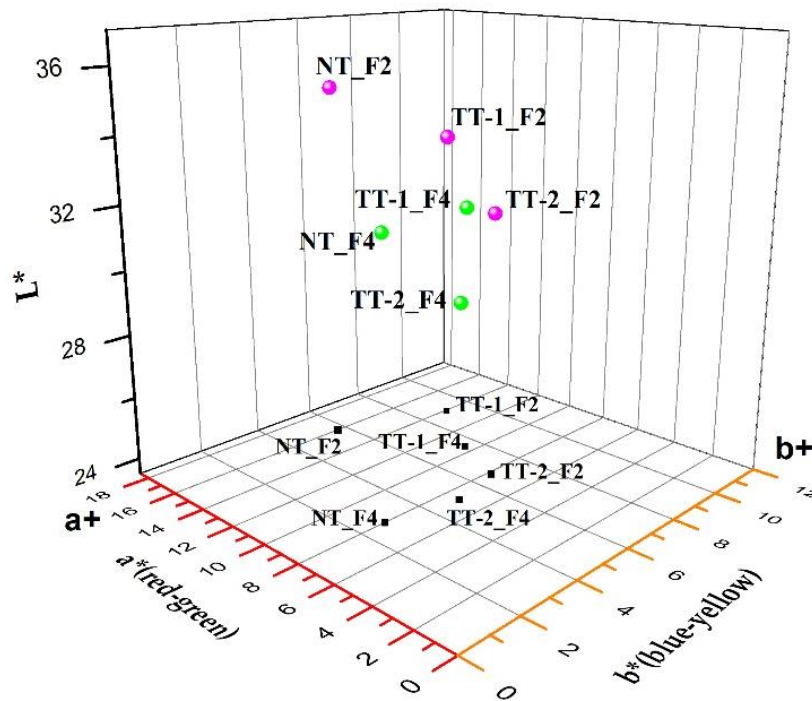


Figure 11.8. CIE Lab graphic representation: L^* a^* b^* chromatic coordinates of the samples produced by heat treatments, projected on the L^* a^* b^* space.

By Raman spectroscopy it was not possible to detect any peaks of metallic copper particles. However, the spectra showed the typical peaks of the soda-lime-silica glass suggesting the presence of metallic copper (fig. 11.9).

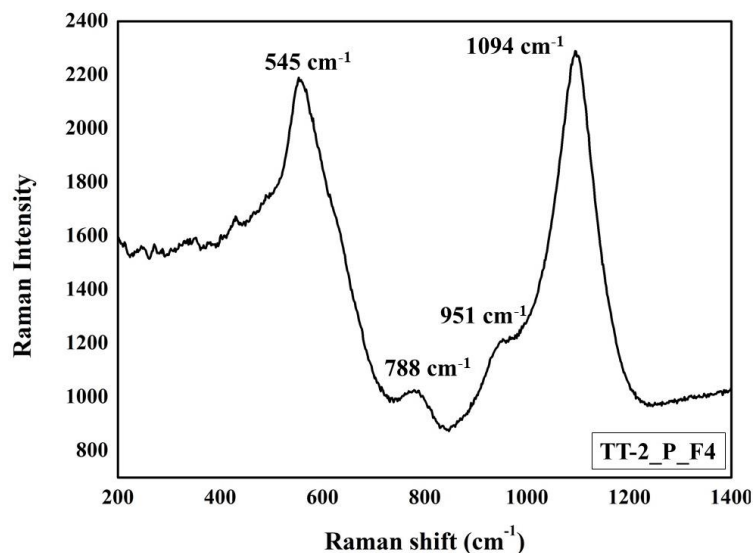


Figure 11.9. Raman spectra of the samples TT-2_P_F4.

Through the X-ray diffraction, two peaks were revealed, at $d=2.09$, $d=1.81$ which were assigned to metallic copper with cubic symmetry, which indicate that metallic copper particles is the colouring agent in these brown samples (fig. 11.10) - (it could be useful to investigate the dimensions and the number of these particles).

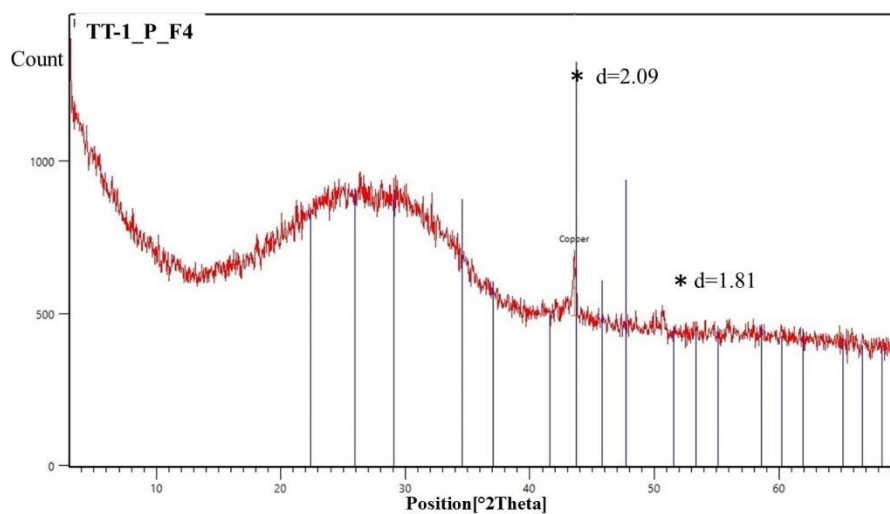


Figure 11.10. X-ray diffraction on the sample TT-1_F4, showing typical peaks of metallic copper particles. No cuprite crystals were revealed.

References

1. Aceto, M.; Agostino, A.; Fenogli, G.; Idone, A.; Gulmini, M.; Picollo, M.; Ricciardi, P.; Delaney, J.K. Characterisation of colourants on illuminated manuscripts by portable fibre optic UV-visible-NIR. Reflectance spectrophotometry. *Anal. Method* **2014**, *6*, 1488–1500.
2. Bacci, M.; Corallini, A.; Orlando, A.; Picollo, M.; Radicati, B. The ancient stained windows by Nicolò di Pietro Gerini in Florence. A novel diagnostic tool for non-invasive in situ diagnosis. *J. Cult. Herit.* **2007**, *8*, 235–241.
3. Möncke, D.; Palles, D.; Palamara, E.; Papageorgiou, M.; Kamitsos, E.I.; Zacharias, N. Coloring Vitreous Materials: Pigments. Colloids and Ions in Glasses and Glazes from the Mycenaean to Medieval Periods—probed by Spectroscopic Techniques. In *Proceedings of the Conference: 3rd ARCH_RNT Archaeological Research and New Technologies, Kalamata, Greece, 22–23 October 2010*; pp. 153–164.
4. Colomban, P.; Schreiber, H.D. Raman signature modification induced by copper nanoparticles in silicate glass. *J. Raman Spectrosc.* **2005**, *36*, 884–890.
5. Colomban, P.; Tourniè, A.; Ricciardi, P. Raman spectroscopy of copper nanoparticle-containing glass matrices: Ancient red stained-glass windows. *J. Raman Spectrosc.* **2009**, *40*, 1949–1955.
6. Cesaratto, A.; Sichel, P.; Bersani, D.; Lottici, P.P.; Montenero, A.; Salvioli-Mariani, E.; Catarsi, M. Characterization of archeological glasses by micro-Raman spectroscopy. *J. Raman Spectrosc.* **2010**, *41*, 1682–1687.

12. Discussion and Conclusions

The results underlined the complexity of the production techniques involved in manufacturing opaque red brown glass. The colour can be affected by several factors, as observed through the laboratory reproduction, which are often difficult to manage, namely achieving the correct oxidation state of the melt, as well as its homogeneity, the nature of the iron- and copper-bearing compounds used to produce it, how and when they have to be added and the amounts of the colouring and reducing agent used, and finally the heat treatment. All of these are parameters which influence the formation of colour, its hue and the homogenous distribution of the colour in the glass.

Although more experiments are required, the results show that the addition of colouring compounds to the batch produces unsatisfactory results, probably because they oxidised when reached the melting temperature, losing their reducing power.

It was highlighted that iron when added as ferrous oxide and/or metallic iron was able to form the colour, reducing the copper dissolved in the melt (Cu^+ or Cu^{2+}) to metallic copper (Cu^0). Hence haematite and magnetite could be ruled out as iron-bearing used in the production of opaque red; while pyrite, although often producing unsatisfactory results, needs more testing to establish its efficiency as a reductant.

More promising is the use of metallic iron, or metallurgical by-product produced by the hammering of incandescent iron could be used in the colouring technique adopted during the Roman Age to manufacture opaque red brown glass. As evidenced by the archaeometric investigations on black Roman glass, opaque red glass dated to the Byzantine period and to the Merovingian Empire, when iron-slugs were utilised. Moreover, this practice (to add iron-slugs to produce opaque red glass) was frequently recommended in Venetian treaties consulted in this research, which could reinforce the hypothesis that during the Roman Age, opaque red glass was also manufactured by adding a similar iron-bearing material.

However, the amounts of iron necessary to cause the formation of opaque red are fundamental to prevent the moving of the colour towards more brownish hues. It was noted that by increasing the amount of iron (by single addition), the colour of the glass moves towards a more brownish colour (P_F3, P_F4), which is often very heterogeneous with the formation of several layers of different hues from reddish orange to reddish brown. In other cases, too much iron content produced too strong reducing conditions favouring their precipitation (P_F5 and P_F6) in the melt.

Even when the correct amount of iron to add (P_F2) was established, the formation of opaque red was not guaranteed, as observed by the experimental results.

By using low copper content (1 g of Cu_2O), very dark opaque red glasses were obtained, which can not be considered good results, due to the extreme heterogeneity of their texture, and the formation of opaque red only in the inside of the samples. This composition needs still more tests. It is likely that the glassmakers started from a minimal addition of both iron and copper and empirically continued to gradually increase the amount of iron and copper until opaque red was formed. Hence, the good results were probably based on the empirical experience of the glassmaker and his/her skills in reproducing the same melting conditions.

A heterogeneous texture was frequently formed in the samples and the origin of this characteristic of the copper-red glass could be due to several factors. In some cases, the amounts of the reducing agent were probably not enough to encourage the precipitation of the Cu° (P_F1). In other cases, the redox conditions were probably not homogenous in the melt; or when the molten glass was poured, different cooling rates occurred causing distinct rates of nucleation and crystal growth. However, these are only theoretical speculations and more accurate analyses and laboratory reproduction are necessary to understand this point. The heat treatments made it possible to manufacture different red hues which moved from reddish-brown to the dark brown. The chemical compositions and the temperatures selected for the thermal treatment were crucial factors in obtaining different red hues. By using the chemical composition to obtain opaque red glass (P_F2), it was possible to obtain different gradations of red which originated mainly from the different crystal size. Indeed, in opaque red (P_F2) the crystals are not distinguishable by OM observation, while when the melt was held at 1000 °C (TT-1_P_F2) and 800 °C (TT-2_P_F2) the particles gradually enlarged and were detected by OM observation.

The heat treatments produced homogeneously coloured glass, and (although it is not the aim of this research) validate (in part) the recipe M110 found in the Montpellier manuscript in which a gradual increase of the reducing and colouring agent, and progressive lowering of the temperature were suggested for producing several red hues.

Using Raman spectroscopy, no crystalline phase and no cuprite peaks were detected, while through x-ray diffraction it was possible to identify only Cu° particles, which can be considered the main colouring and opacifying agent of these laboratory samples. Research performed with FEG-SEM could help to understand more deeply the relationship between the size and number of the particles and the variation in colour.

In conclusion, this research attests that the conjunction between laboratory reproduction, archaeometric data from the literature and the consultation of ancient recipes can be a fruitful practice to understand some aspects of the technological production of opaque red brown glass.

The results obtained from the various experiments helped in understanding the main problems that ancient glassmakers had to face and solve. Moreover, the experimental results could be helpful to better interpret the chemical composition of opaque Roman red glass.

The ancient Venetian glassmaking recipes were revealed to be helpful and a good source for investigating the technical aspects of coloured glass production in ancient times.

However, this work will need further experiments involving different chemical compositions of the base glass (maybe using soda plant ash), other reducing agents or employing more than one reducing agent. Future tests could involve the use of different copper- and iron bearing, or the manipulation of the temperature and cooling rate of the heat treatments to investigate the effects on colour.

MAIN CONCLUSIONS

This study has highlighted how complex and sophisticated is the production of opaque red glass. Over the centuries, the chemical composition, the raw materials, colouring agents and the production technology have changed. These adjustments were probably based on the development in knowledge about furnaces, such as the introduction of new raw materials which brought technical benefits.

During the 2nd century AD, it can be established that two types of opaque red glass were in circulation and were produced: sealing wax and red brown. They represent two distinct technologies. Indeed, to produce sealing wax red glass, high concentrations of copper and lead were necessary to create/form dendritic crystals of cuprite. Moreover, specific control of the melting conditions including the timings, temperature and furnace atmosphere was required to facilitate the formation of this opaque red glass, produced since the 9th century BC. Simultaneously, red brown glass was manufactured, which has a different chemical composition, colouring agent (sub-micrometric particles of metallic copper) and probably different melting procedure, something that is still not completely understood. It is likely that the control of the raw materials and a well-engineered chemical composition were crucial factors in making red brown.

However, the samples from the Lucius Verus villa showed a wide range of red hues, from brick red to sealing wax, from reddish brown to dark red, highlighting the advanced technical skills of the Roman glassmakers. Indeed, each red hue is the result of a specific chemical composition, control of the raw materials and the conditions of the furnaces which involved changing temperatures and timings for each red hue.

Some samples have a base glass chemical composition different from the typical Roman natron glass, and it still represents an unresolved question. In this study, an alternative hypothesis or at least a different point of view has been proposed. This could imply a different organisation of the glassmaking industry in the Roman Age (1st-4th century AD) and could indicate that more than one recipe was used to produce opaque red. Moreover, the probable use of a different fluxing agent points out the presence, somewhere in the Empire, of workshops specialised in the production of opaque red glass and using the own raw glass. However, it is important to remark that this is only a hypothesis and more archaeological evidence are necessary to take in consideration this hypothesis, as well as specific laboratory reproductions which attempt to adopt this recipe to make opaque red.

As future proposal to continue the study of these opaque red glass (*Lucius Verus* villa), should be the identification of the production centres. It is a very difficult task, but maybe with further archaeological information or more data analyses could be possible to understand where they were made.

The laboratory reproduction allowed to understand the complexity to make opaque red glass. They helped to identify the probable procedure used by the ancient glassmakers. The tests allowed to valid the Venetian glassmaking manuscripts, which unveiled the raw materials, and especially the method, the protocol required to make opaque red glass. On the other hand, they (the Venetian manuscripts and the laboratory results) highlighted that, good results were extremely dependent on the knowledge of the glassmakers, which probably kept their recipes secret.

Although, this study answered to the objectives fixed at the beginning of the PhD project, the investigation on opaque red glass cannot be considered concluded. More chemical analyses, such as more laboratory reproductions are required to understand better the ancient production technology. Indeed, testing several base glass compositions made by different raw materials, observing how the base glass composition affects the formation of red colour represent another future propose. Moreover, the use of raw materials similar to those used in ancient times, could show which technical benefit that they could give to the production of opaque red. With its results, considerations and data analyses, I hope that this manuscript may be useful for future investigations and researchers who will study Roman opaque red glass, and has added a new brick to better understand the production technology of opaque red glass during the Roman Age.

APPENDIX

A. How many recipes were there for manufacturing red brown during the Roman Age (1st-4th century AD)? Raw glass, colouring techniques, trade and production

A.1. Introduction

The chemical analyses of opaque red brown glass (Gr-1 group) from the Lucius Verus villa revealed concentrations of K₂O and MgO of about 3wt%, and P₂O₅ of about 1 wt%. These values are unexpected for a natron base glass, raising questions about the organisation of the glassmaking industry. Indeed, the literature has established that natron was the main fluxing agent in the Mediterranean basin since the 5th century BC and during the Roman and Byzantine Age [1, 2]; while soda plant ash base glass was widely used in the Late Bronze Age and never stopped in the Mesopotamian/Persian region [3-5].

The use of soda plant ash as a fluxing agent in the Mediterranean basin was re-introduced from the 8th - 9th century AD, followed by a long period of transition (from natron to soda plant ash) [6]. Natron glass was also found in mosaic tesserae dated to the 12th century, highlighting how long the transition period was [7].

It is thought that the glassmaking industry during the Roman Age was strongly centralised. Indeed, according to archaeological excavations and archaeometric investigations, scholars have established that the glassmaking industry was organised into two stages of production : a) large tanks (primary furnace), producing tons of raw glass; b) the primary furnaces supplying various workshops (secondary furnaces) spread across the Empire that remelted the raw glass to shape or colour it.

This organisation explains the compositional homogeneity of Roman and Byzantine glass. In a well standardised and centralised production organisation, the high potash, magnesia and phosphorus content present in some coloured glasses are considered anomalies.

In order to attempt to explain these anomalies, two main branches were formed in the literature (mentioned in chapter 8) which supported two theses, sometimes in contrast to each other.

a) Some of the writers interpreted the content of K₂O and MgO being higher than 1.5 wt% (the maximum limit for natron base glass) as the result of adding fuel ash to the molten natron glass in order to reach the reducing conditions necessary to facilitate the precipitation of metallic copper (Cu⁰). Due to the presence of carbon or charcoal (strong reductant [8]) in the fuel ash, its addition could bring some technical advantages for manipulating the internal redox conditions. Furthermore, the amounts of K₂O and MgO are often slightly higher than 1.5 wt%, while the unambiguous values for the use of soda plant ash glass had to have been higher than 2 or 2.5 wt% [8]. Moreover, the concentration of P₂O₅ is higher than the usual values detected in the typical soda-plant ash from the medieval period. This theory has been supported by Freestone [10] who analysed opaque red canes present in mosaic glass fragments from the 1st century BC/AD, Fiori [11], Maltoni [12], Paynter [13], and Fiorentino [14] studying mosaic tesserae in Ravenna, Aquileia, Padova, Trento, and West Clacton from the 2nd century AD to 5th/6th century AD.

According to Schibille, the high values of K_2O , MgO and P_2O_5 are due to the intensive recycling of the glass (cullet glass, waste glass) [15-18]. The prolonged melting period used in the secondary furnace to manufacture opaque red glass could suggest pollution by contaminants from the fuel ash [14]. This hypothesis is supported by the study by Paynter [19], who highlighted that the glass during the melting process (in a secondary furnace, thought to be smaller than the primary furnace) was contaminated by the vapour or gases released from the wood fuel which are mainly rich in calcium and potash. The experiments showed that the concentration of K_2O in the glass increased after 54 hours of melting. However, the P_2O_5 content was not revealed by the analyses, while the MgO concentration seemed not to be affected by the prolonged melting period.

In continental Europe during the Medieval period, trees such as beech, bracken and oak were the main fuel for the glass furnace [20, 21]. During the Roman period it is difficult to identify which type of tree was used. Barford recently proposed the use of nuts from olive oil, produced during the extraction of olive oil. Indeed, several of these residues were uncovered close to glass furnace evidence [18]. Nevertheless, Georges Sandys noted that special shrubs were used to fuel the furnace. However, these compounds are rich in potash, calcium, manganese, phosphorus, and poorer in sodium, and showed concentrations similar to those detected in the wood ash used in continental and northern Europe since the medieval period. Also in this case, the chemical composition of these ashes is extremely variable and are affected by the nature of the soil, the season in which they are harvested, the type of tree, and how they were burnt (temperature, oxidation state of the furnace atmosphere, timing etc...) [20, 21].

These hypotheses support the idea that coloured glass production took place “locally” in secondary workshops spread cross the Empire, in which raw glass was re-melted (or recycled) and colourant or opacifier agents were added.

b) Other writers have advanced an alternative theory which supports the manufacture of a specific colour by using soda plant ash as a fluxing agent. Emerald green, black, opaque red and orange glass are the main colours in which these anomalous values have been observed. All these colours require a careful manipulation of the redox conditions and are coloured by copper. Jackson [22] analysed emerald green glass in depth and suggested that they were manufactured by soda plant ash fluxing agents, probably because they were technically beneficial. High K_2O , MgO and P_2O_5 in emerald-green glasses were detected in Adria, Pompei and Bastanis showing almost the same compositional characteristics [23-25].

Nenna and Gratuze analysed several *millefiori* glass samples from the 3rd century BC to 3rd century AD, which were sampled in several parts of the Roman Empire and Mediterranean basin, and they detected a considerable amount of opaque red glass with values of MgO and K_2O ranging between 1.6 wt% to 3 wt% and P_2O_5 0.72-2.50 wt% [26]. Nenna suggested that they are soda-plant ash base glasses and due to the high glassmaking knowledge and skills required by this colour, opaque red glass was produced in specialised workshops.

Verità, studying mosaic *tesserae* and glass *opus sectile* from the 3rd-4th century AD in Rome, found the coexistence of opaque red glass *tesserae* with high MgO and K_2O (both > 2wt%, P_2O_5 0.60-1.2 wt%) and other *tesserae* with the typical Roman natron glass (MgO and K_2O < 1.5 wt%, P_2O_5 0.10-0.20 wt%) [27, 28]. He suggested that the high MgO and K_2O content was due to the use of soda plant ash. As it contained

carbonaceous residues, it would help to reduce the partial pressure of the oxygen inside the melt, necessary to obtaining the metallic copper nanoparticles. Indeed, Verità noted that in the “anomalous” red brown *tesserae*, the concentration of iron (the main reducing agent in red brown) is usually lower than that detected in the typical natron opaque red glass.

These hypotheses imply that specific coloured glass was probably produced by using raw glass. The coloured glass (in this case opaque red) would be produced in the form of canes/rods, cakes or ingots and traded [22, 27, 28].

Cagno detected concentrations of MgO and K₂O higher than 1.5 wt% in black glass from the 2nd century AD. He proposed that glass with these anomalous values was probably manufactured in specific workshops located on the edge of the Roman Empire, which were affected by the glassmaking tradition of the neighbouring empires (such as the Sassanian Kingdom) that were accustomed to melting the glass by adding soda-plant ash [29].

The debate between these contrasting hypotheses is still unresolved and underlines that glass production in the Roman Age (especially between 1st-4th century AD) is still far from being completely understood. Due to the lack of archaeological evidence or written texts which help comprehension of the “anomalous” values, it is not possible to find a definitive resolution of this debate.

This chapter aims to investigate opaque red glass produced from the 1st century BC/AD until the 4th century AD, identifying factors which could be helpful to finding a clearer perspective on this controversial issue. The opaque reds of the Roman Age were compared with those of the Byzantine and Medieval period to find similarities, continuity or breaks among these periods and to understand better the Roman period.

The 421 analyses of red brown glass collected from the literature, and already reported in chapter 3.2.3. were used to investigate in more depth the presence of anomalies in chemical compositions and attempt to identify their origin.

A.2. Methodology

According to the potash (K₂O) and magnesia (MgO) concentration established (conventionally) by the literature [9] and using the reduced composition [30], the samples from the literature were divided into three main groups:

- a) samples with values of K₂O and MgO below 1.5 wt%, are designated the NA group.
- b) samples with values of K₂O and MgO included between 1.5 and 2 wt% are designated the INT group.
- c) the samples which show K₂O and MgO content higher than 2% are designated the PA group.

A.3. Results

A.3.1 Base glass

Fluxing agent

When K₂O and MgO are plotted on a binary graph, the Roman opaque red glasses are divided into two main parts: opaque red with K₂O and MgO > 2wt% (PA group) located in the range of the typical soda-plant ash values, while in the lower part are the natron opaque red glass (NA group). A third group is placed in the middle, with intermediate concentration of potash and magnesia, which are higher than 1.5 wt% but lower than the typical values found in the plant ash (K₂O and MgO > 2 wt%) (INT group) (fig. A.1a). Moreover, PA and INT groups showed concentration of P₂O₅ higher than 0.5 which markedly separates them from the NA group (fig. A.1b). These values suggest the possibility that two different fluxing agents were used to manufacture NA and PA red brown glass, while the identification for INT group samples is more complex.

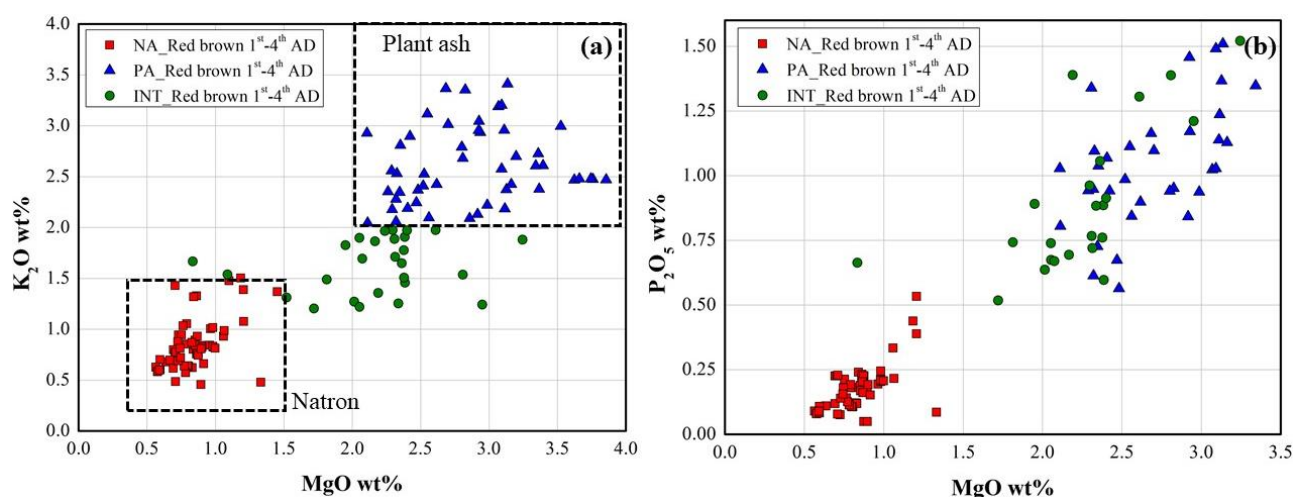


Figure A.1. Bi-plot of weight % a) potash (K₂O) versus magnesia (MgO) (reduced composition) and b) phosphorus (P₂O₅) and magnesia (MgO) (reduced composition) in opaque red glass between the 1st century AD and the 4th century AD.

As can be observed in table A.1, the base glass compositions of the three groups are well distinguished not only for the K₂O and MgO content, but also by the other major and minor elements.

Table A.1. Average chemical composition (reduced composition) of opaque red glass (mosaic tesserae, *opus sectile*, rods/canes) from the 1st century AD to 4th century AD.

Group	Date		SiO ₂	Al ₂ O ₃	Na ₂ O	K ₂ O	CaO	MgO	SO ₃	P ₂ O ₅	Cl	TiO ₂	Fe ₂ O ₃	MnO
PA group	1 st -4 th AD	AV.	64.6	2.3	13.9	2.6	9.4	2.8	0.08	0.80	0.62	0.17	1.9	0.50
		S.D.	2.0	0.54	1.50	0.45	1.10	0.47	0.16	0.59	0.49	0.08	0.63	0.15
NA group	1 st -4 th AD	AV.	65.6	2.8	17.2	0.86	7.5	0.88	0.12	0.18	0.89	0.12	3.1	0.63
		S.D.	1.56	0.44	1.41	0.27	1.17	0.25	0.21	0.16	0.40	0.06	1.06	0.37
INT group	1 st -4 th AD	AV.	63.8	2.9	15.1	1.9	9.0	2.1	0.06	0.85	0.78	0.23	2.6	0.50
		S.D.	1.96	0.52	2.13	1.61	1.62	0.51	0.14	0.44	0.41	0.14	0.83	0.26

From the binary graphs in fig. A.2a-b Na₂O showed a negative tendency with K₂O and CaO content, and the two groups appeared to be well separated. Indeed, the PA group is located down to the right-hand side with a concentration of Na₂O lower than 15 wt%. In contrast, the NA group samples exhibited concentrations of Na₂O higher than 16 wt%. The concentration of CaO in the PA group samples is usually higher (CaO 8-12 wt%)

than the NA group samples (CaO 6-9 wt%) which could indicate the use of two different fluxing agents. The INT group showed variable concentrations of sodium (Na_2O 12-18 wt%) and calcium (CaO 6-13.5 wt%) and are comparable with both NA and PA groups, making this group ambiguous.

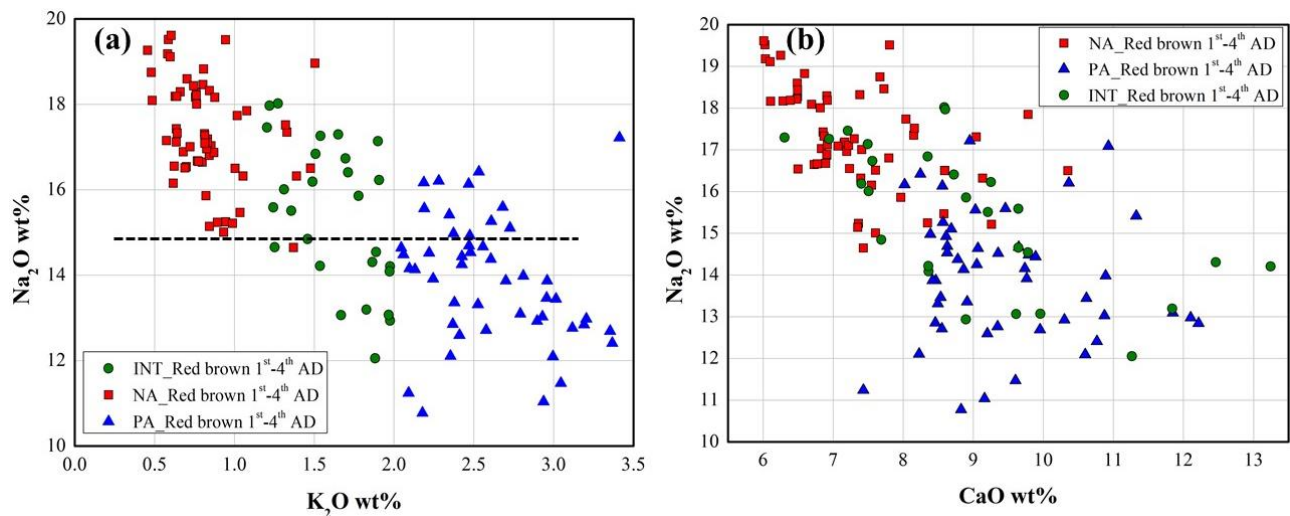


Figure A.2. Bi-plot/Binary graph of **a)** weight % sodium oxide (Na_2O) versus potash (K_2O) (reduced composition); **b)** weight % sodium oxide (Na_2O) versus calcium oxide (CaO) (reduced composition), in opaque red glass between the 1st century AD and the 4th century AD.

The PA and INT group samples exhibit a higher concentration of Sr (Sr 560 and 840 ppm) than the NA group samples (Sr 300-630 ppm). Sr content is positively correlated with CaO (fig. A.3a). No clear tendencies were observed when the concentrations of Ba were plotted against the CaO content (fig. A.3b).

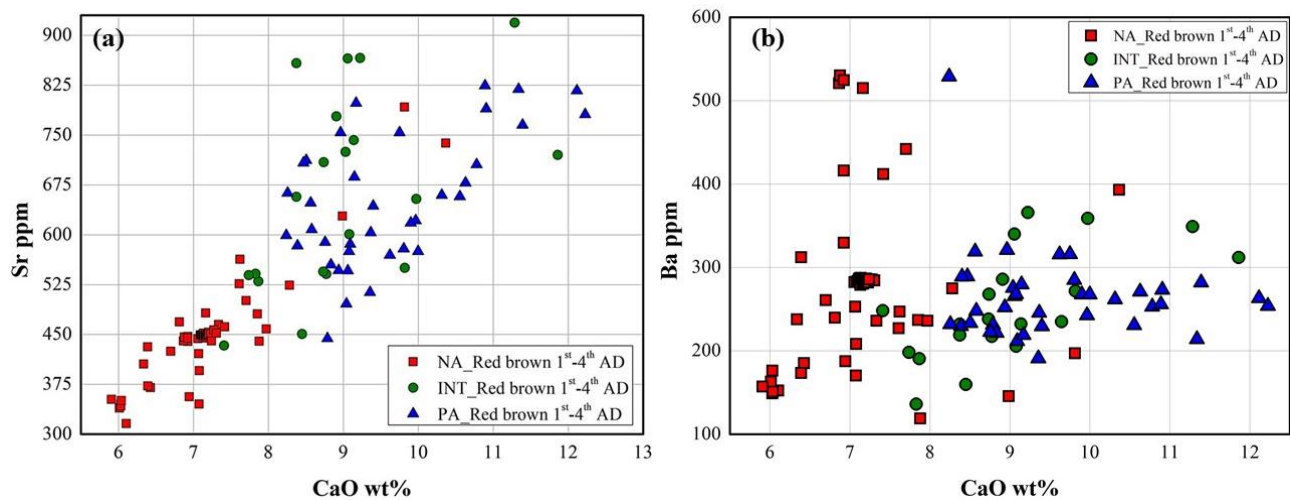


Figure A.3. **a)** Binary graph of Strontium ppm versus weight % of calcium oxide (CaO) (reduced composition), **b)** binary graph of barium (Ba ppm) versus weight % of calcium oxide (CaO) (reduced composition), in opaque red glass between the 1st century AD and the 4th century AD.

Moreover, the Ba content in the PA group is higher (Ba 200-300 ppm) and is located in a “narrow” range, evident when compared with MgO content, without showing any correlation (fig. A.4a). INT group samples with high magnesia ($\text{MgO} > 2$ wt%) exhibit concentrations of Ba comparable with PA group. On the other

hand, the NA group is split into two groups: one between 100 and 200 ppm, showing a positive tendency with MnO, and another ranging between 200 and 500 ppm which does not exhibit correlation with MnO (fig. A.4b).

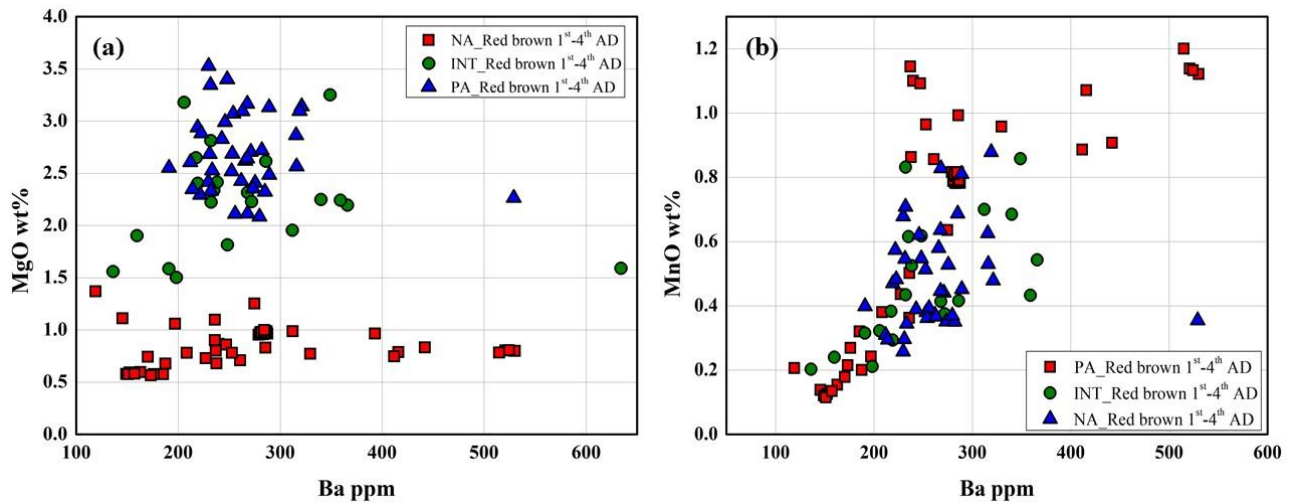


Figure A.4. Binary graph of (a) weight % of magnesia (MgO) against barium (Ba) ppm, (reduced composition); (b) weight % of manganese oxide (MnO) versus barium (Ba) ppm (reduced composition), in opaque red glass between the 1st century AD and the 4th century AD.

The PA group samples usually showed lower concentration of alumina (Al_2O_3 1.1- 2.7 wt%) than NA (2.0-3.5 wt%) and INT (2.5-4.0 wt%) groups samples, while titanium is usually slightly higher in the PA group (TiO_2 0.12-0.25 wt%) than the NA group (0.08-0.15 wt%, except a few samples). The two groups are clearly separated (fig. A.5) suggesting the use of a different silica source, while INT group samples showed comparable values with the two main groups.

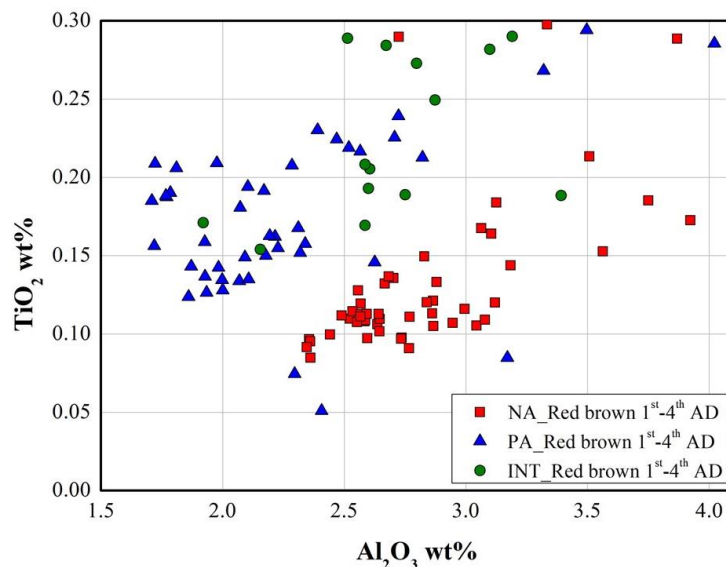


Figure A.5. Binary graph of weight % titanium oxide (TiO_2) versus alumina (Al_2O_3) (reduced composition), in opaque red glass between the 1st century AD and the 4th century AD.

It is thought that in red brown production technology, iron should be intentionally added into the batch or to the molten glass as a reducing agent. Consequently, the high values of iron detected in opaque red glass should

not represent the iron-rich minerals present in the silica source. Nevertheless, when Fe_2O_3 are plotted on a binary graph (fig. A.6) against TiO_2 content, NA and PA samples exhibit different trends. The NA samples showed the highest content of iron and no correlation or positive tendency with TiO_2 , which suggests that iron entered through some Fe-bearing material, deliberately added as a reducing agent. On the other hand, the PA group samples exhibit lower iron content (usually < 2 wt%) and seem to be positively correlated with titanium in most of the samples.

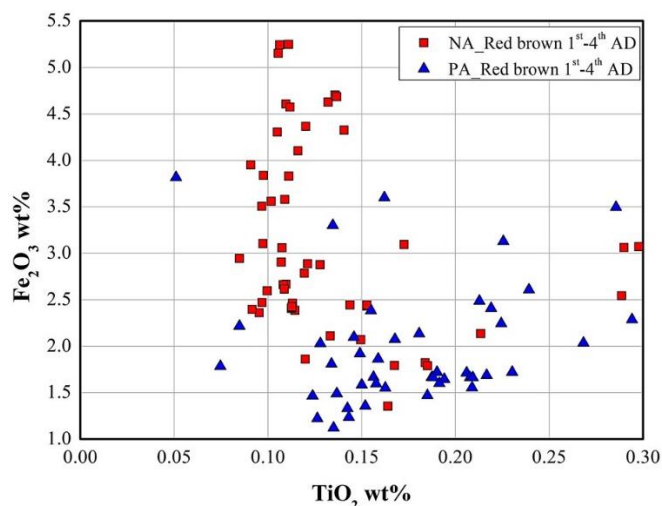


Figure A.6. Binary graph of weight % iron oxide (Fe_2O_3) versus titanium oxide (TiO_2) (reduced composition), in Roman opaque red glass (1st - 4th century AD).

A.3.2 Colouring and reducing agents

PA samples are usually richer in copper ($\text{CuO} > 1.5\text{wt}\%$) and poorer in iron (Fe_2O_3 1.5 and 3wt%) than NA samples (CuO 0.50 – 3 wt%; Fe_2O_3 1.8 – 4.7 wt%). INT group samples showed values of CuO and Fe_2O_3 comparable with those of the PA and NA groups.

Lead content varies widely in the three groups from small amounts up to 15-20 wt%. Tin oxide rarely surpasses 1 wt% and it is often detected lower than 0.6 wt%.

The mean concentration of the colouring and reducing agents are reported in table A.2, which is divided according to the main types of glass item.

Table A.2. Average chemical composition (weight %) of opaque red glass (mosaic tesserae, canes/rods, and *opus sectile*) from the 1st century AD to 4th century AD.

PA group		Fe_2O_3	CuO	PbO
1 st AD – 4 th AD				
Tesserae	Av.	1.82	2.16	5.98
	St.Dev.	0.45	1.52	3.59
Canes/rods	Av.	2.13	1.73	6.58
	St.Dev.	0.63	0.35	1.98
Opus sectile	Av.	1.53	2.36	1.53
	St.Dev.	0.32	0.43	2.83
NA group				
1 st AD – 4 th AD				
Tesserae	Av.	2.96	1.35	3.51
	St.Dev.	0.96	1.12	4.58
Canes/rods	Av.	1.93	1.88	8.15

	<i>St.Dev.</i>	0.56	0.63	7.80
Opus sectile	Av.	2.64	1.76	7.95
	<i>St.Dev.</i>	0.06	0.96	3.15
INT group				
1st AD – 4th AD				
Tesserae	Av.	2.08	2.91	4.59
	<i>St.Dev.</i>	0.64	2.98	2.91
Canes/rods	Av.	2.56	1.99	9.46
	<i>St.Dev.</i>	0.61	0.54	5.38
Opus sectile	Av.	3.00	2.05	14.78
	<i>St.Dev.</i>	0.60	0.45	5.22

A.4 Discussion

A.4.1 Base glass

A.4.1.1.1 A simple anomaly?

The number of PA samples is slightly lower than those contained in the NA group during the Roman Age (1st-4th century AD) while in the Late Antique (5th-8th c. AD), the number of PA samples decreased (fig. A.7), and increased again in the period between 9th-13th century AD in which the number of NA samples decreased considerably. Hence, the PA group should not be considered a simple anomaly but a practise well consolidated during the Roman Age. According to the compositional differences, as underlined through the comparison of the data collected from this research, it was thought that different raw materials were used both for the base glass and for the colouring and reducing agents. Although it is not possible to establish if soda plant ashes were used as a fluxing agent, due to the lack of clear archaeological evidence or written technical sources, this evidence implies the existence of at least two main recipes adopted to manufacture red brown glass during the Roman Age (1st-4th century AD).

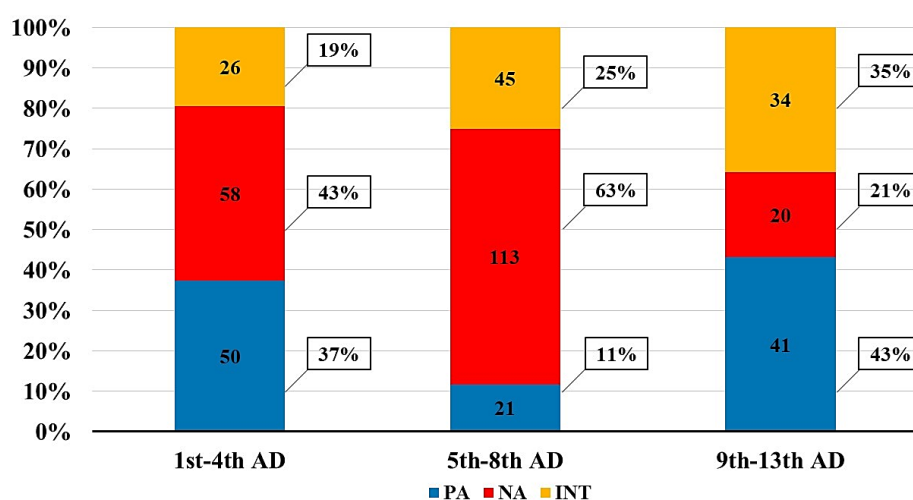


Figure A.7. Histogram showing the number of PA, NA and INT samples reported in the literature and divided into three different periods: Roman Age (1st-4th c. AD); Lat Antique (5th-8th c. AD); Medieval (9th-13th c. AD).

When the PA samples were compared with the medieval opaque red glass (9th-13th c. AD), they showed comparable concentrations of potash and magnesia (fig. A.8), suggesting that a similar fluxing agent was used.

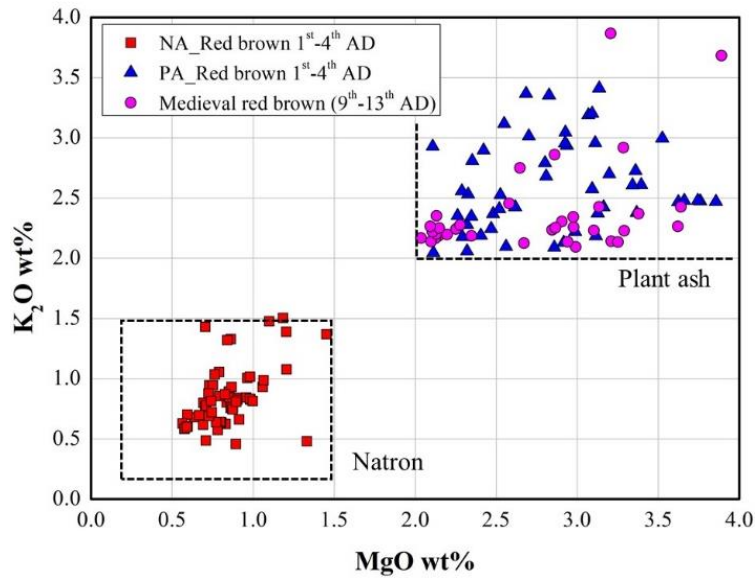


Figure A.8. Binary graph with the concentration of potash (K_2O wt%) versus magnesia (MgO) (reduced composition) content detected in the Roman PA and NA samples (1st-4th c. AD), and medieval opaque red glass (9th-13th c. AD).

A comparison between the PA samples with the naturally coloured soda-plant ash dated between the 3rd – 12th century AD in the Levantine region or in the Mesopotamian area (fig. A.9) exhibits comparable concentrations of K_2O and MgO.

However, PA samples have similar values of K_2O and MgO with the early Islamic glass made mainly in the region of modern-day Syria and northern Iraq, as well as with some samples from Damascus, Beirut and Khirbat al-Minya [31]. Compositional similarities were observed between the PA samples and samples from the early Islamic Egyptian (8th-10th century AD) glass [32] and from the site at Ramla (7th-12th century AD) [33].

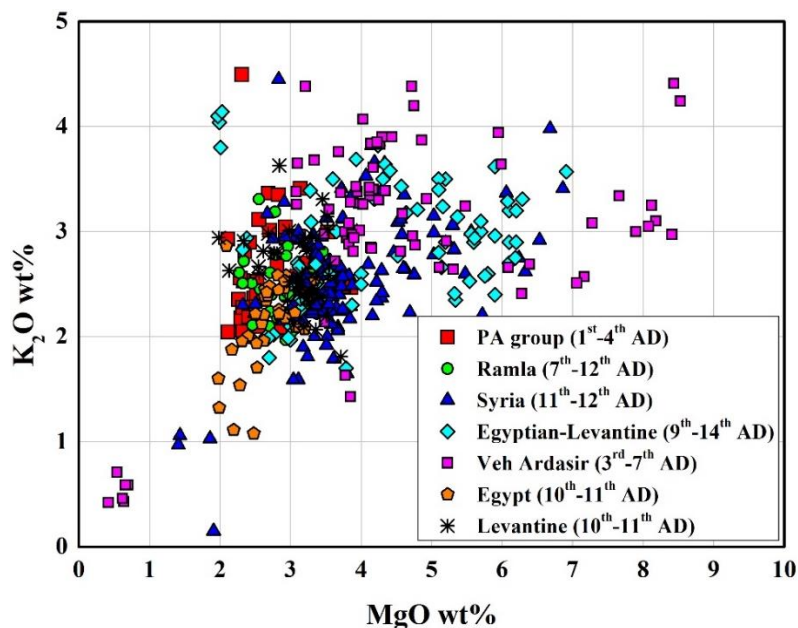


Figure A.9. Binary graph with the concentration of potash (K_2O wt%) versus magnesia (MgO wt%) (reduced composition) content detected in the Roman PA and the soda-plant ash glass from different regions of the Eastern coast of the Mediterranean Sea and ancient Mesopotamian region. Comparative data: [31-34].

In contrast, the samples from Veh Ardasir (3rd -7th century AD) [4, 5] are richer in magnesia and poorer in CaO (5-6 wt%) than the PA samples.

Despite the high variability of the Na₂O concentration detected in the samples from Al-Raqqqa, Damascus, Beirut and Cairo [31, 34], minimal differences distinguish them from the PA samples, while the samples from Ramla (7th-12th c. AD) [33], Egypt (10th-10th c.AD) and the Levant (10th-11th c. AD) (Na₂O 11-15 wt%) [32] match well with the PA samples. The concentration of CaO in the PA samples is generally very close to those exhibited by the plant ash base glass, which ranges between 7.5 wt% and 12 wt%.

These data should discourage the hypothesis that PA samples were produced or imported from other Empires (Mesopotamia or the Sassanian Empire), which used soda plant ash as a fluxing agent. The origin of the PA samples could be located in the Eastern Mediterranean area (the Levant or Egypt).

A.4.1.1.2 High phosphorus

The P₂O₅ concentration in the PA samples is two or three times higher than the common values found in soda plant ash glass. In general, P₂O₅ in soda plant ash glass varies between 0.2 and 0.5 wt%, only in rare cases reaching 0.6 wt% up to 0.8wt%.

This evidence markedly distinguishes PA samples from the early Islamic soda plant ash glass (fig. A.10) and medieval opaque red glass which, also, showed (table A.3) higher amount of iron than the PA samples.

Table A.3. Average chemical composition of the base glass (calculated by mean of reduced composition) of opaque red glass (mosaic tesserae, *opus sectile*, rods/canes) from the 1st to 4th century AD and mosaic tesserae from the 5th to 13th century AD.

Group	Date		SiO ₂	Al ₂ O ₃	Na ₂ O	K ₂ O	CaO	MgO	SO ₃	P ₂ O ₅	Cl	TiO ₂	Fe ₂ O ₃	MnO
PA group	1 st -4 th AD	AV.	64.6	2.3	13.9	2.6	9.4	2.8	0.08	0.80	0.62	0.17	1.9	0.50
		S.D.	2.0	0.54	1.50	0.45	1.10	0.47	0.16	0.59	0.49	0.08	0.63	0.15
	5 th -8 th AD	AV.	64.4	2.2	13.7	2.7	9.35	2.7	0.12	1.01	0.99	0.16	2.1	0.48
		S.D.	1.15	0.27	1.66	0.56	0.60	0.33	0.09	0.30	0.16	0.06	0.66	0.29
	9 th -13 th AD	AV.	66.2	2.0	11.8	2.4	8.98	2.8	0.10	0.48	0.64	0.11	3.2	1.1
		S.D.	3.10	0.60	1.82	0.52	0.86	0.54	0.11	0.29	0.16	0.07	1.16	0.51

However, the high variability of the soda plant ash glass, and how it is affected by the procedure adopted to be prepared [35] should be noted. Indeed, French samples dated between the 13th and 16th century AD (soda plant ash glass) exhibited a concentration of P₂O₅ higher than the typical soda plant ash and comparable with those of the PA samples [36]. This evidence could indicate the use of a soda plant ash richer in phosphorus than those commonly used in the other soda-plant ash glass.

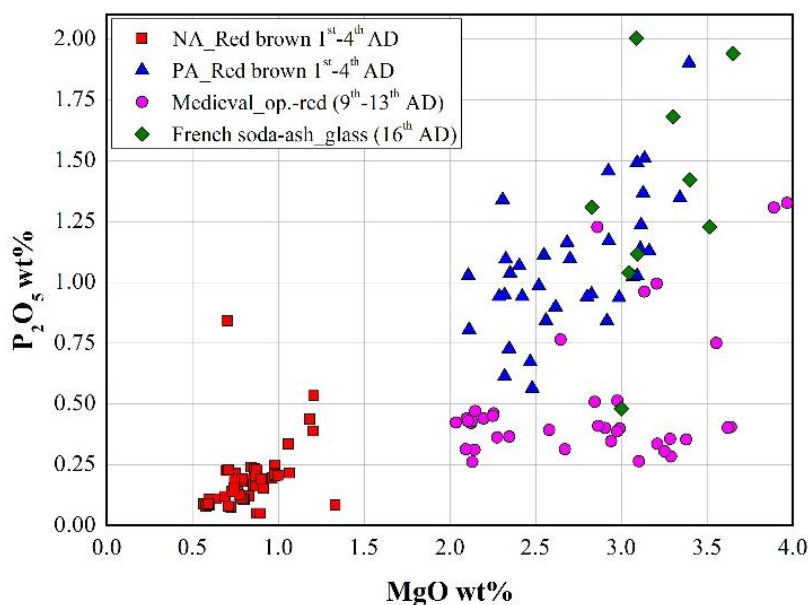


Figure A.10. Binary graph with the concentration of phosphorus versus magnesium (reduced composition) content detected in the Roman PA and NA red brown samples, compared with Medieval opaque red glass and French soda-plant ash glass dated to the 16th century AD.

A.4.1.1.3 Addition of fuel ash

The hypothesis of an addition of fuel ash as a reducing agent is reasonable and this could have contributed to increasing the P₂O₅ content in a natron glass or in a soda-plant ash glass but would not have been the main cause.

The concentration of Sr (450-850 ppm) detected in the PA samples is higher than the common Roman natron glass. However, when the PA samples are compared in a binary graph with the early soda-plant ash found in Ramla (dated to 7th-12th century AD - identified as Tyre-1), the CaO and Sr content are comparable [33] (fig. A.11). Similar results were observed between PA samples and the 10th century AD Egyptian and Levantine plant ash [32]. On the other hand, the soda plant ash glass from Mesopotamian/Persian production [4, 5, 32] is usually poorer in calcium and strontium than the PA samples.

These discrepancies concerning the Sr and CaO content could be considered another proof to underline the high variability of the soda plant ash glass; hence, the high Sr concentration revealed in the PA samples could be due to the use of soda-plant ashes as a fluxing agent to manufacture them. However, the addition of fuel ash cannot be ruled out, but should not be considered the only origin of these compositional differences between PA and the NA samples.

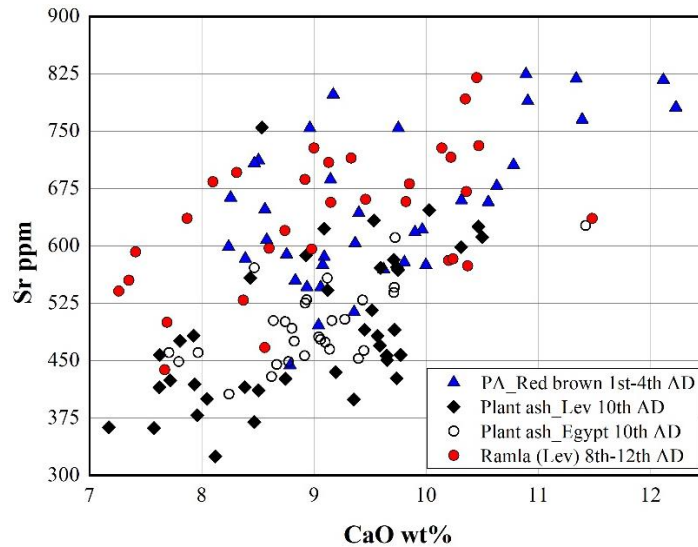


Figure A.11. A binary graph of strontium content (Sr ppm) versus weight % calcium oxide (CaO wt%), comparing the PA group samples with the Islamic soda plant ash glass. Comparative data: [31-34].

A.4.1.1.4 Recycling glass, pollutants from the furnace atmosphere

The study by Paynter [19] showed that in a secondary workshop, the chemical composition of the glass is strongly affected by the K-Ca-rich pollutants produced by the fuel ash during a prolonged melting period. The analyses of glass exhibited a general increase in the potash content (K_2O 1.6 – 8.56 wt%) and a constant low quantity of MgO (MgO 1.42-1.62 wt%). In addition, the CaO and Na_2O concentrations were affected, and based on the points analysed showed a wide variation. Unfortunately, the concentration of P_2O_5 is not measured.

Schibille and Barford noted how the combination of recycling of the glass and fuel pollution from the furnace can affect the concentration of potash and phosphorus [17, 18].

In the NA samples, the potash, magnesia and P_2O_5 content are higher than the typical Roman natron glass, (fig. A.12a-b). They indicate intense recycling activity or maybe the addition of fuel ash, as well as possible pollution from the furnace atmosphere, as a possible origin of the phenomenon.

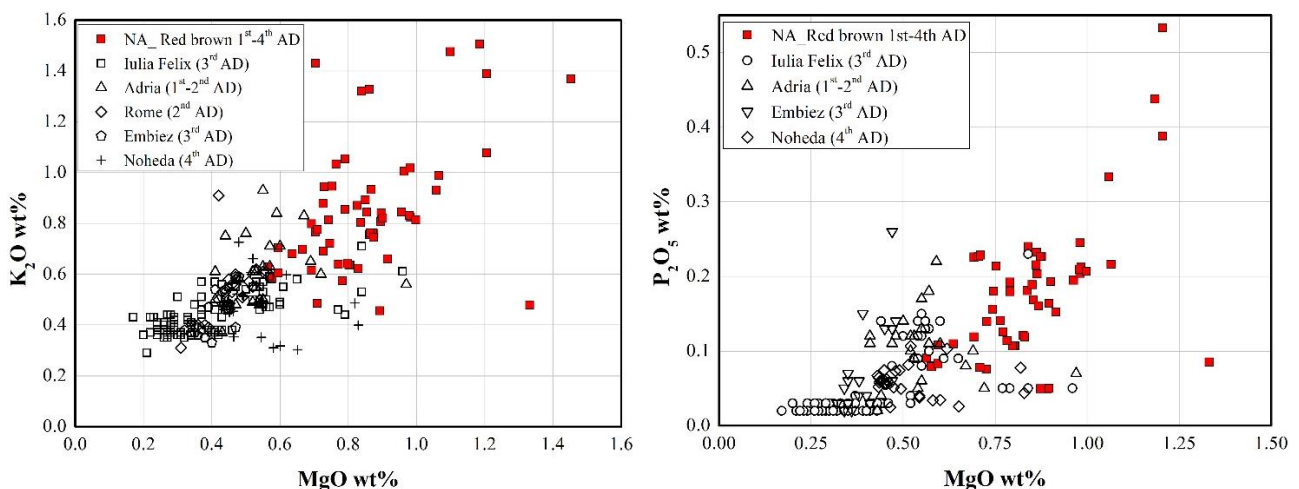


Figure A.12. (a) Binary graph of weight % potash versus magnesia content (reduced composition); (b) Binary graph of weight % phosphorus versus magnesia content (reduced composition). NA samples compared with natural/ colourless Roman natron glass. Comparative data: [23, 37-41].

However, the P_2O_5 content detected in the studies by [17, 18] is lower than 0.40 wt%, while in the PA and INT samples P_2O_5 is higher than 0.70 and 0.50 wt% respectively. Moreover, MgO and CaO in the samples by [17, 18] seem not to be affected by the contamination phenomena, while in the INT and PA samples, the amount of MgO is higher than 2wt%.

This does not exclude the possibility that the furnace atmosphere would contaminate the melt, or that recycled glass was not used, and that they probably affected the chemical composition of the INT samples, but they probably cannot be considered the main factors which produced the “anomalous” concentration of K_2O , MgO and P_2O_5 detected in the PA samples.

A.4.1.2 Silica source

PA and NA samples have higher TiO_2 content (usually > 0.10 wt%) than colourless Roman natron glass (1st-4th c. AD) (fig. A.13), while a comparable concentration of alumina was observed (except for a few samples with higher alumina content, both PA and NA groups).

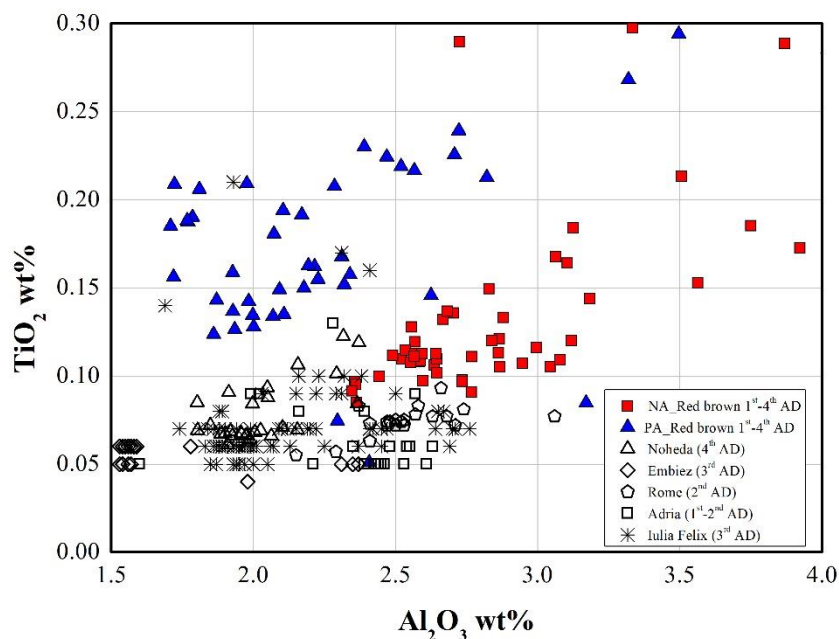


Figure A.13. Binary graph with titanium concentration vs alumina concentration (reduced composition) in the PA and NA samples, Comparative data: [23, 37-41].

On the other hand, by plotting Zr and TiO_2 content, it transpired that NA samples are very close to the positive trend exhibited by the Roman colourless/naturally transparent coloured glass, while PA samples are far from these two groups (fig. A.14).

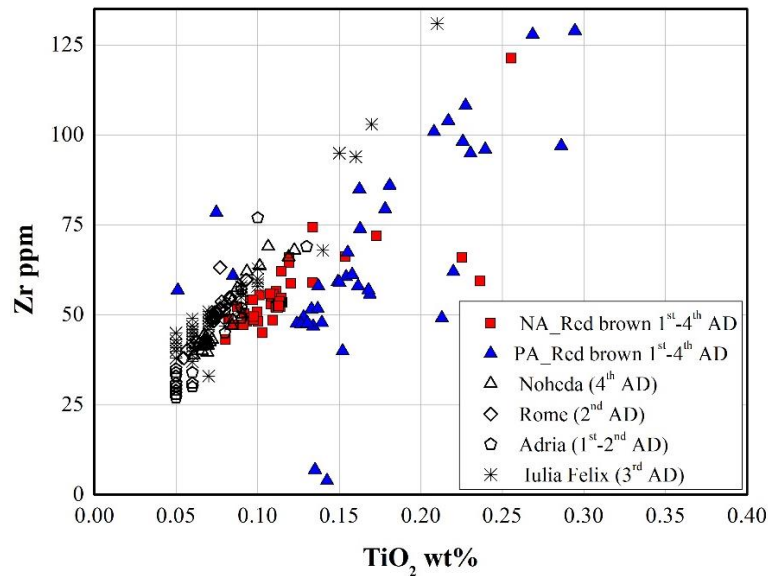


Figure A.14. binary graph with zircon concentration (Zr ppm) versus titania concentration (TiO₂ wt%) (reduced composition). Comparative data: [23, 37-41].

The compositional differences found in the elements regarding the silica source could indicate that sand with a different mineralogical composition or a distinct silica source were used. In the manufacture of the PA samples, the re-melting of the same raw glass used for NA and colourless/naturally transparent coloured samples may not have been adopted. This could suggest that fresh raw glass was produced using a different silica source and soda plant ash to make PA samples. As proposed by Verità [27], the use of fresh soda plant ash, containing carbonaceous residues, could affect the redox condition of the base glass facilitating the formation of Cu⁰ particles, while the addition of vegetable ash in an already made raw glass could not create the same effect. However, this could be a hypothesis, but more studies and maybe more laboratory tests are necessary to validate a thesis like this.

A.4.1.3. Production centres

In the last few decades, archaeometric investigations have been focused on identifying the provenance of the glass. Although researchers have provided fundamental information regarding colourless glass vessels, making it possible to understand every step of the glassmaking process (production and trade), for coloured glass this is still difficult.

Based on the high Zr content, some writers have suggested that PA samples could be made somewhere in Egypt [40]. A similar thesis was advanced by Rosenow concerning emerald green glass, showing concentrations of potash and magnesia higher than 1.5 wt% [24]. Other writers, performing isotopic analyses, indicate a generic Eastern Mediterranean area [37, 39, 41].

NA samples could be produced locally by re-melting the same raw glass (exported from the Syria-Palestinian coast) used to manufacture colourless/naturally coloured glass vessels.

A.4.2 Colouring techniques

The PA samples usually showed a higher copper concentration ($\text{CuO} > 1.5 \text{ wt\%}$) and lower iron content ($\text{Fe}_2\text{O}_3 < 2 \text{ wt\%}$, except some samples) than the NA samples ($\text{CuO} < 1.5 \text{ wt\%}$; $\text{Fe}_2\text{O}_3 > 2 \text{ wt\%}$, except some samples) (fig. A.15a). There is no clear tendency between iron and copper; however, in the PA samples the concentration of iron appears constant between 1-2 wt% with copper ranging between 1.5 wt% and 3 wt% (except for a few samples with lower copper amounts). A considerable number of NA samples showed copper lower than 1.5 wt%, and iron concentration varying between 2 wt% and 5 wt%.

Furthermore, the ratio $\text{Fe}_2\text{O}_3/\text{CuO}$ (the amount of iron added for each wt% of copper) showed that in the PA samples the amount of iron added was usually lower than the copper content (fig. A.15b). However, in some PA samples ($\text{CuO} 1\text{-}1.5 \text{ wt\%}$), the iron addition was similar to the copper concentration and up to three times higher than the amount of copper.

In most of the NA samples ($\text{CuO} 0.5\text{-}1.5 \text{ wt\%}$) the amount of iron added increased, varying from two up to nine times higher than the copper concentration; only in a few samples ($\text{CuO} 1.5 \text{ wt\%}\text{-}3 \text{ wt\%}$), was an addition of iron lower than two times the amount of copper observed.

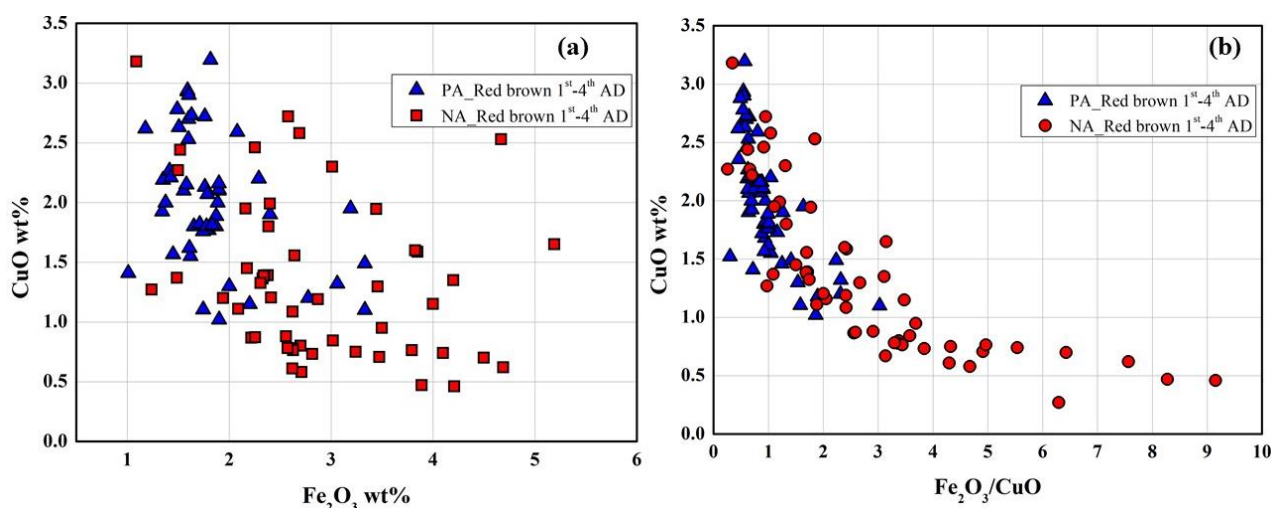


Figure A.15. (a) Binary graph with the concentration of copper oxide (CuO wt%) versus the iron content (Fe_2O_3 wt%); (b) Binary graph with the concentration of copper oxide (CuO wt%) versus the ratio between iron and copper ($\text{Fe}_2\text{O}_3/\text{CuO}$).

According to these graphs, the two different tendencies indicate that more iron was required to produce red brown glass in the NA samples than the PA samples. Although the origin of these compositional differences is still unclear, they could be related to the main factors.

a) *The nature of the probable iron- and copper-bearing.*

Although it has not been established with certainty which iron-bearing was used in red brown technology dated to Roman times (1st-4th century AD), it could be that iron metal scraps, or a mixture of metallic iron and iron oxides produced during the shaping of iron items were used as a reducing agent. This has been suggested by the detection of several iron compound inclusions in several archaeometric studies [12, 42-45]. Moreover, in the 15th – 17th Venetian recipes, adding metallic iron, or steel to the molten glass, as iron-bearing is frequently suggested.

Hence, the different concentrations of iron could be due to different iron-bearing, maybe the iron used in the PA samples had a stronger reducing effect than that used in the NA samples. But why the use of different iron-bearing? Maybe, because it was being manufactured in a specific part of the Empire which was supplied by different metallic iron.

Brass, bronze or leaded bronze have been considered as the main copper-bearing, which should be roasted and powdered [46]. The composition of the copper-alloy used could contain amounts of tin or lead useful for the formation of Cu° particles and require less iron.

Freestone hypothesized the use of a complex metallurgical by-product rich in lead (about 75 wt%), copper (10-15wt%) and silica (SiO_2 15wt%), produced during the affination of silver. This scrap could contain variable concentrations of other elements such as tin and zinc which could bring technological benefits [47].

Although this should not be ruled out, no positive tendencies were noted between copper and lead, which could point to the use of these scraps. Moreover, the addition of metallic iron and other metals could induce an increase in the reducing conditions inside the melt, and an excess of metals could precipitate [48].

b) The base glass composition.

Another hypothesis was the use of own raw glass composed of sand and soda-plant ash, still containing carbonaceous residues, that would have helped to reach the correct reducing conditions inside the molten glass, requiring less addition of iron [27, 28].

Copper-red glass produced without a reducing agent (Fe-Sn-Sb) was observed in most of the samples dated to the Late Bronze Age (high copper-no lead; CuO 5-12 wt%) [49]. The base glass composition and a well-engineered melting and heat treatments procedures could avoid the addition of a reducing agent or require small amounts of iron to obtain opaque red.

Another example is represented by red stained glass from the 12th-14th c. AD, produced without the addition of reducing agents, but the precipitation of the metallic copper particles in the glass is affected by the different base glass composition [50].

A.5 Conclusion

It is accepted that the production of opaque red glass was a very demanding colour which needed extensive glassmaking knowledge. Through the data two probable recipes emerged:

a) The NA recipe probably used raw natron glass supplied by the main primary furnaces, which exhibited comparable chemical composition with those of the common Roman natron glass items. However, the concentrations of K_2O and P_2O_5 are slightly higher than the common Roman natron glass, suggesting the recycling of glass. Moreover, this recipe usually used small amounts of copper (0.5 up to 1.5 wt%) and added considerable amounts of iron, from two up to nine times higher than the copper concentration.

b) In the second recipe (PA samples), it is likely that a different raw glass was used, composed of a distinct sand, or silica source, and a fluxing agent, probably soda plant ash. Due to the lack of clear archaeological evidence that can confirm the production of soda plant ash during the Roman Age, the literature discredits this hypothesis. However, the comparison between the PA samples and the “true” plant ash glass (colourless or

Medieval opaque red), should support this hypothesis. In the PA recipe, higher amounts of copper and a lower concentration of iron than the NA recipe were used. It is likely that the use of soda plant ash containing carbonaceous residues could affect the internal redox conditions of the base glass, requiring less addition of iron, or the addition of another vegetable ash, such as fuel ash. Moreover, specific melting conditions such as a reducing atmosphere in the furnaces, or well-engineered heat treatment could be adopted to obtain red brown glass.

A third red brown group showed an intermediate composition between the two previous recipes which required more investigation.

The existence of two recipes, which were manufactured by a distinct type of base glass composition, raises the question of how the Roman glassmaking industry was organised. The hypothesis that the glasses were coloured in secondary workshops by re-melting raw glass and adding the colourants seems to be confirmed by the NA samples but does not explain the existence of the PA samples.

Maybe, as occurred in the Late Bronze Age, specialised workshops devoted to the production of coloured glass, maybe located near the primary furnaces, or somewhere in the Empire, manufactured opaque red glass using their own raw glass to make rods or cakes/ingots. Then they were shipped to the secondary workshops to make coloured glass items.

Nevertheless, from the data in the literature it seems that the existence of these two recipes disappeared after the 4th-6th century AD. The organisation of the glassmaking industry may have changed due to the collapse of the Western Roman Empire, and the imminent Islamic invasion of the Levantine and Egyptian region.

This work does not establish a certain and conclusive solution to the debate about the anomalous values of K₂O and MgO in red brown glass during the Roman Age, but attempts to offer another prospective or alternative point of view to approach this controversial issue.

References

1. Sayre, E.V.; Smith, R.W. Compositional categories of ancient glass. *Science* **1961**, *133*, 1824–1826.
2. Freestone, I.C. The Provenance of Ancient Glass through Compositional Analysis. In *Materials Issues in Art and Archaeology VII*, edited Vandiver, P.B., Mass, J.L., Murray A. (Mater. Res. Soc. Symp. Proc. 852, Warrendale, PA, 2005), OO8.1.1 -OO8.1.13
3. Andreescu-Treadgold, I.; Henderson, J.; Roe, M. Glass from the Mosaic of the west wall of the Torcello's Basilica, Extract from *Arte medieval* 2006, 2, 87-140.
4. Mirti, P.; Pace, M.; Negro Ponzi, M.M.; Aceto, M. ICP-MS Analysis of glass fragments of Parthian and Sasanian epoch from Seleucia and Veh Ardasir (Central Iraq). *Archaeometry* **2008**, *50* (3), 429–450.
5. Mirti, P.; Pace, M.; Malandrino, M.; Negro Ponzi, M.M. Sasanian glass from Veh Ardasir: new evidences by ICP-MS analysis. *J. Archaeol. Sci.* **2009**, *36*, 1061–1069.
6. Gratuze, B.; Barrandon, J.-N. Islamic glass weights and stamps: analysis using nuclear techniques, *Archaeometry* **1990**, *32* (2), 155-162.
7. Verità, M. Le tessere vitree dei mosaici Medievali a Roma. Tecnologia e degrado. In *Mosaici Medievali a Roma Attraverso il Restauro Dell'ICR 1991–2004*; Andaloro, M., D'Angelo, C., Eds.; Gangemi Editore: Rome, Italy, 2017; pp. 437–477.
8. Weyl, W.A. Copper in copper-ruby glasses (Hematinone and copper aventurine). In *Coloured Glasses*; Society of Glass Technology: Sheffield. UK. 1951, pp. 420-432; ISBN 9780900682063.
9. Lilyquist, C.; Brill, R.H. Analytical procedure. In *Studies in Early Egyptian Glass*; Metropolitan Museum of Art: New York, NY, USA, 1993, pp. 47-58; ISBN 978-0300200195.
10. Freestone, I.; Stapleton, P.C. Composition, technology and production of coloured glasses from mosaic vessels of the early Roman Empire. In *Glass of the Roman Empire*; Bayley, J., Freestone, I., Jackson, C., Eds.; Oxbow: Oxford, UK, 2013, pp. 61-76.
11. Fiori, C. Production technology of Byzantine red mosaic glasses. *Ceram. Int.* **2015**, *41*, 3152–3157.
12. Maltoni, S.; Silvestri, A.; Molin, G. Opaque red glass tesserae from Roman and early-Byzantine sites of north-eastern Italy: New light on production technologies. In *Proceedings of the Annales du 20e Congrès de l'Association Internationale pour l'Histoire du Verre, Fribourg, Switzerland, 7–11 September 2015*; Wolf, S., de Pury-Gysel, A., Eds.; Verlag Marie Leidorf GmbH: Rahden, Germany, 2017; pp. 280–287.
13. Paynter, S.; Kearns, T.; Cool, H.; Chenery, S. Roman coloured glass in the Western provinces: The glass cakes and tesserae from West Clacton in England. *J. Archaeol. Sci.* **2015**, *62*, 66–81.
14. Fiorentino, S.; Chinni T.; Vandini, M. Ravenna, its mosaics and the contribution of archaeometry. A systematic reassessment on literature data related to glass tesserae and new considerations. *J. Cult. Her.* **2020**, *46*, 335-349.
15. Schibille, N.; Degryse, P.; Corremans, M.; Specht, C.G. Chemical characterisation of glass mosaic tesserae from sixth-century Sagalassos (south-west Turkey): chronology and production techniques. *J. Archaeol. Sci.* **2012**, *39*, 1480-1492.
16. Schibille, N.; McKenzie, J. Glass tesserae from Hagios Polyuktos, Constantinople: Their early Byzantine affiliations. In *Neighbours and Successors of Rome. Tradition of Glass Production and Use in Europe and the*

Middle East in the Later 1st Millenium AD; Keller, D., Price, J., Jackson, C.M., Eds.; Oxbow Books: Oxford, UK, 2014; pp. 114–127, ISBN 978178297397.

17. Schibille, N.; Neri, E.; Ebanista, C.; Ammar, M.R.; Bisconti, F. Something old, something new: The late antique mosaics from the catacomb of San Gennaro (Naples). *J. Archaeol. Sci. Rep.* **2018**, *20*, 411–422.

18. Barfod, G.H.; Freestone, I.C.; Lichtenberger, A.; Raja, R.; Schwarzer, H. Geochemistry of Byzantine and Early Islamic glass from Jerash, Jordan: Typology, recycling, and provenance. *Geoarchaeology* **2018**, *33*, 623–640.

19. Paynter S. Experiments in the reconstruction of Roman wood-fired glassworking furnaces: waste products and their formation processes, *J. Glass Stu.* **2008**, *50*, 271-90.

20. Jackson, C.M.; Booth, C.A.; Smedley, J.W. Glass by design? Raw materials, recipes and compositional data. *Archaeometry* **2005**, *47* (4), 781–795.

21. Misra, M.K.; Ragland, K.W.; Baker A.J. Wood ash composition as a function of furnace temperature *Biomass And Bioenergy* **1993**, *4* (2), 103-116.

22. Jackson, C.M.; Cottam, S. ‘A green though in a green shade’; Compositional and typological observation concerning the production of emerald green glass vessels in the 1st century AD. *J. Archaeol. Sci.* **2015**, *61*, 139-148.

23. Gallo, F.; Silvestri, A.; Molin, G. Glass from the Archaeological Museum of Adria (North-East Italy): new insights into Early Roman production technologies, *J. Archaeol. Sci.* **2013**, (40), 2589-2605.

24. Rosenow, D.; Rehren, Th. Herding cats e Roman to Late Antique glass groups from Bubastis, northern Egypt. *J. Archaeol. Sci.* **2014**, (49), 170e184.

25. Boschetti, C.; Henderson, J.; Evans, J.; Leonelli, C. Mosaic tesserae from Italy and the production of Mediterranean coloured glass (4rd century BCE–4th century CE). Part I: Chemical composition and technology. *J. Archaeol. Sci. Report.* **2016**, *7*, 303-311.

26. Nenna, M.D.; Gratuze, B. Etude diachronique des compositions de verres employes dans les vases mosaïques antiques: Resultats preliminaires. In *Proceedings of the Annales du 17e Congrès de l'Association Internationale pour l'Histoire du Verre, Antwerp, Belgium, 4–8 September 2006*; Janssens, K., Degryse, P., Cosyns, P., Caen, J., Van't dack, L., Eds.; University Press Antwerp: Antwerp, Belgium, 2009; pp. 199-205.

27. Verità, M.; Santopadre, P. Unusual Glass Tesserae from a Third-century Mosaic in Rome. *J. Glass. Stud.* **2015**, *57*, 287-292.

28. Verità, M.; Arena, M.S.; Carruba, A.M.; Santopadre, P. Materiali vitrei nell'opus sectile di Porta Marina (Ostia antica), *BOLL. ICR* **2008**, 16-17, 78-94.

29. Cagno, S.; Cosyns, P.; Izmer, A.; Vanhaecke, F.; Nys K.; Janssens, K. Deeply colored and black-appearing Roman glass: a continued research. *J. Archaeol. Sci.* **2014**, *42*, 128-139.

30. Brill, R.H. Chemical Analyses of Early Glasses. Volume 2 Tables of Analyses; The Corning Museum of Glass: Corning, NY, USA, 1999; ISBN 0-872900-143-2.

31. Henderson, J.; Chenery S.; Faber, E.; Kröger, J. The use of electron probe microanalysis and laser ablation-inductively coupled plasma-mass spectrometry for the investigation of 8th–14th century plant ash glasses from the Middle East. *Microch. J.* **2016**, *128*, 134–152

32. Schibille, N.; Gratuze, B.; Ollivier, E.; Blondeauec, É. Chronology of early Islamic glass compositions from Egypt. *J. Archaeol. Sci.* **2019**, *104*, 10–18.

33. Phelps, M. Glass supply and trade in early Islamic Ramla: An investigation of the plant ash glass. In *Things that travelled-Mediterranean Glass in the First Millennium CE*. Rosenow, D., Phelps, M., Meek, A., Freestone I., Eds.; Publisher: UCL Press University College London, UK, 2018, pp. 236-282.
34. Henderson, J.; Mcloughlin, S.D.; McPhail, D.S. Radical changes in Islamic glass technology: evidence for conservatism and experimentation with new glass recipes from Early and Middle Islamic Raqqa, Syria. *Archaeometry* **2004**, 46 (3), 439–468.
35. Tite, M.S.; Shortland, A.; Maniatis, Y.; Kavoussanaki, D.; Harris S.A. The composition of the soda-rich and mixed alkali plant ashes used in the production of glass. *J. Archaeol. Sci.* **2006**, 33, 1284-1292.
36. Barrera, J.; Velde, B. A study of french medieval glass composition. In: *Archéologie médiévale, tome 19*, **1989**, pp. 81-130.
37. Silvestri, A.; Molin, G.; Salviulo, G. The colourless glass of Iulia Felix. *J. Archaeol. Sci.* **2008**, 35, 331-341.
38. Gliozzo, E. The composition of colourless glass: a review. *Archaeol. Anthropol Sci* **2017**, 9, 455–483.
39. Ganio, M.; Boyen, S.; Fenn, T.; Scott, R.; Vanhoutte, S.; Gimeno, D.; Degryse P. Roman glass across the Empire: an elemental and isotopic characterization. *J. Anal. At. Spectrom.* **2012**, 27, 743-753
40. Schibille, N.; Boschetti, C.; Valero M.A.; Veron E.; Juan. J. The Color Palette of the Mosaics in the Roman Villa of Noheda (Spain). *Minerals* **2020**, 10, 272.
41. Silvestri, A. The coloured glass of Iulia Felix. *J. Archaeol. Sci.* **2008**, 35, 1489-1501
42. Cholakova, A.; Rehren, Th. Producing black glass during the Roman period—notes on a crucible fragment from Serdica, Bulgaria. In *Proceedings of the 39th International Symposium for Archaeometry, Leuven, Belgium, 2012, 28May-1June*; Scott, R., Braekmans, M., Degryse P., (eds.); Centre for Archaeological Sciences, Leuven, Belgium, 2014; pp. 261-267.
43. Rehren, T.; Cholakova, A.; Zivanovi, C. M. The making of black glass in Late Roman Doclea. In *New Antique Doclea, 2012, 3(7)*, 71-90.
44. Peake, J.R.; Freestone, I.C. Cross-Craft Interactions between Metal and Glass Working: Slag Additions to Early Anglo-Saxon Red Glass. In *Integrated Approaches to the Study of Historical Glass—IAS12*; Meulebroeck, W., Nys, K., Vanclooster, D., Thienpont, H., Eds.; Proceedings of SPIE: Cergy, France, 2012; Volume 8422, p. 842204.
45. Heck m., Hoffmann, P. Coloured opaque glass beads of the Merovingians. *Archaeometry* **2000**, 42 (2), 341-357.
46. Brill, R.H.; Cahill, N.D. A Red Opaque Glass from Sardis and Some Thoughts on Red Opaque in General. *J. Glass Stud.* **1988**, 30, 16–27.
47. Freestone, I.C.; Stapleton, C.P.; Rigby, V. The production of red glass and enamel in the Late Iron Age. Roman and Byzantine periods. In *Through a Glass Brightly: Studies in Byzantine and Medieval Art and Archaeology*; Presented to David Buckton; Entwistle, C. Buckton, D. Eds.; Oxbow Books: Oxford. UK. 2003; pp. 142–154. ISBN 978-1785702518.
48. Ahmed, A.A.; Ashour, G.M. Effect of heat treatment on the crystallisation of cuprous oxide in glass. *Glass Technol.* **1981**, 22, 24–33.
49. Th. Rehren, Ramesside glass-colouring crucibles. *Archaeometry* **1997**, 39(2), 355-368.

50. Kunicki-Goldfinger, J.; Freestone, I.C.; McDonald, I.; Hobot, J.A.; Gilderdale-Scott, H.; Ayers, T. Technology, production and chronology of red window glass in the medieval period – rediscovery of a lost technology. *J. Archaeol. Sci.* **2014**, 41, 89-105.

B. Adulteration of natron Roman glass by wood ash

B.1. The aim

This work addresses key outstanding questions related to the “anomalous” concentration of K_2O , MgO and P_2O_5 revealed in the Roman opaque red glass (1st century BC- 4th century AD). The aim of this work is to understand the probable cause that could generated these anomalous values. The theory that fuel ash (wood ash) were added to the melt (or to the batch) was chosen among the several hypotheses proposed in the literature, which attempted to explain these anomalous values, and it will be investigated.

This work proposes to adulterate the typical Roman natron base glass (1st-4th century AD) with a hypothetical addition of wood ash, which are considered fuel ash in this text. It will observe which elements will be affected in their concentration and how they change by the addition of wood ash. Moreover, the adulterated glass will be compared with the “anomalous” Roman opaque red glass (PA group) to identify similarities and dissimilarities among them.

B.2. Methodology

In order to study and understand how the addition of fuel/wood ash would modify the concentration of specific elements of the natron glass, simulations were conducted. The trees chemical composition of beech, oak and bracken ashes chemical composition were chosen from the literature. Due to the high variability of their chemical composition, it was established to use average chemical compositions of the wood ash collected from [1].

A set of 100 colourless or natural natron coloured glass composition from the 1st to 4th century AD were collected. They belong to the analyses of glass discovered in the shipwrecks of Embiez (South France, 2nd century AD) [2] and Iulia Felix (Adriatic Sea, 3rd century AD) [3]. Other colourless glass from Noheda (Spain, 4th century AD) [4] and Adria (Italy, 1st-3rd century AD) [5] were used. Based on their sodium content, these samples were divided into three groups: N-16, N-18, N-20.

The chemical compositions of the natron base glass reported in the literature were then diluted of 5%, 10%, 15% and 20% in order to include the equivalent amount of fuel ash. In this way the adulterated natron glass should be for instance composed of 95 % by original natron glass and 5% by the added wood ash. The calculate compositions were then compared with the three groups of Roman opaque red glass identified in the previous chapter (NA, INT and PA group).

The same method mentioned above was applied to adulterate soda plant ash (naturally coloured) glass composition collected from the literature: Ramla 7th-12th century AD [6]; Syria 10th-12th century AD [7]; Egyptian-Levantine 10th-14th century AD [8]; Veh Ardasir 3rd-7th century AD [9, 10]; Egypt and Levantine 10th-11th century AD [11]. The adulterated soda plant ash glass were compared with PA samples to underline the main compositional differences which would allow to establish if PA samples were melt by using soda plant ash or not.

B.3. Results

B.3.1. Adulteration of natron glass with wood ash

In order to show a general view of the changes caused by the addition of wood ash to natron base glass, in the [fig. B.1-2-3](#) three histograms are shown, which are related to the adulteration of natron glass N_16 by beech, bracken and oak respectively. In these histograms, only the concentration of sodium (Na_2O), calcium (CaO), potash (K_2O), magnesia (MgO) and phosphorus (P_2O_5) are reported, since they can be considered indicators of the addition of vegetable ash to a natron glass. In each histogram the PA group mean values are reported, to compare the compositional differences and identify the main changes in the concentration of the selected elements.

By adding different amounts of wood ashes, a general trend was observed: a progressive decrease in the sodium content and increase of the CaO concentration.

The beech ash ([fig. B.1](#)) is rich in potash, calcium, and phosphorus rather than magnesia. Hence, when 10 wt% or more of beech ash is added, the adulterated natron glass exhibits a chemical composition extremely rich in calcium and higher in K_2O and P_2O_5 than the mean values of the PA samples. On the other hand, the magnesia content never surpassed the concentration of 2 wt%, and sodium also remains higher than PA samples.

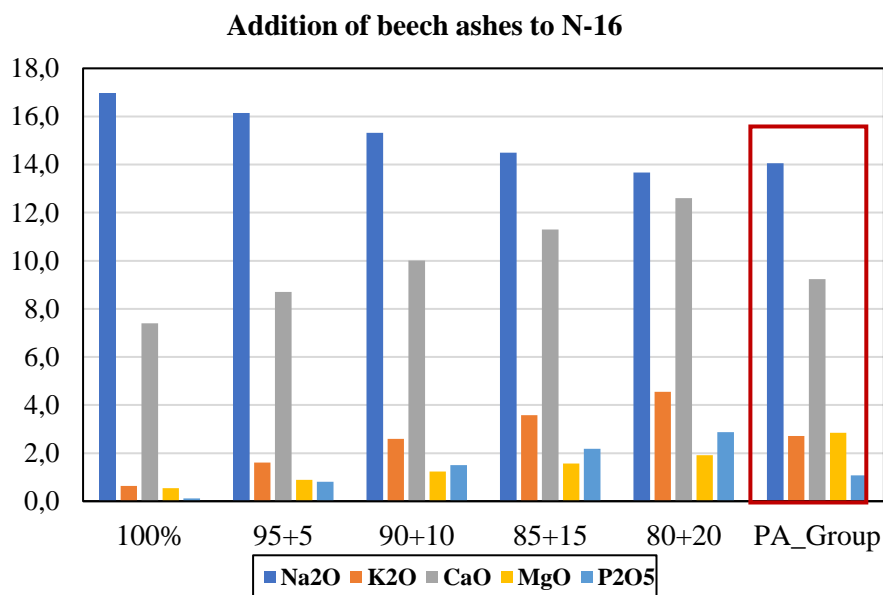


Figure B.1. Histogram showing the variation in sodium, potassium, calcium, magnesium and phosphorus by addition of different amounts of beech ashes to the N_16 natron glass. The composition of the PA group is also reported.

The bracken ashes are extremely rich in potash ([fig. B.2](#)), and by adding more than 5 wt% of ashes, the adulterated natron glass should contain a concentration of potash higher than 5 wt%, an amount which was not detected in the PA samples. Moreover, the Na_2O content is still higher than the PA samples, and MgO concentration is lower than 2 wt%.

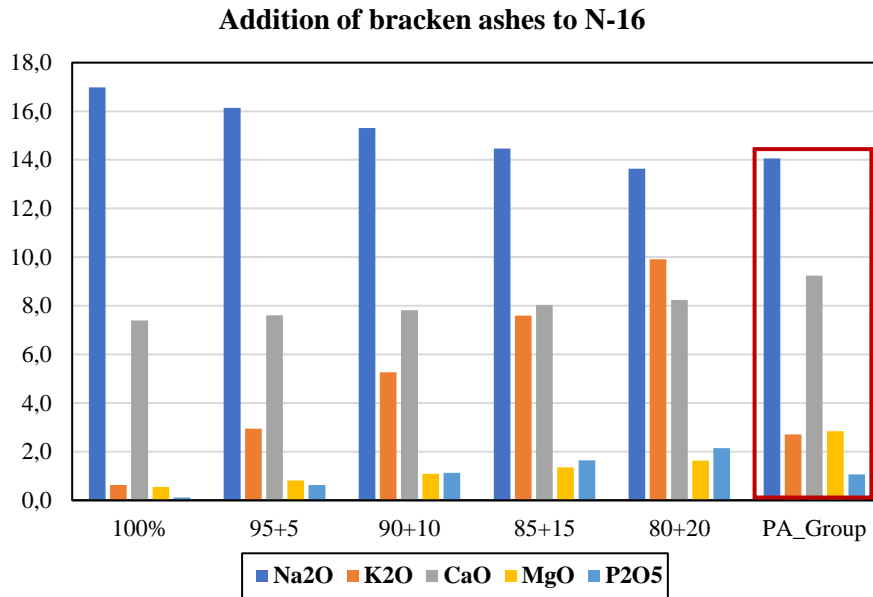


Figure B.2 Histogram showing the variation in sodium, potassium, calcium, magnesium and phosphorus by addition of different amounts of bracken ashes to the N_16 natron glass. The composition of the PA group is also reported.

Oak ashes are very rich in calcium (fig. B.3), and a small addition of them (5 wt%) increases the CaO content in the adulterated glass to more than 10 wt% (higher than in the PA samples). At the same time the concentrations of potash, magnesia and phosphorus are much lower than in the PA samples, and the concentration of Na₂O in the adulterated glass is still higher than the PA samples.

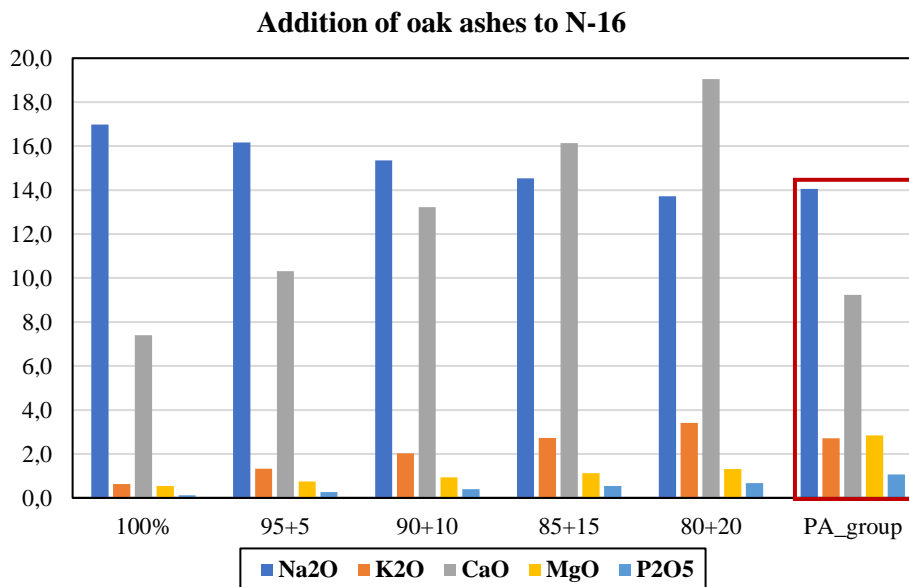


Figure B.3. Histograms showing the variation in sodium, potassium, calcium, magnesium and phosphorus by addition of different amounts of oak ashes to the N_16 natron glass. The composition of the PA group is also reported.

Henceforth, for the comparison with the Roman opaque PA red glass, only the glass adulterated by adding 5% of beech will be mainly considered.

Due to the low Na₂O content in the wood ashes, the adulterated glass does not exhibit any evident change in the concentration of sodium (fig. B.4a), which is still higher than most of the PA samples and is comparable with INT samples. A slight increase is observed in the concentration of calcium.

When the Na₂O content is plotted on a binary graph against K₂O (fig. B.4b), it is possible to observe that, although the Na₂O content is still higher and potash lower than the PA samples, the adulterated natron glass (with an addition of 5% of beech ashes) matches with the samples from the INT group, especially the sample of the N_16 and N_18 type.

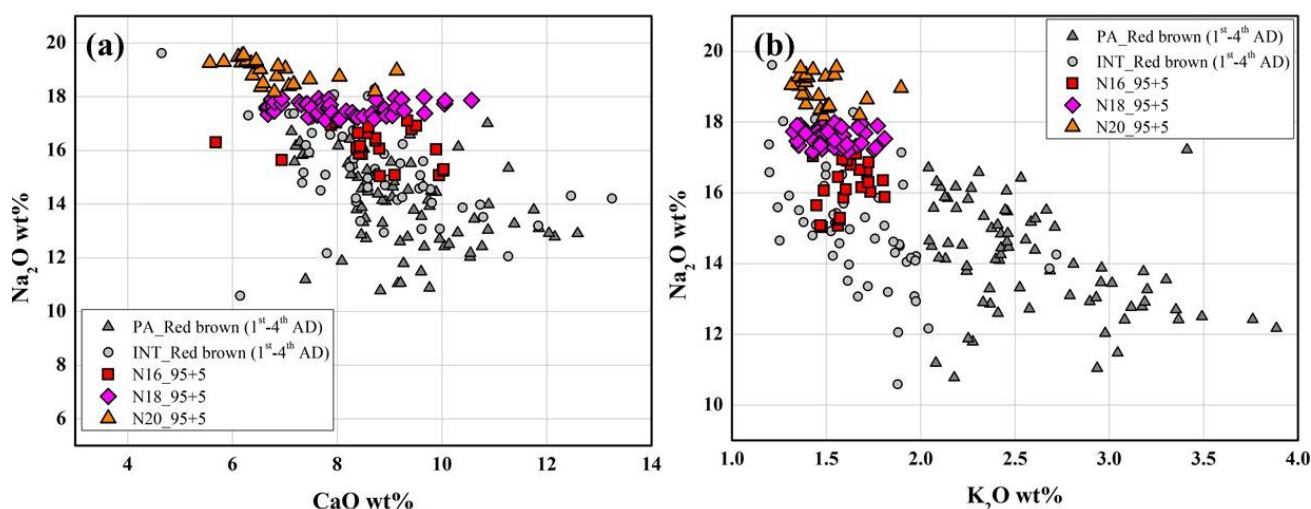


Figure B.4. a) Binary graph between sodium content (Na₂O) versus lime content (CaO) Roman natron base glass adulterated with 5% of beech ashes compared with the PA and INT samples. b) Binary graph of sodium content (Na₂O) versus potassium content (K₂O) between adulterated natron glass (with 5% of beech ashes) and the PA and INT samples. (Reduced composition)

In fig. B.5a the concentration of K₂O and MgO are plotted in a binary graph. The three natron glass types, with different Na₂O content (N_16, N_18 and N_20), form a unique cluster when 5 wt% of the wood ashes (of the three types of trees) are added. It should be noted that the quantities of K₂O increase significantly, while the MgO concentration remains very low. Indeed, the adulterated glass does not fit with the PA samples or the INT samples. It is also interesting to note that the natron glass adulterated with oak and in part also with beech ashes is still included in the range of natron glass.

Plotting the content of P₂O₅ and K₂O (fig. B.5b), the natron glass adulterated with the wood ash forms three different cluster. The glass adulterated by 5% of oak ashes showed comparable content of K₂O and P₂O₅ with the NA samples, while the glass adulterated by 5% of bracken ashes has a concentration of potash comparable with the PA samples, but the P₂O₅ is still lower or out of the tendency. The glass adulterated by 5 wt% of beech ash matches well with the INT samples. However, a further addition of the beech ashes (10%) should produce an adulterated glass with too much P₂O₅ and K₂O which should surpass the PA samples.

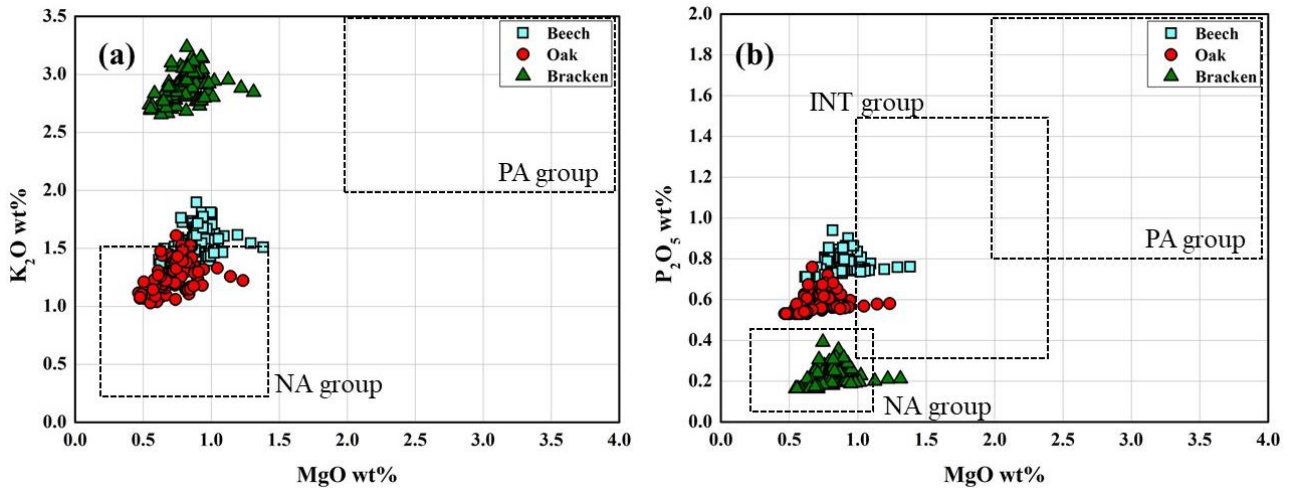


Figure B.5. a) Binary graph of potash (K₂O wt%) versus magnesia (MgO). N₁₆ type natron glass adulterated by 5 wt% of bracken, beech and oak ashes. b) Binary graph of potash (K₂O wt%) versus phosphorus (P₂O₅ wt%) of the Roman natron glass adulterated by 5 wt% of bracken, beech and oak ashes.

The presence of elements such as strontium (SrO) and barium (BaO) would increase with the addition of wood ash to the glass, since wood ash is extremely rich in barium (>3000 ppm) and strontium.

Through the addition of 5% of beech ash, a slight increase of strontium is noted in the adulterated glass (fig. B.6a). However, the values of Sr are still lower than those of the PA samples. The adulterated glass matches with the INT samples.

The BaO content in the glasses adulterated by 5% of beech ashes increases considerably, and their values do not match with the PA samples (lower than the adulterated glass) (fig. B.6b). Indeed, BaO ranges between 0.04-0.08 wt%, while the average values of the PA samples are lower than 0.04 wt%. Instead, the adulterated glasses overlap the INT group showing the same concentration of K₂O and very close values of BaO.

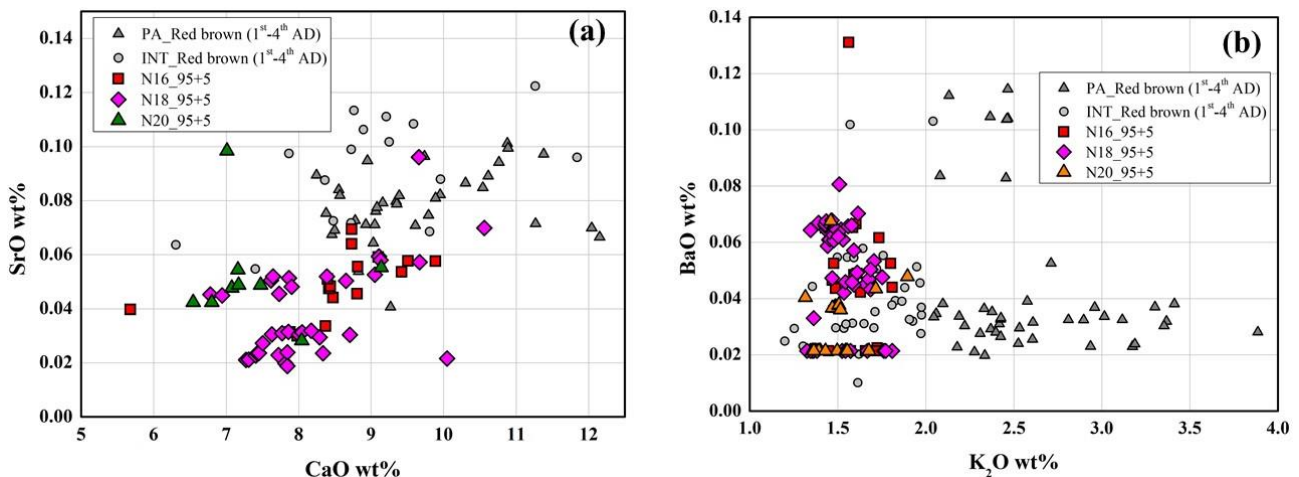


Figure B.6. a) Binary graph of weight % strontium (SrO wt%) versus calcium oxide (CaO wt%) of the adulterated Roman natron glass, and compared with the PA and INT. b) Binary graph of weight % barium oxide (BaO) versus potash (K₂O), of the adulterated Roman natron glass, and compared with the PA and INT. (Reduced composition)

B.3.2 Comparison of the PA group samples with the adulterated soda plant ash glass

To explain the high values of P_2O_5 and SrO , soda plant ash glass from Ramla (7th-12th century AD) [6], from Veh Ardasir (Sassanian 3rd-7th century AD) [9, 10], and from Egypt (10th-11th century AD) [11] was adulterated with an addition of 5 wt% of beech ash, as was done for the Roman natron glass, mentioned above.

In fig. B.7a the K_2O and MgO content of the soda plant ash glass is plotted and compared with the PA samples. Most of the adulterated soda plant ash has potash and magnesia higher than 3wt%. However, some samples from Egypt and Ramla exhibit values of K_2O and MgO comparable with the PA samples. In contrast, the samples from Ver Ardasir are richer in magnesia.

In fig. B.7b the concentration of P_2O_5 in the adulterated soda plant ash increased (about 1 wt%) and is comparable with that detected in the PA samples.

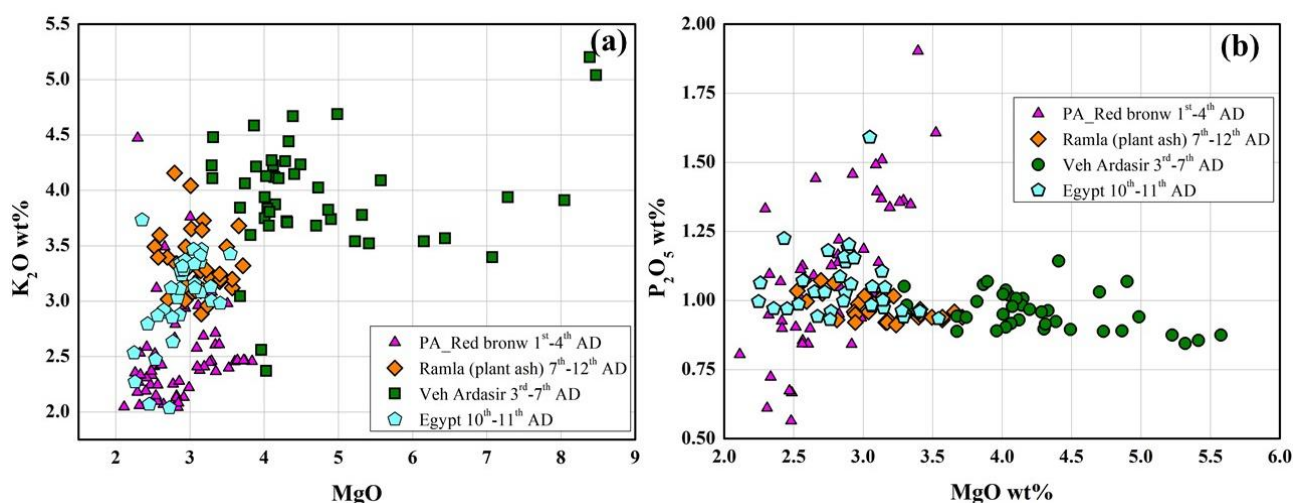


Figure B.7. a) Binary graph with the concentration of potash (K_2O wt%) versus magnesia (MgO) content detected in the Roman PA and the adulterated soda-plant ash. b) Binary graph with the concentration of phosphorus (P_2O_5 wt%) versus magnesia content detected in the Roman PA and the adulterated soda-plant ash glass. (Reduced composition)

Fig. B.8a shows that the sodium content in the adulterated soda plant ash decreased in the samples from Egypt and Ramla - only a few samples fit with the values exhibited by the PA samples. On the other hand, the adulterated samples from Veh Ardasir have sodium content comparable with the PA samples. The concentration of calcium in the adulterated soda plant ash is in agreement with that detected in the PA samples. In fig. B.8b the concentration of Sr detected in the PA samples fits well with the adulterated soda-plant ash glass from Ramla and the Levantine region [11]. The dissimilarities between the Sassanian glass and the PA samples are still present, which could support the hypothesis that the PA samples were not imported from other regions beyond the borders of the Roman Empire.

As observed in the adulteration of the natron glass, in the soda-plant ash glass the addition of 5% of wood ash also increased the amount of Ba considerably. Indeed, the adulterated soda-plant ash glass exhibited a Ba concentration higher than the PA samples, and only in some cases do they fit well with the PA samples.

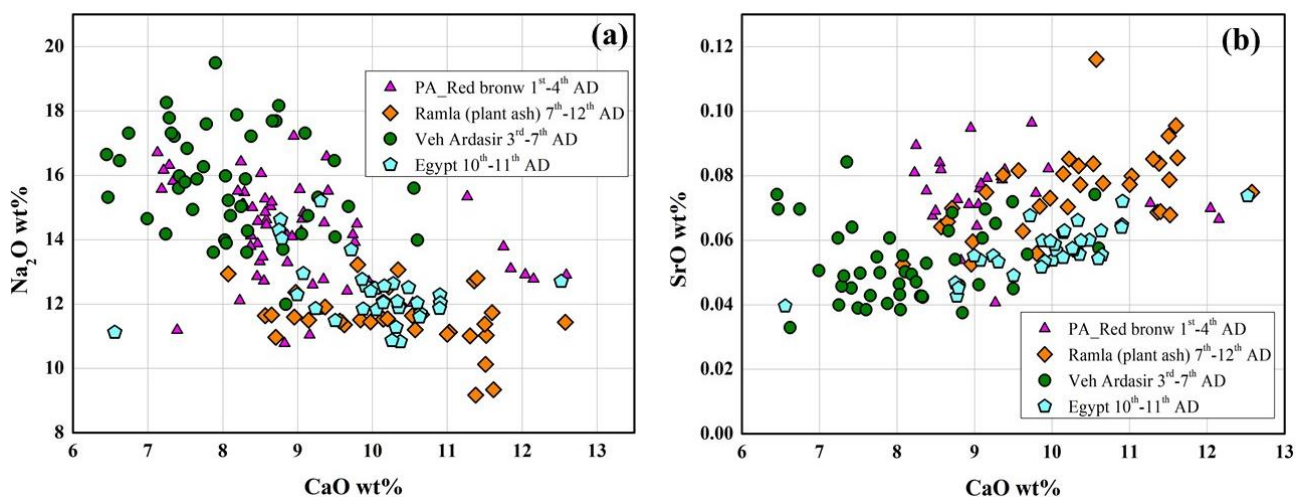


Figure B.8. **a)** Binary graph with the concentration of sodium (Na₂O wt%) versus calcium oxide (CaO wt%) content detected in the Roman PA and the adulterated soda plant ash glass. **b)** Binary graph with the concentration of strontium (SrO wt%) versus calcium (CaO wt%) content detected in the Roman PA and the adulterated soda plant ash. (Reduced composition)

B.4. Conclusions

The results from the simulation, adopted in this work, have to be taken with the due caution. Based on the nature of the fuel ash (plant or shrub) used, how it was prepared and which part was introduced, the chemical composition of the glass would change. Moreover, regional workshops would have used regional plants, increasing the compositional variability.

However, these results offer an overall perspective of the probable composition, or how the composition of a natron glass could be affected by adding wood ash. Moreover, more accurate research is required to identify the probable fuel ash, and it could be very useful to study the composition of other ashes, in order to determine their effect. Finally, systematic reproduction in a laboratory could help to understand not only the changes in the chemical composition but also the technical advantages in adopting the use of fuel ash/wood ash to produce opaque red glass.

Taking into consideration the chemical composition of wood ash from the literature, beech ash is the only one which gives results close to the PA group. The composition of the glass induced a moderate increase in K₂O, P₂O₅ and CaO, which fitted well with the INT samples. On the other hand, the low MgO content detected in wood ash does not provide a chemical composition similar to the PA samples, which are richer in magnesia. Moreover, the addition of wood ash did not diminish the concentration of Na₂O in the adulterated natron glass, which showed Na₂O content still higher than the average Na₂O concentration detected in the PA samples.

In conclusion the adulterated natron glasses never formed a cluster similar to PA samples, while they showed a composition similar to the INT samples. Instead, the comparison between PA samples with the soda plant ash base glass and adulterated soda plant ash, showed numerous similarities.

The concentration of P₂O₅ higher than 0.5 wt% detected in the PA samples did not find a clear and definitive answer, and only conjectures could be advanced to understand this point. One explanation could be the well-known high compositional variability of the plants. The chemical composition of the plants is strongly

connected with the type of plant, the geochemistry of the soil in which they grow, which part is used (the trunk, the branches or the leaves), and also the season in which the plants were gathered [12, 13]. Another possible cause of the differences concerns how the ashes were prepared. Misra [14] underlined that the temperature and the time required in the production of ashes strongly modify the concentration of K_2O , CaO , Na_2O , P_2O_5 . High temperatures ($T > 900$ °C) can cause the decomposition of the carbonates such as $CaCO_3$ or K_2CO_3 , and the atmosphere during this process also affects the concentration of specific compounds. Afterwards, the composition of the ashes could be modified by the mixing of different types of them. Furthermore, the fritting process, which again involves temperature and timing, could affect the chemical composition of the final product [1].

Another explanation could concern the practice of adding a phosphorus-rich material to a soda plant ash base glass, such as bone ash or fuel ash. The hypothesis that bone ash was used to manufacture opaque red does not find any specific evidence from the analyses present in the literature. Bone ash was used as an opacifier in the Islamic glassmaking industry, in which its use was very common, or in the Byzantine glassmaking industry [15, 16]. However, in Roman and early Byzantine opaque red glass, undissolved calcium phosphate (compounds from the bone ash) has not been detected (yet), making this hypothesis less probable.

Finally, the addition of 5% beech ash to a soda plant ash glass showed that the adulterated glass has a composition very close to the PA samples; indeed potash, magnesia and phosphorus content fitted very well, suggesting the hypothesis that soda-plant ash adulterated by wood ash is not to be ruled out.

Trace elements such as Sr matched between PA samples and the adulterated soda-plant ash glass. The Sr content in the adulterated glass is comparable with those detected in the PA samples.

These data highlighted the possibility that specialised workshops used different recipes to manufacture red brown. Besides the recipe in which iron represents the main reducing agent, there is another recipe in which distinct base glass composition and a (probable) further addition of vegetable ashes were adopted for technical advantage.

References

1. Jackson, C.M.; Booth, C.A.; Smedley, J.W. Glass By Design? Raw Materials, Recipes And Compositional Data. *Archaeometry* **2005**, 47 (4), 781–795.
2. Ganio, M.; Boyen, S.; Fenn, T.; Scott, R.; Vanhoutte, S.; Gimeno, D.; Degryse P. Roman glass across the Empire: an elemental and isotopic characterization. *J. Anal. At. Spectrom.* **2012**, 27, 743-753.
3. Silvestri, A.; Molin, G.; Salviulo, G. The colourless glass of Iulia Felix. *J. Archaeol. Sci.* **2008**, 35, 331-341.
4. Schibille, N.; Boschetti, C.; Valero M.A.; Veron E.; Juan. J. The Color Palette of the Mosaics in the Roman Villa of Noheda (Spain). *Minerals* **2020**, 10, 272.
5. Gallo, F.; Silvestri, A.; Molin, G. Glass from the Archaeological Museum of Adria (North-East Italy): new insights into Early Roman production technologies, *J. Archaeol. Sci.* **2013**, (40), 2589-2605.
6. Phelps, M. Glass supply and trade in early Islamic Ramla: An investigation of the plant ash glass. In *Things that travelled-Mediterranean Glass in the First Millennium CE*. Rosenow, D., Phelps, M., Meek, A., Freestone I., Eds.; Publisher: UCL Press University College London, UK, 2018, pp. 236-282.

7. Henderson, J.; Mcloughlin, S.D.; McPhail, D.S. Radical Changes In Islamic Glass Technology: Evidence For Conservatism And Experimentation With New Glass Recipes From Early And Middle Islamic Raqqa, Syria. *Archaeometry* **2004**, 46 (3), 439–468.
8. Henderson, J.; Chenery S.; Faber, E.; Kröger, J. The use of electron probe microanalysis and laser ablation-inductively coupled plasma-mass spectrometry for the investigation of 8th–14th century plant ash glasses from the Middle East. *Microch. J.* **2016**, 128, 134–152
9. Mirti, P.; Pace, M.; Negro Ponzi, M.M.; Aceto, M. ICP–MS Analysis of glass fragments of Parthian and Sasanian epoch from Seleucia and Veh Ardasir (Central Iraq). *Archaeometry* **2008**, 50 (3), 429–450.
10. Mirti, P.; Pace, M.; Malandrino, M.; Negro Ponzi, M.M. Sasanian glass from Veh Ardasir: new evidences by ICP-MS analysis. *J. Archaeol. Sci.* **2009**, 36, 1061–1069.
11. Schibille, N.; Gratuze, B.; Ollivier, E.; Blondeauc, É. Chronology of early Islamic glass compositions from Egypt. *J. Archaeol. Sci.* **2019**, 104, 10–18.
12. Tite, M.S.; Shortland, A.; Maniatis, Y.; Kavoussanaki, D.; Harris S.A. The composition of the soda-rich and mixed alkali plant ashes used in the production of glass. *J. Archaeol. Sci.* **2006**, 33, 1284-1292.
13. Barkoudah, Y.; Henderson, J. Plant ashes from Syria and the manufacture of ancient glass: ethnographic and scientific aspects. *J. Glass Stu.* **2006**, 48, 291-231.
14. Misra, M.K.; Ragland, K.W.; Baker A.J. Wood ash composition as a function of furnace temperature. *Biomass And Bioenergy* **1993**, 4 (2), 103-116.
15. Verità, M. Le tessere vitree dei mosaici Medievali a Roma. Tecnologia e degrado. In *Mosaici Medievali a Roma Attraverso il Restauro Dell'ICR 1991–2004*; Andaloro, M., D'Angelo, C., Eds.; Gangemi Editore: Rome, Italy, 2017; pp. 437–477.
16. Verità M.; Santopadre, P.; De Palma, G. Scientific investigation of Glass Mosaic tesserae from the 8th Century aD archaeological Site of Qusayr' amra (Jordan). *Bollett. ICR*, **2016**, 32, 5-20

C. Archaeometric analysis of a Roman opaque red jar in the Museu da Farmácia, Lisbon

C.1. Introduction

Bottles, vessels or jars made from opaque red glass have rarely been uncovered from archaeological excavations, and usually they are broken into several fragments. However, a few examples are exhibited in some museums. Weinberg reported and described a monochrome opaque red bottle from the collection of the National Archaeological Museum of Athens, uncovered from a Macedonian grave and dated to the late 1st century BC. The bottle was chemically analysed, detecting high concentrations of copper (CuO 11.3 wt%) and lead (PbO 19.2 wt%), which are compositional features of sealing wax red glass [1].

Another example of a red monochrome jar (N^o. inv. 13829) dated between 1st century BC and 1st century AD is exhibited in the *Museu da Farmácia* in Lisbon. The exact provenance is still unknown, as is the chemical composition and the colouring agent. Moreover, there are still various questions around its production technique.

The aim of these analyses is to chemically characterise the vessel, and identify the colouring agent, in order to understand which type of opaque red glass was used to manufacture it. Moreover, it is a good opportunity to test the application of PIXE and μ Raman analyses as a non-destructive analytical technique without sampling operations.

C.2. Materials and method

The jar is 10 cm high, and the circumference of the rounded body is approximately 6 cm in the middle and 4 cm at the bottom, while the mouth on top is 4 cm in diameter.



Figure C.1. The red jar (N^o. inv. 13829) from the Museu da Farmácia, Lisbon.

It seems to be made in two parts: one part composed of the neck and the shoulder, and the second part by the circular body. It is not perfectly symmetrical, as is possible to see by examining the shoulder and the neck.

It is corroded on the top, which has a white greenish layer. There are some parts of the jar exhibiting a different red hue. Furthermore, heavy restoration work is evident all over the body of the jar. Hence, several fragments of different red hues and different materials are probably present in the jar (fig. C.2).

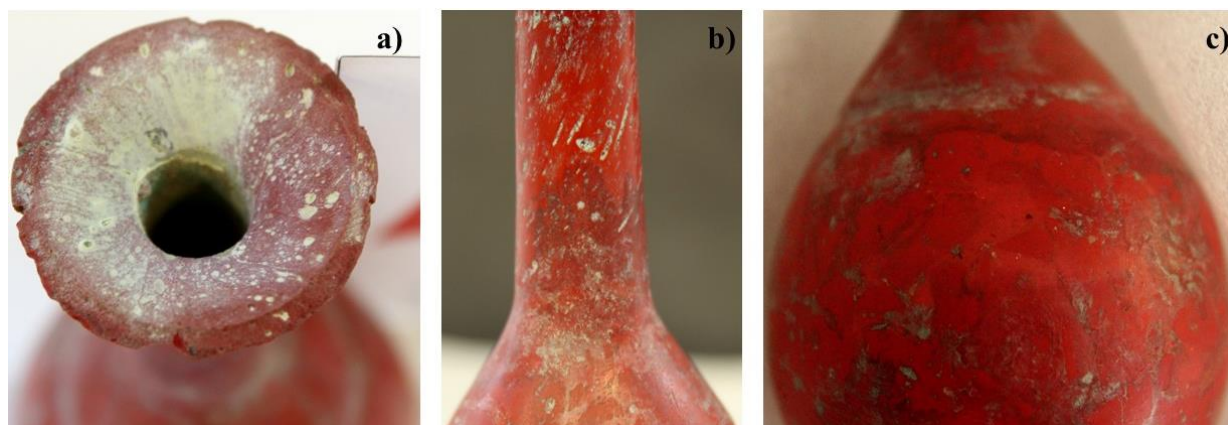


Figure C.2. a) the white greenish layer, probably a decayed product on the mouth of the jar; b) the neck with two different red hues; c) on the round body the presence of an area with fragments showing different red hues.

OM (Optical Microscope)

Images were collected using a Zeiss Axioplan 2 Imaging system (HAL 100) attached to a Nikon DXM1200F digital camera and ACT-1 software. Different illumination modes (bright field and dark field) were used.

PIXE (Particle Induced X-Ray Emission)

Quantitative chemical compositions were achieved using a μ -PIXE ion beam analytical technique, at C2TN (Centre for Nuclear Science and Technology in Lisbon), using an Oxford Microbeams OM150 type scanning nuclear microprobe setup, either with the in-vacuum or with the external beam configuration. The X-rays were collected by an 8 μm thick Be windowed SDD detector with 145 eV resolution. X-ray imaging (2D elemental distribution) and spectra were obtained from an irradiated sample area of $750 \times 750 \mu\text{m}^2$. For trace element quantification (typically elements with atomic number above that of Fe), a 2 MeV proton beam was used. An external beam setup was chosen in order to prevent sample beam-charging and consequently X-ray spectra degradation. X-rays were collected with a SDD detector with 145 eV resolution from a sample area of $800 \times 800 \mu\text{m}^2$. Operation and basic data manipulation, including elemental distribution mapping, was achieved through the OMDAQ software code, and quantitative analysis with GUPIX program.

Reference standards

To calculate the oxide concentration in the semi-quantitative and quantitative chemical analysis, calibration of instruments with glass reference standards was carried out. Standard Corning A, B, C, D were used. These standards have a well-known and certificated composition with different concentrations of several oxides to reproduce the chemical composition of historical glass [2].

μ -Raman microscopy

Raman microscopy was carried out at a scientific laboratory in DCR Lisbon using a Labram 300 Jobin Yvon spectrometer, equipped with a solid state 50-mW laser operating at 532 nm. Spectra were recorded as an extended scan. The system was calibrated using a silicon standard. The laser beam was focused either with a 50 \times or a 100 \times Olympus objective lens. The laser power at the surface of the samples was controlled with neutral density filters (optical densities 0.3 and 0.6). Raman data analysis was performed using LabSpec 5 software. All spectra are presented as acquired without any baseline correction or other treatment.

C.3 Results

Dendritic crystals embedded in the glassy matrix were observed by optical microscope; however, the observations in several cases were difficult to make, due to the presence of other material (used on the surface of the jar) which hampered an accurate view. It is likely that a coating layer was applied in the restoration phase of the jar.

Moreover, the dendritic crystals were not observed on the whole jar, but some parts appear completely different, and by UV-light observation it is possible to see that they are composed of different material, which was probably applied during the restoration to put the fragments of the jar back together. Hence, it should be underlined that the jar is of an original part in which dendritic crystals are visible (fig. C.3), and a restored part in which other material was used (fig. C.4).

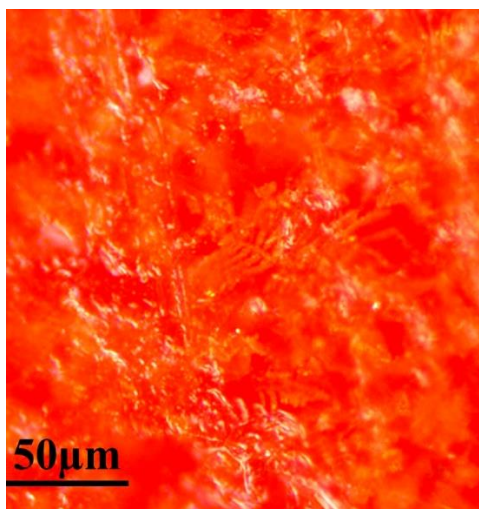


Figure C.3. Dentric crystals observed by optical microscope on the rounded body.

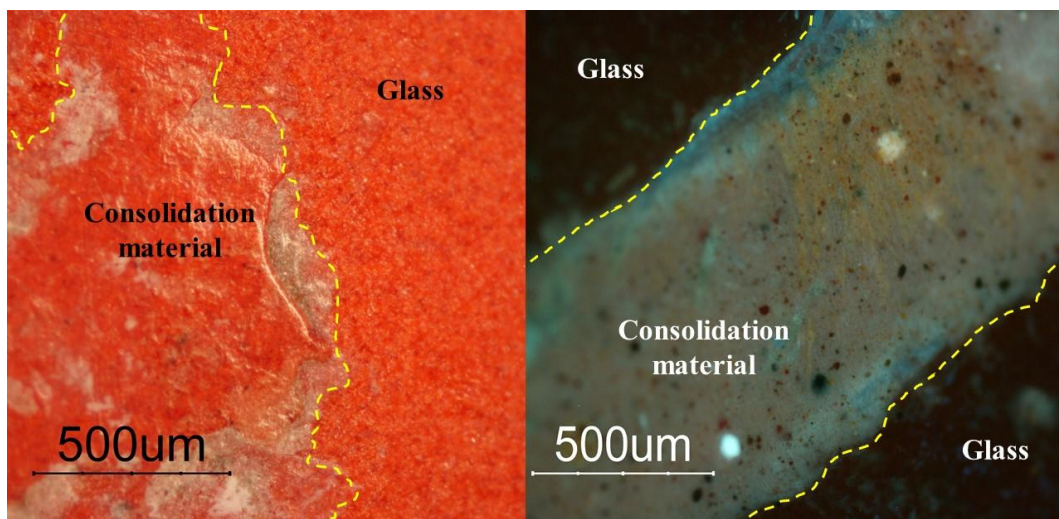


Figure C.4. a) Presence of coating/consolidant layer on the surface of the vessel, observed by reflected light; b) observation by optical microscope by using UV-light.

Chemical composition

The chemical analyses (reported in table C.1) performed on the original parts of the vessel (fig. C.5), revealed high concentrations of copper (CuO 8.5 wt%) and lead (PbO 30.1 wt%), while low quantities of iron (Fe₂O₃ 0.50 wt%) were detected.

By the reduced composition [3], the base glass composition (reported in table C.2) is a soda-lime-silica glass with high sodium content (Na₂O 14.1 wt%) and calcium content 6.5 wt%, while potash and magnesia were detected below 1.5 wt% (K₂O 1.1; MgO 0.85 wt%).

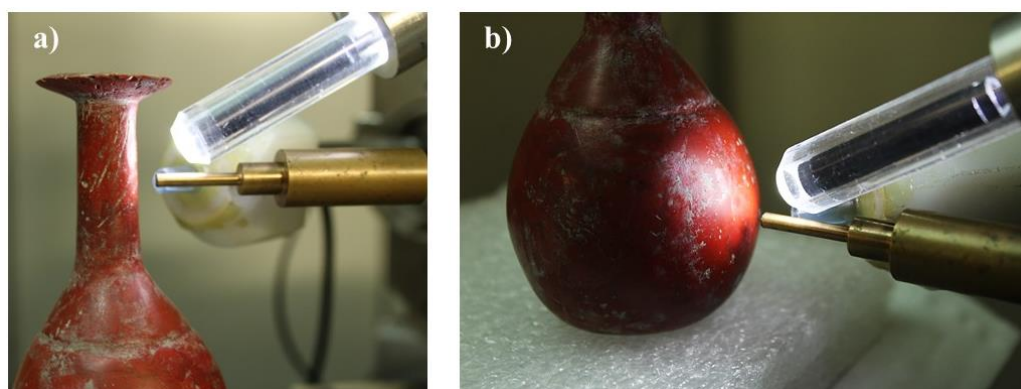


Figure C.5. Some of the points analysed on the vessel. a) Analysing the original part of the neck; b) analysing the original part on the rounded body.

Table C.1. Average oxide composition of the red ampoule.

Oxide	SiO ₂	Al ₂ O ₃	Na ₂ O	K ₂ O	CaO	MgO	P ₂ O ₅	Cl	TiO ₂	Fe ₂ O ₃	MnO	CuO	PbO	ZrO ₂
Wt%	44.1	2.1	8.9	0.68	4.0	0.53	LOD	0.81	0.21	0.50	0.23	8.5	30.1	0.02

Table C.2. Average oxide concentration of the base glass composition (by reduced composition).

Oxide	SiO ₂	Al ₂ O ₃	Na ₂ O	K ₂ O	CaO	MgO	P ₂ O ₅	Cl	TiO ₂	Fe ₂ O ₃	MnO	ZrO ₂
Wt%	71.0	3.4	14.4	1.1	6.5	0.85	LOD	1.3	0.33	0.81	0.36	0.03

By focusing red μ Raman laser (532 nm) on the dendritic crystals, spectra characterised by an intense peak at 218 cm^{-1} , and other weak peaks at 412, 485 and 625 cm^{-1} were obtained (fig. C.6). These features are in good agreement with the Raman spectra of cuprite (Cu_2O) present in the literature, belonging to the Pn3m space group [4]. The peaks at 140 and 160 cm^{-1} , and 630 cm^{-1} are due to a lattice mode, while the peaks at 215-218 cm^{-1} and between 400 and 490 cm^{-1} are attributed to multiphonon Raman scattering [5]. The peak at 142 and 145 cm^{-1} could be related to the crystal lattice vibration of Pb-O [4].

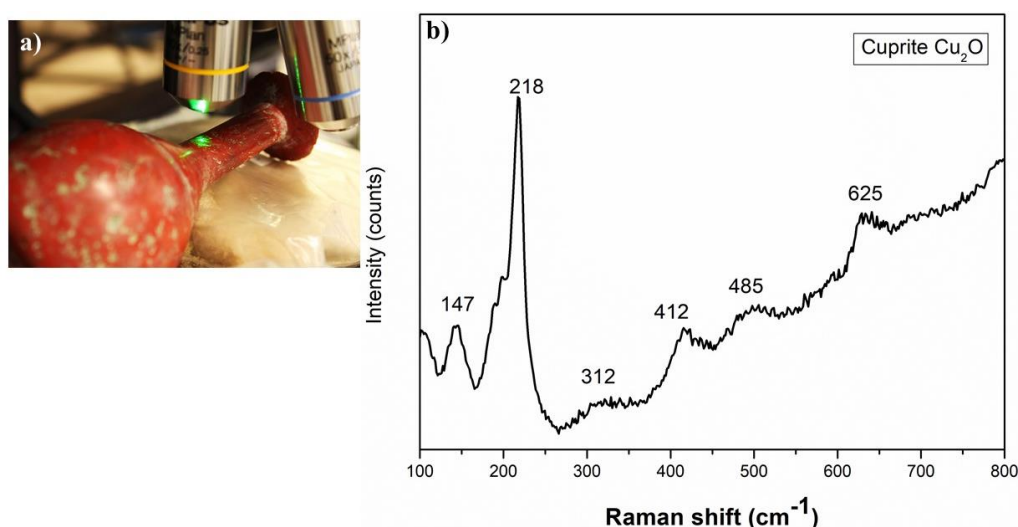


Figure C.6. a) one of the Raman analyses point; b) Raman cuprite spectra.

C. 4 Conclusions

The high quantities of copper and lead oxide revealed in the chemical composition of the jar, and the presence of cuprite crystals in dendritic shape points to the use of sealing wax red glass to manufacture this glass vessel [1, 6].

The base glass composition is in agreement with the typical Roman natron glass, composed of a siliceous-calcareous sand, and (due to the concentration of potash and magnesia both below 1.5wt%) a mineral soda source (natron) was used as a fluxing agent [7]. The concentration of alumina and titanium could be affected by the other material applied to restore the jar, which could contaminate the accuracy of the analyses. Iron is a contaminant from the minerals present in the sand, and it cannot be considered a reducing agent.

Although the bottle reported by [1] is made from the same type of opaque red glass, it exhibits higher potash (K_2O 2.2 wt%) and lower calcium (CaO 3.2 wt%) and magnesia (MgO 0.42 wt%) than the Portuguese jar. Moreover, a higher concentration of copper (CuO 11.3 wt%) and lower lead content (PbO 19.7 wt%) than the Portuguese jar were detected.

In the interior of the neck the vessels were “uneven, while the exterior is smooth” (fig. C.7). According to [1] they are incompatible with free-blowing technique, and suggested “that the bottle might have been blown into a mould”. However, more examples and studies on similar vessels are required to understand the manufacturing technique.

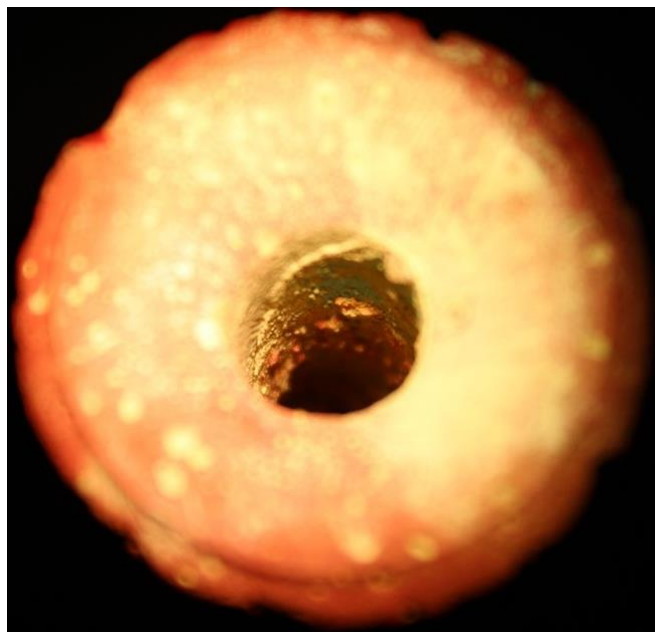


Figure C.7. The interior of the neck vessel, with uneven surface, not smooth.

The provenance of the jar stored in the Museu da Farmácia of Lisbon is still unclear, and needs more analyses. PIXE and μ Raman were confirmed to be good tools to analyse historical glass thanks to their non-destructive character and good sensitivity for obtaining analytical data. However, the quantification of light elements, obtained by the PIXE acquisition system, needs more tests to improve this analytical technique.

References

1. Weinberg, G.D. *Glass Vessels in Ancient Greece. Their History Illustrated from the Collection of the National Archaeological Museum, Athens*; Archaeological Receipt Fund: Athens, Greek, 1992; pp. 112–115.
2. Wagner, B.; Nowak, A.; Bulska, E.; Hametner, K.; Günther, D. Critical assessment of the elemental composition of Corning archeological reference glasses by LA-ICP-MS. *Anal. Bioanal. Chem.* **2012**, 402, 1667–1677.
3. Brill, R.H. *Chemical Analyses of Early Glasses. Volume 2 Tables of Analyses*; The Corning Museum of Glass: Corning, NY, USA, 1999; ISBN 0-872900-143-2.
4. Basso, E.; Invernizzi, C.; Malagodi, M.; La Russa, M.F.; Bersani, D.; Lottici, P.P. Characterization of colorants and opacifiers in roman glass mosaic tesserae through spectroscopic and spectrometric techniques. *J. Raman Spectrosc.* **2014**, 45, 238–245.
5. Meyer, B.K.; Polity, A.; Reppin, D.; Becker, M.; Hering, P.; Kramm, B.; Klar, P.J.; Sander, T.; Reindl, C.; Heiliger, C.; et al. The physics of copper oxide (Cu_2O). *Semicond. Semimet.* **2013**, 88, 201–226.
6. Freestone, I.C. Composition and microstructure of opaque red glass. In Bimson and Freestone. In *Early Vitreous Materials; British Museum Occasional Paper, 56*; Bimson, M., Freestone, I.C., Eds.; British Museum: London, UK, 1987; pp. 173–191. ISBN 978-0861590568.

7. Shortland, A.; Schachner, L.; Freestone, I.; Tite, M. Natron as a flux in the early vitreous materials industry: sources, beginnings and reasons for decline. *J. Archaeol. Sci.* **2006**, 33, 521-530.

D. A comparison between recipes and chemical analyses of Venetian red brown

D.1 Methods and Materials

Twenty Venetian Renaissance red brown glass samples were analysed for their quantitative chemical composition in different laboratories with different methods.

The samples, labelled MG, MH, RBM and GAR, are archaeological shards of blown objects, monochrome and polychrome rods and pressed glass. They were excavated in the Venetian lagoon in a location at the western edge called Fusina. In this area, the embankment of the river Brenta built with natural clays around 1325 to divert the river and impede the silting of the Lagoon, was reinforced since the 15th c. with wastes from the ceramic and glass furnaces of Venice and Murano. The embankment was abandoned in 1610 when the course of the Brenta was changed again [1].

Three samples labelled MG and two samples MH were analysed by Laser Ablation Inductively Coupled Plasma Mass Spectrometry (LA-ICP-MS) at the CNRS laboratories in Orleans (France) and published in [2] and [3] respectively.

Seven samples labelled RBM were analysed by electron probe microanalysis (EPMA) and three samples labelled GAR were analysed by X-ray fluorescence (XRF).

Two mosaic tesserae (SPC-R7 bright red and SPC-R9 brown analysed by EPMA) belonged to the altar piece of the Cappella Lando in the Church of San Pietro di Castello (Venice). The mosaic is signed 1575, but a document dated August 1566 attests that Nicolò verier (Nicolò, glassmaker) was paid for supplying the glass slabs for the mosaic work [4].

Finally, three samples PG-SCV 171, PG-V67 and PG-V74 are 17th c. archaeological shards from the excavation of the Monastery of Sta. Clara-a-Velha (Portugal) and were analysed by EPMA. Comparison of their analyses with the compositional database of Venetian Renaissance glass attested their genuine Venetian provenance [5].

EPMA and XRF analyses were performed at the Stazione Sperimentale del Vetro, Murano-Venice (Italy). EPMA analyses were carried out with a Cameca SX-50 equipped with three wavelength-dispersive spectrometers (PET, LiF and TAP crystals). The operating conditions: accelerating potential 15 kV, beam current 20 nA for major and minor components or 100 nA for trace elements, respectively. A 40 x 50 mm scanning electron beam and limited counting time (10 s for major and minor elements, 20-30 s for trace elements) were used to ensure that no significant alkali drift (ion migration) occurred during the irradiation.

XRF analyses were performed by energy dispersive X-ray micro-fluorescence spectrometry (EDXRF) using a Bruker M4 Tornado spectrometer equipped with a rhodium X-ray tube (maximum power 30 W) with polycapillary lens optics (spot size ~ 30µm) and a Peltier cooled energy dispersive Silicon Drift Detector (SDD) with a 30-mm² sensitive area and an energy resolution ~ 140 eV for Mn K.

For LA-ICP-MS analyses, a VG Laserlab-A was used, comprising a pulsed Nd:YAG laser operating at 1064 nm (spot size 50-200 µm), the repetition rate of the laser may vary from 1 to 10 Hz and the maximum energy of the beam is 2 mJ. The laser beam is focused onto the sample surface through the window of a quartz

sample cell. The cell is flushed by approximately 1.2 l/min of argon carrier gas. ICP-MS instrument was a Plasma Quad2+ EDR.

Further details concerning the analytical methods used for quantitative chemical analysis (device setting, limits of detection and accuracy of the analyses) are given in respectively: LA-ICP-MS in [6], EPMA in [7] and XRF in [8].

Three GAR samples were available for further investigations. They were analysed at the Lisbon University, Conservation and Restoration Department, for optical microscopy observation (Zeiss Axioplan 2 Imaging system -HAL 100- attached to a Nikon DXM1200F digital camera and ACT-1 software under different illumination modes -bright field and dark field-), FORS and μ -Raman spectroscopy and at the CENIMAT laboratory for X-ray diffraction XRD. For the FORS analyses, a MAYA 200 PRO from Ocean Optics spectrophotometer with a single beam dispersive optical fiber was used together with a 2048 CCD Si detector that allows operating in the 200–1050 nm range. The light source is an HL-200-HP 20 W halogen from Ocean Optics, with a single optical path between 360 and 2500 nm. The spectra were taken on the glass surface, in reflectance (R) mode, with a 45°/45° configuration (illumination angle/acquisition) and ca. a 2 mm diameter of the area analysed. Spectra were obtained between 380 and 1050 nm, with an integration time of 8 ms per scan and 15 scans. A Spectralon® surface was used as a reference for calibration. The identification of the crystalline phases was conducted by μ Raman spectroscopy with a Labram 300 Jobin Yvon spectrometer equipped with a solid-state 50mW laser, operating at 532 nm. The spectra were recorded as an extended scan, and the system was calibrated using a silicon standard. The laser beam was focused either with a 50× or a 100× Olympus objective lens and its power at the surface of the samples was controlled with neutral density filters (optical densities 0.3 and 0.6). Raman data were treated using the LabSpec 5 software, and all spectra are presented as acquired without any baseline correction or other treatment. The RUFF database was useful for the identification of some crystalline phases. X-ray diffraction was used on samples where Raman spectroscopy did not allow the identification of the colouring agent. The measurements were performed by X'Pert PRO MPD, equipped with an X-ray tube with Cu anode (1.54059 Å, K α , 45 kV, 40 mA) and an X'Celerator detector (ultra-set X-ray 1D detector based on Real Time Multi Steps -RTMS- technology). The scans were collected in the angular range of 3°- 89° 2 θ with a 0.03° virtual step size and 30 sec/step counting time. The XRD data were processed by the X'Pert HighScore (Panalytical copyright). In order to avoid any contamination of resin peaks, the analyses were performed on bulk samples.

Finally, in Paris at the Centre de Recherche et de Restauration des Musées de France (C2RMF) samples were analysed by field emission scanning electron microscopy (FEG-SEM JEOL 7800F with a EDS BRUKER Quantax 400 system for x-ray microanalysis), to identify the colouring-opacifying particles after platinum coating of samples. The 2 μ m electron beam (current 1 nA) was scanned during analysis to prevent alkali drift.

D.2. Results

The quantitative chemical composition of the Venetian red brown glass samples is reported in wt% of the oxides in [Table D.1](#).

A comparison between recipes and archaeometric investigation on well-dated Venetian red brown confirmed in part what was prescribed by the recipes. Indeed, common glass or *vitrum blanchum* is confirmed by the chemical analyses to be the most frequently used base glass in the production of Venetian red brown glass, and only in three samples did the analyses reveal a *cristallo* glass composition.

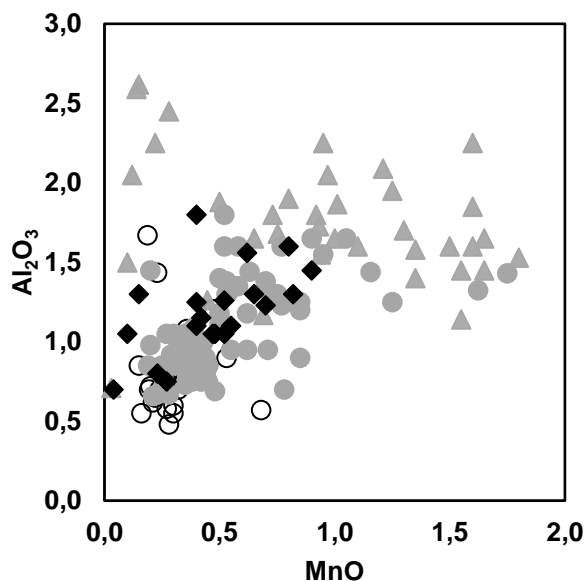


Figure D.1 Alumina vs manganese content (wt% of oxides) of the base glass of analysed red samples (black diamonds) compared with Venetian transparent glass (cristallo: open circles; vitrum blanchum: grey circles; common glass: grey triangles).

The potassium content rarely exceeds 4% (a value considered a limit in Venetian glassmaking). It could indicate small additions of tartar to the base glass as indicated in some Venetian recipes where potassium was deliberately added in the form of tartar. Reported for the first time in the *Trattatelli*, tartar was added in a calcined form (K-carbonate) as a potash-bearing raw material, either unprocessed (raw tartar) or partially calcined tartar (black tartar), acting as a K-bearing compound and as a reducer compound, due to unburned particles.

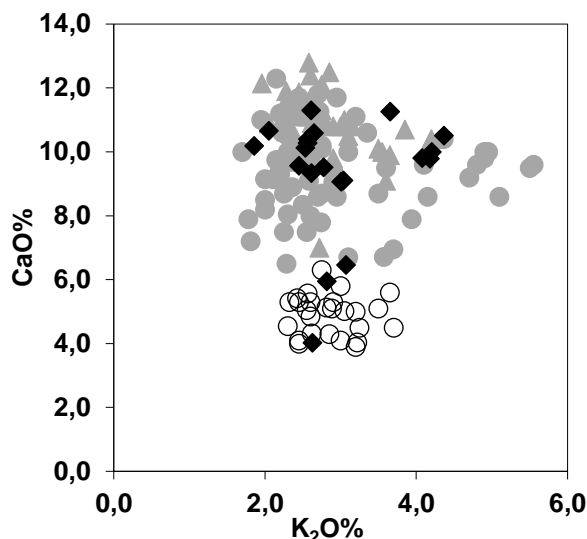


Figure D.2 Calcium vs. potassium contents (wt% of oxides) of the base glass of analysed red samples (black diamonds) compared with Venetian transparent glass (cristallo: open circles; vitrum blanchum: grey circles; common glass: grey triangles).

The analyses reveal that the copper to iron ratio ranges widely. Iron content is always higher than copper (usually from twice to five times) and only in three analyses are these two elements present in comparable concentrations. The recipes also report that iron additions are higher (up to twice) or equal to copper additions. This is probably due to the sources of iron indicated in the recipes: the reducing power of the steel and of the iron flakes from the anvil cannot be predicted.

Although a common procedure is proposed by the manuscripts, the exact amounts of the copper and iron-bearing compounds are rarely mentioned. Hence, the technique for producing opaque red brown glass and the control of the final colour was largely dependent on the skills and the experience of the glassmakers.

In Venetian glassmaking, and probably in the Roman period, the production of red brown glass occurred by re-melting an already made transparent glass in the form of new glass (*cotisso*) or cullet. Several Venetian recipes recommend the use of recycled glass, which is preferred to the well-decolorised crystal glass. The procedure for adding the colouring raw materials directly to the molten glass is highlighted by the manuscripts, a detail not mentioned before in previous research.

In one group the addition of lead-tin calx is recommended and in the other one it is not prescribed.

Lead-tin calx was not added to opacify the glass (insufficient addition and rare cassiterite crystals), but it would have had a different purpose. One possible explanation is to be found in a recipe (D97) to prepare lead-tin calx. It reports a white, more oxidised lead tin calx and a grey one with less oxidised lead and tin. It is likely that the lead-tin calx added to opaque red glass was intended to help copper reduction and the formation of metallic particles. As mentioned above, it is possible that lead and tin were added unintentionally through glass cullet contaminated by opaque white glass in samples where their content is lower than 1%. In this case, lead and tin are fully oxidised and would not affect the formation of colour.

The laboratory reproductions were not aimed at validating the Venetian recipes, but they were used as a reference to offer some suggestions on how to proceed in the manufacture of opaque red glass.

Table D.1 Quantitative chemical composition (wt% of oxides) of the analysed samples. n.a.: not analysed; searched for and not detected: Sb, As, Ba, Zn, Co, Ni. Glass type: VB, vitrum blanchum; CR, cristallo glass.

Analytical technique	sample	object	dating	glass type	SiO ₂	Al ₂ O ₃	Na ₂ O	K ₂ O	CaO	MgO	SO ₂	P ₂ O ₅	Cl	TiO ₂	MnO	Fe ₂ O ₃	CuO	PbO	SnO ₂
EPMA	SPC-R9	mosaic brown	1566	VB	54.5	1.05	13.1	2.48	7.47	2.85	0.19	0.23	0.53	0.05	0.52	6.45	2.25	5.50	2.85
XRF	SPC-R7	mosaic red	1566	VB	63.0	1.56	12.3	2.58	8.85	3.43	0.21	0.34	0.58	0.08	0.62	4.00	1.70	0.35	0.42
EPMA	GAR-R3	bead	15th-17th	CR	62.7	0.70	14.4	2.25	3.45	1.20	0.07	0.10	0.84	0.03	0.04	3.60	3.45	3.60	3.55
LA-ICP-MS	RBM-2H	sherd	15th-17th	CR	67.5	0.75	14.6	2.65	5.60	1.80	0.21	0.12	0.90	0.04	0.27	2.40	2.65	0.25	0.27
LA-ICP-MS	MG-VeR1	sherd	16th-17th	CR	68.0	0.80	14.4	2.90	6.10	1.50	n.a.	0.12	0.60	0.05	0.23	2.40	2.50	0.22	0.21
EPMA	MG-VeR3	sherd	16th-17th	VB	63.7	1.05	13.8	1.75	9.61	3.25	n.a.	0.26	0.73	0.14	0.10	3.80	1.15	0.36	0.34
XRF	RBM-4E	sherd	15th-17th	VB	60.2	1.05	12.5	3.70	8.90	2.90	0.22	0.30	0.83	0.08	0.47	3.30	1.65	2.00	1.90
LA-ICP-MS	GAR-R2	sherd	15th-17th	VB	56.0	1.05	13.8	2.22	9.00	3.20	0.20	0.27	0.70	0.10	0.48	4.05	1.10	3.85	4.00
EPMA	MH-R1	sherd	16th	VB	63.4	1.10	13.0	2.80	8.40	2.50	n.a.	0.20	0.70	0.10	0.40	3.80	1.60	1.00	1.00
EPMA	RBM-4D	sherd	15th-17th	VB	60.7	1.10	12.9	2.40	10.4	3.20	0.17	0.30	0.75	0.07	0.55	5.50	0.70	0.60	0.70
EPMA	RBM-4M	sherd	15th-17th	VB	61.4	1.15	13.2	3.80	8.90	1.00	0.21	0.30	0.85	0.07	0.42	3.20	1.65	1.90	1.90
XRF	PG-V67	applied dots	17th	VB	56.5	1.23	13.4	2.22	8.90	3.10	0.22	0.28	0.63	0.10	0.70	3.17	1.15	5.22	3.16
EPMA	GAR-R1	sherd	15th-17th	VB	57.7	1.25	13.3	2.12	8.30	3.00	0.10	0.25	0.60	0.07	0.40	3.30	1.00	4.20	4.45
EPMA	PG-SCV171	applied dots	17th	VB	58.0	1.26	13.2	2.28	8.15	3.15	0.19	0.28	0.73	0.04	0.52	3.20	0.92	5.10	3.00
EPMA	PG-V74	applied dots	17th	VB	57.3	1.30	12.1	1.77	9.20	3.45	0.20	0.32	0.60	0.09	0.82	3.90	0.70	4.20	4.00
EPMA	RBM-5L	sherd	15th-17th	VB	62.0	1.30	13.4	2.35	9.40	3.30	0.18	0.28	0.50	0.08	0.65	4.80	0.90	0.40	0.50
EPMA	RBM-5B	sherd	15th-17th	VB	62.0	1.30	12.0	2.45	9.80	3.40	0.32	0.35	0.80	0.07	0.15	5.60	1.45	0.20	0.10
EPMA	RBM-2G	sherd	15th-17th	VB	58.3	1.45	11.2	3.70	8.80	3.20	0.18	0.38	0.70	0.07	0.90	4.70	0.85	2.50	3.10
LA-ICP-MS	MG-VeR2	sherd	15th-17th	VB	58.0	1.60	11.6	3.85	9.27	2.80	n.a.	0.27	0.65	0.17	0.80	5.00	1.05	2.65	2.30
LA-ICP-MS	MH-R2	Chevron rod	15th-16th	VB	56.7	1.80	10.2	3.10	9.55	2.65	n.a.	0.20	0.50	0.10	0.40	4.60	0.70	4.80	4.70

References

1. Canal E. Archeologia della laguna di Venezia. Cierre, Verona, 2013.
2. Moretti, C., Gratuze, B. Vetri rossi al rame e avventurina. Confronto di analisi e ricette. *Riv. Staz. Sper. Vetro* **1999**, 3, 147-160.
3. Moretti, C., Hreglich, S. Tecniche di produzione dei vetri opachi impiegate dai vetrai veneziani tra il XV ed il XX secolo. *Riv. Staz. Sper. Vetro* **2005**, 5, 28-32.
4. Zucchetta, E., Verità, M. La pala d'altare in mosaico della Cappella Lando in San Pietro di Castello a Venezia: inedite notizie d'archivio, tecnica di esecuzione, intervento, indagini scientifiche. In *Proceeding of Atti XVIII Convegno Scienza e Beni Culturali. Biscontin G, Driussi G, Eds.*; Bressanone (Italy), 2002, p. 813-821.
5. Lima, A., Medici, T., Pires de Matos, A., Verità, M. Chemical analysis of 17th century Millefiori glasses excavated in the Monastery of Sta. Clara-a-Velha, Portugal: Comparison with Venetian and façon-de-Venise production. *J. Archaeol. Sci.* **2012**, 39 (5), 1238-48.
6. Gratuze, B., Giovagnoli, A., Barrandon, J. N., Telouk, Ph. & Imbert J. L. Apport de la methode ICP-MS couplee a l'ablation laser pour la caracterisation des archeomateriaux. *Revue d'Archéométrie* **1993**, 17, 89-104.
7. Verità, M., Basso, R., Wypyski, M. T. & Koestler, R. J. X-ray microanalyses of ancient glassy materials: a comparative study of wavelength dispersive and energy dispersive techniques. *Archaeometry* **1994**, 36, 241-51.
8. Tesser, E., Verità, M., Lazzarini, L., Falcone, R., Saguì, L. & Antonelli, F. Glass in imitation of exotic marbles: An analytical investigation of 2nd century AD Roman sectilia from the Gorga collection. *J. Cult. Herit.* **2020**, 42, 202-12.

E. First attempts to reproduce opaque red glass in the laboratory

In the first attempt called E1, the base glass was produced in the laboratory using a common laboratory reagent such as SiO_2 , Al_2O_3 , K_2CO_3 , Na_2CO_3 , CaCO_3 with the following chemical composition:

Chemical composition of the base glass (wt.%):

- SiO_2 : 69 wt%
- Al_2O_3 : 2.60 wt%
- K_2O : 2.40 wt%
- Na_2O : 17 w%
- CaO : 9 wt%

Three batches of 50 g of crushed glass were melted at 1300°C for three hours. Then 1 g of cupric oxide was added, and after half an hour ferrous oxide was added in each batch in three different quantities: 0.5 g, 1 g and 1.5 g. The melt was stirred a couple of times, out of the furnace. The temperature was successively lowered to 1100°C and after half an hour the crucibles were transferred to a muffle furnace at 550°C , and then left to cool spontaneously.



Figure E.1 Sequences of the P1 procedure: **a)** three batches in the furnace melted at 1300°C for 3 hours; **b)** the three crucibles after half hour at 1100°C and the addition of iron; **c)** the crucibles were placed in the muffle furnace for the entire night at 550°C .

The procedure P1 (table E.1) produced a blue glass with the formation of red layers only in the bottom of the crucible.

Table E.1 Results by using the P1 procedure.

Glass	Cross section	Bottom
P1-1: 1 g CuO 0.5 g FeO		
P1-2: 1 g CuO 1 g FeO		






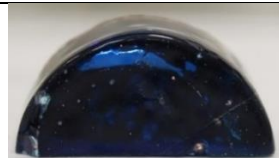
In the second attempt (P2), two batches of 50 g of crushed glass (Effe3 Murano) were prepared: in the first attempt (P2-1) ferrous oxide and cupric oxide in the selected quantities (both 1 g) were added to the batch which was covered by pieces of graphite on the top. The batch was transferred to the furnace and melted at 1300 °C, and then the temperature was lowered to 1100 °C and maintained at this temperature for two hours. Afterwards, the crucible was moved into a muffle furnace at 550 °C, left for one hour and then left to cool spontaneously (between 10-12 hours).

In the second batch (P2-2) only copper (1 g) was added to the glass grains, and about 30 g of graphite pieces were deposited on the top of the batch at room temperature, in an attempt to substitute the role of iron oxide. The batch was melted at 1300 °C for two hours, and then the temperature was lowered to 1100 °C and maintained. Afterward, the crucible was moved into a muffle furnace at 550 °C for 1 hour. The muffle furnace was switch off and left to cool spontaneously (between 10-12 hours).

The sample P2-1 is composed of different coloured regions (Table E.2). On the top (in contact with the graphite) a transparent red layer formed; an extensive area in the middle is colourless pale blue on the bottom. On the bottom of the sample, opaque red glass formed in a thin layer which turned black in the part in contact with the bottom of the crucible.

In sample P2-2, only a thin transparent red layer on the top of the sample formed, which was in contact with the graphite. On the bottom metallic particles of considerable size precipitated. However, the resulting glass was blue-copper.

Table E.2 Results by using the P2 procedure.

Glass	Cross section	Bottom
(P2)-1: CuO (1 g) + FeO (1 g) + CO		
(P2)-2: CuO (1 g) + CO		

In the third procedure (P3) two iron oxides were tested: ferrous oxide (FeO) and magnetite (Fe₃O₄).

In the first batch (P3-1), 2 g of cupric oxide and 2 g of Fe₃O₄ were added to 100 g of crushed glass (Effe3), at room temperature and then 15 g of vegetable carbon was put on the top of the batch. This batch was transferred


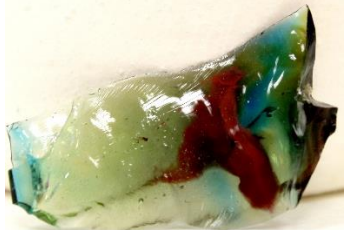
into the furnace and melted at 1100°C for two hours without stirring. Afterwards the furnaces were switched off and the molten glass was left to cool spontaneously (10-12 hours).

In the second batch (P3-2), 2 g of cupric oxide and 2 g of FeO were added to 100 g of crushed glass (Effe3), and then graphite was put on the top of the batch. This batch was transferred into the furnace at room temperature and melted at 1100°C for two hours (without stirring the melt). Afterwards the furnace was switched off and the molten glass was left to cool spontaneously (10-12 hours).

P3-1 sample resulted to be colourless on the top in contact with the vegetable carbon, or pale blue and green with some parts in which opaque red layers formed on the entire body of the sample (Table E.3).

The P3-2 sample appeared very dark. Some opaque red formed on the bottom of the sample and on the top in contact with the vegetable carbon. The central part is a transparent pale green-blue colour.

Table E.3 Results by using the P1 procedure.

Glass	Cross section	Cross section
<p>(P3)-1: CuO (2 g) + 2g of Fe₃O₄ + 15 g CO</p>		
<p>(P3)-2: CuO (2 g) + 2 g of FeO + 15 g CO</p>	